

Impact of symmetries: A phenomenological study on neutrino mass models

by

Roopam Sinha

Enrolment No.: PHYS05201304008

Saha Institute of Nuclear Physics
Kolkata

*A thesis submitted to the
Board of Studies in Physical Science Discipline
In partial fulfillment of requirements
For the Degree of*

DOCTOR OF PHILOSOPHY

of

HOMI BHABHA NATIONAL INSTITUTE



May, 2019

Homi Bhabha National Institute

Recommendations of the Viva Voce Committee

As members of the Viva Voce Committee, we certify that we have read the dissertation prepared by Roopam Sinha entitled "Impact of symmetries: A phenomenological study on neutrino mass models" and recommend that it may be accepted as fulfilling the thesis requirement for the award of Degree of Doctor of Philosophy.

Debasish Majumdar

Date : 14/10/2019

Chairman : Prof. Debasish Majumdar, SINP

Ambar Ghosal

Date : 14/10/19

Guide & Convener : Prof. Ambar Ghosal, SINP

M. K. Parida (M. K. Parida)

Date : 14.10.19

Examiner : ~~NA, NA~~ Prof. M. K. Parida,
SOA Univ.

Pratik Majumdar

Date : 14/10/19

Member : Prof. Pratik Majumdar, SINP

Debades Bandyopadhyay

Date : 14.10.2019

Member : Prof. Debades Bandyopadhyay, SINP

Final approval and acceptance of this thesis is contingent upon the candidate's submission of the final copies of the thesis to HBNI.

I hereby certify that I have read this thesis prepared under my direction and recommend that it may be accepted as fulfilling the thesis requirement.

Date : 14/10/19

Place : Kolkata.

Ambar Ghosal

Guide

STATEMENT BY AUTHOR

This dissertation has been submitted in partial fulfillment of requirements for an advanced degree at Homi Bhabha National Institute (HBNI) and is deposited in the Library to be made available to borrowers under rules of the HBNI.

Brief quotations from this dissertation are allowable without special permission, provided that accurate acknowledgement of source is made. Requests for permission for extended quotation from or reproduction of this manuscript in whole or in part may be granted by the Competent Authority of HBNI when in his or her judgment the proposed use of the material is in the interests of scholarship. In all other instances, however, permission must be obtained from the author.

ROOPAM SINHA

DECLARATION

I, hereby declare that the investigation presented in the thesis has been carried out by me. The work is original and has not been submitted earlier as a whole or in part for a degree / diploma at this or any other Institution / University.

ROOPAM SINHA

List of Publications and Preprints related to the thesis

1. **“Generalized $\mathbb{Z}_2 \times \mathbb{Z}_2$ in scaling neutrino Majorana mass matrix and baryogenesis via flavored leptogenesis,”**
R. Sinha, R. Samanta and A. Ghosal
[JHEP **1712**, 030 \(2017\).](#)
2. **“Maximal Zero Textures in Linear and Inverse Seesaw,”**
R. Sinha, R. Samanta and A. Ghosal
[Phys. Lett. B **759**, 206 \(2016\).](#)
3. **“CP transformed mixed $\mu\tau$ antisymmetry for neutrinos and its consequences.”**
R. Sinha, P. Roy and A. Ghosal,
[Phys. Rev. D **99** \(2019\) no.3, 033009.](#)
4. **“Importance of generalized $\mu\tau$ symmetry and its CP extension on neutrino mixing and leptogenesis,”**
R. Samanta, R. Sinha and A. Ghosal
[arXiv:1805.10031 \[hep-ph\].](#)
5. **“Phenomenological implications of the Friedberg-Lee transformation in a neutrino mass model with $\mu\tau$ -flavored CP symmetry,”**
R. Sinha, S. Bhattacharya, R. Samanta
[JHEP **1903**, 081 \(2019\).](#)

DEDICATED TO

my parents

ACKNOWLEDGMENTS

First I thank my father who always encouraged me to pursue my passion and my mother for her patience and support. I would also like to thank Prof. Tapas Mitra for his encouragement. Prolonged interactions with him have not only enriched my understanding but shaped my approach to physics as a whole. This period of Ph.D journey was one of the most delightful chapters of my life in the august company of wonderful friends and faculties at my home institute. Writing a few lines will not suffice to pay gratitude towards them. I would like to express a deep sense of gratitude to my Ph.D supervisor Prof. Ambar Ghosal for his continuous guidance, motivation and invaluable suggestions during my Ph.D career. He was always there to entertain my questions with generosity. Discussion with him have always been enlightening and enabled me to think independently. Next I would like to thank Prof. Palash Baran Pal who is unequivocally an outstanding teacher we have learned from. I am indebted to him for useful discussions during the early years of my journey. I would also express my genuine thanks to Prof. Biswajit Adhikary for several discussions and to my collaborator Prof. Probir Roy for his penetrating insights. I would like to thank Prof. Debasish Majumdar, Prof. Debadesh Bandopadhyay and Prof. Pratik Majumder for their generosity and help in various occasions.

Among the seniors, I must start by thanking Mainak da (Mainak Chakraborty) for his help and guidance during the early years of my Ph.D and other seniors, Amitda, Prasantada, Anshuda, Kamakshyada, Dipankarda, Anirbanda, Apurbada, Susnata di, Aminulda, Goutamda, Aritrada, Chiruda, Kuntalda (theory), Kuntalda (CMS), Suvankarda, Naosadda for a friendly environment. This also gives me an opportunity to thank my college friends, Manas, Chiranjit, Sudipto, Dip, Swarnali, Sohini, Biplab,

Debayan and Joy with whom I have enjoyed at lot and M.Sc friends, Suman, Sanjib, Noor, Soumya, Sobhit, Ayan, Arup, Moin, Raja, Subhadeep, Sangkhya, Sumit, Indranil, Budhha, Dibyashree, Chunki, Camelia, Bijita, Priyadarshini, Sushmita for making it a memorable journey. Now it's the turn to acknowledge my SINP friends some of whom require a special mention. I must start by thanking Rome who apart from being immensely talented is a wonderful human being I ever came to interact with. He has significant contributions in my research. Next, I thank Amit, a very down-to-earth person and with whom it was always a pleasure to talk with. Since I first heard, I became an admirer of Shamik as a vocalist and guitarist and Sukannya for her great sense of humour and talents beyond physics. It will be strange to thank you guys for your unconditional support. I will genuinely miss times spent with you. Biswajit, Mugdha, Srimanta, Sourav, Susmita, Maireyee, Arnab, Biswarup, Mithun you guys have always been very supportive. I would also like to thank some of my juniors, Avik (theory), Avik (APC), Madhurima, Upala, Sazad, Gaurav, Pritam, Prashant, Sayan with whom I have spent a lot of memorable moments.

Finally I acknowledge Saha Institute of Nuclear Physics for providing me adequate infrastructure to carry out my research and the Department of Atomic Energy (DAE), Government of India for financial support. I should acknowledge the cluster computational facility provided by the Astroparticle Physics and Cosmology (APC) division.

ROOPAM SINHA

Contents

Synopsis	xvii
List of Figures	xxiii
List of Tables	xxxix
1 Introduction	1
1.1 A brief tour of history	2
1.2 Theory of neutrino oscillations	4
1.3 Neutrino masses: Dirac versus Majorana	11
1.4 Ultra High Energy (UHE) cosmic neutrinos	23
1.5 Baryogenesis via Leptogenesis	25
1.5.1 Baryogenesis via leptogenesis in Type-I seesaw	27
1.6 An overview of the present work	36
2 Importance of $\mu\tau$ mixing symmetry and its CP extension on leptogenesis	45
2.1 Introduction	45
2.2 Model independent correlations in $\mu\tau$ mixing	50
2.2.1 Consequences of $G_1^{g\mu\tau}$ invariance	50
2.2.2 Consequences of $G_2^{g\mu\tau}$ invariance	54
2.2.3 $\mu\tau$ mixing in some neutrino mass models	57
2.3 CP extension of the $\mu\tau$ mixing symmetry	59
2.3.1 CP symmetry in a general light neutrino mass term	59
2.3.2 CP symmetry in Type-I seesaw	63
2.4 Leptogenesis in extended CP framework	65
2.5 Conclusions	80
3 Mixed $\mu\tau$ antisymmetry for neutrinos with nonstandard CP extension	83
3.1 Introduction	83
3.2 Complex mixed $\mu\tau$ antisymmetry of the neutrino Majorana mass matrix	86
3.3 Neutrino mixing angles and phases	88
3.4 Numerical analysis	90
3.4.1 Neutrinoless double beta decay	93

3.4.2	CP asymmetry in neutrino oscillations	96
3.4.3	Flavor flux ratios at neutrino telescopes	101
3.5	Summary and conclusions	104
4	Complex extension of the residual $\mathbb{Z}_2 \times \mathbb{Z}_2$ symmetry in scaling neutrino Majorana mass matrix	107
4.1	Introduction	107
4.2	Modification to scaling neutrino mass matrix with generalized $\mathbb{Z}_2 \times \mathbb{Z}_2$	109
4.2.1	Case I: Complex extension of $G_{2,3}^{(k)}$ Invariance	112
4.2.2	Case II: Complex extension of $G_{1,3}^{(k)}$ Invariance	113
4.3	Reconstruction of modified scaling matrices with type-I seesaw	117
4.4	Baryogenesis via leptogenesis	121
4.5	Numerical analysis: methodology and discussion	124
4.6	Effect of $N_{2,3}$ on final Y_B	143
4.7	Summary and conclusion	147
5	Implications of the Friedberg-Lee invariance in a neutrino mass model with $\mu\tau$-flavored CP symmetry	149
5.1	Introduction	149
5.2	FL transformed $\text{CP}^{\mu\tau\theta}$ invariance of M_ν	154
5.3	Impact of mass ordering on mixing angles and CP properties	155
5.3.1	Normal ordering	157
5.3.2	Inverted ordering	159
5.4	Numerical analysis	160
5.4.1	Parameter Estimation	160
5.4.2	Neutrinoless double beta ($0\nu\beta\beta$) decay process	161
5.4.3	Effect of CP asymmetry in neutrino oscillations	164
5.4.4	Octant of θ_{23} from flavor flux measurement at neutrino telescope	166
5.5	Summary and conclusion	168
6	Maximal zero textures in the framework of Linear and Inverse Seesaw	171
6.1	Introduction	171
6.2	Maximal zero textures of charged lepton mass matrix	173
6.3	Texture zeros in Linear seesaw	174
6.3.1	Effective M_ν in Linear seesaw	175
6.4	Maximal zero textures in Inverse seesaw	178
6.4.1	Effective M_ν and its parametrization	181
6.4.2	Numerical analysis	182
6.5	Summary	185
7	Summary and conclusions	187

SYNOPSIS

Spectacular developments in neutrino physics since the last couple of decades has been unravelling the properties of elusive neutrinos. Not only has it been firmly established that neutrinos have tiny masses through the evidences of flavor oscillations, experiments with solar, atmospheric and reactor neutrinos have measured the mixing angles and mass-squared differences to a reasonably decent accuracy. In particular, confirmation of a nonzero value of the reactor mixing angle θ_{13} has opened up the possibility of CP violation through the Dirac CP phase δ . Although the absolute scale of light neutrino masses are still unknown a tight upper bound exists on the sum of neutrino masses $\sum_i m_i$ from cosmological observations. From a theoretical perspective, while an extension of the Standard Model (SM) is required to take neutrino masses and lepton flavor mixing into account, the latter is part of an elaborate and challenging theoretical problem which addresses the so-called “flavor puzzle”- widely different mixing angles for quarks and leptons even though in Grand Unified Theories (GUT) they belong to the same multiplet. Besides, there are yet unsettled questions regarding the baffling nature of neutrinos-Dirac or Majorana, the issue of CP violation in the leptonic sector, the neutrino mass ordering, absolute scale of neutrino mass, possibility of lepton flavor violating decays such as $\mu \rightarrow e\gamma$ and so on.

Four of my papers are based on the paradigm of residual (remnant) symmetry as an economical approach to uncover the pattern of flavor mixing, leptonic CP properties in addition to general neutrino phenomenology such as the prediction of sum of the light neutrino masses $\sum_i m_i$, neutrinoless double ($\beta\beta 0\nu$) decay parameter $|M_\nu^{ee}|$ and behaviour of Ultra High Energy (UHE) flavor flux at neutrino telescopes. It has been shown in the literature that irrespective of the actual high energy flavor group, existence of nondegenerate light Majorana neutrinos lead to a $\mathbb{Z}_2 \times \mathbb{Z}_2$ [1, 2] invariance of the light Majorana neutrino mass term in the low-energy Lagrangian

which in turn dictates the flavor mixing. The vanishing of the reactor mixing angle θ_{13} in such scenarios can be avoided in two different ways. Either one of the residual symmetries have to be broken or supplemented with a nonstandard CP transformation, namely, a CP-transformation combined with flavor symmetry which not only allows a nonvanishing θ_{13} but predicts (non)maximal Dirac CP violation. While one of the Majorana phases α is always restricted to lie at its CP conserving values, the other phase β can lead to Majorana CP violation if δ is nonmaximal.

In one of these papers [3], the prediction of Dirac CP violation arising as a consequence of the existence of two \mathbb{Z}_2 type residual symmetries $\mathcal{G}_{1,2}^{g\mu\tau}$ accompanying a ‘ $\mu\tau$ mixing symmetry’ $\mathcal{G}_3^{g\mu\tau}$ – a generalization of the canonical $\mu\tau$ interchange symmetry – has been worked out assuming the latter to be broken to avoid a vanishing θ_{13} . We refer them as ‘associated $\mu\tau$ mixing’ symmetries. It is well-known [4] that both the \mathbb{Z}_2 type ‘associated $\mu\tau$ interchange’ ($\mathcal{G}_{1,2}^{\mu\tau}$) symmetries lead to a precise correlation between the Dirac CP violating phase δ and the atmospheric mixing angle θ_{23} in a model-independent manner and the correlation is such that a maximal value of θ_{23} inevitably leads to a maximal value of δ . However, such a simultaneous maximality appears to be in tension with the present global status of the neutrino oscillation parameters; a large deviation in δ from its maximal value is still allowed for the near maximality of θ_{23} . Our analysis of the associated $\mu\tau$ mixing using the non-uniqueness of PMNS matrix indeed reveals that such a stringent condition of simultaneous maximality δ and θ_{23} can be relaxed i.e. either of the quantities δ or θ_{23} can be nonmaximal while the other being maximal. However, the parameter that generalizes $\mu\tau$ interchange to $\mu\tau$ mixing, cannot be arbitrarily large. Even a tiny departure from the $\mu\tau$ interchange have been shown to lead to a drastic deviation in δ . We have made a comparison of the $\mu\tau$ interchange symmetry with the proposed $\mu\tau$ mixing symmetry. We obtain a distribution of $\cos \delta$ by randomly generating all the mixing angles assuming a normal distribution with a standard

deviation of 1σ . For associated $\mu\tau$ interchange $\mathcal{G}_1^{\mu\tau}$, $\cos\delta$ peaks around 0.18, i.e., corresponding $\delta \approx \pm 79.63^\circ$ ($\delta \approx \pm 117^\circ$). On the other hand, $\cos\delta$ peaks around 0.43, i.e., corresponding $\delta \approx \pm 64.53^\circ$ for $\mathcal{G}_1^{g\mu\tau}$ for an hypothetical value $\pi/60$ of the $\mu\tau$ mixing parameter $\theta_g - \pi/4$ with 10% uncertainty. The rapid progress of the experiments such as T2K and NO ν A is expected to lead to confirmation regarding a definitive statement about the (non)maximality in the atmospheric mixing angle if δ . If the latter deviate largely from its maximal value, the proposal of $\mu\tau$ mixing shall become a potentially viable scenario.

The next paper [5] too, is based on the residual $\mathbb{Z}_2 \times \mathbb{Z}_2$ approach. To avoid a vanishing θ_{13} , we have generalized the well-known Strong Scaling Ansatz (SSA) [6, 7] on the light neutrino Majorana mass matrix M_ν by complementing the residual symmetry with a nonstandard CP-transformation on the neutrino fields as $\nu_{L\alpha} \rightarrow iG_{\alpha\beta}\gamma^0\nu_{L\beta}^C$ with $G_{\alpha\beta}$ being the generators of any one of the two independent \mathbb{Z}_2 symmetries and $\nu_{L\beta}^C$ being the CP conjugated left-handed flavor neutrino field. As a result, the real invariance of M_ν i.e. $G^T M_\nu^{SSA} G = M_\nu^{SSA}$ is replaced by its complex counterpart: $G^T M_\nu^{MS} G = (M_\nu^{MS})^*$ referred to as ‘Modified Scaling’. Since only two of the three $G_a^{(k)}$ ’s ($a = 1; 2; 3$) are independent, there are three ways in which generalized CP symmetry can be implemented: $G_{1,2}, G_{2,3}$ and $G_{1,3}$. The complex invariance relations of M_ν related to $G_{2,3}^{(k)}$ i.e. $G_{2,3}^{(k)T} M_\nu^{MS} G_{2,3}^{(k)} = (M_\nu^{MS})^*$ (Case-I) is equivalent the real invariance $G_1^{(k)T} M_\nu^{MS} G_1^{(k)} = (M_\nu^{MS})$. Similarly, complex (real) invariance relations holds under $G_{1,3}^{(k)}$ ($G_2^{(k)}$) (Case-II) while the complex (real) invariance under $G_{1,2}^{(k)}$ ($G_3^{(k)}$) have to be abandoned because of vanishing θ_{13} . For each of the viable cases, the existence of complex invariance under $G_3^{(k)}$ ensures $\cos\delta = 0$ and $\sin\alpha = \sin\beta = 0$. We assume hierarchical mass eigenvalues for the RH Majorana neutrino mass matrix M_R . With the assumption that the required CP violation for leptogenesis is created by the decay of lightest (N_1) of the heavy Majorana neutrinos while the asymmetry originating from the decays of $N_{2,3}$, being washed out, we numerically

worked out the possibility of flavored vs. unflavored leptogenesis in the three mass regimes (1) $M_1 < 10^9$ GeV, (2) 10^9 GeV $< M_1 < 10^{12}$ GeV and (3) $M_1 > 10^{12}$ GeV for both a normal and an inverted mass ordering separately for Case-I and II. It turns out partially flavored or unflavored leptogenesis does not occur and τ -flavored leptogenesis remains the only possibility. For a normal (inverted) ordering of light neutrino masses, θ_{23} is found to be less (greater) than its maximal value, for the final baryon asymmetry Y_B to be in the observed range. Besides, an upper and a lower bound on the mass of N_1 have also been estimated. Effect of the heavier neutrinos $N_{2,3}$ on final Y_B has been worked out subsequently.

In the work [8], we propose a complex extension of $\mu\tau$ mixing antisymmetry in the neutrino Majorana mass matrix M_ν by a nonstandard CP transformation $\nu_{\alpha L} \rightarrow i\mathcal{G}_{\alpha\beta}^{\mu\tau\theta} \gamma^0 \nu_{\beta L}^C$ where \mathcal{G} is a \mathbb{Z}_4 generator related to the \mathbb{Z}_2 generator G through the relation $\mathcal{G} = iG$. This leads to interesting implications for leptonic CP violation. The $\mu\tau$ mixing parameter θ gets related with δ and θ_{23} as $\sin \delta = \pm \sin \theta / \sin 2\theta_{23}$. For arbitrary θ , both θ_{23} and δ are nonmaximal. For a nonmaximal δ , one of the two Majorana phases is different from 0 or π , leading to substantial Majorana CP violation with observable consequences for $\beta\beta 0\nu$ decay process. For all possible combinations of α, β and δ the entire parameter space corresponding to the inverted mass ordering shall be ruled out if nEXO, covering its entire reach, does not observe any $\beta\beta 0\nu$ signal. We have made a quantitative study of the effect of the CP asymmetry parameter $A_{\mu e}$ in long baseline neutrino oscillation experiments. We also make quantitative predictions of our scheme on Ultra High Energy (UHE) neutrino flavor flux ratios at neutrino telescopes. While exact CP transformed $\mu\tau$ interchange antisymmetry ($\theta = \pi/2$) leads to an exact equality among those ratios, taking a value 0.5, a tiny deviation can cause a drastic change in them. Measurement of UHE flavor flux with improved statistics will further constrain the parameter θ .

In the remaining work [9] on residual symmetry, we propose a neutrino mass

model with $\mu\tau$ -flavored CP symmetry which leads to a highly predictive scenario when the effective light neutrino Lagrangian enjoys an additional invariance under a Friedberg-Lee (FL) transformation on the left-chiral flavor neutrino fields. While both types of mass ordering, i.e., Normal Ordering (NO) and Inverted Ordering (IO) are allowed, the absolute scale of the light neutrino masses is fixed by the vanishing determinant of light Majorana neutrino mass matrix \mathcal{M}_ν . For both NO and IO, while θ_{23} is in general nonmaximal ($\theta_{23} \neq \pi/4$), the Dirac CP phase δ is exactly maximal ($\delta = \pi/2, 3\pi/2$) for IO and nearly maximal for NO due to $\cos \delta \propto \sin \theta_{13}$. For the NO, very tiny nonvanishing Majorana CP violation might appear through one of the Majorana phases β , otherwise the model predicts vanishing Majorana CP violation. From the future precision measurement of θ_{23} , it is difficult to rule out the model. However, any large deviation of δ from its maximality, will exclude the model. Beside fitting the neutrino oscillation global fit data, we also explore $\nu_\mu \rightarrow \nu_e$ oscillation which is expected to reveal CP violation in different long baseline experiments. Finally, assuming pp and $p\gamma$ collisions as the source of the Ultra High Energy (UHE) neutrinos, statements have been made about the octant of θ_{23} . Conversely, a precision measurement of θ_{23} can be used to predict the allowed ranges of flavor flux ratios.

The last paper [10] is based on a pedagogical analysis of maximal texture zeros i.e., vanishing of certain elements in the light neutrino Majorana mass matrix in low energy seesaw scenarios. In the simplest Type-I seesaw extension of the SM, the light neutrino Majorana masses are generated by incorporating of three right-handed (RH) singlet neutrino fields ν_{Ri} and a corresponding lepton number violating Majorana mass term M_R with a new mass scale close to the GUT (10^{12} GeV). Probing the new physics at such a high scale is beyond the reach of ongoing collider experiments while, a seesaw scale in the TeV range can be realized in some other variants, such as Inverse seesaw and Linear seesaw in which the effective light Majorana neutrino

mass matrices read

$$m_\nu \approx m_D(m^{-1})^T \mu_S m^{-1} m_D^T, \quad (1)$$

and

$$m_\nu = -M(m^{-1}m_D^T) - [M(m^{-1}m_D^T)]^T \quad (2)$$

respectively. These mechanisms have been investigated with maximal zero textures of the constituent matrices subjected to the assumption of non-vanishing determinant of the neutrino mass matrix M_ν and charged lepton mass matrix M_ℓ . We restrict to the minimally parametrized non-singular M_ℓ it gives rise to only 6 possible textures of M_ℓ . Nonvanishing determinant of m dictates six possible textures of the constituent matrices. It turns out that Inverse seesaw leads to phenomenologically allowed maximal zero textures while the Linear seesaw leads to only one. In Inverse seesaw, we show that 2 is the maximum number of independent zeros that can be inserted into μ 's to obtain all seven viable two-zero textures of M_ν . On the other hand, in Linear seesaw mechanism, the minimal scheme allows maximum 5 zeros to be accommodated in 'm' so as to obtain viable effective neutrino mass matrices (M_ν). Interestingly, we find that our minimalistic approach in Inverse seesaw leads to a realization of all the phenomenologically allowed two-zero textures whereas in Linear seesaw only one such texture is viable.

In conclusion, the important issues leptonic CP violation which might have implications in the matter-antimatter asymmetry of the Universe, determination of absolute neutrino mass scale and mass ordering has been addressed from the approach of residual symmetry. The predictions of all these models will be tested in the experiments such as nEXO [11], LEGEND, GERDA-II, T2K, NO ν A, DUNE etc.

List of Figures

1.1	Neutrino mass generation at one-loop in the Zee-Wolfenstein model. The flavor indices have been suppressed for simplicity.	21
1.2	One-loop diagram for light neutrino mass generation in the Ma model.	22
2.1	For $G_1^{g\mu\tau}$ (left): Variation of δ with θ_d (a measure of the deviation from $\mu\tau$ interchange symmetry). Here, $2\pi - \delta$ is also an allowed solution for the same values of θ_d . For $G_1^{\mu\tau}$ (right): Variation of δ with θ_{23} . These plots are generated using the best-fit values for θ_{13} and θ_{12} for NO. .	52
2.2	For $G_1^{\mu\tau}$ (left): Probability distribution of δ with θ_{23} . For $G_1^{g\mu\tau}$ (left): The same plot but for $\theta_d = \pi/12$. Here we have used Gaussian distribution for each of the mixing angles with 1σ errors.	53
2.3	For $G_2^{g\mu\tau}$ (left): Variation of δ with θ_d (a measure of the deviation from $\mu\tau$ interchange symmetry). Here, $2\pi - \delta$ is also an allowed solution for the same values of θ_d . For $G_2^{\mu\tau}$ (right): Variation of δ with θ_{23} . These plots are generated using the best-fit values for θ_{13} and θ_{12} for NO. .	55

2.4	For $G_2^{\mu\tau}$ (left): Probability distribution of δ with θ_{23} . For $G_2^{g\mu\tau}$ (left): The same plot but for $\theta_d = \pi/12$. Here we have used Gaussian distribution for each of the mixing angles with 1σ errors.	56
2.5	For the real invariance $(G_1^{g\mu\tau})^T M_\nu G_1^{g\mu\tau} = M_\nu$ (top): Probability distribution of δ with θ_{23} . For the real invariance $(G_2^{g\mu\tau})^T M_\nu G_2^{g\mu\tau} = M_\nu$ (bottom): Probability distribution of δ with θ_{23} . Here we have used Gaussian distribution for each of the mixing angles with 1σ errors. . .	62
2.6	Variation of N_{B-L} with z assuming $4\delta_x K_{i\tau}^I \cos 2\xi = 0.1$ and $ \varepsilon_{i\tau} \simeq 1.5 \times 10^{-3}$. The blue line is the contribution from a single RH neutrino. The red line, matching the observed range, denotes contributions from both the RH neutrinos.	75
2.7	Variation of N_{B-L} with z assuming $\overline{m}_{\max} \frac{4\delta_x}{m^*} = 8$ and $ \varepsilon_{i\tau} \simeq 2.67 \times 10^{-5}$. The blue line is the asymmetry injected in the electron flavor through flavor couplings. The green line is net contribution from the muon and tau flavor asymmetries. The red line which matches the observed range after taking into account the injected asymmetry in the electron flavor.	78
3.1	Plots of $m_{1,2,3}$ for normal (left) and inverted (right) mass ordering with the lightest mass eigenvalue is plotted in the ordinate. The red, green and blue bands refer to m_1, m_2 and m_3 respectively.	92
3.2	Plots of $ M_\nu^{ee} $ vs. m_{min} for both types of mass ordering with four possible choices of the Majorana phases α and β . NO and IO refer to Normal and Inverted ordering respectively.	94

3.3	$A_{\mu e}$ (for $E = 1$ GeV), plotted against the baseline length L , for the four cases in Table 3.5. Each plot stands for both NO and IO since numerically, within the 3σ range of θ_{23} , the two types of ordering are practically indistinguishable. The bands are caused by θ_{23} and θ varying in their 3σ range and phenomenologically allowed range respectively with the other parameters kept at their best fit values.	97
3.4	Variation of the CP asymmetry parameter with beam energy E for different baselines lengths of $L = 295$ km, 810 km and 1300 km corresponding to T2K, NO ν A and DUNE respectively for both NO and IO; the numerical distinction between the two types of ordering is insignificant for the 3σ range of θ_{23}	99
3.5	Flux ratios R_e, R_μ, R_τ vs. the $\mu\tau$ -mixing parameter θ for normal ordering. where the three mixing angles have been allowed to vary over their 3σ ranges. The green(red) line in each plot of the upper(lower) panel corresponds to the best fit value of the mixing angles. The plots in the upper (lower) panel correspond to $\cos \delta \geq 0(\leq 0)$	103
3.6	Flux ratios R_e, R_μ, R_τ vs. the $\mu\tau$ -mixing parameter θ for inverted ordering where the three mixing angles have been allowed to vary over their 3σ ranges. The green(red) line in each plot of the upper(lower) panel corresponds to the best fit value of the mixing angles. The plots in the upper (lower) panel correspond to $\cos \delta \geq 0(\leq 0)$	104
4.1	Case-I: Plots of the primed parameters for a normal mass ordering.	126
4.2	Case-I: Plots of the primed parameters for a inverted mass hierarchy.	127
4.3	Case-II: Plots of the primed parameters for a normal mass ordering.	127

4.4	Case-II: Plots of the primed parameters for a normal mass ordering.	128
4.5	Plot of $ M_{ee} $ vs. the lightest neutrino mass: the top two figures represent Case A: $\alpha = \pi, \beta = 0$ (left) and Case B: $\alpha = \pi, \beta = \pi$ (right) while the figures in the lower panel represent Case C: $\alpha = 0, \beta = 0$ (left) and Case D: $\alpha = 0, \beta = \pi$ (right).	130
4.6	The plot on the left panel shows the range of the wash-out parameters. The red dot corresponds to the minimum value of χ^2 for which a set of primed parameters has been taken to compute Y_B . The plot on the right panel shows a variation of Y_B vs k . The red band in the same plot indicates the observed range of Y_B	135
4.7	A plot of the final Y_B for different values of M_1 for a normal light neutrino mass ordering.	135
4.8	The plot on the left panel shows the range of the wash-out parameters. The red dot corresponds to the minimum value of χ^2 for which a set of primed parameter has been taken to compute Y_B . The plot on the right panel shows final Y_B for different values of M_1 for the inverted light neutrino mass ordering.	138
4.9	The plot on the left panel shows the range of the wash-out parameters. The red dot corresponds to the minimum value of χ^2 for which a set of primed parameter has been taken to compute Y_B . The plot on the right panel shows a variation of Y_B vs k . The red band in the same plot indicates the observed range of Y_B	139
4.10	A plot of the final Y_B for different values of M_1 for the normal light neutrino mass ordering.	140

4.11	The plot on the left panel shows the range of the wash-out parameters. The red dot corresponds to the minimum value of χ^2 for which a set of primed parameter has been taken to compute Y_B . The plot on the right panel shows final Y_B for different values of M_1 for the inverted light neutrino mass ordering.	141
4.12	Plots of the wash-out parameters Δ_1 and Δ_2 for inverted light neutrino mass ordering for both the cases. The red dot corresponds to the corresponding χ_{min}^2 for which we calculate the final baryon asymmetry.	146
5.1	Probability distribution of the Dirac CP phase δ for normal mass ordering. It is evident that the values which are very close to 270° are most probable. To be numerically precise, $\int_{270}^{270\pm 0.2} PDF(\delta) d\delta = 0.795$. Thus upon a large number of random trial (we choose that number to be 10^6), there is 80 % probability that δ will be in the range 270 ± 0.2 .	159
5.2	Plots of $ M^{ee} $ vs. m_{min} for both types of mass ordering with four possible choices of the Majorana phases α and β	163
5.3	Variation of $P_{\mu e}$ and $A_{\mu e}$ against the baseline length L for IO ($E = 1$ GeV). The plots are for $\delta = 3\pi/2$ and the bands correspond to 3σ ranges in θ_{12} and θ_{13} . The three vertical dashed lines indicate observations at three different baseline lengths: $L = 295\text{Km}$ (T2K), $L = 810\text{Km}$ (No ν A) and $L = 1300\text{Km}$ (DUNE).	164

- 5.4 Plots of $A_{\mu e}$ with energy E for fixed baseline lengths corresponding to different experiments in case of IO. Fig.(a) is for T2K with $L = 295\text{Km}$; fig.(b) is for NO ν A with $L = 810\text{Km}$ and fig.(c) is for DUNE with $L = 1300\text{Km}$. The plot is for $\delta = 3\pi/2$, while the bands and the horizontal dashed lines have the same specifications as in fig. 5.3. . . . 165
- 5.5 Plots of $P_{\mu e}$ and $A_{\mu e}$ with different baseline lengths L for NO ($E = 1\text{GeV}$). The bands of the plots correspond to 3σ ranges of the mixing angles and also the ranges for the parameters $79.6^\circ < \theta < 101.6^\circ$ and $1.79 < |\eta_1/\eta_2| < 2.11$. In this case, δ is not fixed, but varies over a range predicted from (5.29) with the same ranges of the mixing angles, and model parameters θ and η_1/η_2 . The three vertical dashed lines and the horizontal dotted line specify the same as in Fig.5.3. 165
- 5.6 Plots of $A_{\mu e}$ with energy E for fixed baseline lengths corresponding to different experiments in case of NO. Fig.(a) is for T2K with $L = 295\text{Km}$; fig.(b) is for NO ν A with $L = 810\text{Km}$ and fig.(c) is for DUNE with $L = 1300\text{Km}$. The plots and their widths have same specifications as in fig. 5.5. The horizontal dotted lines $A_{\mu e} = 0$ specify CP conservation. 166
- 5.7 Variation of the flavor the flux ratios R_e (red), R_μ (blue) and R_τ (green) with θ for NO (left panel) and for IO (right panel). The solid lines represent plots for the best-fit values of the mixing angles and the bands are caused by the current 3σ ranges of the mixing angles θ_{12} and θ_{13} . The horizontal axes in both plots correspond to the numerically obtained ranges of θ in Table 5.2, which is different in NO and IO. For the NO case, η_1/η_2 is fixed at 1.0. 168

- 6.1 The first two figures of the top row represent the parameter space for M_ν^1 matrix. Left plot of the bottom row is the variation of J_{CP} with δ and the right figure shows the hierarchy (normal) of the model. . . . 184
- 6.2 The first two figures of the top row represent the parameter space for M_ν^2 matrix. Left plot of the bottom row is the variation of J_{CP} with δ and the right figure shows the hierarchy (normal) of the model. . . . 185

List of Tables

3.1	Input values used in the analysis [12]	91
3.2	Output values of the parameters of M_ν	91
3.3	Output values CP phases in the range $\beta \in [0, 2\pi]$	92
3.4	Predictions on the light neutrino masses.	92
3.5	Four possibilities for $A_{\mu e}$	97
3.6	Prediction of the ranges of $ A_{\mu e} $ with $E = 1\text{GeV}$	100
3.7	Prediction of the ranges of $ A_{\mu e} $ in T2K, NO ν A, DUNE	100
3.8	Prediction for the values of flux ratios (R_l) for $\theta \neq \pi/2$ [12]	103
4.1	Parameters of M_ν	119
4.2	Input values fed into the analysis [13].	126
4.3	Predictions on the light neutrino masses and $\sum_i m_i$	128
4.4	Parameters and observables corresponding $\chi^2 = 0.083$ for normal mass ordering.	133

4.5	Parameters and observables corresponding $\chi^2 = 0.261$ for inverted hierarchy.	139
4.6	Parameters and observables corresponding $\chi^2 = 0.256$ for normal mass ordering.	140
4.7	Parameters and observables corresponding $\chi^2 = 0.041$ for inverted hierarchy.	142
4.8	Final statements on Y_B for different mass regimes.	142
4.9	Bounds on M_1 for different mass ratios of the RH neutrinos ($i = 1, 2$).	145
5.1	Input values used in the analysis [12]	161
5.2	Output values of the parameters of M_ν	161
6.1	Maximal zero textures of the charged lepton mass matrix M_ℓ	174
6.2	Six zero textures of m_D with $\det(m_D) \neq 0$	175
6.3	Six zero textures of M with $\det(M) \neq 0$	175
6.4	Minimal (6-zero) textures of m with $\det(m) \neq 0$	175
6.5	Compositions for Allowed Realizations of M_ν	176
6.6	Viable 5-zero textures of m	177
6.7	Minimal (6-zero) textures of m	179
6.8	Minimal (4-independent zero) textures of μ_S	179
6.9	2-independent zero textures for μ_S	180

6.10	Compositions for Realization of two-zero M_ν textures with $m_D = m_D^1$	180
6.11	Effective allowed M_ν from Inverse seesaw	181
6.12	Input experimental values [14]	182
6.13	Parameter ranges of the matrices with $ M_{11} \neq 0$	183

Chapter 1

Introduction

Although the speculations about the fundamental indivisible constituents of matter dates back to the era of Democritus the scientific enterprise really started to gather momentum with Becquerel's discovery of radioactivity in 1896 and that of electron by Thomson in the subsequent year. In the twentieth century, after the continuous β -spectrum was conclusively established, Pauli suggested the existence of an elusive particle, called neutrino which was incorporated by Fermi in his effective theory of nuclear β -decay. Since then it has been an exhilarating journey which ultimately led to the Standard Model (SM) of particle physics. The predictions of the SM has been verified with incredible precision. The discovery of the Higgs boson, the last missing piece of the puzzle, has bolstered physicists faith in the SM as an effective theory. However, it is still an incomplete theory. Among others, the discovery of neutrino oscillations by Super-Kamiokande and SNO necceciate the existence of tiny neutrino masses and therefore, extension of the SM with new degrees of freedom.

In this thesis we focus on some aspects related to massive neutrinos. Since it was first proposed by Pauli, the intriguing nature of neutrinos has been baffling the

physicists. For a long time, neutrinos were assumed to be massless fermions, and was thought to be described by Weyl spinors. In 1937, Majorana suggested that neutrinos can be their own antiparticles and Giulio Racha proposed that such a conjecture would lead to neutrinosless double beta ($0\nu\beta\beta$) decay. Though compelling evidences of flavor oscillation has firmly established that neutrinos have tiny masses, the nature of neutrinos, whether Dirac or Majorana, still remains buried in mystery. Many issues such as the theoretical origin of the observed pattern of flavor mixing, leptonic CP violation and lepton flavor violating decays remain to be answered; experimental questions such as determination of the sign of the atmospheric mass-squared difference Δm_{31}^2 (or Δm_{32}^2), i.e., the “neutrino mass ordering”, mass spectrum (hierarchical or quasidegenerate), the octant of the atmospheric mixing angle θ_{23} are yet to be settled. Moreover, due to other important roles played by the neutrinos, the subject of neutrino physics is now a rapidly evolving field of research. For example, neutrinos have profound impact on BigBang Nucleosynthesis (BBN) and the formation of Large-Scale Structures (LSS) of the Universe. Besides, neutrinos can be a window to probe the physics beyond the SM, in particular, generation of baryon asymmetry through the decays of heavy Majorana neutrinos. In the following, we discuss a brief history of the neutrinos and some theoretical aspects related to them.

1.1 A brief tour of history

Neutrinos were actually discovered in 1956 in Reines and Cowan’s experiment [15] which detected an electron anti-neutrino ($\bar{\nu}_e$) from a radioactive source. The idea of neutrino-antineutrino oscillation was first proposed by Pontecorvo in 1957-58 as an elegant solution to the solar neutrino problem. On the other hand, the possibility of electron-neutrino (ν_e) oscillating into muon-neutrino (ν_μ) was proposed by Maki,

Nakagawa and Sakata in 1962 in - same year (ν_μ) was detected by its rescattering to produce muon (μ^-) in 1962 by Lederman, Schwartz, Steinberger [16] in Brookhaven National Laboratory. It was followed by Pontecorvo's theory of $\nu_\mu \rightarrow \nu_e$ oscillation. Though there were various indirect evidences regarding the existence of the third generation of neutrino, i.e., the tau-neutrino (ν_τ), for its direct detection, physicists had to wait till 2000 when it was observed at Fermilab [17]. Experiments were carried out in search of fourth generation of neutrino and the measurement of the decay width of Z boson confirmed the non-existence of such a fourth type of neutrino with mass less than 40 GeV. The earliest experiment designed to detect solar neutrinos was led by Raymond Davis at the Homestake mines in South Dakota, USA. They detected neutrinos through the inverse beta decay process $\nu_e + {}^{37}\text{Cl} \rightarrow e^- + {}^{37}\text{Ar}$, and found that the measured flux was about one third of the flux predicted from the standard solar model. Assuming that the model of the Sun is reliable, where did the missing neutrinos go? This anomaly was known as the Solar Neutrino Problem (SNP). Atmospheric neutrinos are produced when the nuclei in the earth's atmosphere are bombarded by the cosmic rays (predominantly protons) producing pions via the process:

$$p + X \rightarrow \pi^\pm + Y. \quad (1.1)$$

Next, the charged pions decay through

$$\begin{aligned} \pi^\pm &\rightarrow \mu^\pm + \nu_\mu(\bar{\nu}_\mu), \\ \mu^\pm &\rightarrow e^\pm + \nu_e(\bar{\nu}_e) + \bar{\nu}_\mu(\nu_\mu). \end{aligned} \quad (1.2)$$

Clearly, twice as many ν_μ were expected to be produced compared to the number of ν_e . However, water Cherenkov detectors such as Kamiokande [18], iron calorimeter detector Soudan II [19] detected flux which were less than expected which further consolidated the flavor oscillation conjecture. While atmospheric neutrino oscillation

was definitely established when the SK-detector demonstrated a strong dependence on the zenith angle for the upward going neutrinos a definitive confirmation of solar neutrino oscillation had to wait till 2002. Experiments such as GALLEX [20] and SAGE [21] confirmed the deficit observed in Homestake experiment and the Super Kamiomande collaboration reported the deficit with enhanced statistics. The SNP was finally resolved in 2002 by Sudbury Neutrino Observatory (SNO) which was capable of detecting all three flavors of neutrinos and confirmed flavor oscillation in solar neutrinos.

In Sec.1.2, we lay out the basic theory of neutrino oscillation in vacuum and in presence of matter. In Sec.1.3 we give a short summary of some of the mechanisms of neutrino mass generation. Sec.1.4 deals with a brief discussion of Ultra High Energy neutrinos as relevant to this thesis. Sec.1.5 contains a review of the framework of baryogenesis via leptogenesis.

1.2 Theory of neutrino oscillations

Oscillations in vacuum

Neutrinos are produced in weak interaction eigenstates or flavor states. Each flavor state $|\nu_l\rangle$ ($l = e, \mu, \tau$) can be written as a coherent superposition of mass eigestates $|\nu_i\rangle$ ($i = 1, 2, 3$) i.e., at $t = 0$

$$|\nu_l(0)\rangle = \sum_{i=1}^3 U_{li}^* |\nu_i\rangle \quad (1.3)$$

where U is a 3×3 ¹ unitary matrix, known in the literature as the PMNS matrix.

¹Despite the hints of light sterile neutrino in LSND and Mini-Boone, we adhere to the three-flavor scenario.

The mass eigenstates evolve according to the Schrodinger equation

$$i\partial_t|\nu_i\rangle = H|\nu_i\rangle = E_i|\nu_i\rangle \quad (1.4)$$

with $E_i = \sqrt{p_i^2 + m_i^2} \approx p_i + m_i^2/2E$ assuming extremely relativistic neutrinos. Therefore, at a later time $t > 0$, $|\nu_l\rangle$ evolves to

$$|\nu_l(t)\rangle = \sum_{i=1}^3 U_{li}^* e^{-iE_i t} |\nu_i\rangle = e^{-ipt} \sum_{i=1}^3 U_{li}^* e^{-im_i^2 t/2E} |\nu_i\rangle \quad (1.5)$$

assuming each mass eigenstates are produced with same momenta p . The amplitude of finding the flavor state $|\nu_m\rangle$ in $|\nu_l(t)\rangle$ is given by

$$\mathcal{A}_{lm} \equiv \mathcal{A}(\nu_l \rightarrow \nu_m) = \langle \nu_m | \nu_l(t) \rangle = e^{-ipt} \sum_i U_{li} U_{mi}^* e^{-im_i^2 t/2E}. \quad (1.6)$$

Therefore, assuming $L \sim t$ for extremely relativistic neutrinos, the transition probability is given by

$$\begin{aligned} P_{lm} \equiv P(\nu_l \rightarrow \nu_m) &= |\mathcal{A}(\nu_l \rightarrow \nu_m)|^2 = \left| \sum_i U_{li}^* U_{mi} e^{-im_i^2 L/2E} \right|^2 \\ &= \sum_{i,j} U_{li}^* U_{mi} U_{lj} U_{mj}^* e^{-i\Delta m_{ij}^2 L/2E} \end{aligned} \quad (1.7)$$

where $\Delta m_{ij}^2 = m_i^2 - m_j^2$. For convenience, (1.7) can be written in a different form

$$P_{lm} = \delta_{lm} - 4 \sum_{i>j} \text{Re}(U_{li}^* U_{mi} U_{lj} U_{mj}^*) \sin^2 \Delta_{ij} + 2 \sum_{i>j} \text{Im}(U_{li}^* U_{mi} U_{lj} U_{mj}^*) \sin(2\Delta_{ij}), \quad (1.8)$$

where $\Delta_{ij} = \Delta m_{ij}^2 L/4E$. If $l = m$, the quantity in the bracket is real, and therefore, the imaginary part drops out to give the survival probability (the corresponding

experiment is called a *disappearance* experiment):

$$P_{ll} = 1 - 4 \sum_{i < j} |U_{li}|^2 |U_{lj}|^2 \sin^2 \Delta_{ij} = 1 - 4 \sum_{j < i} \tilde{P}_{li} \tilde{P}_{lj} \sin^2 \Delta_{ij} \quad (1.9)$$

where the sum is over all i and j , subject to the condition $j < i$. Here, the quantity $\tilde{P}_{li} = |U_{li}|^2$ is the probability to find the l -flavor state in the i^{th} mass eigenstate. If $l \neq m$, P_{lm} is called conversion probability (the corresponding experiment is called an *appearance* experiment).

The matrix U in (1.3) is a 3×3 unitary matrix with nine independent real parameters. A convenient parametrization of U in terms of three a priori independent mixing angles and six phases is given by

$$U = P_\phi U_{\text{PMNS}} = P_\phi \begin{pmatrix} c_{12}c_{13} & e^{\frac{i\alpha}{2}} s_{12}c_{13} & s_{13}e^{-i(\delta-\beta/2)} \\ -s_{12}c_{23} - c_{12}s_{23}s_{13}e^{i\delta} & e^{\frac{i\alpha}{2}} (c_{12}c_{23} - s_{12}s_{23}s_{13}e^{i\delta}) & e^{\frac{i\beta}{2}} s_{23}c_{13} \\ s_{12}s_{23} - c_{12}c_{23}s_{13}e^{i\delta} & e^{\frac{i\alpha}{2}} (-c_{12}s_{23} - s_{12}c_{23}s_{13}e^{i\delta}) & e^{\frac{i\beta}{2}} c_{23}c_{13} \end{pmatrix} \quad (1.10)$$

where $c_{ij} = \cos \theta_{ij}$, $s_{ij} = \sin \theta_{ij}$ with $\theta_{ij} = [0, \pi/2]$ being the mixing angles. The diagonal phase matrix $P_\phi = \text{diag}(e^{i\phi_1}, e^{i\phi_2}, e^{i\phi_3})$ consists of three unphysical phases $\phi_{1,2,3}$ which can always be absorbed through a redefinition of Dirac-type charged lepton fields. The phases $\delta \in [0, 2\pi]$ and $\alpha, \beta \in [0, 2\pi]$ are respectively known as the Dirac CP-violating phase and the Majorana phases. If the neutrinos are Majorana in nature, the latter phases cannot be removed. However, if neutrinos are Dirac type in nature, the only irremovable phase is δ in which case U_{PMNS} in (1.10), known as the Pontecorvo-Maki-Nakagawa-Sakata (PMNS) matrix, coincides with the standard parameterization of the CKM matrix U_{CKM} in the quark sector. Though the Majorana CP phases do not affect the oscillation probabilities they can affect experiments like neutrinoless double beta decay. Solar and atmospheric neutrino oscillation data suggests that $\Delta m_{21}^2 \ll \Delta m_{31}^2$ and $\Delta m_{23}^2 \approx \Delta m_{13}^2 \equiv \Delta m_{\text{atm}}^2$. For small baseline

experiments with small L/E ratio, a vanishing value can be assumed for $\Delta m_{21}^2 L/2E$ so that the oscillation is effectively controlled by Δm_{31}^2 . Therefore, (1.8) and (1.9) reduce to a simplified expressions

$$\begin{aligned}
 P_{ee} &= 1 - \sin^2 2\theta_{13} \sin^2 \left(\frac{\Delta m_{\text{atm}}^2 L}{4E} \right), \\
 P_{\mu\mu} &= 1 - 4s_{23}^2 c_{13}^2 (1 - s_{23}^2 c_{13}^2) \sin^2 \left(\frac{\Delta m_{\text{atm}}^2 L}{4E} \right), \\
 P_{\tau\tau} &= 1 - 4c_{23}^2 c_{13}^2 (1 - c_{23}^2 c_{13}^2) \sin^2 \left(\frac{\Delta m_{\text{atm}}^2 L}{4E} \right), \\
 P_{e\mu} &= P_{\mu e} = s_{23}^2 \sin^2 2\theta_{13} \sin^2 \left(\frac{\Delta m_{\text{atm}}^2 L}{4E} \right), \\
 P_{e\tau} &= P_{\tau e} = c_{23}^2 \sin^2 2\theta_{13} \sin^2 \left(\frac{\Delta m_{\text{atm}}^2 L}{4E} \right), \\
 P_{\mu\tau} &= P_{\tau\mu} = c_{13}^4 \sin^2 2\theta_{23} \sin^2 \left(\frac{\Delta m_{\text{atm}}^2 L}{4E} \right).
 \end{aligned} \tag{1.11}$$

For long baseline experiments with large L/E , and using $\Delta m_{13}^2 L/2E \simeq \Delta m_{23}^2 L/4E$, one obtains

$$P(\nu_e \rightarrow \nu_{\mu+\tau}) = c_{13}^2 \sin^2 2\theta_{12} \sin^2 \left(\frac{\Delta m_{12}^2 L}{4E} \right) + \frac{1}{2} \sin^2 2\theta_{13}. \tag{1.12}$$

It is to be noted that in the limit $\theta_{13} \rightarrow 0$, Eqs.(1.11),

$$\begin{aligned}
 P_{ee} &= 1, P_{e\mu} = P_{e\tau} = 0, \\
 P_{\mu\mu} &= P_{\tau\tau} = 1 - \sin^2 2\theta_{23} \sin^2 \left(\frac{\Delta m_{\text{atm}}^2 L}{4E} \right), \\
 P_{\mu\tau} &= P_{\tau\mu} = \sin^2 2\theta_{23} \sin^2 \left(\frac{\Delta m_{\text{atm}}^2 L}{4E} \right)
 \end{aligned} \tag{1.13}$$

while (1.12) reduces to

$$P(\nu_e \rightarrow \nu_{\mu+\tau}) = \sin^2 2\theta_{12} \sin^2 \left(\frac{\Delta m_{12}^2 L}{4E} \right). \tag{1.14}$$

These formulae describe the two-flavor oscillation scenarios where (1.14) is attributed

to solar neutrino oscillation and (1.13) to atmospheric oscillation.

The antineutrino oscillation probability $P_{\bar{l}m} \equiv P(\bar{\nu}_l \rightarrow \bar{\nu}_m; t)$ can be obtained from P_{lm} as:

$$P_{\bar{l}m} = P_{lm}(U_{li} \rightarrow U_{li}^*). \quad (1.15)$$

The CP and CPT-transformation property of P_{lm} are given by

$$P_{lm} \xrightarrow{\text{CP}} P_{\bar{l}m} \quad \text{and} \quad P_{lm} \xrightarrow{\text{CPT}} P_{\bar{m}l} \quad (1.16)$$

from which it follows that the CPT invariance is automatically satisfied i.e., $P_{lm} = P_{\bar{m}l}$. In particular, it implies that the neutrino and antineutrino survival probabilities are identical i.e. $P_{\bar{l}l} = P_{ll}$ i.e., a disappearance experiment is not sensitive to CP-violation. The CP-asymmetry is written as

$$A_{\text{CP}}^{(lm)} = P_{lm} - P_{\bar{l}m} = 4 \sum_{i>j} \text{Im}(U_{li}^* U_{mi} U_{lj} U_{mj}^*) \sin\left(\frac{\Delta m_{ij}^2 L}{2E}\right) = -A_{\text{CP}}^{(ml)} \quad (1.17)$$

where the quantity $\text{Im}(U_{li}^* U_{mi} U_{lj} U_{mj}^*) \equiv J_{\text{CP}}$ is called the Jarlskog invariant. Using the parameterization (1.10) and unitarity property of U it can be easily shown that

$$A_{e\mu} = A_{\mu\tau} = A_{\tau e} = \sin 2\theta_{12} \sin 2\theta_{23} \sin 2\theta_{13} c_{12} \sin \delta \\ \times \left[\sin\left(\frac{\Delta m_{12}^2 t}{2E}\right) + \sin\left(\frac{\Delta m_{23}^2 t}{2E}\right) + \sin\left(\frac{\Delta m_{31}^2 t}{2E}\right) \right]. \quad (1.18)$$

Clearly, all CP asymmetries will vanish if (i) $\delta = 0, \pi$, and (ii) any of the mixing angles $\theta_{12}, \theta_{23}, \theta_{13}$ is 0 or π even when $\delta \neq 0, \pi$. In other words, CP violation will show up in the appearance experiments if $J_{\text{CP}} \neq 0$.

Oscillations in matter

So far our discussion was confined to neutrino oscillations in vacuum. However,

since matter effects [22] can dramatically affect the oscillation probabilities P_{lm} , propagation of neutrinos through matter must be taken into account for a realistic description. In particular, it might lead to the resonance enhancement of P_{lm} i.e., it may exceed $\sin^2 2\theta$ (where θ is the two-flavor mixing angle in vacuum), and may be close to unity even if θ is very small. This is known as the Mikheyev-Smirnov-Wolfenstein (MSW) effect. As the neutrinos pass through normal matter, all three flavors (ν_e, ν_μ, ν_τ) interact with the constituent electrons, protons and neutrons via neutral current (NC) interaction while only ν_e s experience the charged current (CC) interaction with the electrons. At low energies, the latter is governed by the effective Hamiltonian

$$H_{CC} = \frac{G_F}{\sqrt{2}} [\bar{e}\gamma^\mu(1 - \gamma_5)e][\bar{\nu}_e\gamma_\mu(1 - \gamma_5)\nu_e]. \quad (1.19)$$

where a Fierz transformation has been used. The matter-induced potential that contributes to the coherent forward scattering ν_e can be obtained by integrating over the variables corresponding to the electron so as to obtain following expression quadratic in ν_e :

$$H_{\text{eff}}(\nu_e) = \langle H_{CC} \rangle_{\text{electron}} \equiv \bar{\nu}_e V_e \nu_e. \quad (1.20)$$

The average of the term in the first parenthesis of (1.19) i.e., $\langle \bar{e}\gamma_\mu(1 - \gamma_5)e \rangle$ contributes to the background for the neutrino propagation. We have,

$$\langle \bar{e}\gamma^0 e \rangle = \langle e^\dagger e \rangle = N_e, \langle \bar{e}\boldsymbol{\gamma} e \rangle = \langle \mathbf{v}_e \rangle, \langle \bar{e}\gamma_0\gamma_5 e \rangle = \left\langle \frac{\boldsymbol{\sigma}_e \mathbf{P}_e}{E_e} \right\rangle, \langle \bar{e}\boldsymbol{\gamma}\gamma_5 e \rangle = \langle \boldsymbol{\sigma}_e \rangle \quad (1.21)$$

where N_e is the number density of electrons. If the medium is unpolarized and has a vanishing total momentum, only the first term survives to give

$$(V_e)_{CC} \equiv V_{CC} = \sqrt{2}G_F N_e. \quad (1.22)$$

Since NC interactions do not distinguish between the flavors, the corresponding contributions to the matter-induced potentials, V_{NC} , has the same value for all flavors. In an electrically neutral medium, the contributions to V_{NC} from electrons and protons mutually cancel but the scattering of neutrinos off neutrons gives $(V_a)_{\text{NC}} = -G_F N_n / \sqrt{2}$ with N_n being the number density of neutrons. Together with (1.22) this gives

$$V_e = \sqrt{2}G_F(N_e - \frac{N_n}{2}), \quad V_\mu = V_\tau = -\sqrt{2}G_F(\frac{N_n}{2}). \quad (1.23)$$

Restricting to the two-flavor case, the effective hamiltonian in flavor basis can now be written as

$$H_{\text{eff}} = U \begin{pmatrix} E_1 & 0 \\ 0 & E_2 \end{pmatrix} U^\dagger + a\mathbb{I} + \begin{pmatrix} \sqrt{2}G_F N_e & 0 \\ 0 & 0 \end{pmatrix}, \quad (1.24)$$

where \mathbb{I} is the 2×2 identity matrix, H is the Hamiltonian in absence of all matter effects and $a = -G_F \frac{N_n}{\sqrt{2}}$ and

$$U = \begin{pmatrix} \cos \theta & \sin \theta \\ -\sin \theta & \cos \theta \end{pmatrix}. \quad (1.25)$$

For relativistic neutrinos, $E_i \approx p + \frac{m_i^2}{2E}$ so that H_{eff} in (1.25) can be approximated as

$$H_{\text{eff}} = b\mathbb{I} + \begin{pmatrix} -\frac{\Delta m^2}{4E} \cos 2\theta + \sqrt{2}G_F N_e & \frac{\Delta m^2}{4E} \sin 2\theta \\ \frac{\Delta m^2}{4E} \sin 2\theta & \frac{\Delta m^2}{4E} \cos 2\theta \end{pmatrix} \quad (1.26)$$

where $b = a + p + \frac{m_1^2 + m_2^2}{4E}$. This matrix in (1.26) can be diagonalized to obtain the

splitting between the energy eigenvalues in matter as

$$E'_1 - E'_2 = \sqrt{\left(\frac{\Delta m^2}{2E} \cos 2\theta - \sqrt{2}G_F N_e\right)^2 + \left(\frac{\Delta m^2}{2E}\right)^2 \sin^2 2\theta} \quad (1.27)$$

The effective mixing angle θ_m is given by

$$\sin^2 2\theta_m = \frac{\left(\frac{\Delta m^2}{4E}\right)^2 \sin^2 2\theta}{\left(\frac{\Delta m^2}{2E} \cos 2\theta - \sqrt{2}G_F N_e\right)^2 + \left(\frac{\Delta m^2}{2E}\right)^2 \sin^2 2\theta} \quad (1.28)$$

which attains the maximum value of unity when the MSW resonance condition is satisfied i.e.

$$\sqrt{2}G_F N_e = \frac{\Delta m^2}{2E} \cos 2\theta \quad (1.29)$$

This gives $\theta_m = \pi/4$. Since the LHS of (1.29) is positive, Δm^2 is also positive with the convention $\cos 2\theta > 0$. This is the two-flavor oscillation scenario in matter. The three-flavor case can also be similarly obtained at the cost of a tedious algebra [23, 24]. The matter effect plays a crucial role for a realistic computation of oscillation probabilities.

1.3 Neutrino masses: Dirac versus Majorana

If a fermionic field ψ can be decomposed into two *independent* chiral projections ψ_L and ψ_R as

$$\psi = \psi_L + \psi_R \quad (1.30)$$

where ψ_L and ψ_R are defined as $\psi_L = P_L \psi$ and $\psi_R = P_R \psi$ with $P_{R,L} = \frac{1}{2}(1 \pm \gamma_5)$. Such a fermion is called a Dirac fermion. The Lagrangian for mass term couples the independent chiral fields ψ_L and ψ_R as

$$\mathcal{L}_{\text{mass}} = -m_D \bar{\psi} \psi = -m_D (\bar{\psi}_L \psi_R + \bar{\psi}_R \psi_L). \quad (1.31)$$

This is known as a Dirac mass term. Under particle-anti[article conjugation \hat{C} , the chiral fields transform as

$$\hat{C} : \psi_L \rightarrow (\psi_L)^C, \psi_R \rightarrow (\psi_R)^C. \quad (1.32)$$

Clearly, $\psi_L, (\psi_L)^C, \psi_R, (\psi_R)^C$ represents four independent degrees of freedom of the Dirac field. For n species of Dirac fermions, (1.31) generalizes to

$$-\mathcal{L}_{\text{mass}} = -(\bar{\psi}_L m_D^T \psi_R + \bar{\psi}_R m_D \psi_L) \quad (1.33)$$

where m_D is a $n \times n$ matrix and $\psi = (\psi_1 \ \psi_2 \ \dots \ \psi_n)^T$. Such a term in the SM manifestly breaks $SU(2)_L \times U(1)_Y$ gauge invariance but respects $U(1)_Q$.

If a fermion field admits a decomposition of the form

$$\psi = \psi_L + e^{i\theta_1}(\psi^C)_R, \quad \text{or} \quad \psi = \psi_R + e^{i\theta_2}(\psi^C)_L \quad (1.34)$$

with $e^{i\theta_{1,2}}$ being arbitrary phases, it can be easily seen that

$$\psi^C = e^{-i\theta_{1,2}}\psi \quad (1.35)$$

which implies that the particles created by ψ are their own antiparticles. These particles are called Majorana fermions. Clearly, for the fields ψ in (1.34) the left-chiral and right-chiral components are not independent, and in particular, one is the \hat{C} -conjugate of the other:

$$C : \psi_L \rightarrow (\psi_L)^C = (\psi^C)_R, \quad \psi_R \rightarrow (\psi_R)^C = (\psi^C)_L. \quad (1.36)$$

The mass term for a Majorana spinor

$$-\mathcal{L}_{\text{mass}} = \frac{1}{2}m_M[\overline{(\psi_L)^C}\psi_L + \overline{\psi_L}(\psi_L)^C] \quad (1.37)$$

Again for n species of Majorana fermions (1.37) generalizes to

$$\mathcal{L}_{\text{mass}} = -\frac{1}{2}[\overline{(\psi_L)^C}m_M\psi_L + \overline{\psi_L}m_M^T(\psi_L)^C] = -\frac{1}{2}[\psi_L^T C m_M \psi_L + \text{h.c.}] \quad (1.38)$$

where m_M is a $n \times n$ matrix and $\psi_L = \begin{pmatrix} \psi_1 & \psi_2 & \dots & \psi_n \end{pmatrix}^T$. Such a term is Lorentz invariant but violates any $U(1)$ quantum number two units. Hence, such a mass is not allowed for any charged fermion of the SM but neutrinos. In chiral basis, a Dirac field ψ can be written in terms of two two-component Weyl spinors, χ and ϕ as [25]

$$\psi = \begin{pmatrix} \chi \\ \phi \end{pmatrix} \quad (1.39)$$

so that the mass term in (1.37) becomes $-\mathcal{L}_{\text{mass}} = m\bar{\psi}\psi = m(\chi^\dagger\phi + \phi^\dagger\chi)$. For Majorana particles, ϕ is constructed out of χ as $\phi = i\sigma_2\chi^*$ so that the Majorana mass in (1.37) becomes

$$-\mathcal{L}_{\text{mass}} = \frac{1}{2}(\chi^\dagger i\sigma_2\chi^* - \chi^T i\sigma_2\chi) \quad (1.40)$$

The SM can be considered to be an effective field theory with a cut-off Λ i.e., an approximation to a high energy renormalizable theory valid for energies $E \ll \Lambda$. In such a scenario, nonrenormalizable operators of dimension $d > 4$, suppressed by a factor Λ^{4-d} , must be taken into account. The greatest contribution comes from the $d = 5$ term. With the SM Higgs ϕ and left-chiral lepton doublets l_{Li} , the unique $d = 5$ operator is given by

$$\mathcal{O}_5 = \frac{f_{ij}}{\Lambda}(l_{Li}^T C i\tau_2\tau_a l_{Lj})(\phi^T C i\tau_2\tau_a \phi) \quad (1.41)$$

which clearly leads to a Majorana neutrino mass

$$(M_{\nu_L})_{ij} = \frac{f_{ij}}{\Lambda} \frac{v^2}{2} (\nu_{Li})^C \nu_{Lj} \quad (1.42)$$

after the spontaneous breakdown of electroweak symmetry when the neutral component of ϕ acquires a vacuum expectation value (VEV) of $v/\sqrt{2}$. However, the term violates $B - L$ by two units. Since the SM conserves $B - L$ both at perturbative and nonperturbative levels such a term is not allowed. Weinberg's non-renormalizable operator might come from the renormalizable vertex (i) $\bar{l}_L \phi N_R$ as in type-I seesaw extension, or (ii) $\phi \phi \Delta$ and $l_L l_L \Delta$ in type-II seesaw extensions of the SM upon integrating out N_R or Δ as explained below.

Type-I Seesaw

This is the most basic framework of generating small Majorana neutrino masses where the SM is extended to include right-chiral electroweak singlets N_{Ri} . Since they are singlets of the SM gauge group, they cannot have interaction with gauge bosons and hence, referred to as “sterile”. Though their number need not coincide with the number of fermion generations, we shall consider in the following only three active and three sterile species. With this the most general gauge invariant Lagrangian is given by

$$-\mathcal{L} = f_{ij}^{(\nu)} \bar{l}_{Li} \tilde{\phi} N_{Rj} + \frac{1}{2} \overline{(N_{Ri})^C} (M_R)_{ij} N_{Rj} + \text{h.c.} \quad (1.43)$$

where $\tilde{\phi} = i\tau_2 \phi^*$, $f_{ij}^{(\nu)}$ are new Yukawa couplings, l_{Li} is the lepton doublet. The second term in (1.43) represents the bare $(B - L)$ violating Majorana mass term. Clearly, in this high-energy theory (1.43), the Higgs is coupled to the leptons via the exchange of the heavy fermion singlets N_{Ri} . When the neutral component of ϕ acquires a vacuum expectation value (VEV) i.e., $\langle \phi^0 \rangle = v/\sqrt{2}$, the neutrinos acquire a Dirac mass of the form $\bar{\nu}_L m_D N_R + \text{h.c.}$ where $m_D = v f^\nu / \sqrt{2}$ represents a 3×3 matrix. Suppressing

the generational indices, the Lagrangian of (1.43) can be written as

$$-\mathcal{L} = \bar{\nu}_L m_D N_R + \frac{1}{2} \overline{(N_R)^C} M_R N_R + \text{h.c.} \quad (1.44)$$

Replacing the first term by its h.c., we rewrite (1.45) as

$$-\mathcal{L} = \bar{N}_R m_D^T \nu_L + \frac{1}{2} \overline{(N_R)^C} M_R N_R + \text{h.c.} \quad (1.45)$$

Next, using the identity $\bar{\psi}_1 \psi_2 = \overline{(\psi_2)^C} \psi_1^C$, (1.45) can be written as

$$-\mathcal{L} = \frac{1}{2} \bar{N}_R m_D^T \nu_L + \frac{1}{2} \overline{(\nu_L)^C} m_D (N_R)^C + \frac{1}{2} \overline{(N_R)^C} M_R N_R + \text{h.c.} \quad (1.46)$$

In the basis $\eta_L = (\nu_L \ (N_R)^C)$ basis and with 6×6 matrix \mathcal{M} , (1.46) becomes

$$-\mathcal{L} = \frac{1}{2} \begin{pmatrix} \overline{(\nu_L)^C} & \bar{N}_R \end{pmatrix} \begin{pmatrix} 0 & m_D \\ m_D^T & M_R \end{pmatrix} \begin{pmatrix} \nu_L \\ (N_R)^C \end{pmatrix} = \frac{1}{2} \overline{(\eta_L)^C} \mathcal{M} \eta_L + \text{h.c.} \quad (1.47)$$

The matrix \mathcal{M} in (1.47) can now be block diagonalized the matrix using a 6×6 unitary matrix with 3×3 blocks given by

$$U = \begin{pmatrix} 1 & \rho \\ -\rho^\dagger & 1 \end{pmatrix} \quad (1.48)$$

where $U^\dagger U = 1 + O(\rho^\dagger \rho)$. Assuming ρ to be real, and using the diagonalization condition, $U^T \mathcal{M} U = \text{diag}(M_1, M_2)$, one obtains

$$U^T \mathcal{M} U = \begin{pmatrix} -\rho m_D^T - m_D \rho^T & m_D - \rho M_R \\ m_D^T - M_R \rho^T & m_D^T \rho + \rho^T m_D + M_R \end{pmatrix} \quad (1.49)$$

With the assumption $M_R \gg m_D$, \mathcal{M} is diagonalized with $\rho \simeq m_D M_R^{-1}$. The 3×3

mass matrices M_1 and M_2 is evaluated to be

$$M_1 \approx -m_D M_R^{-1} m_D^T; \quad M_2 \approx M_R \quad (1.50)$$

Therefore, in the diagonal basis, (1.47) can be written as

$$-\mathcal{L} = \frac{1}{2} \overline{(\eta_L)^C} \mathcal{M} \eta_L + h.c. = \frac{1}{2} \overline{(\chi_L)^C} \mathcal{M}_d \chi_L + h.c. \quad (1.51)$$

where

$$\chi_L = \begin{pmatrix} \chi_{1L} \\ \chi_{2L} \end{pmatrix} = U^\dagger \begin{pmatrix} \nu_L \\ (N_R)^C \end{pmatrix} = \begin{pmatrix} 1 & -m_D M_R^{-1} \\ m_D M_R^{-1} & 1 \end{pmatrix} \begin{pmatrix} \nu_L \\ (N_R)^C \end{pmatrix} \quad (1.52)$$

so that

$$\chi_{1L} = \nu_L - m_D M_R^{-1} (N_R)^C, \quad \chi_{2L} = m_D M_R^{-1} \nu_L + (N_R)^C. \quad (1.53)$$

If we now define $\chi_i = \chi_{iL} + (\chi_{iL})^C$ ($i = 1, 2$), (1.51) can be written as

$$\mathcal{L}_{mass} = M_1 \overline{\chi_1^C} \chi_1 + M_2 \overline{\chi_2^C} \chi_2 \quad (1.54)$$

where the mass eigenstates χ_1 and χ_2 are given by,

$$\chi_1 = (\nu_L + (\nu_L)^C) - \frac{m_D}{M_R} ((N_R)^C + N_R) = \chi_1^C, \quad (1.55)$$

$$\chi_2 = ((N_R)^C + N_R) + \frac{m_D}{M_R} (\nu_L + (\nu_L)^C) = \chi_2^C \quad (1.56)$$

which clearly are Majorana in nature. Since $m_D \sim 10^2$ GeV (EW scale), if one considers $M_R \sim 10^{15}$ GeV (GUT scale), the elements of $M_1 \sim \mathcal{O}(0.1)$. Therefore, $M_1 \simeq -m_D M_R^{-1} m_D^T$ is called the effective light Majorana neutrino mass matrix while $M_2 \simeq M_R$ is called the effective heavy Majorana neutrino mass matrix. M_1 can be diagonalized to find the light neutrino mass eigenvalues and eigenstates. Thus, N_R

setting the scale of new physics at the GUT scale makes the χ_1 states (predominantly composed of ν_L) to be light and χ_2 (predominantly composed of ν_L) to be heavy. This is the Type-I Seesaw mechanism. Since the scale of grand unified theories (GUT) (10^{15} GeV) is beyond the reach of current colliders, we will discuss a few possibilities of lowering this scale as relevant to this thesis.

Type-II Seesaw

Though the SM neutrinos of each generation contains ν_L and $(\nu_L)^C$ degrees of freedom, a bare Majorana mass of the form $\overline{(\nu_L)^C}\nu_L$ cannot be included in a gauge invariant Lagrangian. However, instead of N_{Ri} , if the SM is extended with a triplet scalar

$$\Delta = \begin{pmatrix} \Delta^+/\sqrt{2} & \Delta^{++} \\ \Delta^0 & -\Delta^+/\sqrt{2} \end{pmatrix} \sim (3, 2) \quad (1.57)$$

it leads to a gauge invariant Yukawa interaction

$$-\mathcal{L}_Y = f_{ij}^\Delta (l_{iL}^T C i\tau_2 \Delta l_{jL}) \quad (1.58)$$

with $f_{ij}^\Delta = f_{ji}^\Delta$. Since the triplet $T = l_L^T C i\tau_2 l_L$ carries a lepton number $L = 2$, if Δ is assigned a lepton number $L = -2$, the term in (1.58) is L -conserving. However, when Δ^0 acquires a VEV the global lepton number symmetry is spontaneously broken generating a L -violating neutrino Majorana mass. The resulting spectrum will contain a massless pseudoscalar Goldstone boson (J) called a Majoron [26, 27] and in the present context [28], SSB gives rise to a ‘triplet Majoron’. The triplet Majoron is now experimentally excluded [29]. The Majoron problem is eliminated by including

an explicit L -violating, trilinear term $\frac{\Lambda_6}{\sqrt{2}}\phi^T i\tau_2 \Delta^\dagger \phi + \text{h.c}$ in the potential given by

$$\begin{aligned}
 V(\phi, \Delta) &= -\mu^2 \phi^\dagger \phi + \frac{\lambda}{2} (\phi^\dagger \phi)^2 + M_\Delta^2 \text{Tr}(\Delta^\dagger \Delta) + \frac{\lambda_1}{2} [\text{Tr}(\Delta^\dagger \Delta)]^2 \\
 &+ \frac{\lambda_2}{2} ([\text{Tr}(\Delta^\dagger \Delta)]^2 - \text{Tr}[(\Delta^\dagger \Delta)^2]) + \lambda_4 (\phi^\dagger \phi) \text{Tr}(\Delta^\dagger \Delta) + \lambda_5 \phi^\dagger [\Delta^\dagger, \Delta] \phi \\
 &+ \left(\frac{\Lambda_6}{\sqrt{2}} \phi^T i\tau_2 \Delta^\dagger \phi + \text{h.c.} \right). \tag{1.59}
 \end{aligned}$$

By minimizing $V(\phi, \Delta)$ w.r.t ϕ and Δ , and with $\langle \phi^0 \rangle = v/\sqrt{2}$ and $\langle \Delta^0 \rangle = v_\Delta/\sqrt{2}$ the scalar masses are evaluated to be

$$m_\phi^2 = \frac{1}{2} \lambda v^2 - \Lambda_6 v_\Delta + \frac{1}{2} (\lambda_4 - \lambda_5) v_\Delta^2, \tag{1.60}$$

$$M_\Delta^2 = \frac{1}{2} \frac{\Lambda_6 v^2}{v_\Delta} - \frac{1}{2} (\lambda_4 - \lambda_5) v^2 - \frac{1}{2} \lambda_1 v_\Delta^2. \tag{1.61}$$

Clearly, the triplet VEV v_Δ contributes to the W and Z masses, and therefore, to the ρ parameter of the SM. Since the latter is constrained by the electroweak (EW) precision data it implies an upper limit $v_\Delta < 5$ GeV. Thus in the limit $v \gg v_\Delta$, and $M_\Delta \gg v^2$ (or $\lambda_4 = \lambda_5$), the neutrino mass matrix is given by

$$(M_\nu)_{ij} = \sqrt{2} v_\Delta (f^\Delta)_{ij} \equiv \frac{\Lambda_6 v^2}{\sqrt{2} M_\Delta^2} (f^\Delta)_{ij}. \tag{1.62}$$

Inverse and Linear Seesaw

In addition to N_{Ri} , if a different species of fermionic singlets (S_{Li}) are incorporated for each generation of the SM fermions, the relevant Lagrangian consisting of bare masses and Yukawa sectors after SSB reads

$$-\mathcal{L} = \bar{\nu}_L m_D N_R + \bar{\nu}_L M S_L^C + \bar{S}_L m N_R + \frac{1}{2} \bar{S}_L \mu_S S_L^C + \frac{1}{2} \bar{N}_R M_R N_R^C + \text{h.c.} \tag{1.63}$$

The effective mass matrix \mathcal{M} in the basis $(\nu_L^C \ N_R \ S_L^C)$ has the form

$$\mathcal{M} = \begin{pmatrix} 0 & m_D & M \\ m_D^T & M_R & m^T \\ M^T & m & \mu_S \end{pmatrix} \quad (1.64)$$

where \mathcal{M} is a 9×9 matrix. Symmetries of a model might lead to vanishing of some entries of \mathcal{M} , and might be explored [30]. For example, zeros in the diagonal entries of \mathcal{M} i.e., $M_R = \mu_S = 0$ is referred to as the standard linear seesaw mechanism while $M_R = M = 0$ is called the inverse seesaw. Setting only $M_R = 0$, \mathcal{M} can be written as

$$\mathcal{M} = \left(\begin{array}{c|cc} 0 & m_D & M \\ \hline m_D^T & 0 & m^T \\ M & m & \mu_S \end{array} \right) = \left(\begin{array}{c|cc} 0_{3 \times 3} & (\tilde{m}_D)_{3 \times 6} \\ \hline (\tilde{m}_D)^T_{6 \times 3} & (\tilde{M}_R)_{6 \times 6} \end{array} \right)$$

where

$$\tilde{m}_D = \begin{pmatrix} m_D & M \\ m_D & M \end{pmatrix}, \quad \tilde{M}_R = \begin{pmatrix} 0 & m^T \\ m & \mu_S \end{pmatrix}. \quad (1.65)$$

Now \mathcal{M} has a structure similar to that of Type-I seesaw, can be diagonalized by a unitary matrix U of the form

$$U = \begin{pmatrix} 1_{3 \times 3} & \varrho_{3 \times 6} \\ -\varrho_{6 \times 3}^\dagger & 1_{6 \times 6} \end{pmatrix} \quad (1.66)$$

with $U^\dagger U = 1 + \mathcal{O}(\varrho^2)$. Assuming the type-I seesaw hierarchy, the effective light

neutrino mass matrix M_ν turns out to be

$$M_\nu \simeq m_D m^{-1} \mu_S (m_D m^{-1})^T - M(m^{-1} m_D^T) - [M(m^{-1} m_D^T)]^T. \quad (1.67)$$

With $\mu_S = 0$, the linear seesaw formula comes out to be

$$M_\nu^{\text{Linear}} \simeq -M(m^{-1} m_D^T) - [M(m^{-1} m_D^T)]^T \quad (1.68)$$

and with $M = 0$, the inverse seesaw formula becomes

$$M_\nu^{\text{Inverse}} \simeq m_D m^{-1} \mu_S (m_D m^{-1})^T. \quad (1.69)$$

Note that in the limit $\mu \rightarrow 0$, lepton number conservation which is an accidental symmetry of the SM, is restored. Though m_D is again fixed at the EW scale i.e., $m_D \sim 10^2$ GeV, there are two more scales to play with. Assuming the scale of new physics $M_{RS} \sim 10$ TeV and the lepton number breaking mass $\mu \sim 1$ KeV one can generate neutrino mass $\mathcal{O}(\text{eV})$. Interesting point in this variant of seesaw is that only $\mathcal{O}(\text{TeV})$ heavy neutrinos are now required to realize the light neutrino masses. Since the seesaw scale is lowered from the GUT scale to TeV scale, inverse seesaw bears testability in collider experiments.

Radiative neutrino masses Naturally small neutrino masses can be generated radiatively at some n -loop level with loop suppression factor $\frac{1}{(16\pi^2)^n}$. This allows the scale of new physics to be much lower than the canonical seesaw scale which makes them testable at collider experiments.

Zee model

The Zee model [31] is an extension of the SM with a singly charged singlet

Higgs h^- and a scalar doublet ϕ' in addition to the SM Higgs doublet ϕ . While both ϕ and ϕ' , can in principle, couple to the lepton doublets l_{iL} , such a scenario leads to the flavor changing neutral current (FCNC) processes mediated by Higgs. To avoid FCNC, a variant of the Zee model was proposed by Wolfenstein [32] where only ϕ couples to l_{iL} . The relevant part of the Lagrangian has the form

$$-\mathcal{L}_Y^{(1)} = y_{ij}\bar{l}_{iL}\phi e_{jR} + \mu\phi^T i\tau_2\phi' h^- + f_{ij}\bar{l}_{iL}i\tau_2 l_{jL}^C h^- + \text{h.c.} \quad (1.70)$$

The second and third term taken together violate the lepton number by 2 units, and predicts lepton flavor violating (LFV) decays e.g., $h \rightarrow e_i\nu_j$, $e_i \rightarrow e_j\gamma$, $Z \rightarrow e_i e_j$ etc. Although the neutrino mass is forbidden at the tree-level it can be induced radiatively through one-loop (cf. Fig.1.1) and can potentially account for its smallness. Though

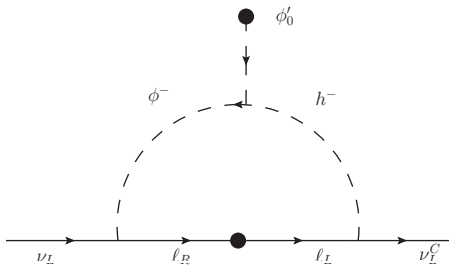


Figure 1.1: Neutrino mass generation at one-loop in the Zee-Wolfenstein model. The flavor indices have been suppressed for simplicity.

the current experimental data rules out the primitive version of this model at 3σ , several variants have been proposed to accommodate the oscillation data.

Ma model

This model [33] incorporates three singlet right-chiral fields N_{Ri} and one inert scalar doublet $\eta = \begin{pmatrix} \eta^+ & \eta^0 \end{pmatrix}^T$ with vanishing VEV to generate tiny neutrino masses at one loop (c.f. Fig.1.2). An additional \mathbb{Z}_2 symmetry is imposed in addition to the $SU(2)_L \times U(1)_Y$ invariance of the SM under which the newly added fields transform

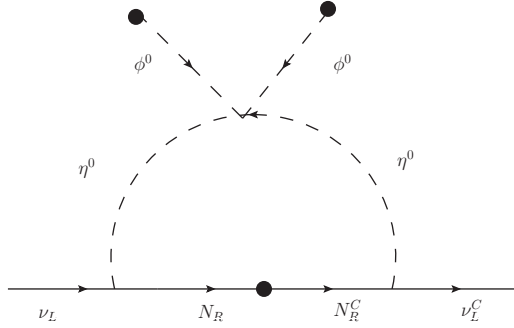


Figure 1.2: One-loop diagram for light neutrino mass generation in the Ma model.

as $N_{Ri} \rightarrow -N_{Ri}$ and $\eta \rightarrow -\eta$ while the SM fields are \mathbb{Z}_2 -even. Therefore, the Yukawa coupling of N_{Ri} with the SM Higgs ϕ and l_{Li} is forbidden while a similar interaction with η , given by

$$h_{ij} \overline{l_{Li}} \eta N_{Rj}, \quad (1.71)$$

is allowed. On integrating out the heavy N_{Ri} fields, a dimension-5 Weinberg operator is induced at one loop which after electroweak symmetry breaking, when ϕ^0 acquires a VEV v , gives rise to a neutrino Majorana mass $\mathcal{M}_\nu \overline{(\nu_L^C)} \nu_L$ with

$$(\mathcal{M}_\nu)_{ij} = \frac{\lambda_5 v^2}{8\pi^2} \sum_k \frac{h_{ik} h_{jk} M_k}{m_0^2 - M_k^2} \left[1 - \frac{M_k^2}{m_0^2 - M_k^2} \ln \frac{m_0^2}{M_k^2} \right] \quad (1.72)$$

where m_0 represents the mass of η^0 , and M_i is the Majorana mass for N_{Ri} . The appropriate scalar potential invariant under these symmetries is given by

$$\begin{aligned} V_{\text{scalar}}(\phi, \eta) &= m_1^2 \phi^\dagger \phi + m_2^2 \eta^\dagger \eta + \frac{1}{2} \lambda_1 (\phi^\dagger \phi)^2 + \frac{1}{2} \lambda_2 (\eta^\dagger \eta)^2 \\ &+ \lambda_3 (\phi^\dagger \phi) (\eta^\dagger \eta) + \lambda_4 (\phi^\dagger \eta) (\eta^\dagger \phi) + \frac{1}{2} \lambda_5 [(\phi^\dagger \eta)^2 + \text{h.c.}] \end{aligned} \quad (1.73)$$

where the \mathbb{Z}_2 symmetry together with the vanishing VEV of η ensures that there be no term in (1.73) linear in η preventing its decay. However, depending on the mass, the interaction (1.71) may contribute to the decay of the heavier particle between

N_{Ri} and η while the lighter one can be a potential candidate for the DM which is an appealing feature of this model.

As an endnote, we emphasize that the entire thesis is based only on the consideration of Type-I, the inverse and linear seesaw mechanisms. However, we have also proposed low-energy symmetries of the neutrino Majorana mass matrix without addressing their high-energy realizations, and in building explicit models mechanisms such as the Type-II seesaw or radiative mass generation might play a crucial role. Other scenarios of light neutrino mass generation include double seesaw [30], Type-III seesaw [34], Left-Right symmetric model [35,36], GUT models such as $SU(5)$ [37] and $SO(10)$ [38,39], supersymmetric models [40] etc, which however, are beyond the scope of this thesis.

1.4 Ultra High Energy (UHE) cosmic neutrinos

The recent discovery [41–45] of Ultra High Energy (UHE) neutrino events at IceCube has unfolded a brand new era in neutrino astronomy. Including track plus shower, the IceCube collaboration reported 82 High-Energy Starting Events (HESE) which constitute more than 7σ excess over the atmospheric background [46]. Moreover, no significant spatial clustering has been observed and the data appears to be consistent with isotropic neutrino flux from uniformly distributed point sources [46] and suggests extragalactic origin of the observed events. Though the aforementioned HESE events are not consistent with the standard astrophysical one component unbroken isotropic power-law spectrum $\Phi(E_\nu) \propto E_\nu^{-2}$ and also suffer constraints from multi-messenger gamma-ray observation [47], two component explanation of the observed neutrino flux from pure astrophysical sources is still a plausible scenario [48]. Since in Chapters 3 and 5, we discuss the predictions of our models based on the flavor

flux ratios, statements on which could be made from enhanced statistics at neutrino telescopes (e.g., IceCube) and fits [48], we lay out a short summary of the subject as a necessary prerequisite.

The dominant source of UHE cosmic neutrinos are pp (hadro-nuclear) collisions in cosmic ray reservoirs such as galaxy clusters and $p\gamma$ (photo-hadronic) collisions in cosmic ray accelerators [49, 50] such as gamma-ray bursts, active galactic nuclei and blazars. In pp collisions, protons of TeV–PeV range produce neutrinos via the decays $\pi^+ \rightarrow \mu^+\nu_\mu$, $\pi^- \rightarrow \mu^-\bar{\nu}_\mu$, $\mu^+ \rightarrow e^+\nu_e\bar{\nu}_\mu$ and $\mu^- \rightarrow e^-\bar{\nu}_e\nu_\mu$. Therefore, the normalized flux distributions over flavor are [51]

$$\{\phi_{\nu_e}^S, \phi_{\bar{\nu}_e}^S, \phi_{\nu_\mu}^S, \phi_{\bar{\nu}_\mu}^S, \phi_{\nu_\tau}^S, \phi_{\bar{\nu}_\tau}^S\} = \phi_0 \left\{ \frac{1}{6}, \frac{1}{6}, \frac{1}{3}, \frac{1}{3}, 0, 0 \right\}, \quad (1.74)$$

where the superscript S denotes ‘source’. On the other hand, the $p\gamma$ collisions involve relatively less energetic γ -rays (GeV- 10^2 GeV range). Therefore, the center-of-mass energy of γp system is such that it can only produce $\gamma p \rightarrow \Delta^+ \rightarrow \pi^+ n$, which in turn give rise to the decays $\pi^+ \rightarrow \mu^+\nu_\mu$ and $\mu^+ \rightarrow e^+\nu_e\bar{\nu}_\mu$. The corresponding normalized flux distributions over flavor

$$\{\phi_{\nu_e}^S, \phi_{\bar{\nu}_e}^S, \phi_{\nu_\mu}^S, \phi_{\bar{\nu}_\mu}^S, \phi_{\nu_\tau}^S, \phi_{\bar{\nu}_\tau}^S\} = \phi_0 \left\{ \frac{1}{3}, 0, \frac{1}{3}, \frac{1}{3}, 0, 0 \right\}. \quad (1.75)$$

In either case, if we take $\phi_l^S = \phi_{\nu_l}^S + \phi_{\bar{\nu}_l}^S$ with $l = e, \mu, \tau$,

$$\{\phi_e^S, \phi_\mu^S, \phi_\tau^S\} = \phi_0 \left\{ \frac{1}{3}, \frac{2}{3}, 0 \right\}. \quad (1.76)$$

As neutrino oscillations will change flavor distributions from a source (S) to the

telescope (T) [52] the flux reaching the T will be given by

$$\phi_l^T = \phi_{\nu_l}^T + \phi_{\bar{\nu}_l}^T = \sum_m \left[\phi_{\nu_m}^S P(\nu_m \rightarrow \nu_l) + \phi_{\bar{\nu}_m}^S P(\bar{\nu}_m \rightarrow \bar{\nu}_l) \right]. \quad (1.77)$$

Since the distance from S to T is much larger than the oscillation length, the oscillation probability averaged over many oscillations is given by

$$P(\nu_m \rightarrow \nu_l) = P(\bar{\nu}_m \rightarrow \bar{\nu}_l) \approx \sum_i |U_{li}|^2 |U_{mi}|^2. \quad (1.78)$$

Thus the flux reaching the telescope is given by

$$\phi_l^T = \sum_i \sum_m \phi_m^S |U_{li}|^2 |U_{mi}|^2 = \frac{\phi_0}{3} \sum_i |U_{li}|^2 (|U_{ei}|^2 + 2|U_{\mu i}|^2) \quad (1.79)$$

where ϕ_0 is the overall flux normalization. The unitarity of the PMNS matrix implies

$$\phi_l^T = \frac{\phi_0}{3} \left[1 + \sum_i |U_{li}|^2 (|U_{\mu i}|^2 - |U_{\tau i}|^2) \right] = \frac{\phi_0}{3} \left[1 + \sum_i |U_{li}|^2 \Delta_i \right]. \quad (1.80)$$

where $\Delta_i = |U_{\mu i}|^2 - |U_{\tau i}|^2$. Therefore, the existence of exact $\mu\tau$ symmetry or antisymmetry, dictates that $\Delta_i = 0$, and $\phi_e^T = \phi_\mu^T = \phi_\tau^T$. We work out the predictions on these UHE neutrino flavor flux ratios in relation to deviations from $\mu\tau$ symmetry in Chapter 3 and Chapter 5.

1.5 Baryogenesis via Leptogenesis

Cosmological observations reveal that the Universe has an overwhelming dominance of matter over antimatter. There is no evidence of primordial antimatter except those arising from the collision of cosmic ray particles with the interstellar medium. The observed baryon asymmetry of the Universe can be expressed in two

equivalent ways [53]

$$\begin{aligned}\eta_B &= \frac{n_B - n_{\bar{B}}}{n_\gamma}|_0 = (5.94 \pm 6.17) \times 10^{-10}, \\ Y_B &= \frac{n_B - n_{\bar{B}}}{s}|_0 = (8.43 - 8.76) \times 10^{-11}\end{aligned}\quad (1.81)$$

where $(n_{\bar{B}})n_B$, n_γ are the number densities of the (anti)baryons and photons respectively. The subscript ‘0’ indicates that the values quoted in (1.81) are for the present epoch, and has been obtained from precise measurements of the angular distribution of the temperature anisotropies of the cosmic microwave background (CMB). Unless the Universe is unnaturally fine-tuned, the baryon symmetry must have been generated dynamically, known as the phenomenon of baryogenesis [54–56].

In 1967, Sakharov pointed out that particle physics interactions can dynamically generate a baryon asymmetry starting from a baryon-symmetric Universe if three necessary conditions are satisfied [57]. These are (i) *Baryon number (B) violation*, (ii) *C and CP violation* and (iii) *Departure from equilibrium*. Baryon number conservation is an *accidental* global symmetry of the SM and (i) can be satisfied once we go beyond the SM. One example would be the inclusion of *Majorana mass term* that explicitly breaks the lepton number conservation. There are other ways of including Baryon non-conserving interactions. If (ii) is not satisfied, any excess amount of baryon generated in a B-number violating process will be compensated by the generation of an equal amount of antibaryons in the conjugated process occurring at the same rate. Finally, in equilibrium, the thermal average of the baryon number is given by

$$\langle B \rangle = \text{Tr}(Be^{-\beta H}) = \text{Tr}(O^{-1}Oe^{-\beta H}B) = \text{Tr}(Be^{-\beta H}) = \text{Tr}(O^{-1}BOe^{-\beta H}B) \quad (1.82)$$

with $O = CPT$ and $[H, O] = 0$ assuming a CPT invariant quantum field theory. Since

the baryon number operator B is invariant (even) under parity and time reversal but odd under charge conjugation, $O^{-1}BO = -B$. This immediately gives $\langle B \rangle = 0$ implying that unless (iii) is satisfied there can be no baryon asymmetry. Though, in principle, the SM has all the necessary ingredients required for baryogenesis a substantial body of works suggest that the amount of CP violation provided by the CKM phase is not enough to generate Y_B in the observed range. Various mechanisms for baryogenesis, namely, GUT baryogenesis [58–60], Electroweak Baryogenesis [61, 62], the Affleck-Dine mechanism [63, 64] etc are popular in the literature. However, in this thesis, we exclusively focus on the mechanism of baryogenesis via leptogenesis [65–69] due to its immediate connection to the neutrino physics, especially with the Type-I seesaw scenario. The newly introduced heavy Majorana neutrinos decay out of equilibrium via a lepton number and CP violating process. The produced lepton number is then converted to baryon number by the nonperturbative sphalerons [70]. Before the construction of an explicit theoretical framework let's first construct a general setup that acts as a prerequisite.

1.5.1 Baryogenesis via leptogenesis in Type-I seesaw

In this mechanism, a dynamically generated lepton asymmetry is converted into a baryon asymmetry via sphaleron transitions. In this thesis, we shall confine our discussion to type-I seesaw leptogenesis. In this framework, the complex Yukawa couplings of the RH neutrinos and the lepton doublets offer the required CP asymmetry via the out-of-equilibrium decay of heavy Majorana neutrinos. In the first step one has to compute the CP asymmetry parameter which depends upon the flavor structure of the Dirac mass matrix and hence, upon the model under consideration. Depending upon the temperature scale of leptogenesis, the CP asymmetries can be flavor dependent or independent. Finally, the CP asymmetries can be used to work

out the lepton asymmetry either by numerically solving the network of Boltzmann equations or using the appropriate approximate solution.

Evaluation of CP asymmetry parameter

The pertinent Lagrangian for the generation of CP asymmetry in type-I seesaw is

$$-\mathcal{L}_D = \lambda_{i\alpha} \bar{N}_{Ri} \tilde{\phi}^\dagger l_{L\alpha} + \frac{1}{2} \bar{N}_{iR} (M_R)_i \delta_{ij} N_{Rj} + \text{h.c.}, \quad (1.83)$$

where $l_{L\alpha} = (\nu_{L\alpha} \ e_{L\alpha})^T$ is the left-chiral SM lepton doublet of flavor α and $\tilde{\phi} = i\tau_2 \phi^*$ with $\phi = (\phi^+ \ \phi^0)^T$ being the Higgs doublet. It is clear from (1.83) that the possible decays of N_i are $N_i \rightarrow e_\alpha^- \phi^+$, $N_i \rightarrow \nu_\alpha \phi^0$, $N_i \rightarrow e_\alpha^+ \phi^-$ and $N_i \rightarrow \nu_\alpha^C \phi^{0*}$. We are interested in the flavor-dependent CP asymmetry parameter defined as

$$\epsilon_i^\alpha = \frac{\Gamma(N_i \rightarrow e_\alpha^- \phi^+, \nu_\alpha \phi^0) - \Gamma(N_i \rightarrow e_\alpha^+ \phi^-, \nu_\alpha^C \phi^{0*})}{\Gamma(N_i \rightarrow e_\alpha^- \phi^+, \nu_\alpha \phi^0) + \Gamma(N_i \rightarrow e_\alpha^+ \phi^-, \nu_\alpha^C \phi^{0*})} \quad (1.84)$$

where Γ denotes the decay width. The partial widths of N_i -decay in a process and its conjugate are identical leading to a vanishing ϵ_i^α . However, a nonzero value of ϵ_i^α arises from the interference between the tree level, one loop self-energy and one-loop vertex diagrams for N_i -decay. For leptogenesis with hierarchical heavy RH neutrinos, (1.84) can be evaluated to be

$$\epsilon_i^\alpha = \frac{1}{4\pi v^2 h_{ii}} \sum_{j \neq i} \left[g(x_{ij}) \text{Im}[h_{ij}(m_D)_{i\alpha} (m_D^*)_{j\alpha}] + \frac{\text{Im}[h_{ji}(m_D)_{i\alpha} (m_D^*)_{j\alpha}]}{(1-x_{ij})} \right] \quad (1.85)$$

where $m_D = v\lambda/\sqrt{2}$, $v = \sqrt{2}\langle\phi^0\rangle$ $h = m_D m_D^\dagger$ and $x_{ij} = M_j^2/M_i^2$. Furthermore, the loop function $g(x_{ij})$ has the expression

$$g(x_{ij}) = \frac{\sqrt{x_{ij}}}{1-x_{ij}} + f(x_{ij}) \quad (1.86)$$

where the first term on the RHS of (1.86) arises from the interference of one loop self-energy term with the tree-level diagram while the second term $f(x_{ij})$ given by

$$f(x_{ij}) = \sqrt{x_{ij}} \left[1 - (1 + x_{ij}) \ln \left(\frac{1 + x_{ij}}{x_{ij}} \right) \right] \quad (1.87)$$

originates from the interference between one loop vertex diagram with the tree-level [65]. The formalism for a quasi-degenerate RH neutrino mass is given in Ref. [71].

Depending upon the temperature regime in which leptogenesis takes place, the lepton flavors may be fully distinguishable, partly distinguishable or indistinguishable. In a hierarchical scenario, e.g., $M_3 \gg M_2 \gg M_1$, it has been shown in Ref. [72] that only the decays of N_1 matter for the creation of lepton asymmetry while the latter created from the heavier neutrinos get washed out. Obviously there are certain circumstances when the decays of $N_{2,3}$ are also significant [73]. With the reasonable assumption that the leptogenesis takes place at a scale $T \sim M_1$, the rates of the Yukawa interaction classify leptogenesis into three categories. (i) $M_1 > 10^{12}$ GeV, when all interactions with all flavors are out of equilibrium: unflavored leptogenesis. In this case all three flavors are indistinguishable and thus the total CP asymmetry is a sum over all flavors, i.e., $\epsilon_i = \sum_{\alpha} \epsilon_i^{\alpha}$, (ii) 10^9 GeV $< M_1 < 10^{12}$ GeV, when only the τ flavor is in equilibrium so that only τ flavor can be identified separately while e and μ acts indistinguishably: τ -flavored leptogenesis. In this regime there are two relevant CP asymmetry parameters $\epsilon_i^{(2)} = \epsilon_i^e + \epsilon_i^{\mu}$ and ϵ_i^{τ} , and (iii) $M_1 < 10^9$ GeV, when all the flavors (e, μ, τ) are in equilibrium and distinguishable: fully flavored leptogenesis. One requires three CP asymmetry parameters $\epsilon_i^e, \epsilon_i^{\mu}, \epsilon_i^{\tau}$ for each generation of RH neutrinos i . Let us mention that for the unflavored case the flavor-summed CP asymmetry parameter admits a simpler expression. Summing over all flavors α ,

$$\sum_{\alpha} \text{Im} h_{ji} (m_D)_{i\alpha} (m_D^*)_{j\alpha} = \text{Im} h_{ji} h_{ji}^* = \text{Im} |h_{ji}|^2 = 0, \quad (1.88)$$

i.e., the second term in (1.85) vanishes to gives

$$\epsilon_i = \sum_{\alpha} \epsilon_i^{\alpha} = \frac{1}{4\pi v^2 h_{ii}} \sum_{j \neq i} \left[f(x_{ij} + \frac{\sqrt{x_{ij}}}{(1-x_{ij})}) \right] \text{Im} h_{ij}^2. \quad (1.89)$$

Now we turn our attention to the Boltzmann equations that govern the evolution of the number densities of the hierarchical heavy neutrinos N_i and the left-chiral lepton doublets $l_{L\alpha}$. They involve decays $N_i \rightarrow l_{L\alpha} \phi$ and $N_i \rightarrow l_{L\alpha}^C \phi^\dagger$ as well as the scattering transitions $qu^C \leftrightarrow N_i l_{L\alpha}, l_{L\alpha} q^C \leftrightarrow N_i u^C, l_{L\alpha} u \leftrightarrow N_i q, l_{L\alpha} \phi \leftrightarrow N_i V_\mu, \phi^\dagger V_\mu \leftrightarrow N_i l_{L\alpha}$ and $l_{L\alpha} V_\mu \leftrightarrow N_i \phi^\dagger$. Here q denotes the left-chiral quark doublet given by $q = (u_L \ d_L)^T$ and V_μ stands for either B_μ or W_μ^a ($a = 1, 2, 3$). Next, we introduce a new parameter η_a defined as $\eta_a(z) = n_a(z)/n_\gamma(z)$ where $z = M_1/T$, n_γ is the number density of photons given by

$$n_\gamma(z) = \frac{2T^3}{\pi^2} = \frac{2M_1^3}{\pi^2 z^3} \quad (1.90)$$

and n_a is the number density of a particle of species a given by

$$n_a(T) = \frac{g_a m_a^2 T e^{\mu_a(T)/T}}{2\pi^2} K_2\left(\frac{m_a}{T}\right). \quad (1.91)$$

Here, m_a and g_a respectively denote the particle's mass and the number of internal degrees of freedom. K_2 is the modified Bessel function of the second kind of order 2. In thermal equilibrium, the quantities η_a and n_a are denoted by η_a^{eq} and n_a^{eq} where the latter is given by setting the chemical potential $\mu_a(T)$ equal to zero, i.e.,

$$n_a^{eq}(T) = \frac{g_a m_a^2 T}{2\pi^2} K_2\left(\frac{m_a}{T}\right). \quad (1.92)$$

Now one can use the Boltzmann equations given in Ref. [74] and generalized with flavor [71]. Since the active flavor in the temperature regime under consideration may not correspond to the actual lepton flavors (e, μ or τ) but some combination, a

general flavor index λ has been used for the lepton asymmetry. This enables us to write

$$\begin{aligned}
 \frac{d\eta_{N_i}}{dz} &= \frac{z}{H(z=1)} \left[\left(1 - \frac{\eta_{N_i}}{\eta_{N_i}^{\text{eq}}}\right) \sum_{\beta=e,\mu,\tau} \left(\Gamma^{\beta Di} + \Gamma_{\text{Yukawa}}^{\beta Si} + \Gamma_{\text{Gauge}}^{\beta Si} \right) \right. \\
 &\quad \left. - \frac{1}{4} \sum_{\beta=e,\mu,\tau} \eta_L^\beta \varepsilon_i^\beta \left(\Gamma^{\beta Di} + \tilde{\Gamma}_{\text{Yukawa}}^{\beta Si} + \tilde{\Gamma}_{\text{Gauge}}^{\beta Si} \right) \right], \\
 \frac{d\eta_L^\lambda}{dz} &= -\frac{z}{H(z=1)} \left[\sum_{i=1}^3 \varepsilon_i^\lambda \left(1 - \frac{\eta_{N_i}}{\eta_{N_i}^{\text{eq}}}\right) \sum_{\beta=e,\mu,\tau} \left(\Gamma^{\beta Di} + \Gamma_{\text{Yukawa}}^{\beta Si} + \Gamma_{\text{Gauge}}^{\beta Si} \right) \right. \\
 &\quad \left. + \frac{1}{4} \eta_L^\lambda \left\{ \sum_{i=1}^3 \left(\Gamma^{\lambda Di} + \Gamma_{\text{Yukawa}}^{\lambda Wi} + \Gamma_{\text{Gauge}}^{\lambda Wi} \right) + \Gamma_{\text{Yukawa}}^{\lambda \Delta L=2} \right\} \right]. \tag{1.93}
 \end{aligned}$$

The expressions for the various transition widths Γ in (1.93) are given in Ref. [74].

Consider the first equation in (1.93) to start with. Its second RHS term has been neglected for an assumed hierarchical leptogenesis since both η_L^β and ε_i^β are each quite small and their product much smaller². Using some shorthand notation, as explained in Eqs. (1.95) - (1.97) below, we can now write

$$\frac{dY_{N_i}(z)}{dz} = \{D_i(z) + D_i^{\text{SY}}(z) + D_i^{\text{SG}}(z)\} \{Y_{N_i}^{\text{eq}}(z) - Y_{N_i}(z)\}, \tag{1.94}$$

where

$$D_i(z) = \sum_{\beta=e,\mu,\tau} D_i^\beta(z) = \sum_{\beta=e,\mu,\tau} \frac{z}{H(z=1)} \frac{\Gamma^{\beta Di}}{\eta_{N_i}^{\text{eq}}(z)}, \tag{1.95}$$

$$D_i^{\text{SY}}(z) = \sum_{\beta=e,\mu,\tau} \frac{z}{H(z=1)} \frac{\Gamma_{\text{Yukawa}}^{\beta Si}}{\eta_{N_i}^{\text{eq}}(z)}, \tag{1.96}$$

$$D_i^{\text{SG}}(z) = \sum_{\beta=e,\mu,\tau} \frac{z}{H(z=1)} \frac{\Gamma_{\text{Gauge}}^{\beta Si}}{\eta_{N_i}^{\text{eq}}(z)}. \tag{1.97}$$

Turning to the second equation in (1.93) and neglecting the $\Delta L = 2$ scattering terms,

²In order of magnitude this product is $10^{-6} \times 10^{-5} \sim 10^{-11}$, as compared with the first term which is $\mathcal{O}(1)$.

we rewrite it as

$$\begin{aligned} \frac{d\eta_L^\lambda(z)}{dz} = & - \sum_{i=1}^3 \varepsilon_i^\lambda \{D_i(z) + D_i^{\text{SY}}(z) + D_i^{\text{SG}}(z)\} (\eta_{N_i}^{\text{eq}}(z) - \eta_{N_i}(z)) \\ & - \frac{1}{4} \eta_L^\lambda \sum_{i=1}^3 \left\{ \frac{1}{2} D_i^\lambda(z) z^2 K_2(z) + D_i^{\lambda\text{YW}}(z) + D_i^{\lambda\text{GW}}(z) \right\} \end{aligned} \quad (1.98)$$

with

$$D_i^{\text{YW}}(z) = \sum_{\beta=e,\mu,\tau} \frac{z}{H(z=1)} \Gamma_{\text{Yukawa}}^{\beta W i}, \quad (1.99)$$

$$D_i^{\text{GW}}(z) = \sum_{\beta=e,\mu,\tau} \frac{z}{H(z=1)} \Gamma_{\text{Gauge}}^{\beta W i}. \quad (1.100)$$

Lepton asymmetry to Baryon asymmetry

Having discussed the ways of generating a lepton asymmetry and its evolution, we turn our attention to the mechanism of converting that lepton asymmetry into a baryon asymmetry. In the SM, B and L are conserved at the classical level due to two accidental global symmetries, namely, $U(1)_B$ and $U(1)_L$. However, both symmetries are violated at the quantum level due to ABJ or chiral anomaly [75] i.e., the divergences of the associated Noether currents do not vanish. In particular,

$$\partial_\mu J_B^\mu = \partial_\mu J_L^\mu = \frac{n_f}{32\pi^2} (g^2 W_{\mu\nu}^a \tilde{W}^{a\mu\nu} - g'^2 B_{\mu\nu} B^{\mu\nu}), \quad (1.101)$$

where $J_B^\mu = \frac{1}{3} \sum (\bar{q}_L \gamma^\mu q_L + \bar{u}_R \gamma^\mu u_R + \bar{d}_R \gamma^\mu d_R)$, $J_L^\mu = \frac{1}{3} \sum (\bar{l}_L \gamma^\mu l_L + \bar{e}_R \gamma^\mu e_R)$ with the summation over all families and colors (for quarks). Here, $W_{\mu\nu}^a$ and $B_{\mu\nu}$ respectively denote the $SU(2)$ and $U(1)$ gauge field strengths of SM. g, g' are the gauge coupling constants and n_f represents the number of fermion generations. Since $B = \int J_B^0 d^3x$ and $L = \int J_L^0 d^3x$, Eq.(1.101) clearly shows that $(B - L)$ is conserved while $(B + L)$ is violated nonperturbatively due to instanton effects [76]. The violation arises due

to the nontrivial vacuum structure of the non-abelian gauge theories and given by

$$\Delta(B + L) = 2n_f N_{CS} \quad (1.102)$$

where $N_{CS} = \frac{g^2}{32\pi^2} W_{\mu\nu}^a \tilde{W}^{a\mu\nu}$ is called the winding number or Chern-Simons number. There are infinitely many degenerate vacua characterized by the winding number $n = \pm 1, \pm 2, \dots$ etc and two such consecutive vacua are separated by energy barriers. These vacua are connected by nonperturbative gauge field configurations, called instantons and mediate tunneling between the vacua. This gives rise to an effective operator at the leading order

$$\mathcal{O}_{B+L} = \prod_i (q_{Li} q_{Li} q_{Li} l_{Li}). \quad (1.103)$$

At zero temperature the tunneling rate [77, 78]

$$\Gamma(T = 0) \approx e^{-2S_E} = e^{-8\pi/g^2} = 10^{-170} \quad (1.104)$$

and hence, too heavily suppressed to consider. However, in a thermal bath, the transition between different vacua is dominantly controlled by hopping over the energy barrier [79] induced by *sphalerons* [80]. For temperatures below that of the EW phase transition the transition rate [81] is given by

$$\frac{\Gamma_{B+L}}{V} \sim e^{-\frac{M_W}{\alpha k T}}, \quad (1.105)$$

which, once again, is very small. However, for temperatures above that of the EW phase transition, the rate [77, 78] becomes

$$\frac{\Gamma_{B+L}}{V} \sim \alpha^5 \ln \alpha^{-1} T^4. \quad (1.106)$$

Thus, the baryon number violating processes are not suppressed in the $T > T_{EW}$

phase and give rise to the required baryon asymmetry of the universe.

Chemical equilibrium relations

At temperatures much higher than the weak scale, the scale of leptogenesis, the leptons, quarks and Higgs interact and scatter via SM Yukawa interactions and sphaleron transitions. If all such processes were assumed to be in chemical equilibrium it gives rise to various relations between the chemical potentials. Under the assumption that $\beta\mu_\psi \ll 1$, the difference between the number density of a particle ψ (q, l, ϕ etc) and its antiparticle $\bar{\psi}$ in an assembly of noninteracting massless particles is [67]

$$\begin{aligned} n_\psi - n_{\bar{\psi}} &= \frac{g_\psi T^3}{6} \beta\mu_\psi \quad \text{for fermions,} \\ n_\psi - n_{\bar{\psi}} &= \frac{g_\psi T^3}{3} \beta\mu_\psi \quad \text{for bosons.} \end{aligned} \quad (1.107)$$

As explained earlier, the $SU(2)$ electroweak sphaleron transitions give rise to an effective operator $\prod_i q_{Li} q_{Li} q_{Li} l_{Li}$ where q_{Li} (l_{Li}) represents the left-chiral quark (lepton) doublet. This gives rise to a constraint [67]

$$\sum_i (3\mu_{q_i} + \mu_{l_i}) = 0 \quad (1.108)$$

where the sum is over all generations. Similarly, QCD instantons will induce an effective operator $\prod_i q_{Li} q_{Li} u_{Ri}^C d_{Ri}^C$ where u_{Ri}^C (d_{Ri}^C) represents the right-chiral up-type (down-type) quark singlet. The corresponding constraint on the chemical potential is

$$\sum_i (2\mu_{q_i} - \mu_{u_i} - \mu_{d_i}) = 0. \quad (1.109)$$

Irrespective of the temperature regime, there exists a robust constraint due to

hypercharge neutrality of the plasma

$$\sum_i N(\mu_{q_i} + 2\mu_{u_i} - \mu_{d_i} - \mu_{l_i} - \mu_{e_i}) + 2N_\phi\mu_\phi = 0. \quad (1.110)$$

The Yukawa interactions give rise to the following conditions:

$$\mu_{q_i} - \mu_\phi - \mu_{d_i} = 0, \quad \mu_{q_i} + \mu_\phi - \mu_{u_i} = 0, \quad \mu_{l_i} - \mu_\phi - \mu_{e_i} = 0. \quad (1.111)$$

Finally, the $\Delta L = 2$ interactions give rise to

$$\mu_{l_i} + \mu_\phi = 0. \quad (1.112)$$

Using (1.107), the baryon and lepton number densities can be expressed as

$$\begin{aligned} n_L - n_{\bar{L}} &= \mu_L T^2/6, \quad \text{where } \mu_L = \sum_i (2\mu_{l_i} + \mu_{e_i}), \\ n_B - n_{\bar{B}} &= \mu_B T^2/6, \quad \text{where } \mu_B = \sum_i (2\mu_{q_i} + \mu_{u_i} + \mu_{d_i}). \end{aligned} \quad (1.113)$$

Solving the chemical potential relations one obtains [82, 83]

$$\begin{aligned} Y_B &= \frac{n_B - n_{\bar{B}}}{s} = \frac{8N + 4m}{22N + 13N_\phi} Y_\Delta = C Y_\Delta, \\ Y_L &= \frac{n_L - n_{\bar{L}}}{s} = -\frac{14N + 9m}{22N + 13N_\phi} Y_\Delta = (C - 1) Y_\Delta. \end{aligned} \quad (1.114)$$

where N_ϕ is the number of Higgs doublets and N is the number of fermion generations, and $Y_\Delta = Y_{B-L} = Y_B - Y_L$. With $N_\phi = 1$, and $N = 3$, one obtains $C = 28/79$. One important thing to mention is that if the temperature scale of leptogenesis is below 10^9 GeV, all the lepton flavors are separately identifiable. In that case, the conserved quantity in sphaleronic transition is $\Delta_\lambda = B/3 - L_\lambda$ a linear relation holds between

them. For convenience, we define a new variable

$$Y_\lambda = \frac{n_L^\lambda - n_{\bar{L}}^\lambda}{s} = \frac{\eta_\gamma}{s} \eta_L^\lambda, \quad (1.115)$$

where $n_L^\lambda(n_{\bar{L}}^\lambda)$ is the number density of (anti)leptons of the active flavor λ normalized to the entropy density. The factor s/η_γ is known to equal $1.8g_{*s}$ with g_{*s} being the number of effective relativistic degrees of freedom. For $T > 10^2$ GeV, g_{*s} remains nearly constant with temperature at a value of about 112 [84] with three right chiral neutrinos. Sphaleron transitions convert the lepton asymmetry created by the decay of the right chiral heavy neutrinos into a baryon asymmetry by keeping $\Delta_\lambda = \frac{1}{3}B - L^\lambda$ conserved. Y_{Δ_λ} , defined as $s^{-1}\{1/3(n_B - n_{\bar{B}}) - (n_L - n_{\bar{L}})\}$, and Y_λ are linearly related, as under

$$Y_\lambda = \sum_\rho A_{\lambda\rho} Y_{\Delta_\rho}, \quad (1.116)$$

where $A_{\lambda\rho}$ is a set of numbers which are obtained by the chemical equilibrium conditions as explained in the previous section and depends on which of the three mass regimes M_1 lies in. The final baryon asymmetry Y_B which varies linearly with Y_{Δ_λ} [67] can be obtained depending upon the mass regime in which M_1 is located. We discuss this in detail in the next chapters.

1.6 An overview of the present work

In this thesis, we shall consider the light neutrinos to be Majorana in nature. The effective light neutrino mass matrix M_ν may have its origin in one of the mechanisms discussed in Sec.1.3. In general, M_ν is complex symmetric, and therefore, contains twelve real independent parameters which determine the low-energy neutrino

observables. However, the current experimental data cannot uniquely determine all the low-energy observables. Till date, there exists only five experimentally measured quantities, namely, the three mixing angles, the solar and the atmospheric mass-squared differences. The absolute scale of the light neutrino masses, the neutrino mass ordering and the leptonic CP phases δ, α, β are yet to be determined. Thus the rationale is to invoke some symmetry/ansatz at low energy which reduces the number of parameters of M_ν . In this regard, there exists a substantial body of research [85–90] in the Beyond Standard Model (BSM) framework. The use of discrete symmetries [91–94] turns out to be the most economical approach to unveil the flavor structure of M_ν which governs the pattern of mixing. Assuming $\theta_{13} = 0$ and $\theta_{23} = \pi/4$, the mixing matrix U at the leading order can be parameterized as

$$U = \begin{pmatrix} c_{12} & s_{12} & 0 \\ -\frac{s_{12}}{\sqrt{2}} & \frac{c_{12}}{\sqrt{2}} & \frac{1}{\sqrt{2}} \\ \frac{s_{12}}{\sqrt{2}} & -\frac{c_{12}}{\sqrt{2}} & \frac{1}{\sqrt{2}} \end{pmatrix} \quad (1.117)$$

where $s_{12} = \sin \theta_{12}$. The TBM mixing [92] corresponds to the special case with $\theta_{12} = \sin^{-1}(1/\sqrt{3})$. The mixing pattern given in (1.117) had its origin in a low-energy flavor symmetry, known as the $\mu\tau$ interchange symmetry. It proposes an invariance of the neutrino Majorana mass term

$$-\mathcal{L} = \frac{1}{2} \overline{\nu_{Ll}^C} M_{\nu lm} \nu_{Lm} + \text{h.c.} \quad (1.118)$$

under the linear transformation $\nu_{Ll} \rightarrow G_{lm}^{\mu\tau} \nu_{Lm}$ where G is a unitary matrix in flavor space with $G_{ee}^{\mu\tau} = G_{\mu\tau}^{\mu\tau} = G_{\tau\mu}^{\mu\tau} = 1$ and all other entries are zero. This implies an invariance $(G^{\mu\tau})^T M_\nu G^{\mu\tau} = M_\nu^{\mu\tau}$ which immediately dictates the structure of M_ν to

be:

$$M_\nu^{\mu\tau} = \begin{pmatrix} A & B & B \\ B & C & D \\ B & D & C \end{pmatrix}, \quad (1.119)$$

where A, B, C and D are in general complex parameters. In general, if under any linear transformation of the neutrino fields $\nu_{L\alpha} \rightarrow G_{\alpha\beta}\nu_{L\beta}$ the effective neutrino Majorana mass term (1.118) enjoys an invariance, then M_ν must satisfy the equation

$$G^T M_\nu G = M_\nu. \quad (1.120)$$

It has been shown in Ref. [1] that if an unitary matrix U diagonalizes M_ν , so does the matrix $U' = GU$. Eq.(1.120), coupled with the diagonalization condition $U^T M_\nu U = \text{diag}(m_1, m_2, m_3)$ for nondegenerate m_i implies

$$U^\dagger G U = d, \text{ with } d_{ij} = \pm\delta_{ij}. \quad (1.121)$$

Among the eight possible choices for d , two are trivial, $d = \pm I$, and the corresponding G matrices are also trivial, namely, $G = \pm I$. Out of the remaining six d matrices, three are negatives of the other three, and the corresponding G matrices are negatives of each other. Hence, without any loss of generality we can confine to $\det G = +1$ which corresponds to

$$\begin{aligned} d_1 &= \text{diag}(1, -1, -1) \rightarrow G_1, \\ d_2 &= \text{diag}(-1, 1, -1) \rightarrow G_2, \\ d_3 &= \text{diag}(-1, -1, 1) \rightarrow G_3. \end{aligned} \quad (1.122)$$

Out of three G matrices G_1, G_2 and G_3 , only two are independent, on account of a

relation $G_a G_b = G_b G_a = G_c$ with $a \neq b \neq c$. These two independent G matrices define a $\mathbb{Z}_2 \times \mathbb{Z}_2$ symmetry since $d^2 = G^2 = I$ as dictated by Eq.(1.121). It has been demonstrated in Ref [1,95] that irrespective of the structure of M_ν , it enjoys a $\mathbb{Z}_2 \times \mathbb{Z}_2$ residual symmetry.

Apart from $\mu\tau$ interchange, there exists other interesting residual symmetries such as scaling ansatz in neutrino mass matrix. It predicts vanishing values for θ_{13} and m_3 together with a nonmaximal θ_{23} in general. All these effective symmetries are well motivated from the larger symmetry group such as A_4 , S_3 , D_4 etc. However, since current data has firmly established a nonvanishing θ_{13} and opened up the door for CP violation, these residual symmetries should be suitably modified. The current thesis deals with two such approaches.

To discuss the first approach, we note that for an arbitrary mixing matrix U , one can uniquely construct the G matrices. However, the converse is not true due to the degeneracies in the eigenvalues of d matrices. In such a case, given a leading order mixing matrix, e.g., U^0 , first the G matrices are uniquely constructed. Due to the said degeneracy, the degrees of choice of the mixing matrix U is enhanced. It possible to appropriately ‘rotate’ U^0 in accordance with the phenomenological requirement [4,96–98].

In the second approach, the real invariance of M_ν is extended to its complex counterpart by means of a nonstandard CP transformation $\nu_\alpha \rightarrow iG_{\alpha\beta}\gamma^0\nu_\beta^C$ [99–101] which leads to a complex invariance

$$G_{2,3}^T M_\nu G_{2,3} = M_\nu^* \tag{1.123}$$

since the R.H.S of (1.120) is now replaced with its complex conjugate in (1.123). Thus one can implement a nonstandard \mathbb{Z}_2^{CP} transformation in the low energy effective

Lagrangian.

It remains a nontrivial challenge to consistently combine CP symmetry with a flavor group [102–104]. However, it has been shown in Ref. [105] that this can be achieved if certain consistency conditions are satisfied. In a top-down approach, a CP combined flavor symmetry existing at high energy ($G_{\text{flav}} \times G_{CP}$) is spontaneously broken down to two distinct residual symmetries- $G_{\text{flav}}^l \times G_{CP}^l$ in the charged lepton sector and $G_{\text{flav}}^\nu \times G_{CP}^\nu$ neutrino sector [99]. The neutrino mixing arises as a result of this mismatch between the residual symmetries of the two sectors. A bottom-up approach has also been proposed [106] to construct a minimal flavor group with the residual symmetries in the charged lepton and the neutrino sector. In this thesis, without going into the explicit model building, we rather zero in on the low energy predictions of the neutrino parameters such as CP phases, sum of the light neutrino masses $\Sigma_i m_i$ and neutrinoless double ($\beta\beta 0\nu$) decay parameter $|M_{ee}|$.

One of my research work is based on the first approach. We show how the well-known relation between δ and θ_{23} , arising as a consequence of two \mathbb{Z}_2 symmetries accompanying the $\mu\tau$ interchange symmetry, is changed if the latter is generalized to a symmetry that mixes the ν_μ and ν_τ flavors. In particular, we show that the stringent condition of simultaneous maximality of δ and θ_{23} can be lifted even with a very tiny departure from the exact $\mu\tau$ interchange. Furthermore, the current neutrino data on δ and θ_{23} can be explained better in this framework. We also discuss how the proposed mixing scenario could be realized with two simultaneous CP transformations leading to more predictive correlations between δ and the mixing angles θ_{ij} . Next, we analyze the ‘three flavor regime’ of leptogenesis within the CP extended framework and demonstrate that unlike the CP extended $\mu\tau$ interchange symmetry, a resonant leptogenesis is possible in the $\mu\tau$ mixing case. The resulting baryon asymmetry requires $\theta_{23} \neq \pi/4$ due to the fact that the baryon to photon ratio η_B vanishes in the

exact limit of $\theta_{23} \rightarrow \pi/4$.

Three of my other works [107, 108] are based on the second approach, i.e., we have supplemented the residual \mathbb{Z}_2 symmetries with a nonstandard CP transformation; CP-transformations followed by a flavor symmetry operation [109]. Unlike the canonical CP transformation, which is a CP conserving theory, this nonstandard CP transformation predicts maximally violating value $\pi/2$ or $3\pi/2$ for the Dirac CP phase δ and a CP conserving value for the Majorana phases α or β by restricting them to either 0 or π . High energy symmetry group for models of this kind may be constructed through the induced automorphism approach [102, 106, 110]

In one of the work, we envision a complex extension of $\mu\tau$ mixing antisymmetry in M_ν by a nonstandard CP transformation $\nu_{\alpha L} \rightarrow i\mathcal{G}_{\alpha\beta}\gamma^0\nu_{\beta L}^C$ where \mathcal{G} is a \mathbb{Z}_4 generator related to the \mathbb{Z}_2 generator G through the relation $\mathcal{G} = iG$. As a result $\mu\tau$ mixing parameter θ gets related with δ and θ_{23} as $\sin \delta = \pm \sin \theta / \sin 2\theta_{23}$. For arbitrary θ , both θ_{23} and δ are nonmaximal. For a nonmaximal δ , one of the two Majorana phases is different from 0 or π , leading to substantial Majorana CP violation with observable consequences for $\beta\beta 0\nu$ decay process. For all possible combination of α, β and δ the entire parameter space corresponding to the inverted mass ordering shall be ruled out if nEXO, covering its entire reach, does not observe any $\beta\beta 0\nu$ signal. We have made a quantitative study of the effect of the CP asymmetry parameter $A_{\mu e}$ in long baseline neutrino oscillation experiments. We also make quantitative predictions of our scheme on Ultra High Energy (UHE) neutrino flavor flux ratios at neutrino telescopes. While exact CP transformed $\mu\tau$ interchange antisymmetry ($\theta = \pi/2$) leads to an exact equality among those ratios, taking a value 0.5, a tiny deviation can cause a drastic change in them. Measurement of UHE flavor flux with improved statistics will further constrain the parameter θ .

In a different work [5], we discuss the implications of the CP extension of the

residual symmetries associated with scaling ansatz invariant neutrino Majorana mass matrix M_ν . It changes the real invariances of M_ν to their complex counterparts which are referred to as ‘Modified Scaling’. We determine correlations between the mixing angles θ_{12} and θ_{13} and show that it leads to maximal Dirac CP violation and vanishing Majorana phases. Besides the testable predictions on $0\nu\beta\beta$ decay, we discuss interesting consequences for leptogenesis. Within the hierarchical scenario, we show that only τ -flavored leptogenesis is possible in this framework. For a NO (IO), θ_{23} is found to be less (greater) than $\pi/4$, for the final baryon asymmetry Y_B to lie in the observed range. An upper and a lower bound on the mass of N_1 and the effect of the heavier neutrinos $N_{2,3}$ on final Y_B has been subsequently estimated.

In the work [9], we discuss a neutrino mass model with a CP extended $\mu\tau$ flavored symmetry of the effective light neutrino mass term together with an additional invariance under a Friedberg-Lee (FL) transformation of the neutrino fields. The absolute scale of the light neutrino masses is dictated by the vanishing determinant of \mathcal{M}_ν . For both NO and IO, while θ_{23} is in general nonmaximal, δ is exactly maximal for IO and nearly maximal for NO due to $\cos\delta \propto \sin\theta_{13}$. For the NO, very tiny nonvanishing Majorana CP violation might appear through one of the Majorana phases β , otherwise the model predicts vanishing Majorana CP violation. From the future precision measurement of θ_{23} , it is difficult to rule out the model. However, any large deviation of δ from its maximality, will exclude the model. Beside fitting the neutrino oscillation global fit data, we also explore $\nu_\mu \rightarrow \nu_e$ oscillation which is expected to reveal CP violation in different long baseline experiments. Finally, assuming pp and $p\gamma$ collisions as the source of the Ultra High Energy (UHE) neutrinos, statements have been made about the octant of θ_{23} . Conversely, a precision measurement of θ_{23} can be used to predict the allowed ranges of flavor flux ratios.

Finally, I also worked on a detailed analysis of the minimal textures of the

constituent matrices that comprises the light neutrino Majorana mass matrix M_ν in low energy seesaw schemes [10]. In particular, we thoroughly explore the Inverse and Linear seesaw mechanisms with maximal vanishing elements for the various matrices comprising M_ν with the assumption that its eigenvalues are nonvanishing. We show that the minimal structure of the charged lepton mass matrix allows only six possibilities. For the nonvanishing determinant of m_ν , an extensive analysis is performed to derive the minimal textures of the matrices comprising m_ν in both linear and inverse seesaw. We find that the minimality allows the realization of all the phenomenologically allowed two-zero textures in Inverse seesaw but only one such texture is found to be allowed in linear seesaw.

The next chapters are based on following publications and preprints:

Chapter 2: [arXiv:1805.10031v2](#).

Chapter 3: [Phys.Rev. D99 \(2019\) 033009](#).

Chapter 4: [JHEP 1712 \(2017\) 030](#).

Chapter 5: [JHEP 1903, 081 \(2019\)](#).

Chapter 6: [Phys.Lett. B759 \(2016\) 206-213](#).

Coauthors: Ambar Ghosal, Rome Samanta, Probir Roy and Sukannya Bhattacharya.

Chapter 2

Importance of $\mu\tau$ mixing symmetry and its CP extension on leptogenesis

2.1 Introduction

Till date, the important issues such as the theoretical origin of the mass, pattern of flavor mixing and CP properties [85] of the three light neutrinos remain unresolved. Experimentally, all the three mixing angles and the two independent mass-squared differences have already been known to a good accuracy. In particular, the current best-fit value of the solar mixing angle is known to be $(\theta_{12})^{\text{bf}} = 33.62^\circ$ while that of the reactor mixing angle $(\theta_{13})^{\text{bf}} = 8.5^\circ$. In the present era of precision measurement of the oscillation parameters, the determination of the neutrino mass ordering, the octant of the atmospheric mixing angle θ_{23} and the value of the Dirac CP phase δ have also attracted a lot of attention.

Despite a decent understanding of the leading order lepton flavor mixing [92] and other measurable neutrino observables such as δ [111], the origin of exact pattern

of leptonic mixing is yet unknown. As mentioned in Sec.1.6, the paradigm of residual symmetry [1, 4, 98] turns out to be both a promising and an economical approach in uncovering the mixing pattern. This is because it does not require the values of the elements of M_ν in order to predict the mixing parameters. As laid out in Sec.1.6, for a given M_ν and a representation of the residual symmetries in the flavor space G_a , a horizontal invariance $(G_a)^T M_\nu G_a = M_\nu$ ($a = 1, 2, 3$) together with the condition $U^T M_\nu U = \text{diag}(m_1, m_2, m_3)$ imply

$$G_a = U d_a U^\dagger \text{ with } (d_a)_{ij} = \pm \delta_{ij}. \quad (2.1)$$

Clearly, the columns of U are the eigenvectors of G_a with eigenvalues ± 1 . Since there exists two independent G_a matrices and each G_a generates a \mathbb{Z}_2 symmetry, the neutrino mixing properties could be regarded as a consequence of a residual $\mathbb{Z}_2 \times \mathbb{Z}_2$ invariance. Given a mixing matrix U and $d_{1,2}$, the corresponding \mathbb{Z}_2 generators $G_{1,2}$ can be easily constructed using (2.1). For example, within the PDG convention [112], a leading order mixing matrix $U_0^{\mu\tau}$ could be used with d_3 to construct the well-known $\mu\tau$ interchange symmetry generator $G_3^{\mu\tau}$ [113, 114] matrix:

$$U_0^{\mu\tau} = \begin{pmatrix} p & x & 0 \\ -\frac{x}{\sqrt{2}} & \frac{p}{\sqrt{2}} & \frac{1}{\sqrt{2}} \\ \frac{x}{\sqrt{2}} & -\frac{p}{\sqrt{2}} & \frac{1}{\sqrt{2}} \end{pmatrix} \xrightarrow[(2.1)]{d_3} G_3^{\mu\tau} = \begin{pmatrix} -1 & 0 & 0 \\ 0 & 0 & 1 \\ 0 & 1 & 0 \end{pmatrix}, \quad (2.2)$$

where, $p \equiv \cos \theta_{12}^\circ$ and $x \equiv \sin \theta_{12}^\circ$ with θ_{12}° being the solar mixing angle. Using (2.1) and $d_{1,2}$, the other two matrices, i.e., $G_{1,2}^{\mu\tau}$ can also be trivially constructed. In this chapter, we refer these as the associate $\mu\tau$ symmetries. Since a nonzero θ_{13} has been confirmed at more than 5.2σ [115], $G_3^{\mu\tau}$ invariance must be broken. Even though, $G_3^{\mu\tau}$ does not uniquely determine U , the freedom of rotating $U_0^{\mu\tau}$ in the 1-2 plane still leaves one with a vanishing θ_{13} . However, the symmetry $G_1^{\mu\tau}$ ($G_2^{\mu\tau}$) need not

be broken because they do not uniquely predict the mixing matrix. In particular, one can ‘rotate’ $U_0^{\mu\tau}$ in 2-3 (1-3) plane to obtain a nonzero θ_{13} and hence the phase δ . These rotations are very natural possibilities due to the degenerate eigenvalues of $G_{1,2}^{\mu\tau}$ matrices. For any light neutrino mass matrix that enjoys such an invariance, the authors of Ref. [4] showed that the phase δ could be computed as

$$\cos \delta = \frac{(s_{23}^2 - c_{23}^2)(s_{12}^2 - c_{12}^2 s_{13}^2)}{4c_{12}s_{12}c_{23}s_{23}s_{13}} \quad \text{for } G_1^{\mu\tau}, \quad (2.3)$$

$$\cos \delta = \frac{(c_{23}^2 - s_{23}^2)(c_{12}^2 - s_{12}^2 s_{13}^2)}{4c_{12}s_{12}c_{23}s_{23}s_{13}} \quad \text{for } G_2^{\mu\tau}, \quad (2.4)$$

where $\theta_{23}, \theta_{12}, \theta_{13}$ are respectively the atmospheric, solar and reactor mixing angles. For a given 3σ range of θ_{12} and θ_{13} , the relations in (2.3) and (2.4) predict a simultaneous maximality ($\delta = \pi/2$ or $3\pi/2$ and $\theta_{23} = \pi/4$). Keeping in mind that there are still no definite statements regarding the values of δ and θ_{23} , we propose a generalization of the associate $\mu\tau$ interchange symmetries. We refer to them as the associate $\mu\tau$ mixing symmetries. The mixing symmetry could lift the simultaneous maximality of δ and θ_{23} , i.e., in contrast to the prediction of exact $\mu\tau$ interchange(cf. Eq.(2.3), this scenario allows a nonmaximal value of δ for a maximal value of θ_{23} and vice-versa. General $\mu\tau$ symmetry is basically a ‘mixing’ between μ and τ neutrino flavors unlike the conventional $\mu\tau$ ‘interchange’. Similar to the $G_3^{\mu\tau}$ generator (cf. Eq.2.2), we can derive the same (we designate it as $G_3^{g\mu\tau}$) for the $\mu\tau$ mixing, starting from the zeroth order mixing matrix $U_0^{g\mu\tau}$ as

$$U_0^{g\mu\tau} = \begin{pmatrix} p & x & 0 \\ -xq & pq & y \\ xy & -py & q \end{pmatrix}, \quad (2.5)$$

where $y = \sin \theta_g$ and $q = \cos \theta_g$ with θ_g being the $\mu\tau$ mixing parameter and using

(2.1). Thus $G_3^{g\mu\tau}$ could be constructed as

$$G_3^{g\mu\tau} = \begin{pmatrix} -1 & 0 & 0 \\ 0 & -\cos 2\theta_g & \sin 2\theta_g \\ 0 & \sin 2\theta_g & \cos 2\theta_g \end{pmatrix}. \quad (2.6)$$

It is to be noted that for $\theta_g = \pi/4$, the usual $\mu\tau$ interchange symmetry $G_3^{\mu\tau}$ (cf. Eq.2.2) is recovered. An elaborate account of the high energy flavor models that spontaneously break down to low energy residual symmetries like $G_3^{g\mu\tau}$ can be found in Refs. [116, 117]. Similar to [4], in our proposal also, due to the vanishing θ_{13} , we opt for the predictions of the associate $\mu\tau$ mixing symmetries $G_{1,2}^{g\mu\tau}$ assuming the $G_3^{g\mu\tau}$ is broken. It is now obvious to anticipate, that the deviation of the parameter θ_g from $\pi/4$ is solely responsible for simultaneously maximality of θ_{23} and δ . Having furnished all the necessary prerequisites, in this chapter, we present our work in three steps. In the first step, we obtain δ as $\delta \equiv f(\theta_{23}, \theta_{12}, \theta_{13}, \theta_g)$ (Eq.2.13 & 2.17) for both the associate $\mu\tau$ mixing symmetries in a model independent way. Then we present a very general numerical analysis. For example, for the given maximality of θ_{23} (δ) we try to show how far θ_g could deviate from $\pi/4$ for the allowed nonmaximal value of δ (θ_{23}). We find that the deviation (measured by a parameter $\theta_d = \theta_g - \pi/4$) cannot be very large, in particular for $G_2^{g\mu\tau}$ invariance, the deviation is significantly small. To make a comparison of the results the current framework with $\mu\tau$ interchange, we then present a distribution of $\cos \delta$ for a small value of θ_d taking into account a Gaussian distribution and 1σ error for the mixing angles. In the second step, we discuss how the parameter θ_g could be related to a realistic model parameter in neutrino mass models such as softly broken D_4 [117], Scaling Ansatz [5, 7, 107, 118–121], four texture zeros in neutrino Dirac mass matrix within Type-I seesaw [122] etc. In the third step, we show how the associate mixing symmetries $G_{1,2}^{g\mu\tau}$ could arise a result of two simultaneous CP transformations [100, 123, 124] in the neutrino mass terms. Next,

we derive correlations between δ and the mixing angles θ_{ij} in this class of models. Finally, from the perspective of leptogenesis, we show this CP extended $\mu\tau$ mixing scheme is more interesting than the CP extended $\mu\tau$ interchange which has been a subject of recent interest in neutrino mass models [99, 102–105, 108, 110, 125–130]. We focus, in particular, on the ‘three flavor regime’ of leptogenesis [68, 131, 132]. We also show that unlike the CP extension $\mu\tau$ interchange, a resonant leptogenesis [74] is possible in our proposal. *In this framework, a nonzero baryon asymmetry always requires nonmaximality in θ_{23} .* We also demonstrate that the CP extended $\mu\tau$ mixing symmetry is a novel example that brings out the importance of the off-diagonal terms of the flavor coupling matrix [133–136] which have usually been neglected in the computation of leptogenesis, particularly, in the models with flavor symmetries.

The rest of the chapter is organized as follows. Sec.5.33 and its various subsections deal with the theoretical formalism to derive the model independent constraints and some pictorial representations of the sensitivity of the observables δ and θ_{23} with the newly introduced model parameter θ_g that generalizes $\mu\tau$ interchange to $\mu\tau$ mixing. We then compare our results with the exact $\mu\tau$ interchange symmetry and discuss the significance of the parameter θ_d in neutrino mass models such as Scaling Ansatz. In Sec.2.3, we demonstrate the CP extended $\mu\tau$ mixing and its consequences. In Sec.2.4 we present a qualitative as well as a quantitative description of leptogenesis within the framework of CP extended $\mu\tau$ mixing. Finally, we conclude our work in Sec.2.5.

2.2 Model independent correlations in $\mu\tau$ mixing

This section contains derivations of the analytical correlations among the Dirac CP phase, three mixing angles and the mixing parameter θ_g for both the associate mixing symmetries $G_1^{g\mu\tau}$ and $G_2^{g\mu\tau}$. We also discuss the compatibility of the scenario with current neutrino oscillation data. A systematic analysis is given in the following subsections.

2.2.1 Consequences of $G_1^{g\mu\tau}$ invariance

As already introduced in Sec.2.1, the diagonal matrix $d_1 = \text{diag}(1, -1, -1)$ has two repeated entries. Therefore, given the symmetry $G_1^{g\mu\tau}$ and the diagonalization condition (2.1), the second and third columns of the mixing matrix $U_0^{g\mu\tau}$ are not unique. It can be subjected to a rotation in the 2-3 plane due to this two-fold degeneracy. This is particularly interesting because the phenomenological requirement of a nonvanishing θ_{13} finds a natural justification. With the choice of a most general unitary rotation matrix U_θ^{23} [4] in the 2-3 plane

$$U_\theta^{23} = \begin{pmatrix} 1 & 0 & 0 \\ 0 & c_\theta & s_\theta e^{i\gamma} \\ 0 & -s_\theta e^{-i\gamma} & c_\theta \end{pmatrix} P_\phi, \quad (2.7)$$

where $P_\phi = \text{diag}(e^{i\phi_1}, e^{i\phi_2}, e^{i\phi_3})$, a phenomenologically consistent PMNS matrix $U = U_0^{g\mu\tau} U_\theta^{23}$ is obtained as

$$U = \begin{pmatrix} p & xc_\theta & xs_\theta e^{i\gamma} \\ -xq & (pqc_\theta - ys_\theta e^{-i\gamma}) & (yc_\theta + pqs_\theta e^{i\gamma}) \\ xy & -(pys_\theta e^{-i\gamma}) & (qc_\theta - pqs_\theta e^{i\gamma}) \end{pmatrix} P_\phi. \quad (2.8)$$

Now we compare (2.8) with the PMNS matrix parametrized according to the PDG convention [112] as

$$U_{\text{PMNS}} = P_\chi \begin{pmatrix} c_{12}c_{13} & s_{12}c_{13} & s_{13}e^{-i\delta} \\ -s_{12}c_{23} - c_{12}s_{23}s_{13}e^{i\delta} & c_{12}c_{23} - s_{12}s_{23}s_{13}e^{i\delta} & c_{13}s_{23} \\ s_{12}s_{23} - c_{12}c_{23}s_{13}e^{i\delta} & -c_{12}s_{23} - s_{12}c_{23}s_{13}e^{i\delta} & c_{13}c_{23} \end{pmatrix} P_M, \quad (2.9)$$

where $P_\chi = \text{diag}(e^{i\chi_1}, e^{i\chi_2}, e^{i\chi_3})$ is an unphysical phase matrix and $P_M = \text{diag}(1, e^{i\frac{\alpha}{2}}, e^{i\frac{\beta}{2}})$ represents the Majorana phase matrix.

Comparing the (11), (12) and (13) element of (2.8) and (2.9), we find

$$c_{12}c_{13} = p, \quad \chi_1 = \phi_1, \quad (2.10)$$

$$s_{12}c_{13} = xc_\theta, \quad \frac{\alpha}{2} + \chi_1 = \phi_2, \quad (2.11)$$

$$s_{13} = xs_\theta, \quad \chi_1 - \delta + \frac{\beta}{2} - \gamma = \phi_3. \quad (2.12)$$

Equating the quantity ($|U_{21}|^2 - |U_{31}|^2$) of (2.8) with the same of (2.9) and using (6.8-2.12), we obtain

$$\cos \delta = \frac{(s_{23}^2 - c_{23}^2)(s_{12}^2 - c_{12}^2s_{13}^2) + \cos 2\theta_g(s_{13}^2 + c_{13}^2s_{12}^2)}{4c_{12}s_{12}c_{23}s_{23}s_{13}}, \quad (2.13)$$

In (2.13), we have re-expressed q, y in terms of θ_g . As expected, for $\theta_g = \pi/4$, (2.13) reduces to (2.3) which is the prediction of $G_1^{\mu\tau}$. For the convenience of numerical analysis, we choose $\theta_d = \theta_g - \pi/4$, which is a measure of the deviation from the usual $\mu\tau$ interchange symmetry, as the parameter instead of θ_g . This re-parameterization also makes it easy to understand the variation of the observables w.r.t the deviation from $\mu\tau$ interchange. Introduction of the mixing parameter θ_g now enables us to explore various interesting aspects of (2.13). For example, if we set θ_{23} to be maximal,

the deviation of $\cos \delta$ from its maximal value can be tracked with θ_d from

$$\cos \delta = \frac{\cos 2(\pi/4 - \theta_d)(s_{13}^2 + c_{13}^2 s_{12}^2)}{2c_{12}s_{12}s_{13}}. \quad (2.14)$$

For the best-fit values of θ_{12} and θ_{13} , we present a variation of δ with θ_d (left) for $\mu\tau$ mixing and δ with θ_{23} for $\mu\tau$ interchange¹ (right) in Fig.2.1.

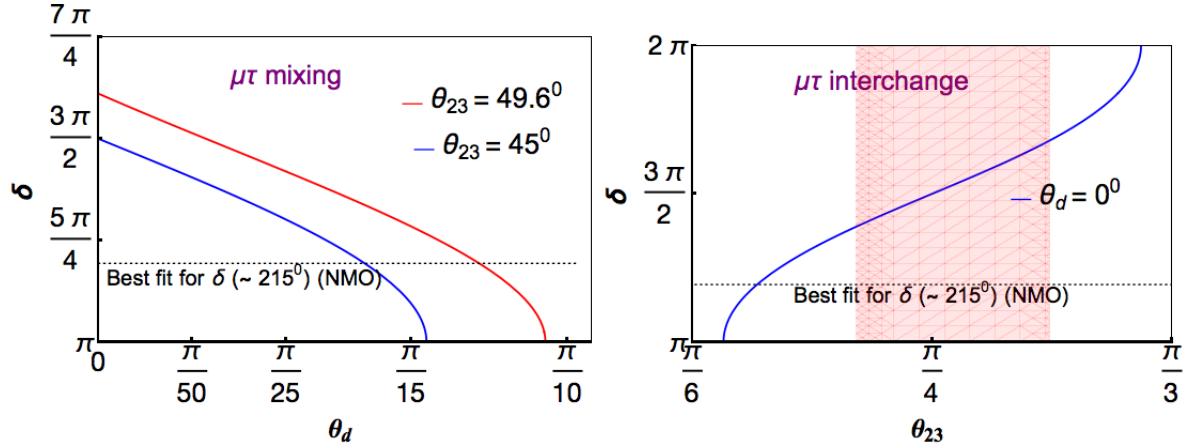


Figure 2.1: For $G_1^{g\mu\tau}$ (left): Variation of δ with θ_d (a measure of the deviation from $\mu\tau$ interchange symmetry). Here, $2\pi - \delta$ is also an allowed solution for the same values of θ_d . For $G_1^{\mu\tau}$ (right): Variation of δ with θ_{23} . These plots are generated using the best-fit values for θ_{13} and θ_{12} for NO.

It is evident from Fig.2.1 (left panel), that the robust prediction of simultaneous maximality arising from $\mu\tau$ interchange (cf. Eq.2.3) has been relaxed (represented by the blue line for $\theta_{23} = 45^\circ$) since θ_d can be different from zero. In fact, the deviation of δ from its maximal value is extremely sensitive to the changes in θ_d , e.g., a deviation of the former from $3\pi/2$ to $5\pi/4$ only requires a value $\approx \pi/20$ for the latter. The red line represents the variation of δ for the current best-fit value $\theta_{23} = 49.6^\circ$ for NO. Clearly one can see that in the $\mu\tau$ interchange limit ($\theta_d = 0$),

¹From now on when we address predictions of $\mu\tau$ mixing or $\mu\tau$ interchange, it could be assumed that we are implying the predictions for the associate symmetries.

the best-fit of θ_{23} is not consistent with the current best-fit of $\delta = 215^\circ$ (denoted by the horizontal black dotted line). However, in our $\mu\tau$ mixing scheme, one can fit the best-fits simultaneously just by tuning a single parameter θ_d ($\sim \pi/12$) as shown by the red line. The figure in the right hand side shows a variation of δ with θ_{23} for the exact $\mu\tau$ interchange symmetry. It is interesting to notice, that even within the 3σ range of θ_{23} , one cannot reconcile the best-fit value of δ . Thus from the view point of current experimental results, the proposed $G_1^{g\mu\tau}$ is a more admissible symmetry than the $G_1^{\mu\tau}$. This can also be realized more clearly from the Fig.2.2 where we present a statistical comparison between the predictions of $\mu\tau$ interchange ($G_1^{\mu\tau}$) and $\mu\tau$ mixing ($G_1^{g\mu\tau}$). The probability density plot in the left hand side in Fig.2.2 shows, for the $G_1^{\mu\tau}$, most probable values of δ lie within a region centered approximately around $\delta \sim 290^\circ$ which is far away (tension is $\sim 2\sigma$) from the best-fit 215° for NO.

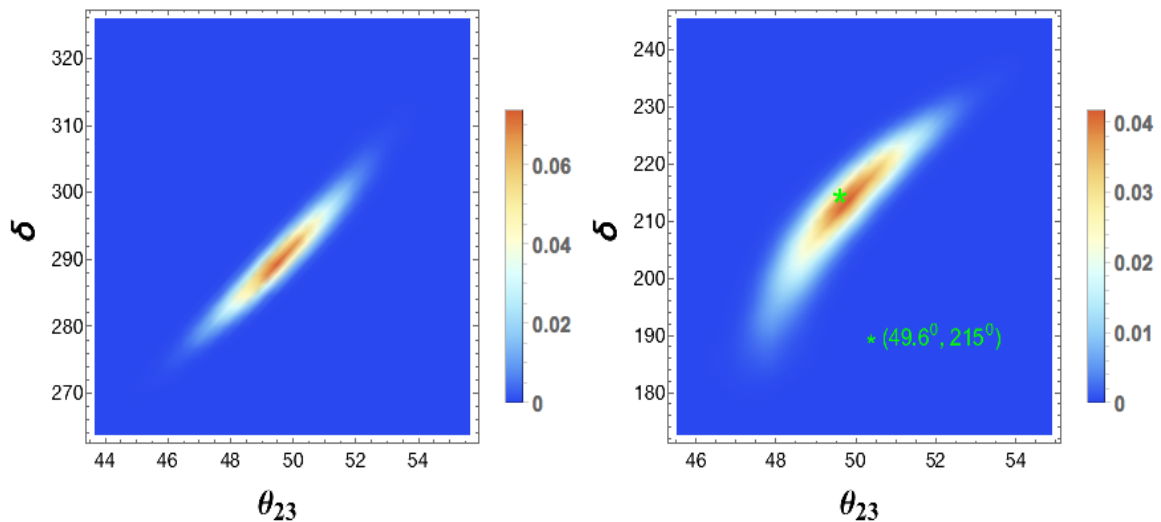


Figure 2.2: For $G_1^{\mu\tau}$ (left): Probability distribution of δ with θ_{23} . For $G_1^{g\mu\tau}$ (left): The same plot but for $\theta_d = \pi/12$. Here we have used Gaussian distribution for each of the mixing angles with 1σ errors.

On the other hand, as also explained earlier, for the best-fit of θ_{23} , the most probable values of δ could be reconciled with the best-fit 215° for $\theta_d = \pi/12^\circ$. As

shown in the figure in the right hand side of Fig.2.2, the entire pattern (shown in the left side) has shifted near the best-fit shown by the green ‘*’. Before we embark on our discussion of $G_2^{g\mu\tau}$, let us briefly articulate some essential points. Firstly, when we say the $\mu\tau$ interchange ($G_1^{\mu\tau}$) is disfavored, we always mean a NO. As one can see from Fig.2.2 (left hand side), best-fit of δ ($= 284^\circ$) for an IO could be well reconciled within 1σ of θ_{23} . However, as mentioned in the introduction, that the IO seems to be disfavored now by the current experimental data. One might also wonder how the mixing parameter $\theta_g = \pi/4 + \theta_d$ could be realized in a realistic neutrino mass model. Because so far it appears to be a model independent tuning parameter, except the mention to Ref. [116, 117] in the introduction. In Sec.2.2.3, we shall briefly discuss some models regarding the relation of θ_g with the model parameters and show indeed there is a large class of models that exhibit $\mu\tau$ mixing at low energy.

2.2.2 Consequences of $G_2^{g\mu\tau}$ invariance

In this case, a rotation in 1-3 plane is possible due to the degeneracy in $d_2 = (-1, 1, -1)$ matrix. By choosing a most general unitary rotation matrix U_θ^{13} [4] as

$$U_\theta^{13} = \begin{pmatrix} c_\theta & 0 & s_\theta e^{i\gamma} \\ 0 & 1 & 0 \\ -s_\theta e^{-i\gamma} & 0 & c_\theta \end{pmatrix} P_\phi \quad (2.15)$$

we construct the phenomenologically viable PMNS matrix $U = U_0^{g\mu\tau} U_\theta^{13}$ which is given by

$$U = \begin{pmatrix} pc_\theta & x & ps_\theta e^{i\gamma} \\ -(xqc_\theta + ys_\theta e^{-i\gamma}) & pq & (yc_\theta - xqs_\theta e^{i\gamma}) \\ (xyc_\theta - qs_\theta e^{-i\gamma}) & -py & (qc_\theta + xys_\theta e^{i\gamma}) \end{pmatrix} P_\phi. \quad (2.16)$$

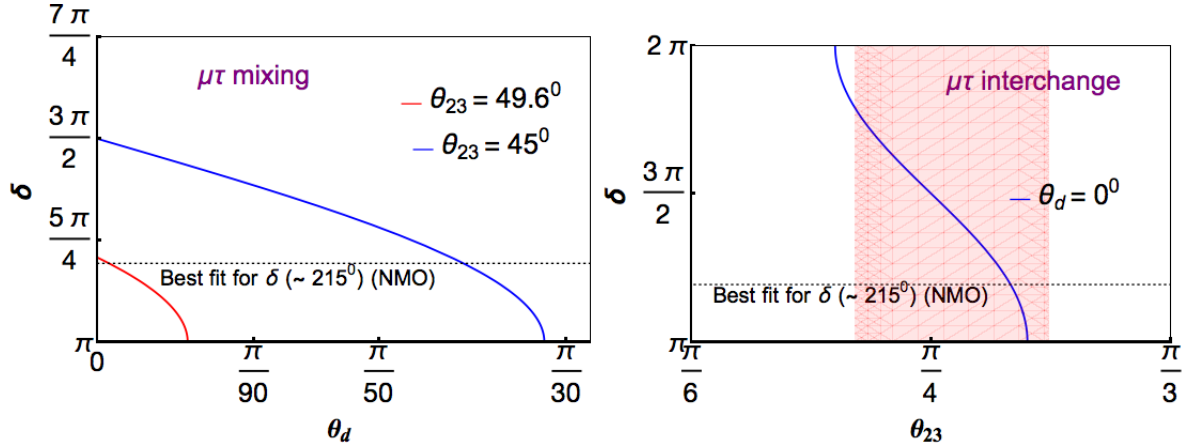


Figure 2.3: For $G_2^{g\mu\tau}$ (left): Variation of δ with θ_d (a measure of the deviation from $\mu\tau$ interchange symmetry). Here, $2\pi - \delta$ is also an allowed solution for the same values of θ_d . For $G_2^{\mu\tau}$ (right): Variation of δ with θ_{23} . These plots are generated using the best-fit values for θ_{13} and θ_{12} for NO.

Following a similar procedure demonstrated previously for $G_1^{g\mu\tau}$, we compare (2.16) with the PMNS matrix of (2.9) and equate the quantity $|U_{22}|^2 - |U_{32}|^2$ of both the matrices. This results in

$$\cos \delta = \frac{(c_{23}^2 - s_{23}^2)(c_{12}^2 - s_{12}^2 s_{13}^2) - \cos 2\theta_g (s_{13}^2 + c_{13}^2 c_{12}^2)}{4c_{12}s_{12}c_{23}s_{23}s_{13}}. \quad (2.17)$$

We note that for $\theta_g = \pi/4$, we recover (2.4). Similar to the previous case parameterizing $\theta_g = \pi/4 + \theta_d$ and setting $\theta_{23} = \pi/4$, one can track the nonmaximality of δ due to the maximal value of θ_{23} (cf. plot in the left hand side in Fig.2.3) with the correlation

$$\cos \delta = \frac{-\cos 2(\pi/4 - \theta_d)(s_{13}^2 + c_{13}^2 c_{12}^2)}{2c_{12}s_{12}s_{13}}. \quad (2.18)$$

In Fig.2.3 (left figure), the red line represents the variation of δ with θ_d for the best-fit of $\theta_{23} = 49.6^\circ$. We find a remarkable ‘coincidence’ of (2.4) with the present data on θ_{23} and δ . It is evident from the figure in the left hand side in Fig.2.3 (also in Fig.2.4),

one requires a really tiny departure (numerically, θ_d less than -0.5°) from exact $\mu\tau$ interchange to fit the most probable values of δ simultaneously with the best-fit of δ and θ_{23} . When we opt for a larger departure from $\mu\tau$ interchange, even with $\theta_d = -1^\circ$, the most probable values of δ start to move towards CP conserving values as shown in the figure in the right hand side of Fig.2.4. Thus as far as the current data on δ and θ_{23} is concerned, undoubtedly, $\mu\tau$ interchange (here $G_2^{\mu\tau}$) is a better symmetry to explain the data than the proposed $\mu\tau$ mixing (here $G_2^{g\mu\tau}$). However, compared to the previously released data [12], the new data shows a tendency to move towards the CP conserving values mainly driven by $\text{NO}\nu\text{A}$ anti-neutrino appearance channel. If this trend continues, one has to think beyond $\mu\tau$ interchange symmetry. In that case, the $\mu\tau$ mixing (as shown in the figure in the right hand side in Fig.2.4) could be a good option to explain the data.

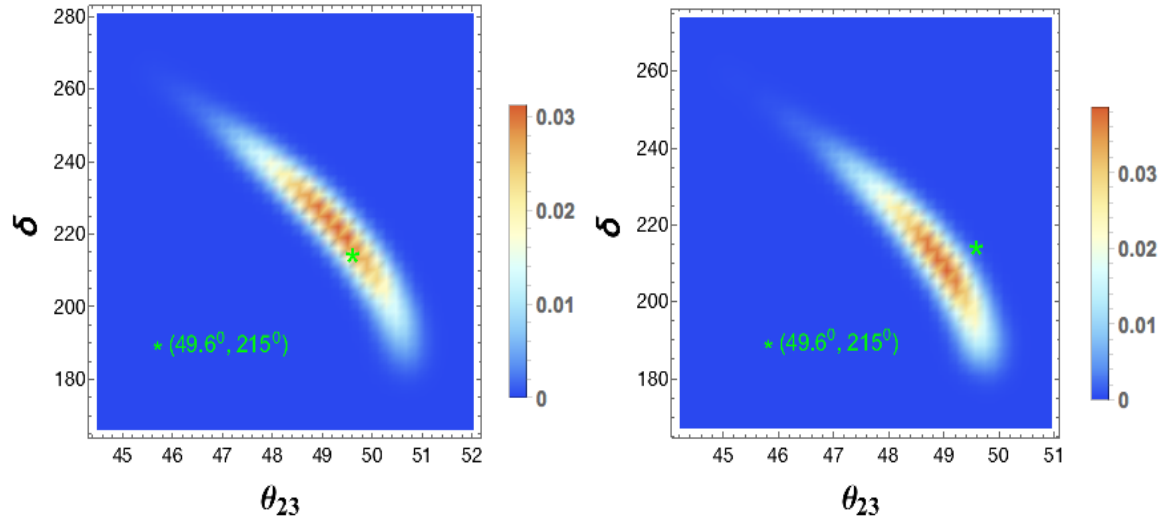


Figure 2.4: For $G_2^{\mu\tau}$ (left): Probability distribution of δ with θ_{23} . For $G_2^{g\mu\tau}$ (left): The same plot but for $\theta_d = \pi/12$. Here we have used Gaussian distribution for each of the mixing angles with 1σ errors.

So we conclude this section with the remark that, to explain the present data, the proposed $G_1^{g\mu\tau}$ (mixing) symmetry has an edge over the $G_1^{\mu\tau}$ (interchange),

whereas the symmetries which are in the class of G_2 , to explain the present data, the interchange scenario is better than the proposed mixing scenario.

2.2.3 $\mu\tau$ mixing in some neutrino mass models

In this section, we discuss some examples of the low energy residual $\mu\tau$ symmetry so that the parameter θ_g could be connected to the model parameter(s). Indeed there is a large class of models that belong to the mixing category. For example the authors of Ref. [116, 117] derive the mixing from explicit symmetry group D_4 where the $\mu\tau$ mixing parameter θ_g could be related to the model parameter as

$$\cos 2\theta_g \sim -\frac{\mu_{\text{soft}}}{M}, \quad (2.19)$$

where μ_{soft} is a soft breaking term in the D_4 model and M is the mass scale of the RH neutrinos needed to obtain Type-I seesaw light neutrino masses. The model predicts the same leading order mixing matrix as shown in (2.5). Now to generate a nonzero θ_{13} we can further add soft breaking terms to the model. However, notice that, here the introduction of new breaking terms corresponds to the rotation of the leading order mixing matrix (cf. Eq.2.7) and the final prediction (cf. Eq.2.13) is independent of the rotation angle. Since in general, generation of nonzero θ_{13} requires small breaking terms, Eq.2.19 still holds at the leading order. But unlike the D_4 model, $\cos 2\theta_g$ is not directly related only to θ_{23} but it connects θ_{23} and δ with the correlations shown in (2.13) or (2.17). The authors of Ref. [116, 117] conclude, that to test a sizable deviation of physical parameters such as θ_{23} one requires the scale of μ_{soft} of same order as the mass scale of the RH neutrinos requiring a large deviation from $\mu\tau$ interchange ($\cos 2\theta_g \simeq 1$). However, as we have shown in the previous section, even with a small departure from the interchange symmetry, one can test the parameters

δ and θ_{23} with the correlations derived this work. Thus the scale of μ_{soft} and M need not be the same. In fact, one requires much smaller scale for μ_{soft} than the scale M . Models with Scaling Ansatz or Simple Real Scaling (SRS) originally proposed in Ref. [7] and then analyzed at length in Ref. [5, 107, 118–121, 137], also belong to the $\mu\tau$ mixing category. As derived in Ref. [119], the residual symmetry for SRS is given by

$$G_3^k = \begin{pmatrix} -1 & 0 & 0 \\ 0 & (1 - k^2)(1 + k^2)^{-1} & 2k(1 + k^2)^{-1} \\ 0 & 2k(1 + k^2)^{-1} & -(1 - k^2)(1 + k^2)^{-1} \end{pmatrix}, \quad (2.20)$$

where ‘ k ’ is the scale parameter of the model that scales, for example, one row of M_ν with the other row or one column with another column [7]. Thus the scale parameter of the model could be constrained simply by the relation

$$k = \frac{1 \pm \cos 2\theta_g}{\sin 2\theta_g} \quad (2.21)$$

along with (2.13) or (2.17). One can also constrain the parameters of models like four zero textures (in charge lepton flavor basis) within Type-I seesaw [122], so called discrete Dark Matter (DM) models [138, 139] as well as the models with global $U(1)$ symmetries [129, 140–142] which at the leading order, show up a $\mu\tau$ mixing scheme at low energy. However, we would like to stress that at this stage, where the precise values of δ and θ_{23} are yet to be measured, if the $\mu\tau$ mixing parameter can be constrained a priori by some other constraints, (e.g., the mass-squared differences, the mixing angles other than θ_{23} or some cosmological phenomenon such as leptogenesis etc.) then (2.13) or (2.17) could be used to predict δ or θ_{23} . So the models with $\mu\tau$ mixing symmetry and lesser number of parameters (such as Scaling Ansatz plus texture zeros [107]) are most welcome.

2.3 CP extension of the $\mu\tau$ mixing symmetry

2.3.1 CP symmetry in a general light neutrino mass term

So far the discussion was quite general. In this section we want to explore some special class of $\mu\tau$ mixing. Since in general, only flavor symmetries are not sufficient to predict the CP violating phases, a lot of effort has been devoted in past few years to ameliorate flavor symmetries with CP symmetries [99] by demanding the invariance of the neutrino mass term with the field transformation

$$\nu_{L\ell} \rightarrow i(G_a)_{\ell m} \gamma^0 \nu_{Lm}^C \quad (a = 1, 2, 3). \quad (2.22)$$

Though one has always to be consistent with the ‘consistency condition’ to have a combined theory of flavor and CP [102,103]. The consistency condition can be written as

$$X_r \rho_r^*(g) X_r^{-1} = \rho_r(g), \quad (2.23)$$

where X_r is a unitary matrix representing CP symmetry which acts on a generic multiplet φ as

$$X_r \varphi(x) \xrightarrow{\text{CP}} X_r \varphi(x') \quad (2.24)$$

with $x' = (t, -\mathbf{x})$ and $\rho_r(g)$ is the representation for the element g of the flavor group in an irreducible representation \mathbf{r} . Eq.2.22 leads to the complex invariance

$$G_a^T M_\nu G_a = M_\nu^*. \quad (2.25)$$

Now at low energy, among the three residual \mathbb{Z}_2 generators, if two of them, say, G_2 and G_3 correspond to the complex invariances

$$G_2^T M_\nu G_2 = M_\nu^*, G_3^T M_\nu G_3 = M_\nu^*, \quad (2.26)$$

the remaining one, i.e., G_1 automatically satisfies a real invariance [124]

$$G_1^T M_\nu G_1 = M_\nu. \quad (2.27)$$

Now it is trivial to show, that (4.24) is satisfied, since in this case, (4.24) would imply

$$G_2 G_1 G_2^{-1} = G_1, \quad (2.28)$$

$$G_3 G_1 G_3^{-1} = G_1 \quad (2.29)$$

and since by construction $G_a G_b = G_c$ for $a \neq b \neq c$, the left and right hand sides of the above equations are consistent. Similarly, one obtains a real invariance for G_2 , for the simultaneous complex invariances for G_1 and G_3 . However, note that, if we demand the complex invariances for G_1 and G_2 , we obtain a real invariance for G_3 which is not acceptable, since, that will correspond to a vanishing θ_{13} . Let us now turn into the computation of the Dirac CP phases for both the acceptable real invariances, i.e., $(G_1^{g\mu\tau})^T M_\nu G_1^{g\mu\tau} = M_\nu$ and $(G_2^{g\mu\tau})^T M_\nu G_2^{g\mu\tau} = M_\nu$. For the both the cases, the second of (2.26) leads to [8, 143]

$$\sin \delta = \pm \frac{\sin 2\theta_g}{\sin 2\theta_{23}}. \quad (2.30)$$

Eliminating θ_g from (2.13) and (2.30) for $G_1^{g\mu\tau}$ whereas doing the same from (2.17) and (2.30) for $G_2^{g\mu\tau}$ we obtain a generic expression for $\cos \delta$ as

$$\cos \delta = \frac{A_i B \pm \sqrt{A_i^2 B^2 - (B^2 + C_i^2 \sin^2 2\theta_{23})(A_i^2 - C_i^2 \cos^2 2\theta_{23})}}{(B^2 + C_i^2 \sin^2 2\theta_{23})}, \quad (2.31)$$

where $i = 1, 2$ corresponds $G_i^{g\mu\tau}$ symmetries. The parameters A_i, B and C_i are the functions of the mixing angles θ_{ij} with the explicit expressions

$$A_1 = (s_{23}^2 - c_{23}^2)(s_{12}^2 - c_{12}^2 s_{13}^2), \quad A_2 = (c_{23}^2 - s_{23}^2)(c_{12}^2 - s_{12}^2 s_{13}^2), \quad (2.32)$$

$$C_1 = (s_{13}^2 + c_{13}^2 s_{12}^2), \quad C_2 = (s_{13}^2 + c_{13}^2 c_{12}^2), \quad (2.33)$$

$$B = 4c_{12}s_{12}c_{23}s_{23}s_{13}. \quad (2.34)$$

The novel correlations obtained in (2.31) are exact and can be further simplified if terms $\mathcal{O}(s_{13}^4)$ is dropped. Interestingly, both the relations are independent of θ_g and coincide with the prediction $\cos \delta = 0$ for CP extended $\mu\tau$ ($\text{CP}^{\mu\tau}$) [109, 144] in the limit $\theta_{23} \rightarrow \pi/4$.

In Fig.2.5, we have shown the predictions of CP extended $\mu\tau$ mixing. The figures in the top panel are for the real invariance for $G_1^{g\mu\tau}$ (for each case there are two solutions due the ‘ \pm ’ sign in (2.31)) and those which are in the bottom panel are for the real invariance for $G_2^{g\mu\tau}$. Notice that unlike the $\text{CP}^{\mu\tau}$ (CP extended $\mu\tau$ interchange [106]) which predicts co-bimaximal mixing ($\delta = \pm 3\pi/2$ and $\theta_{23} = \pi/4$), the current scenario allows nonmaximal atmospheric mixing. However, the most probable values of δ are clustered around their near maximal values. Thus significant deviation from maximality of δ would rule out the scenario (present data on δ for NO is at $\sim 1.37\sigma$ tension with the predictions obtained in the CP extended $\mu\tau$ mixing). Before we proceed further into the discussion of the CP extended $\mu\tau$ mixing in Type-

In seesaw framework with the motivation to explore the implications on baryogenesis via leptogenesis, let's point out an interesting aspect regarding the class of the CP extended $\mu\tau$ mixing. We have seen in Sec.5.33, introduction of $\mu\tau$ mixing instead of the $\mu\tau$ interchange symmetry, adds up two more degrees of freedom. To be precise, for both the cases, whilst simultaneous nonmaximal values for δ and θ_{23} are allowed, only for the $\mu\tau$ mixing scenario, we can test nonmaximality in one parameter for a maximal value of the other.

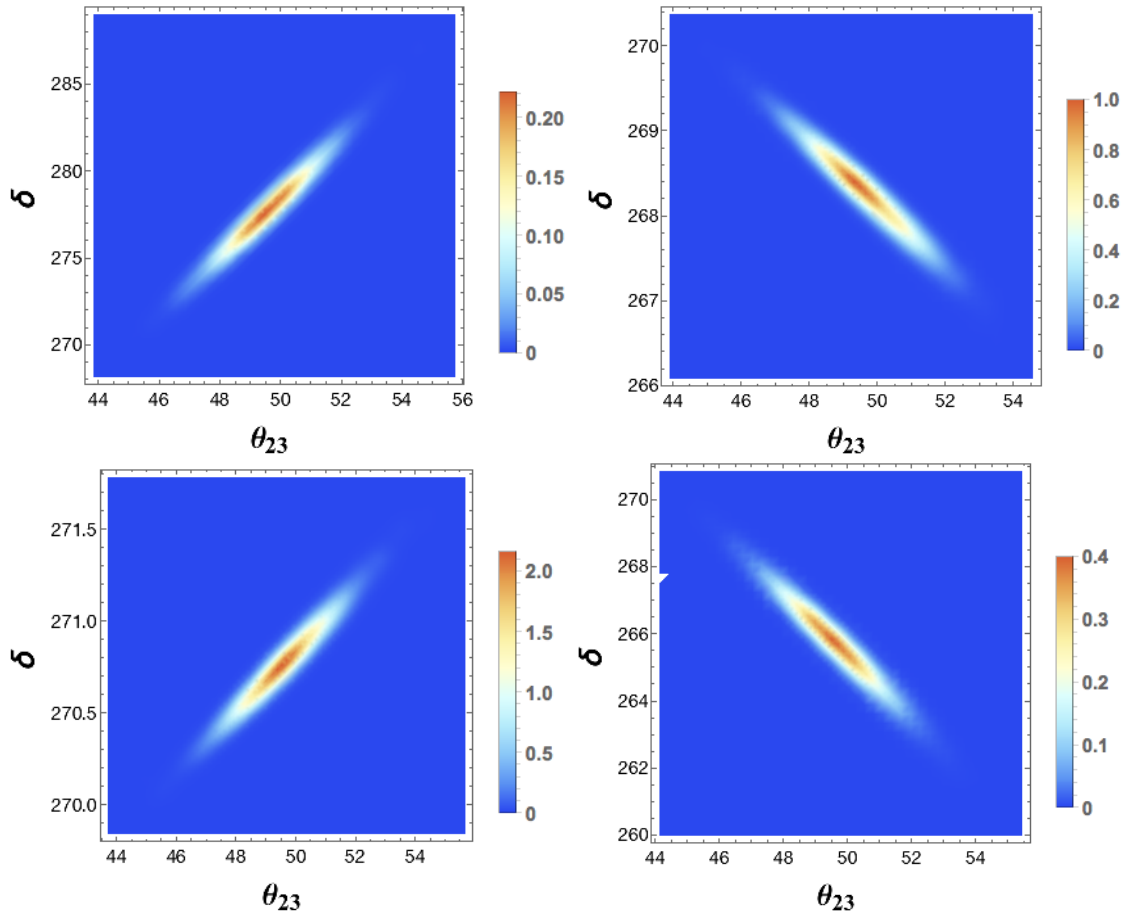


Figure 2.5: For the real invariance $(G_1^{g\mu\tau})^T M_\nu G_1^{g\mu\tau} = M_\nu$ (top): Probability distribution of δ with θ_{23} . For the real invariance $(G_2^{g\mu\tau})^T M_\nu G_2^{g\mu\tau} = M_\nu$ (bottom): Probability distribution of δ with θ_{23} . Here we have used Gaussian distribution for each of the mixing angles with 1σ errors.

Therefore there are two options i) δ could be maximal but θ_{23} is not ii) θ_{23} could be maximal but δ is not.

From Fig.2.5, it is evident that the CP extended $\mu\tau$ mixing belongs (approximately) to the case ‘i’. Explicit flavor models for the case ‘ii’ could also be interesting in future since we don’t have any precise statements on the value of δ and θ_{23} at this moment.

2.3.2 CP symmetry in Type-I seesaw

We may now proceed to the discussion of this extended CP in Type-I seesaw mechanism. It is well known that to obtain light neutrino masses one has to introduce singlet right handed (RH) fields as a minimal extension to the Standard Model (SM). Thus with the introduction of the singlet fields N_{Ri} , in the diagonal basis of the RH neutrinos, the Lagrangian for the Type-I seesaw reads

$$-\mathcal{L}_{\text{mass}}^{\nu} = \bar{N}_{iR}(m_D)_{i\alpha}l_{L\alpha} + \frac{1}{2}\bar{N}_{iR}(M_R)_i\delta_{ij}N_{jR}^C + \text{h.c.} \quad (2.35)$$

with $\alpha = e, \mu, \tau$ and $i = 1, 2, 3$. The first term in (4.28) is a Dirac type and the second term is a Majorana type mass term which together lead to the effective 3×3 light neutrino Majorana mass matrix M_{ν} as

$$M_{\nu} = -m_D^T M_R^{-1} m_D. \quad (2.36)$$

In the diagonal basis of the charged lepton as well as the heavy RH neutrinos, a CP invariant light neutrino mass matrix

$$G^T M_{\nu} G = M_{\nu}^* \quad (2.37)$$

could be obtained with the following transformation on m_D .

$$m_D G = -m_D^* \quad (2.38)$$

We refer to Refs. [5, 106, 145], to realize how in the diagonal basis of charged lepton and heavy neutrinos, CP is applied to the Type-I seesaw Lagrangian. Now in our case, to have a real invariance for $G_1^{g\mu\tau}$ as well as $G_2^{g\mu\tau}$ one needs the following transformations.

$$m_D G_i^{g\mu\tau} = -m_D^*, m_D G_3^{g\mu\tau} = -m_D^*. \quad (i = 1, 2) \quad (2.39)$$

For both the cases, the most general form of m_D that satisfies the second constraint of (2.39) can be parametrized as

$$m_D = \begin{pmatrix} a & b_1 + ib_2 & -b_1 \tan \theta_g + ib_2 \cot \theta_g \\ e & c_1 + ic_2 & -c_1 \tan \theta_g + ic_2 \cot \theta_g \\ f & d_1 + id_2 & -d_1 \tan \theta_g + id_2 \cot \theta_g \end{pmatrix}, \quad (2.40)$$

where all the parameters are real and a priori unknown. There will be other constraints (the parameters b_1, c_1, d_1 could be expressed in terms a, e, f and θ_g) on the mass matrix m_D of (2.40) due to the first transformation in (2.39). However, those transformations are not important in this work, since we present the discussion of leptogenesis with few benchmark values (particularly for the decay parameters $K_{i\alpha}$ and the CP asymmetry parameters $\epsilon_{i\alpha}$ as given in the next section) which are always compatible with those transformations². In any case, those constraint equations could easily be derived as shown in Ref. [5]. But what matters here, the overall structure of m_D shown in (2.40). Having set up all the necessary prerequisites, we are now ready

²Even after considering the constraints from $G_{1,2}^{g\mu\tau}$, the number of effective parameters in m_D are more than the number of experimental constraints.

to explore the baryogenesis via leptogenesis in the CP extended $\mu\tau$ mixing framework.

2.4 Leptogenesis in extended CP framework

Baryogenesis via leptogenesis is a process where CP violating and out of equilibrium decays of the heavy RH neutrinos produce lepton asymmetry which is subsequently converted into baryon asymmetry by non-perturbative sphalerons. For a simplified discussion, we consider a scenario with two RH neutrinos N_1 and N_2 the decays and interactions of which would give rise to the process of leptogenesis. However, the qualitative results drawn in such a scheme would also be relevant for a three RH neutrino case. When the masses of N_1 and N_2 are in the regime $M_i > 10^{12}$ GeV where all the charged lepton flavors are out of equilibrium [68, 131, 132], the quantum states $|\ell_i\rangle$ produced by the decay of N_1 and N_2 can be written as a coherent superposition of the flavor states $|\ell_\alpha\rangle$ as

$$|\ell_i\rangle = \mathcal{A}_{i\alpha} |\ell_\alpha\rangle, \quad |\bar{\ell}_i\rangle = \bar{\mathcal{A}}_{i\alpha} |\bar{\ell}_\alpha\rangle. \quad (i = 1, 2, \alpha = e, \mu, \tau) \quad (2.41)$$

The amplitudes at the tree level are given by

$$\mathcal{A}_{i\alpha}^0 = \frac{m_{D_{i\alpha}}}{\sqrt{(m_D m_D^\dagger)_{ii}}} \quad \text{and} \quad \bar{\mathcal{A}}_{i\alpha}^0 = \frac{m_{D_{i\alpha}}^*}{\sqrt{(m_D m_D^\dagger)_{ii}}}. \quad (2.42)$$

Since there is no interaction to break the coherence of the quantum states before it inversely decays to N_i , the asymmetry will be produced along the direction of $|\ell_i\rangle$ (or $|\bar{\ell}_i\rangle$) in the lepton flavor space. In that case, the set of classical kinetic equations

relevant for leptogenesis could be written as [146]

$$\frac{dN_{N_i}}{dz} = -D_i(N_{N_i} - N_{N_i}^{\text{eq}}), \text{ with } i = 1, 2 \quad (2.43)$$

$$\frac{dN_{B-L}}{dz} = -\sum_{i=1}^2 \varepsilon_i D_i(N_{N_i} - N_{N_i}^{\text{eq}}) - \sum_{i=1}^2 W_i N_{B-L}, \quad (2.44)$$

with $z = M_1/T$. Eq.2.43 tracks the dynamics of the RH neutrinos (production+decay) while (2.44) tracks the lepton asymmetry which survives in the interplay of the production (first term) and washout (second term), as a function of z . N_{N_i} 's and N_{B-L} are the abundances computed per number of N_i 's in ultra-relativistic thermal equilibrium. Defining $x_{ij} = M_j^2/M_i^2$ and $z_i = z\sqrt{x_{1i}}$, the decay terms can be written as

$$D_i = \frac{\Gamma_{D,i}}{Hz} = K_i x_{1i} z \langle 1/\gamma_i \rangle, \quad (2.45)$$

where total decay rates $\Gamma_{D,i}$ are given by $\Gamma_{D,i} = \bar{\Gamma}_i + \Gamma_i = \Gamma_{D,i}(T=0) \langle 1/\gamma_i \rangle$ with $\langle 1/\gamma_i \rangle$ as the thermally averaged dilation factor and can be expressed as the ratio of two modified Bessel functions as

$$\langle 1/\gamma_i \rangle = \frac{\mathcal{K}_1(z_i)}{\mathcal{K}_2(z_i)}. \quad (2.46)$$

The decay parameter K_i is given by

$$K_i \equiv \Gamma_{D,i}(T=0)/H(T=M_i). \quad (2.47)$$

The equilibrium abundance of N_i is given by $N_{N_i}^{\text{eq}} = \frac{1}{2} z_i^2 \mathcal{K}_2(z_i)$ and the CP asymmetry $\varepsilon_i = \sum_{\alpha} \varepsilon_{i\alpha}$ is given by

$$\varepsilon_i = \sum_{\alpha} \frac{\Gamma_{i\alpha} - \bar{\Gamma}_{i\alpha}}{\Gamma_i + \bar{\Gamma}_i} \quad (2.48)$$

with the flavored CP asymmetry $\varepsilon_{i\alpha}$ as [71]

$$\begin{aligned} \varepsilon_{i\alpha} = & \frac{1}{4\pi v^2 h_{ii}} \sum_{j \neq i} \text{Im}\{h_{ij}(m_D)_{i\alpha}(m_D^*)_{j\alpha}\} \left[f(x_{ij}) + \frac{\sqrt{x_{ij}}(1-x_{ij})}{(1-x_{ij})^2 + h_{jj}^2(16\pi^2 v^4)^{-1}} \right] \\ & + \frac{1}{4\pi v^2 h_{ii}} \sum_{j \neq i} \frac{(1-x_{ij})\text{Im}\{h_{ji}(m_D)_{i\alpha}(m_D^*)_{j\alpha}\}}{(1-x_{ij})^2 + h_{jj}^2(16\pi^2 v^4)^{-1}}, \end{aligned} \quad (2.49)$$

where $h_{ij} \equiv (m_D m_D^\dagger)_{ij}$. The final $B - L$ asymmetry could be written as

$$N_{B-L}^f = N_{B-L}^{\text{in}} e^{-\sum_i \int dz' W_i(z')} + N_{B-L}^{\text{lepto}}, \quad (2.50)$$

where N_{B-L}^{in} could be a possible pre-existing asymmetry at an initial temperature T_{in} and N_{B-L}^{lepto} is the contribution from pure leptogenesis. In this work we assume any pre-existing asymmetry (so called strong thermal condition [147]) is strongly washed out by the heavy RH neutrinos. Therefore, we are in a strong washout scenario. Thus in the washout term in (2.44), the $\Delta L = 1$ scattering term $W_i^{\Delta L=1}$ can be safely neglected [131]. However, a particular washout regime is a matter of choice in our discussion. One can neglect the pre-existing asymmetry assuming there is no source of asymmetry production prior to the leptogenesis phase and explore a weak washout regime as well. In that case inclusion of scattering would only affect the asymmetry production efficiency [131] but the qualitative conclusion drawn in a strong washout regime would remain the same. For our purpose, we shall also neglect the non-resonant part of the $\Delta L = 2$ term $W_i^{\Delta L=2}$ which is relevant only at higher temperature. Now the relevant washout term $W_i \simeq W_i^{\text{ID}}$ can be written as (after properly subtracting the real intermediate state contribution of $\Delta L = 2$ process)

$$W_i^{\text{ID}} = \frac{1}{4} K_i \sqrt{x_{1i}} \mathcal{K}_1(z_i) z_i^3. \quad (2.51)$$

The final baryon to photon ratio is given by

$$\eta_B = a_{sph} \frac{N_{B-L}^{\text{lepto}}}{N_\gamma^{\text{rec}}} \simeq 0.96 \times 10^{-2} N_{B-L}^{\text{lepto}}, \quad (2.52)$$

where N_γ is the photon density at the recombination and the sphaleron conversion coefficient $a_{sph} \sim 1/3$. In a given model, this η_B has to be compared with measured value [148]

$$\eta_B^{\text{CMB}}/10^{-10} = 6.3 \pm 0.3. \quad (2.53)$$

In the mass regime $10^9 \text{ GeV} < M_i < 10^{12} \text{ GeV}$, interactions due to τ^- lepton flavor are fast enough to break the coherent evolution of the quantum states $|\ell_i\rangle$ before it inversely decays to N_i . The $|\ell_i\rangle$ is then projected into a two flavor basis characterized by the eigenstates along the directions of τ and $\tau_i^\perp = e + \mu$. In the three flavor regime, i.e. $M_i < 10^9 \text{ GeV}$, the μ^- lepton flavor comes in to equilibrium thus breaking the coherent evolution of the states which is along τ_i^\perp . One resolves all the flavors (e, μ, τ) individually (for both the flavor regimes, we are assuming strong decoherence so that the density matrix³ is flavor diagonal [68, 150]). Thus for each flavor regime, one has to track the lepton asymmetry in the relevant flavors. For example, if we are in the two flavor regime, the lepton asymmetry has to be tracked in τ and τ_i^\perp flavors. The Boltzmann equations for a generic flavor ‘ α ’ could be written as

$$\frac{dN_{N_i}}{dz} = -D_i(N_{N_i} - N_{N_i}^{\text{eq}}), \text{ with } i = 1, 2 \quad (2.54)$$

$$\frac{dN_{\Delta_\alpha}}{dz} = -\sum_{i=1}^2 \varepsilon_{i\alpha} D_i(N_{N_i} - N_{N_i}^{\text{eq}}) - \sum_{i=1}^2 P_{i\alpha}^0 W_i^{\text{ID}} N_{\Delta_\alpha}. \quad (2.55)$$

Here N_{Δ_α} is the asymmetry in the flavor α analytic solution for which can be obtained

³An elaborate computation of leptogenesis in density matrix formalism is given in Ref. [149]

as

$$N_{\Delta\alpha} = - \sum_i^2 \varepsilon_{i\alpha} \kappa_{i\alpha} \quad (2.56)$$

with the efficiency factor

$$\kappa_{i\alpha}(z) = - \int_{z_{\text{in}}}^{\infty} \frac{dN_{N_i}}{dz'} e^{-\sum_i \int_{z'}^z P_{i\alpha}^0 W_i^{\text{ID}}(z'') dz''} dz'. \quad (2.57)$$

For the purpose of numerical integration, one can set very small value of ‘ $z_{\text{in}}(\sim 0)$ ’ and a very large value for ‘ $z(\sim 10^3)$ ’. The final baryon to photon ratio is then given by

$$\eta_B = 0.96 \times 10^{-2} \sum_{\alpha} N_{\Delta\alpha}. \quad (2.58)$$

The quantity $P_{i\alpha}^0$ is the tree level probability of a quantum state produced by the i th heavy neutrino being in the flavor α and has an expression

$$P_{i\alpha}^0 \equiv K_{i\alpha}/K_i, \quad (2.59)$$

where $K_{i\alpha}$ is the flavored decay parameter defined as

$$K_{i\alpha} = \frac{\Gamma_{i\alpha} + \bar{\Gamma}_{i\alpha}}{H(T = M_i)} \equiv \frac{|m_{D_{i\alpha}}|^2}{M_i m^*} \quad (2.60)$$

with $m^* \simeq 10^{-3}$ being the equilibrium neutrino mass. Let us trace out another important parameter $\Delta P_{i\alpha} = P_{i\alpha} - \bar{P}_{i\alpha}$ strongly relevant to our discussion. The tree+loop level projectors are given by $P_{i\alpha} = |\mathcal{A}_{i\alpha}|^2 = P_{i\alpha}^0 + \frac{\Delta P_{i\alpha}}{2}$, $\bar{P}_{i\alpha} = |\bar{\mathcal{A}}_{i\alpha}|^2 = P_{i\alpha}^0 - \frac{\Delta P_{i\alpha}}{2}$. The quantity $\Delta P_{i\alpha}$, the difference between the tree+loop level projectors, is nonzero since, in general $|\mathcal{A}_{i\alpha}| \neq |\bar{\mathcal{A}}_{i\alpha}|$ [67]. Now the flavored CP asymmetry

parameter $\varepsilon_{i\alpha}$ of (2.48) can be simplified as

$$\varepsilon_{i\alpha} = P_{i\alpha}^0 \varepsilon_i + \Delta P_{i\alpha}/2. \quad (2.61)$$

Though the quantity $\Delta P_{i\alpha}$ is not so significant in the washout terms, for the CP asymmetry parameter it is remarkably relevant. In fact, we show that the entire source of CP violation, in a particular flavor ‘ α ’ arises due to $\Delta P_{i\alpha}$.

As mentioned in the introduction, here we discuss only the three flavor regime ($M_i < 10^9$ GeV) of the leptogenesis to show the dramatic difference between the conclusion drawn in case of a CP extended $\mu\tau$ interchange [106, 145, 151] and the proposed CP extended $\mu\tau$ mixing. Let’s clarify explicitly why we do that.

One flavor regime: First of all, for the one flavor regime ($M_i > 10^{12}$ GeV), the second term in (2.49) is vanishing when summed over ‘ α ’, i.e., $\text{Im}\{h_{ji}(m_D)_{i\alpha}(m_D^*)_{j\alpha}\} = \text{Im}[|h_{ji}|^2] = 0$. The first term is proportional to $\text{Im}\{h_{ij}^2\}$. Using (2.40), the ‘ $h = m_D m_D^\dagger$ ’ can shown to be a real matrix. Thus the flavor summed CP asymmetry $\varepsilon_i = \sum_\alpha \varepsilon_{i\alpha}$ vanishes for any ‘ i ’. Therefore successful baryogenesis is not possible in the unflavored regime. This result has also been obtained in CP extended $\mu\tau$ interchange symmetry [106, 145, 151]. One can also show $\varepsilon_{ie} = 0$, since the first column of the m_D matrix in (2.40) is real. Thus similar to CP extended $\mu\tau$ interchange, $\varepsilon_{i\mu} \equiv \Delta P_{i\mu}/2 = -\varepsilon_{i\tau}$. Therefore, in the one flavor regime, the results obtained for leptogenesis in CP extended $\mu\tau$ mixing, are similar to CP extended $\mu\tau$ interchange.

Two flavor regime: As already mentioned, we are probing a strong washout

scenario: any pre-existing asymmetry that was present prior to the phase of leptogenesis has been strongly washed out. This is possible only in the three flavor regime. For the two flavor regime ($10^9 \text{ GeV} < M_i < 10^{12} \text{ GeV}$), this is not possible because though in the direction of τ flavor the asymmetry could be washed out assuming $K_{i\tau} \gg 1$, a component of the asymmetry would always survive in the direction orthogonal to the τ_\perp [73, 150], irrespective of the value of K_{τ_\perp} . Thus a pure leptogenesis scenario breaks down. In any case, as mentioned earlier, along with the strong washout scenario, one can also probe the weak washout regime relaxing the strong-thermal condition (pre-existing asymmetry), which has been done so far in the literature in the context of $\text{CP}^{\mu\tau}$. However, for the latter case, apart from showing a successful baryogenesis, we hardly expect any prediction on low energy neutrino parameters, since the number of parameters in m_D is still larger than the number of experimental constraints. Thus in the two flavor regime, from leptogenesis perspective, there will be no significant difference between a CP extended $\mu\tau$ interchange and a CP extended $\mu\tau$ mixing. But certainly differences will be there if one assumes texture zeros on top of the CP extended $\mu\tau$ mixing [110, 122, 152] or imposes the symmetry in a minimal seesaw framework [151, 152]. Since in that case there would be less number of parameters and one might expect predictions from the baryogenesis constraint on the physical parameters such as θ_{23} which is nonmaximal in general in the $\mu\tau$ mixing scheme.

Three flavor regime: Now coming back to the discussion of leptogenesis in the three flavor regime, first of all one has to go beyond the hierarchical scenario, since in the hierarchical limit the CP asymmetry parameter, say, $\varepsilon_{1\alpha}$ is proportional to M_1 and if $M_1 < 10^9 \text{ GeV}$, one can not generate the observed baryon asymmetry [153]. However if the mass differences of the RH neutrinos are close enough, one expects a significant enhancement in the loop functions, particularly self energy contribution

to the CP asymmetry parameter increases and therefore even if $M_i < 10^9$ GeV, required baryon asymmetry could be generated due to this enhancement in the CP asymmetry parameter [74]. However, in that scenario one has to consider the asymmetry generated by all the heavy neutrinos, since in the standard hierarchical scenario, contribution from the heavier RH neutrinos are washed out by the lighter RH neutrinos. In the limit of quasi-degeneracy (QD) in the RH neutrino spectrum, the contribution from the heavier neutrinos can not be washed out. For an explicit analytical explanation of leptogenesis due to QD mass spectrum, we refer to [154]. For the CP extended $\mu\tau$ interchange symmetry as well as mixing, the N_{B-L} asymmetry could be written as

$$N_{B-L}^f = \sum_{\alpha} N_{\Delta_{\alpha}} = - \sum_i^2 (\varepsilon_{i\tau}\kappa_{i\tau} + \varepsilon_{i\mu}\kappa_{i\mu}) = - \sum_i^2 \varepsilon_{i\tau} (\kappa_{i\tau} - \kappa_{i\mu}) = - \sum_i^2 \varepsilon_{i\tau}\kappa_i^{\text{eff}} \quad (2.62)$$

where we use the fact that $\varepsilon_{ie} = 0$ and $\varepsilon_{i\mu} = -\varepsilon_{i\tau}$ and at $z \rightarrow \infty$, the efficiency factor $\kappa_{i\alpha}$ has the expression

$$\kappa_{i\alpha} = - \int_0^{\infty} \frac{dN_{N_i}}{dz'} e^{-\sum_i \int_{z'}^{\infty} (K_{i\alpha}/K_i) W_i^{\text{ID}}(z'') dz''} dz' \quad \alpha = (\tau, \mu). \quad (2.63)$$

Now notice that, for CP extended $\mu\tau$ interchange ($\theta_g \rightarrow \pi/4$), using (2.40) and (2.60) the decay parameters can be obtained as

$$K_{1\mu}^I = \frac{b_1^2 + b_2^2}{M_1 m^*} = K_{1\tau}^I, \quad K_{2\mu}^I = \frac{c_1^2 + c_2^2}{M_2 m^*} = K_{2\tau}^I, \quad (2.64)$$

where ‘I’ stands for ‘Interchange’. Thus from (2.63) one concludes $\kappa_{i\mu} = \kappa_{i\tau}$ and hence, from (2.62), $N_{B-L}^f = 0$. Therefore, even if we are in the resonance regime of leptogenesis, baryon asymmetry vanishes due to the exact cancellation of the efficiency factors. But for the CP extended $\mu\tau$ mixing this is not the case. This is since, though the decay parameters $K_{i\mu}$ have the same expression as shown in (2.64), since $\theta_g \neq 0$

in general, $K_{i\tau}^M$ can be obtained as

$$K_{i\tau}^M = \frac{[\text{Re}(m_D)_{i\mu}]^2 \tan^2 \theta_g + [\text{Im}(m_D)_{i\mu}]^2 \cot^2 \theta_g}{M_i m^*} \quad (2.65)$$

which reduces to $K_{i\tau}^I$ of (2.64) in the limit $\theta_g \rightarrow \pi/4$. Here ‘ M ’ stands for ‘Mixing’. In fact, given the distribution of δ in Fig.2.5, we can approximate $\sin \delta \sim 1$ and therefore using (2.30), we can recast $K_{i\tau}^M$ as

$$K_{i\tau}^M = \frac{[\text{Re}(m_D)_{i\mu}]^2 \tan^2 \theta_{23} + [\text{Im}(m_D)_{i\mu}]^2 \cot^2 \theta_{23}}{M_i m^*}. \quad (2.66)$$

Thus since $K_{i\tau}^M \neq K_{i\mu}^M$, from (2.62) N_{B-L} is nonvanishing. It is now clear that to obtain a nonzero baryon asymmetry, in this CP extended $\mu\tau$ mixing framework, one always needs deviation of θ_{23} from maximality. Now parameterizing θ_{23} as $\theta_{23} = (\pi/4 + \delta_x)$, where the parameter δ_x accounts for the nonmaximality of θ_{23} , (2.66) could further be simplified as

$$K_{i\tau}^M = K_{i\tau}^I (1 + 4\delta_x \cos 2\xi_i), \quad \xi_i = \tan^{-1} \frac{\text{Im}[(m_D)_{i\mu}]}{\text{Re}[(m_D)_{i\mu}]}. \quad (2.67)$$

Thus except for a very special solution $\cos 2\xi_i = 0$, a nonvanishing baryon asymmetry is guaranteed by a nonmaximal value of θ_{23} . Now, the κ_i^{eff} of 2.62 can be obtained as

$$\kappa_i^{\text{eff}} = 4\delta_x K_{i\tau}^I \cos 2\xi \int_0^\infty \frac{dN_{N_i}}{dz'} e^{-\sum_i \int_{z'}^\infty K_{i\tau}^I K_i^{-1} W_i^{\text{ID}}(z'') dz''} \sum_i \int_{z'}^\infty K_i^{-1} W_i^{\text{ID}}(z'') dz'' d\mathcal{A} \quad (2.68)$$

For convenience, we may choose $\cos 2\xi_i \equiv \cos 2\xi = 1$ ⁴. Then we may further

⁴This is always not the case. The parameter ξ is model dependent. However, as we have already pointed out earlier, the models with CP symmetries, one can not constrain the mass matrix element only by oscillation data, unless some special conditions are assumed [110]. Thus $\cos 2\xi$ would be a probable solution.

parametrize the κ_i^{eff} as

$$\kappa_i^{\text{eff}} \leq \bar{m}_{\text{max}} \frac{4\delta_x}{m^*} \int_0^\infty \frac{dN_{N_i}}{dz'} e^{-\sum_i \int_{z'}^\infty K_{i\tau}^I K_i^{-1} W_i^{\text{ID}}(z'') dz''} \sum_i \int_{z'}^\infty K_i^{-1} W_i^{\text{ID}}(z'') dz'' dz' \quad (2.69)$$

where \bar{m} denotes the overall mass scale of the light neutrinos. The effective efficiency factor in (2.69) has few interesting features. First, from the perspective of κ_1^{eff} i.e., effective production efficiency due of N_1 , it suffers a two step suppression. The first one comes from the N_2 -washout, since in contrast to the hierarchical scenario, in the QD limit N_2 washout significantly reduces the asymmetry produced by N_1 [154]. The second one is due the parameter δ_x which appears as a pre-factor in (2.69). In case of κ_2^{eff} , firstly it increases since the N_1 interactions cannot fully washout the asymmetry produced by N_2 (the production from N_2 is still on), however again similar to κ_1^{eff} , it faces a suppression by δ_x . However, due to the small mass splitting between the masses of the RH neutrinos, one obtains comparable production efficiencies ($\kappa_1^{\text{eff}} \simeq \kappa_2^{\text{eff}}$). Let us now have a numerical estimate of the final baryon asymmetry. From (2.53), it is evident that $N_{B-L} = \sum_\alpha N_{\Delta_\alpha} \simeq 6.3 \times 10^{-8}$. Now if we choose a very small value of the pre-factor in (2.68), say, $4\delta_x K_{i\tau}^I \cos 2\xi \simeq 0.1$ (this can be done, e.g., either by choosing a very small value of $\cos 2\xi$ or very small value of δ_x), a numerical integration of (2.68) gives $\kappa_i^{\text{eff}} \simeq 2 \times 10^{-5}$, where we have assumed $K_{i\mu} = K_{i\tau} = 25$. Therefore, to be consistent with the observed value of N_{B-L} , we require $|\varepsilon_{i\tau}| \simeq 1.5 \times 10^{-3}$. This has also been reproduced in Fig.2.6 by solving the Boltzmann equations, assuming both the RH neutrinos contribute equally (this is justified when one chooses very small mass splitting between RH neutrinos, which is needed in this scheme to obtain resonance in the three flavor regime). One can also comment on the mass scale of the RH neutrinos. For example, let say the resonant enhancement of the CP asymmetry happens when the mass difference $\Delta = \sqrt{x_{12}} - 1 \simeq 10^{-8}$. Then assuming the elements of m_D in (2.49) as $m_D \sim \sqrt{M\bar{m}}$ one obtains the mass scale of the RH neutrinos

$M \sim 10^7$ GeV. One can explore another interesting situation, assuming $\cos 2\xi = 1$, $\bar{m}_{\max} \simeq \sqrt{|\Delta m_{23}^2|}$ and the current best-fit of $\theta_{23} \simeq 49.6^\circ$ ($\delta_x \sim 4.6^\circ$). This would correspond to the value of the pre-factor in (2.69) as $\bar{m}_{\max} \frac{4\delta_x}{m^*} \simeq 8$. In that case the correct value of η_B could be generated with $|\varepsilon_{i\tau}| \simeq 2.6 \times 10^{-5}$ and consequently the mass scale of the RH neutrinos could be lowered to ~ 100 TeV.

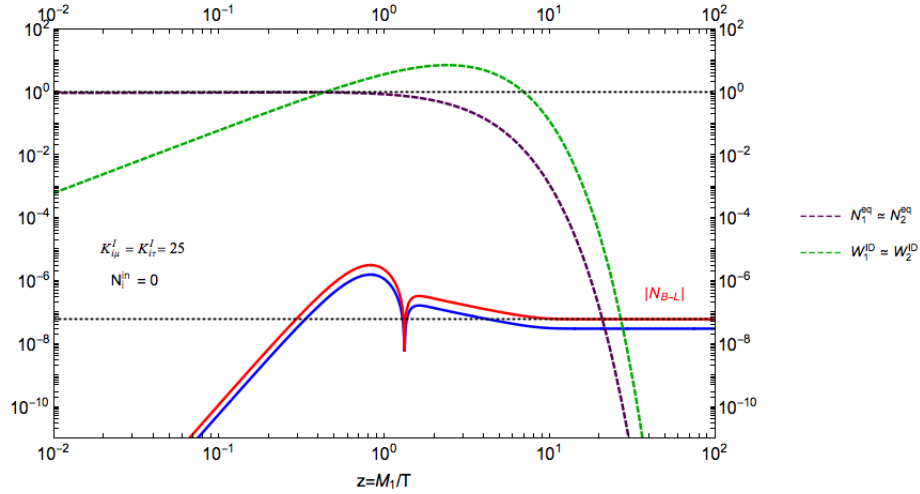


Figure 2.6: Variation of N_{B-L} with z assuming $4\delta_x K_{i\tau}^I \cos 2\xi = 0.1$ and $|\varepsilon_{i\tau}| \simeq 1.5 \times 10^{-3}$. The blue line is the contribution from a single RH neutrino. The red line, matching the observed range, denotes contributions from both the RH neutrinos.

Having established the possibility of resonant leptogenesis in the CP extended $\mu\tau$ mixing scheme, the main purpose of the leptogenesis study in this work is served. However, still one would like to consider some other interesting possibilities such as flavor coupling [133–135]. So far we have discussed the leptogenesis scenario without flavor coupling matrix [132] in the Boltzmann equations. With flavor couplings the Boltzmann equation of (2.54) and (2.55) will be modified as

$$\frac{dN_{N_i}}{dz} = -D_i(N_{N_i} - N_{N_i}^{\text{eq}}), \quad \text{with } i = 1, 2 \quad (2.70)$$

$$\frac{dN_{\Delta_\alpha}}{dz} = -\sum_{i=1}^2 \varepsilon_{i\alpha} D_i(N_{N_i} - N_{N_i}^{\text{eq}}) - \sum_{i=1}^2 P_{i\alpha}^0 W_i^{\text{ID}} \sum_{\beta=e,\mu,\tau} C_{\alpha\beta} N_{\Delta_\beta}, \quad (2.71)$$

where the flavor coupling matrix $C_{\alpha\beta}$ is given by

$$C_{\alpha\beta} = \begin{pmatrix} 188/179 & 32/179 & 32/179 \\ 49/358 & 500/537 & 142/537 \\ 49/358 & 142/537 & 500/537 \end{pmatrix} \quad (2.72)$$

which accounts for the asymmetry in lepton doublets as well as Higgs asymmetry. One might wonder whether the flavor coupling effect can save the situation for the CP extended $\mu\tau$ interchange symmetry, i.e., whether the entries of the flavor coupling can create a mismatch between the decay parameters so that one obtains a nonzero κ_i^{eff} . Starting from the simplest case, i.e., assuming a diagonal C matrix (which is usual in the study of leptogenesis in the neutrino mass models), if one writes the Boltzmann equations, the scenario remains unchanged. This is because the elements $C_{\mu\mu}$ and $C_{\tau\tau}$ are the same and therefore, are unable to produce any mismatch between the decay parameters. Thus similar to the previous case ($C = \mathbb{I}$), no net lepton asymmetry will generate. Interestingly, even if one assumes the nondiagonal C matrix, one cannot generate a nonzero lepton asymmetry. Since, $P_{i\mu}^0 = P_{i\tau}^0$, the μ and τ flavor will couple each other with equal strength ($P_{i\mu}^0 = 142/537$). Therefore, there will be no net asymmetry mismatch because the production is equal an opposite ($\varepsilon_{i\mu} = -\varepsilon_{i\tau}$). Mathematically, this can be understood in the following way. We can go to a basis where the Boltzmann equation in (2.71) is diagonal in a generic flavor, say α' . This can be done by the means of a unitary transformation as

$$\frac{dN_{\Delta_{\alpha'}}}{dz} = - \sum_{i=1}^2 \varepsilon_{i\alpha'} D_i (N_{N_i} - N_{N_i}^{\text{eq}}) - \sum_{i=1}^2 W_i^{\text{ID}} V^{-1} P_{i\alpha}^0 C_{\alpha\beta} V N_{\Delta_{\beta'}}, \quad (2.73)$$

where

$$N_{\Delta_{\beta'}} = V^{-1} N_{\Delta_{\beta}}, \quad \varepsilon_{i\alpha'} = V^{-1} \varepsilon_{i\alpha}, \quad V^{-1} P_{i\alpha}^0 C_{\alpha\beta} V = P_{i\beta'}^0 \delta_{\alpha'\beta'}. \quad (2.74)$$

Now similar to (2.56), the N_{B-L} in the prime basis can be written as

$$N_{B-L} = \sum_{\alpha'} N_{\Delta_{\alpha'}} = - \sum_{\alpha'} \sum_i^2 \varepsilon_{i\alpha'} \kappa_{i\alpha'}. \quad (2.75)$$

For numerical computation, we assume that the total decay parameter $K_i = 60$, $K_{i\mu} = K_{i\tau} = 25$. Thus, the matrix V which diagonalizes $P_{i\alpha}^0 C_{\alpha\beta}$ is given by

$$V = \begin{pmatrix} 0.125 & 0.000 & -0.971 \\ 0.701 & -0.707 & 0.166 \\ 0.701 & 0.707 & 0.166. \end{pmatrix}. \quad (2.76)$$

This implies

$$\begin{pmatrix} \varepsilon_{ie'} \\ \varepsilon_{i\mu'} \\ \varepsilon_{i\tau'} \end{pmatrix} = \begin{pmatrix} 0.125 & 0.000 & -0.971 \\ 0.701 & -0.707 & 0.166 \\ 0.701 & 0.707 & 0.166. \end{pmatrix}^{-1} \begin{pmatrix} \varepsilon_{ie} \\ \varepsilon_{i\mu} \\ \varepsilon_{i\tau} \end{pmatrix} = \begin{pmatrix} 0 \\ 1.414\varepsilon_{i\tau} \\ 0 \end{pmatrix}. \quad (2.77)$$

Therefore the asymmetry vector in the prime basis is given by

$$\begin{pmatrix} N_{\Delta_{e'}} \\ N_{\Delta_{\mu'}} \\ N_{\Delta_{\tau'}} \end{pmatrix} = \begin{pmatrix} 0 \\ -1.414 \sum_i \varepsilon_{i\tau} \kappa_{i\mu'} \\ 0 \end{pmatrix} \quad (2.78)$$

which should then be transformed in the unprimed basis (original basis of leptogenesis) as

$$\begin{pmatrix} N_{\Delta_e} \\ N_{\Delta_\mu} \\ N_{\Delta_\tau} \end{pmatrix} = \begin{pmatrix} 0.125 & 0.000 & -0.971 \\ 0.701 & -0.707 & 0.166 \\ 0.701 & 0.707 & 0.166. \end{pmatrix} \begin{pmatrix} 0 \\ -1.414 \sum_i \varepsilon_{i\tau} \kappa_{i\mu} \\ 0 \end{pmatrix} = \begin{pmatrix} 0 \\ 0.996 \sum_i \varepsilon_{i\tau} \kappa_{i\mu'} \\ -0.996 \sum_i \varepsilon_{i\tau} \kappa_{i\mu'} \end{pmatrix} \quad (2.79)$$

Thus $\sum_{\alpha} N_{\Delta_{\alpha}} = 0$ and we have vanishing N_{B-L} . However, for the proposed $\mu\tau$ mixing, where in general, $P_{i\mu}^0 \neq P_{i\tau}^0$, the asymmetry in the μ and τ flavor will couple to each other with different coupling strength. Thus, even if we consider diagonal C matrix, we obtain a nonzero lepton asymmetry. But most interestingly, when we consider the general nondiagonal C matrix, a part of the net asymmetry, generated due to the interplay between the μ and τ flavor, will also be injected in the e flavor.

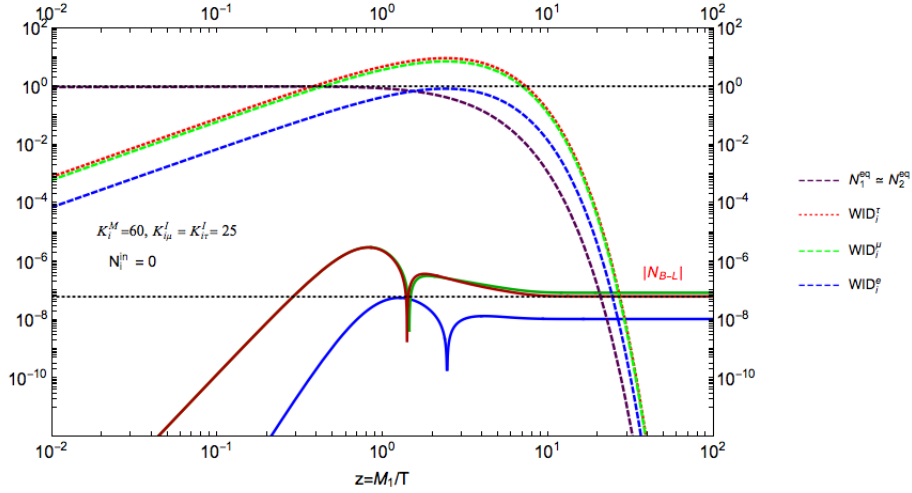


Figure 2.7: Variation of N_{B-L} with z assuming $\overline{m}_{\max} \frac{4\delta_x}{m^*} = 8$ and $|\varepsilon_{i\tau}| \simeq 2.67 \times 10^{-5}$. The blue line is the asymmetry injected in the electron flavor through flavor couplings. The green line is net contribution from the muon and tau flavor asymmetries. The red line which matches the observed range after taking into account the injected asymmetry in the electron flavor.

Thus even if we start from a scenario with vanishing production term in the electron flavor ($\varepsilon_{ie} = 0$) due to the off-diagonal terms mainly due to the $C_{e\mu}$ and $C_{e\tau}$ term we can generate a nonvanishing lepton asymmetry in the electron flavor. Though, for a fixed value of $\varepsilon_{i\alpha}$, magnitude of the injected asymmetry will depend on how strong the mismatch of the asymmetry in muon and tau flavor. In Fig.2.7, along with number densities of the RH neutrinos and flavored inverse decay rates

(dashed lines), we present the variation of $|N_{B-L}|$ (solid lines). The blue line (solid) represents the injected asymmetry in the electron flavor. The green (solid) represents the net asymmetry generated by muon and tau flavor. The red (solid) line is the final N_{B-L} when we combine all the flavors. This is clear that after taking into account the asymmetry in electron flavor, we obtain correct value of N_{B-L} . This shows the importance of the off-diagonal terms in the flavor coupling matrix which are neglected in general in the computation in leptogenesis. The discussed CP extended $\mu\tau$ mixing is thus a novel low energy model which facilitates the understanding of flavor couplings in Boltzmann equations for leptogenesis in a very clear way.

Before concluding, we would like to highlight the main results discussed in this chapter and make few remarks regarding future prospect of this work.

- We derive model independent correlations between the Dirac CP phase and the light neutrino mixing angles for generalized associate $\mu\tau$ symmetries which we name as the associate $\mu\tau$ mixing symmetries.

- We have shown that the current data on δ and θ_{23} could be better explained by the proposed mixing symmetry.

- After a general discussion on $\mu\tau$ mixing which can be realized in many of the neutrino mass models, we discuss the CP extension of it and find novel testable correlations between δ and the light neutrino mixing angles.

- We then discuss the baryogenesis via leptogenesis mechanism in the three flavor regime and show unlike the CP extended $\mu\tau$ interchange, a resonant leptogenesis is possible in the CP extended $\mu\tau$ mixing and a nonzero baryon to photon ratio always requires nonmaximal θ_{23} which is now preferred by the current data.

- We have shown quantitatively, even after inclusion of flavor coupling effect in

leptogenesis computation, the usually drawn conclusion of a vanishing asymmetry in the fully flavored regime is still valid for the CP extended $\mu\tau$ interchange symmetry.

- The proposed CP extended $\mu\tau$ mixing is a novel example of a neutrino mass model where the role of flavor couplings in leptogenesis mechanism is very explicit.

This chapter is written entirely from the perspective of neutrino mixing. While both the $\mu\tau$ mixing and its CP extensions are very appealing for predictions of the light neutrino mixing, they do not entertain predictions in the mass sector. Therefore, explicit mass models with less number of parameters and with $\mu\tau$ mixing or its CP extension would be of special interest to look for. Since in that case, in addition to all the model independent correlations derived in this chapter, one would have definite statements on the neutrino masses. These models would also carry interesting features for leptogenesis. For instance, as we have demonstrated that in the CP extension of $\mu\tau$ mixing, since we do not have predictions on the masses, we have assumed conditions such as $\cos 2\xi = 1$, $K_{i\tau} = 25$ etc. But in the models with lesser number of parameters, one would have exact statements on the assumed parameters. In such a case, we can also have precise statement on the nonmaximality of θ_{23} required to generate the observed baryon asymmetry via resonant leptogenesis even when the RH mass scale is of $\mathcal{O}(\text{TeV})$ [74, 155]. To constrain the parameter space of such predictive models, it would be interesting to consider the heavy neutrino flavor oscillation effects [156–158] to increase the robustness of the low energy predictions.

2.5 Conclusions

In this Chapter, we promote the idea of $\mu\tau$ mixing symmetry—a generalization of the $\mu\tau$ interchange symmetry. First we present a systematic derivation of the

model independent correlations between δ and the mixing angles θ_{ij} in this scenario. It shows that the simultaneous maximality of δ and θ_{23} (currently disfavored by the neutrino oscillation data) which follows as a robust outcome of the $\mu\tau$ interchange symmetry can be relaxed. We show that the present data as well as the current trend on δ and θ_{23} demands a deviation from the $\mu\tau$ interchange scenario. Parameterizing the deviation from $\mu\tau$ interchange through a single real parameter θ_g , we comment on the range of deviation as allowed by the current data. We also demonstrate that the parameter θ_g can be related to the parameters of those mass models that exhibit $\mu\tau$ mixing at low energies. In particular, we discuss the CP extended version of the $\mu\tau$ mixing symmetry and derive novel correlations among δ and the neutrino mixing angles. Particularly, we show that in this class of models, the most probable values of δ prefers maximal Dirac CP violation while θ_{23} is not necessarily maximal. Unlike the CP extended version of the $\mu\tau$ interchange, we show that the mixing scenario is able to explain the observed baryon asymmetry in the three flavor regime via the mechanism of resonant leptogenesis. Particularly we show that except a very special choice in the parameter space, the observed baryon asymmetry is proportional to the deviation of θ_{23} from its maximality. Thus to explain baryon asymmetry simultaneously with neutrino mixing, the CP extended $\mu\tau$ mixing symmetry favors nonmaximal values of θ_{23} . After a qualitative as well as quantitative comparison of the leptogenesis scenario in the three flavor regime between the CP extended interchange and mixing symmetry, we show, while for the interchange scenario, even if we include off-diagonal flavor coupling matrix (C) in the Boltzmann equation for the leptonic number densities, the usual conclusion of obtaining a vanishing asymmetry in the three flavor regime is unchanged, however, in the mixing scheme, the off-diagonal terms of the C matrix play a crucial role. In particular, the advocated CP extension of $\mu\tau$ mixing turns out to be a novel example of a low energy model of neutrino mass, in which even in absence of any source term for the lepton asymmetry in a flavor, a sizable asymmetry

can get injected to that flavor through the off-diagonal elements of the flavor coupling matrix. This emphasizes the importance of using the general structure of the flavor coupling matrix (usually assumed to be diagonal in most of the leptogenesis studies) in the network of Boltzmann equations.

Chapter 3

Mixed $\mu\tau$ antisymmetry for neutrinos with nonstandard CP extension

3.1 Introduction

Various discrete flavor symmetries have been proposed in the $\mu\tau$ sector of neutrinos to understand the observed pattern of neutrino mixing. One class of such symmetries assume $\mu\tau$ mixing as discussed in Chapter 2. It is an invariance under the transformation

$$\nu_{Ll} \rightarrow G_{lm}^\theta \nu_{Lm} \quad (3.1)$$

where G^θ denotes the generator of a residual \mathbb{Z}_2 symmetry while the subscript L stands for the left-chiral flavor neutrino fields. The indices l, m denote the lepton flavors e, μ, τ . In flavor space, G^θ has the generic form

$$G^\theta = \begin{pmatrix} -1 & 0 & 0 \\ 0 & -\cos \theta & \sin \theta \\ 0 & \sin \theta & \cos \theta \end{pmatrix}, \quad (3.2)$$

where θ is a mixing parameter. The signs in (3.2) are in accordance with our choice $\det G^\theta$ to be +1 without any loss of generality. The special case of (3.1) for $\theta = \pi/2$ is known in the literature as $\mu\tau$ interchange symmetry which can arise from some high energy flavor symmetry such as S_4 [94]. Further, there exists a substantial body of work [98, 113, 114, 159–164] investigating the phenomenological consequences of (3.1). It has been found that the reactor mixing angle θ_{13} vanishes if one imposes the symmetry (3.1) with (3.2). Since this possibility has now been excluded at more than 10σ [115], this symmetry has to be abandoned.

An interesting variant of (3.1) is the symmetry of CP transformed [99–105, 110, 123–130, 165–175] $\mu\tau$ mixing, as proposed in Ref. [143]. This is an invariance of the neutrino Majorana mass term under the transformation

$$\nu_{Ll} \rightarrow iG_{lm}^\theta \gamma^0 \nu_{Lm}^C \quad (3.3)$$

with G^θ as in (3.2) and $\nu_{Ll}^C = C(\overline{\nu_{Ll}})^T$. The corresponding phenomenological consequences have been studied [143]. A different approach using the idea of littlest $\mu\tau$ seesaw [176, 177] has also been recently proposed allowing slight deviations from maximal θ_{23} and maximal Dirac CP violation. It should be noted that the $\theta \rightarrow \pi/2$ limit of (3.3), referred to as a CP transformed $\mu\tau$ interchange symmetry ($\text{CP}^{\mu\tau}$), had earlier been extensively studied [109] and avoids the problem of a vanishing reactor angle. However, it predicts maximal values for the atmospheric mixing angle θ_{23} and the Dirac CP phase δ , namely $\theta_{23} = \pi/4$ and $\cos \delta = 0$. Such a possibility, though still allowed by current experimental limits, is being challenged by ongoing and forthcoming precision measurements of these quantities. In case the maximality of either quantity is ruled out in future, CP transformed $\mu\tau$ interchange symmetry will be excluded.

In this work, we propose a complex antisymmetric extension of (3.3) using a \mathbb{Z}_4 generator $\mathcal{G}^\theta = iG^\theta$

$$\nu_{Li} \rightarrow i\mathcal{G}_{lm}^\theta \gamma^0 \nu_{Lm}^C. \quad (3.4)$$

A special case of such an invariance with $\theta = \pi/2$ was proposed by some of us in Ref. [151]. The latter avoids the problem of a vanishing θ_{13} but leads to maximal values of the atmospheric mixing angle θ_{23} and the Dirac CP phase δ . As explained above, these results may not survive for much longer. In this situation our proposal of an invariance under (3.4) with $\theta \neq \pi/2$ assumes a special significance since it allows any arbitrary nonzero value of θ_{13} and nonmaximal θ_{23} depending on the parameter θ . Since in this work we concentrate on the low-energy phenomenological consequences, we start from the effective field transformation (3.4) without providing a larger symmetry that embeds it. In case of CP combined with a flavor symmetry, a nontrivial challenge would be to satisfy the consistency conditions [99, 100, 102–105, 110, 123–130, 165–175]. Now real $\mu\tau$ interchange antisymmetry [178] has been shown to arise in a class of explicit models with larger discrete symmetries including \mathbb{Z}_4 while Ref. [179, 180] discusses that the neutrino (Majorana) mass matrix can enjoy pure flavor antisymmetry under some discrete subgroups contained in A_5 . Again, a real mixed $\mu\tau$ symmetry [181] arises in a model where the charged lepton and neutrino mass matrices are invariant under specific residual symmetries contained in the finite discrete subgroups of $O(3)$. The latter work provides an explicit model based on A_5 maintaining the mixed $\mu\tau$ symmetry. However, such a demonstration is lacking in the literature for the corresponding CP-transformed (complex extended) cases.

The rest of the work is organized as follows. Sec.5.2 deals with the symmetries of the neutrino Majorana mass matrix M_ν and the most general parametrization of M_ν that is invariant under (3.4). Sec.5.3 contains the evaluation of Majorana phases and a definite relation between the leptonic Dirac CP phase and the atmospheric

mixing angle θ_{23} that involves the $\mu\tau$ mixing parameter θ . In Sec.5.4 a numerical analysis of our proposal is presented utilizing neutrino oscillation data; this entails the extraction of the allowed parameter space and the prediction of light neutrino masses. It consists of three subsections. The first considers neutrinoless double beta decay; the second includes the range of variation of the CP asymmetry parameter $A_{\mu e}$ in experiments such as T2K, No ν A and DUNE for both types of mass ordering; the variation of flavor flux ratios at neutrino telescopes is considered in the third. In Sec.3.5 we summarize the results of our analysis.

3.2 Complex mixed $\mu\tau$ antisymmetry of the neutrino Majorana mass matrix

The effective neutrino Majorana mass term in the Lagrangian density reads

$$-\mathcal{L}_{mass}^{\nu} = \frac{1}{2} \overline{\nu_{Ll}^C} (M_{\nu})_{lm} \nu_{Lm} + h.c. \quad (3.5)$$

with $\nu_{Ll}^C = C \overline{(\nu_{Ll})}^T$ and the subscripts l, m spanning the lepton flavor indices e, μ, τ while the subscript L denotes left-chiral neutrino fields. Here, M_{ν} is a complex symmetric matrix ($M_{\nu}^* \neq M_{\nu} = M_{\nu}^T$) in lepton flavor space. It can be diagonalized by a similarity transformation with a unitary matrix U :

$$U^T M_{\nu} U = M_{\nu}^d \equiv \text{diag} (m_1, m_2, m_3). \quad (3.6)$$

Here m_i ($i = 1, 2, 3$) are real and we assume that $m_i \geq 0$. Without any loss of generality, we work in the diagonal basis of the charged leptons so that U can be

related to the PMNS matrix U_{PMNS} :

$$U = P_\phi U_{PMNS} \equiv P_\phi \begin{pmatrix} c_{12}c_{13} & e^{i\frac{\alpha}{2}}s_{12}c_{13} & s_{13}e^{-i(\delta-\frac{\beta}{2})} \\ -s_{12}c_{23} - c_{12}s_{23}s_{13}e^{i\delta} & e^{i\frac{\alpha}{2}}(c_{12}c_{23} - s_{12}s_{13}s_{23}e^{i\delta}) & c_{13}s_{23}e^{i\frac{\beta}{2}} \\ s_{12}s_{23} - c_{12}s_{13}c_{23}e^{i\delta} & e^{i\frac{\alpha}{2}}(-c_{12}s_{23} - s_{12}s_{13}c_{23}e^{i\delta}) & c_{13}c_{23}e^{i\frac{\beta}{2}} \end{pmatrix}, \quad (3.7)$$

where $P_\phi = \text{diag}(e^{i\phi_1}, e^{i\phi_2}, e^{i\phi_3})$ is an unphysical diagonal phase matrix and $c_{ij} \equiv \cos\theta_{ij}$, $s_{ij} \equiv \sin\theta_{ij}$ with the mixing angles $\theta_{ij} \in [0, \pi/2]$. We follow the PDG convention [112] but denote our Majorana phases by α and β instead of α_{21} and α_{31} . CP-violation enters through nontrivial values of the Dirac phase δ and of the Majorana phases α, β with $\delta, \alpha, \beta \in [0, 2\pi]$.

The effect of our proposed invariance under (3.4) on the neutrino Majorana mass matrix would be

$$\mathcal{G}^{\theta T} M_\nu \mathcal{G}^\theta = -M_\nu^*. \quad (3.8)$$

\mathcal{G}^θ in (3.8) is given by iG^θ where G^θ was defined in (3.2). In flavor space, the most generally parameterized 3×3 complex symmetric mass matrix obeying (3.8) is given by

$$M_\nu^{CP\theta A} = \begin{pmatrix} ix & a_1 + ia_2 & a_1 t_\theta^{-1} - ia_2 t_\theta \\ a_1 + ia_2 & y_1 + iy_2 & y_1 c_\theta s_\theta^{-1} + ic \\ a_1 t_\theta^{-1} - ia_2 t_\theta & y_1 c_\theta s_\theta^{-1} + ic & -y_1 + i(y_2 + 2cc_\theta s_\theta^{-1}) \end{pmatrix}, \quad (3.9)$$

where $c_\theta \equiv \cos\theta$, $s_\theta \equiv \sin\theta$ and $t_\theta \equiv \tan\frac{\theta}{2}$. In (3.9), there are seven real free parameters $x, a_{1,2}, c, y_1, y_2$ and θ . As expected, the limit $\theta \rightarrow \pi/2$ gives back the mass matrix $M_\nu^{CP\mu\tau A}$ invariant under CP transformed $\mu\tau$ interchange antisymmetry [151], namely

$$M_\nu^{CP\mu\tau A} = \begin{pmatrix} ix & a_1 + ia_2 & a_1 - ia_2 \\ a_1 + ia_2 & y_1 + iy_2 & ic \\ a_1 - ia_2 & ic & -y_1 + iy_2 \end{pmatrix}. \quad (3.10)$$

It should be emphasized that complex mixed $\mu\tau$ antisymmetry, which can be abbreviated as $CP^{\theta\mu\tau A}$ and gets generated by \mathcal{G}^θ , must now be broken in the charged lepton sector. This is because a nonzero Dirac CP violation is equivalent to the criterion

$$\text{Tr} [H_\nu, H_\ell]^3 \neq 0, \quad (3.11)$$

where H_ν and H_ℓ are two hermitian matrices defined as $H_\ell = M_\ell^\dagger M_\ell$, M_ℓ being the charged lepton mass matrix and $H_\nu = M_\nu^\dagger M_\nu$. [182, 183]. A common CP symmetry \mathcal{G}_{CP} would imply

$$\mathcal{G}_{CP}^T H_\nu^T \mathcal{G}_{CP}^* = H_\nu, \quad \mathcal{G}_{CP}^T H_\ell^T \mathcal{G}_{CP}^* = H_\ell. \quad (3.12)$$

From (3.12) it follows that $\text{Tr}[H_\nu, H_\ell]^3 = 0$ which, in turn, leads to $\sin \delta = 0$ i.e. a vanishing Dirac CP violation. As mentioned earlier, this is disfavored by current experiments.

3.3 Neutrino mixing angles and phases

Eqs.(5.10) and (3.8) together imply [109] that

$$\mathcal{G}^\theta U^* = U \tilde{d} \quad (3.13)$$

where $\tilde{d}_{ij} = \pm \delta_{ij}$. Next, we take $\tilde{d} = \text{diag}(\tilde{d}_1, \tilde{d}_2, \tilde{d}_3)$ where each \tilde{d}_i ($i = 1, 2, 3$) is either +1 or -1. (5.12) can explicitly be written as

$$\begin{pmatrix} -i & 0 & 0 \\ 0 & -ic_\theta & is_\theta \\ 0 & is_\theta & ic_\theta \end{pmatrix} \begin{pmatrix} U_{e1}^* & U_{e2}^* & U_{e3}^* \\ U_{\mu1}^* & U_{\mu2}^* & U_{\mu3}^* \\ U_{\tau1}^* & U_{\tau2}^* & U_{\tau3}^* \end{pmatrix} = \begin{pmatrix} \tilde{d}_1 U_{e1} & \tilde{d}_2 U_{e2} & \tilde{d}_3 U_{e3} \\ \tilde{d}_1 U_{\mu1} & \tilde{d}_2 U_{\mu2} & \tilde{d}_3 U_{\mu3} \\ \tilde{d}_1 U_{\tau1} & \tilde{d}_1 U_{\tau2} & \tilde{d}_1 U_{\tau3} \end{pmatrix}. \quad (3.14)$$

Eq. (5.13) leads to nine independent relations corresponding to the three rows:

$$\begin{aligned}
 -iU_{e1}^* &= \tilde{d}_1 U_{e1}, & -iU_{e2}^* &= \tilde{d}_2 U_{e2}, & -iU_{e3}^* &= \tilde{d}_3 U_{e3}, \\
 -iU_{\mu 1}^* c_\theta + iU_{\tau 1}^* s_\theta &= \tilde{d}_1 U_{\mu 1}, & -iU_{\mu 2}^* c_\theta + iU_{\tau 2}^* s_\theta &= \tilde{d}_2 U_{\mu 2}, & -iU_{\mu 3}^* c_\theta + iU_{\tau 3}^* s_\theta &= \tilde{d}_3 U_{\mu 3}, \\
 iU_{\mu 1}^* s_\theta + iU_{\tau 1}^* c_\theta &= \tilde{d}_1 U_{\tau 1}, & iU_{\mu 2}^* s_\theta + iU_{\tau 2}^* c_\theta &= \tilde{d}_2 U_{\tau 2}, & iU_{\mu 3}^* s_\theta + iU_{\tau 3}^* c_\theta &= \tilde{d}_3 U_{\tau 3}
 \end{aligned} \tag{3.15}$$

In order to calculate the Majorana phases in a way that avoids unphysical phases, it is useful to construct two rephasing invariants [184]

$$I_1 = U_{e1} U_{e2}^*, I_2 = U_{e1} U_{e3}^*. \tag{3.16}$$

Using the relations in the first row of (5.14), we obtain

$$I_1 = \tilde{d}_1 \tilde{d}_2 U_{e1}^* U_{e2}, \quad I_2 = \tilde{d}_1 \tilde{d}_2 U_{e1}^* U_{e3}. \tag{3.17}$$

On inserting the two different expressions for $I_{1,2}$, in (5.15) and (5.16), we find that

$$c_{12} s_{12} c_{13}^2 e^{-i\alpha/2} = \tilde{d}_1 \tilde{d}_2 c_{12} s_{12} c_{13}^2 e^{i\alpha/2} \tag{3.18}$$

and

$$c_{12} s_{13} c_{13} e^{i(\delta-\beta/2)} = \tilde{d}_1 \tilde{d}_3 c_{12} s_{13} c_{13} e^{-i(\delta-\beta/2)}. \tag{3.19}$$

From (5.17) and (5.18), it follows that

$$e^{i\alpha} = \tilde{d}_1 \tilde{d}_2, \quad e^{2i(\delta-\beta/2)} = \tilde{d}_1 \tilde{d}_3, \tag{3.20}$$

i.e., either $\alpha = 0$ or $\alpha = \pi$, and either $\beta = 2\delta$ or $\beta = 2\delta - \pi$. In other words, the Majorana phases can have four possible pairs of values for a given value of δ . From

the absolute square of the third relation in the third row of (5.14), we obtain

$$|U_{\tau 3}|^2 = (U_{\mu 3}^* s_\theta + U_{\tau 3}^* c_\theta)(U_{\mu 3} s_\theta + U_{\tau 3} c_\theta) \quad (3.21)$$

which implies that

$$\cot 2\theta_{23} = \cot \theta \cos(\phi_2 - \phi_3) \quad (3.22)$$

reducing to $\theta_{23} \rightarrow \pi/4$ in the $\mu\tau$ interchange limit $\theta \rightarrow \pi/2$, as expected. Taking the absolute square of the second relation in the third row of (5.14), and eliminating the unphysical phase difference $\phi_2 - \phi_3$, we obtain

$$\sin \delta = \pm \sin \theta / \sin 2\theta_{23}. \quad (3.23)$$

This result was originally derived in Ref. [143] which proposed a CP transformed mixed $\mu\tau$ symmetry for neutrinos. Eq.(3.23), as expected, reproduces the result $\sin \delta = \pm 1$ (equivalently, $\cos \delta = 0$) in the $\mu\tau$ interchange limit $\theta = \pi/2$ and $\theta_{23} = \pi/4$. Note also that, if the unphysical phase combination $\phi_2 - \phi_3$ is put equal to zero, $\cot 2\theta_{23}$ becomes equal to $\cot \theta$ and $\cos \delta$ vanishes i.e., leptonic Dirac CP violation becomes maximal. However, such is not the case in general. We should also mention that another relation between δ and θ_{13} was obtained recently in Ref. [185].

3.4 Numerical analysis

In order to demonstrate the phenomenological viability of our theoretical proposal we present a numerical analysis of its consequences in substantial detail. It is organized as follows. In Table 5.1, we display the 3σ ranges of neutrino mixing angles and mass squared differences obtained from globally fitted neutrino oscillation data [12]. The allowed ranges of parameters of M_ν , CP phases and the consequent

predictions on the light neutrino masses are tabulated in Table 5.2, 3.3 and Table 4.3 respectively. These have been obtained by using the exact analytical formulae for the mixing angles and light neutrino masses [186], the entries in Table 5.1 and the upper bound [187] of 0.17 eV on the sum of the light neutrino masses from PLANCK and other cosmological observations. In Fig.4.6 each mass eigenvalue m_1, m_2 and m_3 is plotted against the smallest mass eigenvalue m_{min} for both types of mass ordering. The neutrino mass spectrum is clearly hierarchical ($m_{2,1} \gg m_3$ for NO and $m_{2,1} \ll m_3$ for IO).

Table 3.1: Input values used in the analysis [12]

Parameter	θ_{12} degrees	θ_{23} degrees	θ_{13} degrees	Δm_{21}^2 $10^{-5}(\text{eV})^2$	$ \Delta m_{31}^2 $ $10^{-3}(\text{eV}^2)$
3σ ranges (NO)	31.42 – 36.05	40.3 – 51.5	8.09 – 8.98	6.80 – 8.02	2.399 – 2.593
3σ ranges (IO)	31.43 – 36.06	41.3 – 51.7	8.14 – 9.01	6.80 – 8.02	2.369 – 2.562
Best fit values (NO)	33.62	47.2	8.54	7.40	2.494
Best fit values (IO)	33.62	48.1	8.58	7.40	2.465

Table 3.2: Output values of the parameters of M_ν

Parameters	$x/10^{-2}$	$a_1/10^{-2}$	$a_2/10^{-2}$	$y_1/10^{-2}$	$y_2/10^{-2}$	$c/10^{-2}$	$\theta(^{\circ})$
NO	-2.2 – 2.2	-4.5 – 4.5	-3.2 – 3.2	-3.5 – 3.5	-4.5 – 4.5	-3.5 – 3.5	12-174
IO	-2.5 – 2.5	-4.5 – 4.5	-0.4 – 0.4	-2.5 – 2.5	-3.5 – 3.5	-2.5 – 2.5	2-156

Table 3.3: Output values CP phases in the range $\beta \in [0, 2\pi]$

Ordering	δ	$\beta = 2\delta$	$\beta = 2\delta - \pi$
NO($\sin \delta > 0$)	$[6^\circ, 174^\circ]$	$[12^\circ, 348^\circ]$	$[0^\circ, 168^\circ], [192^\circ, 360^\circ]$
NO($\sin \delta < 0$)	$[186^\circ, 354^\circ]$	$[12^\circ, 348^\circ]$	$[0^\circ, 168^\circ], [192^\circ, 360^\circ]$
IO($\sin \delta > 0$)	$[4^\circ, 176^\circ]$	$[8^\circ, 352^\circ]$	$[0^\circ, 172^\circ], [188^\circ, 360^\circ]$
IO($\sin \delta < 0$)	$[184^\circ, 356^\circ]$	$[8^\circ, 352^\circ]$	$[0^\circ, 172^\circ], [188^\circ, 360^\circ]$

Table 3.4: Predictions on the light neutrino masses.

Normal Ordering ($m_3 > m_2$)			Inverted Ordering ($m_3 < m_1$)		
$m_1/10^{-3}$	$m_2/10^{-3}$	$m_3/10^{-3}$	$m_1/10^{-3}$	$m_2/10^{-3}$	$m_3/10^{-3}$
(eV)	(eV)	(eV)	(eV)	(eV)	(eV)
$8.4 \times 10^{-2} - 49$	$9 - 51$	$50 - 71$	$48 - 64$	$49 - 66$	$4.4 \times 10^{-2} - 42$

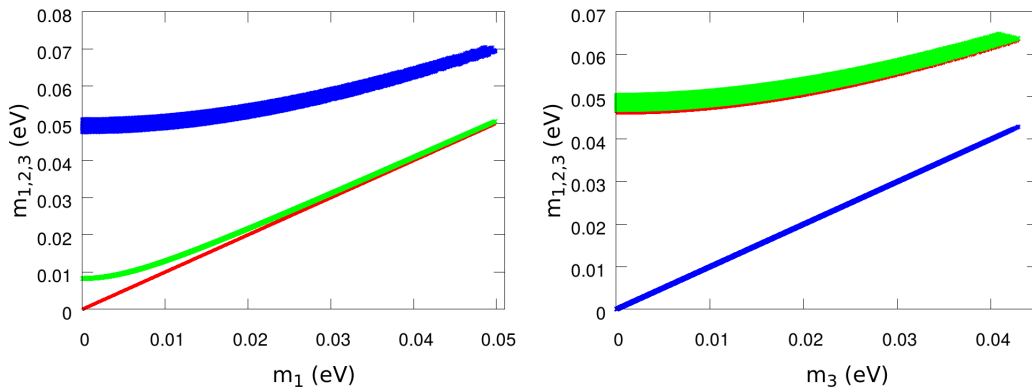


Figure 3.1: Plots of $m_{1,2,3}$ for normal (left) and inverted (right) mass ordering with the lightest mass eigenvalue is plotted in the ordinate. The red, green and blue bands refer to m_1, m_2 and m_3 respectively.

Next, we discuss the numerical results of CP-transformed mixed $\mu\tau$ antisym-

metry. In particular, we discuss the implications of the symmetry for the neutrinoless double beta decay, effect of CP asymmetry in neutrino oscillations and flavor flux ratios at neutrino telescopes in three separate subsections.

3.4.1 Neutrinoless double beta decay

For certain nuclei such as Ge-76, it is energetically favourable to undergo a double beta decay ($2\nu\beta\beta$) instead of a singular β -decay emitting two electrons and two neutrinos. Moreover, if the neutrino is a Majorana particle those two neutrinos can annihilate each other to give rise to a neutrinoless double beta decay ($0\nu\beta\beta$):

$$(A, Z) \longrightarrow (A, Z + 2) + 2e^- \quad (3.24)$$

which clearly violates the lepton number by 2 units. Observation of such decay will firmly establish the Majorana nature of the neutrinos. The half-life [188] corresponding to the above decay is given by

$$\frac{1}{T_{1/2}^{0\nu}} = G_{0\nu} |\mathcal{M}|^2 |M_{ee}|^2 m_e^{-2}, \quad (3.25)$$

where $G_{0\nu}$ denote the two-body phase space factor, \mathcal{M} is the nuclear matrix element (NME), m_e is the mass of the electron and M_{ee} is the (1,1) element of the effective light neutrino mass matrix M_ν .

In the PDG parametrization convention for U_{PMNS} , M_ν^{ee} is given most generally by

$$M_\nu^{ee} = c_{12}^2 c_{13}^2 m_1 + s_{12}^2 c_{13}^2 m_2 e^{i\alpha} + s_{13}^2 m_3 e^{i(\beta-2\delta)}. \quad (3.26)$$

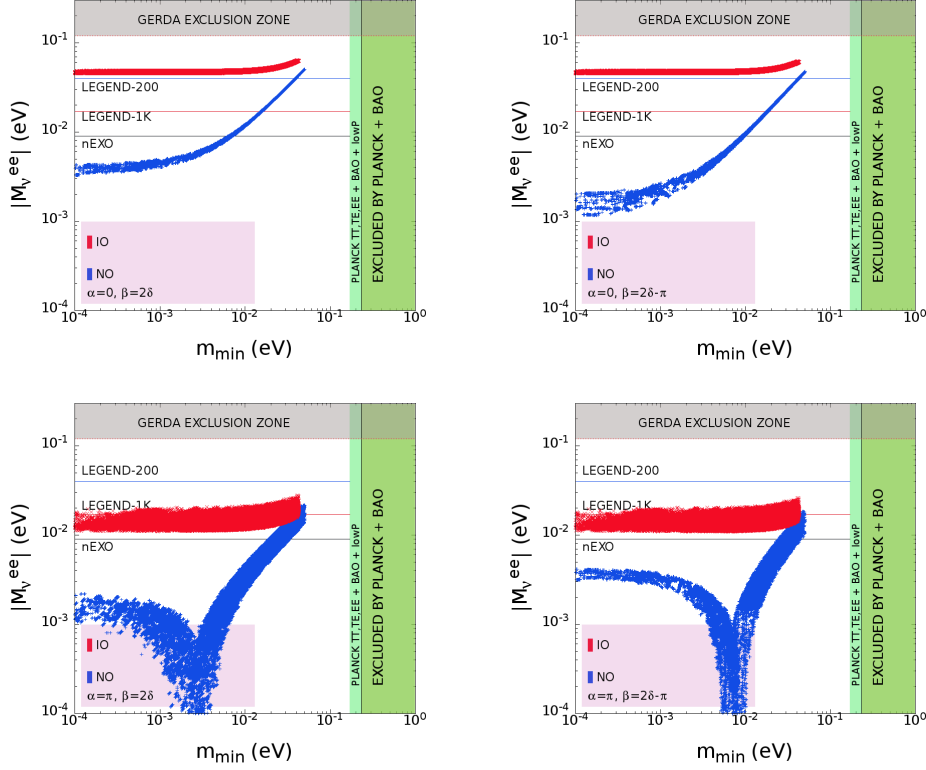


Figure 3.2: Plots of $|M_\nu^{ee}|$ vs. m_{min} for both types of mass ordering with four possible choices of the Majorana phases α and β . NO and IO refer to Normal and Inverted ordering respectively.

In our case, (5.37) simplifies to the following four expressions for our four different possibilities:

$$(i) |M_\nu^{ee}| = c_{12}^2 c_{13}^2 m_1 + s_{12}^2 c_{13}^2 m_2 + s_{13}^2 m_3 \text{ for } \alpha = 0, \beta = 2\delta,$$

$$(ii) |M_\nu^{ee}| = c_{12}^2 c_{13}^2 m_1 + s_{12}^2 c_{13}^2 m_2 - s_{13}^2 m_3 \text{ for } \alpha = 0, \beta = 2\delta - \pi,$$

$$(iii) |M_\nu^{ee}| = c_{12}^2 c_{13}^2 m_1 - s_{12}^2 c_{13}^2 m_2 + s_{13}^2 m_3 \text{ for } \alpha = \pi, \beta = 2\delta$$

and

$$(iv) |M_\nu^{ee}| = c_{12}^2 c_{13}^2 m_1 - s_{12}^2 c_{13}^2 m_2 - s_{13}^2 m_3 \text{ for } \alpha = \pi, \beta = 2\delta - \pi.$$

In $0\nu\beta\beta$ decay, M_ν^{ee} depends on α and $\beta - 2\delta$ (cf. Eq.(4.3)). In a generic case, α and $\beta - 2\delta$ varies in the range $[0, 2\pi]$ (or $[-\pi, \pi]$, since angles are defined modulo 2π) to cover the largest possible parameter space. However, a notable feature of our scenario is that it uniquely fixes (i) α to be 0 or π and (ii) the combination $\beta - 2\delta$ to 0 or $-\pi$ rather than the entire range of variation $[0, 2\pi]$ (or $[-\pi, \pi]$) as in a generic situation. This constraint tightly controls the range of variation of M_ν^{ee} and is implicitly reflected in the parameter space of $0\nu\beta\beta$ decay. The resulting plots of $|M_\nu^{ee}|$ versus the smallest mass eigenvalue m_{min} (m_1 for NO and m_3 for IO) are presented in Fig.5.2 with significant upper limits on $|M_\nu^{ee}|$ for ongoing and future experiments. At the moment the most stringent exclusion zone on M_{ee} has been reported by the GERDA Phase II [189] experiment to be 0.12 – 0.26eV depending on the value of the nuclear matrix element used. It is evident from Fig.5.2 that $|M_{ee}|$ in each plot leads to an upper limit which is below the reach of the GERDA phase-II experimental data. The sensitivity reach of several other experiments such as LEGEND-200 (40 meV), LEGEND-1K (17 meV) and nEXO (9 meV) [11], shown in Fig.5.2, can probe our model. In particular, if LEGEND-1K fails to observe a signal, the inverted mass ordering in our model corresponding to $\alpha = 0$ shall be excluded. Note that, for each case, the entire parameter space corresponding to the inverted mass ordering is likely to be ruled out for both $\alpha = 0$ and π if nEXO, covering its entire reach, does not observe any $\beta\beta 0\nu$ signal. However, the latter exclusion is likely to be a generic feature of many models.

3.4.2 CP asymmetry in neutrino oscillations

In this subsection, we discuss the effect of the presence of leptonic Dirac CP violation in long baseline neutrino oscillation experiments. CP violating phase δ makes its appearance in the CP asymmetry parameter A_{lm} , defined as

$$A_{lm} = \frac{P(\nu_l \rightarrow \nu_m) - P(\bar{\nu}_l \rightarrow \bar{\nu}_m)}{P(\nu_l \rightarrow \nu_m) + P(\bar{\nu}_l \rightarrow \bar{\nu}_m)}, \quad (3.27)$$

where $l, m = (e, \mu, \tau)$ are flavor indices and the P 's are transition probabilities. The $\nu_\mu \rightarrow \nu_e$ transition probability is given by

$$P_{\mu e} \equiv P(\nu_\mu \rightarrow \nu_e) = P_{atm} + P_{sol} + 2\sqrt{P_{atm}}\sqrt{P_{sol}} \cos(\Delta_{32} + \delta). \quad (3.28)$$

where $\Delta_{ij} = \Delta m_{ij}^2 L/4E$ is the kinematic phase factor in which L denotes the baseline length and E represents the beam energy. The quantities P_{atm}, P_{sol} are respectively defined as

$$\sqrt{P_{atm}} = \sin \theta_{23} \sin 2\theta_{13} \frac{\sin(\Delta_{31} - aL)}{(\Delta_{31} - aL)} \Delta_{31}, \quad (3.29)$$

$$\sqrt{P_{sol}} = \cos \theta_{23} \sin 2\theta_{12} \frac{\sin aL}{aL} \Delta_{21}, \quad (3.30)$$

where $a = G_F N_e / \sqrt{2}$ with G_F being the Fermi constant and N_e being the electron number density in the medium of propagation which takes into account the matter effects in neutrino propagation through the earth. An approximate value of a for the earth is 3500km^{-1} . In the limit $a \rightarrow 0$, (3.28) leads to the oscillation probability in vacuum. With this, the CP asymmetry parameter is given by

$$A_{\mu e} = \frac{P(\nu_\mu \rightarrow \nu_e) - P(\bar{\nu}_\mu \rightarrow \bar{\nu}_e)}{P(\nu_\mu \rightarrow \nu_e) + P(\bar{\nu}_\mu \rightarrow \bar{\nu}_e)} = \frac{2\sqrt{P_{atm}}\sqrt{P_{sol}} \sin \Delta_{32} \sin \delta}{P_{atm} + 2\sqrt{P_{atm}}\sqrt{P_{sol}} \cos \Delta_{32} \cos \delta + P_{sol}} \quad (3.31)$$

where $\sin \delta$, given by (3.23), has two possible values and same goes for $\cos \delta$. Hence there are two pairs of choices which give rise to two pairs of possibilities for $A_{\mu e}$ as given in Table 3.5.

 Table 3.5: Four possibilities for $A_{\mu e}$

Possibilities	$\sin \delta$	$\cos \delta$
Case A	$+\sin \theta (\sin 2\theta_{23})^{-1}$	$+(\sin 2\theta_{23})^{-1} \sqrt{\cos^2 \theta \sin^2 2\theta_{23} - \sin^2 \theta \cos^2 2\theta_{23}}$
Case B	$-\sin \theta (\sin 2\theta_{23})^{-1}$	$+(\sin 2\theta_{23})^{-1} \sqrt{\cos^2 \theta \sin^2 2\theta_{23} - \sin^2 \theta \cos^2 2\theta_{23}}$
Case C	$+\sin \theta (\sin 2\theta_{23})^{-1}$	$-(\sin 2\theta_{23})^{-1} \sqrt{\cos^2 \theta \sin^2 2\theta_{23} - \sin^2 \theta \cos^2 2\theta_{23}}$
Case D	$-\sin \theta (\sin 2\theta_{23})^{-1}$	$-(\sin 2\theta_{23})^{-1} \sqrt{\cos^2 \theta \sin^2 2\theta_{23} - \sin^2 \theta \cos^2 2\theta_{23}}$

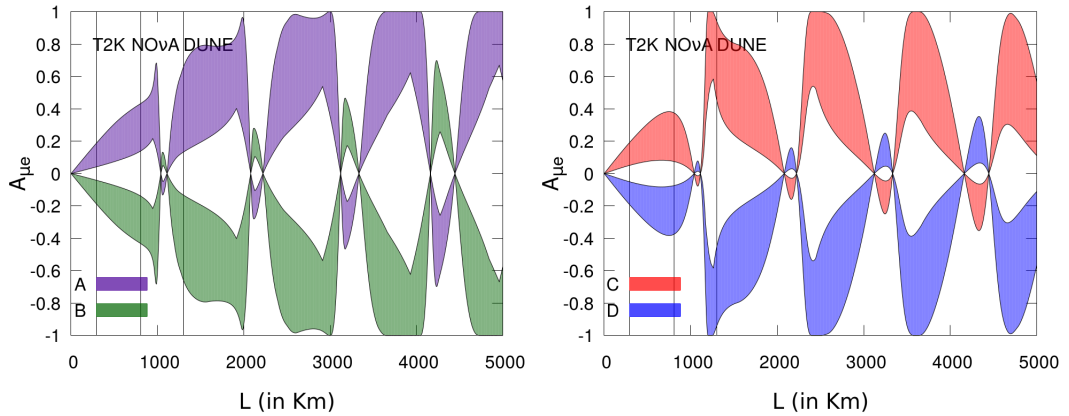


Figure 3.3: $A_{\mu e}$ (for $E = 1$ GeV), plotted against the baseline length L , for the four cases in Table 3.5. Each plot stands for both NO and IO since numerically, within the 3σ range of θ_{23} , the two types of ordering are practically indistinguishable. The bands are caused by θ_{23} and θ varying in their 3σ range and phenomenologically allowed range respectively with the other parameters kept at their best fit values.

In Fig.3.3 the CP asymmetry parameter $A_{\mu e}$, for both types of mass ordering, is plotted against the baseline length L for four possibilities (Table 3.5) and for a

fixed beam energy ($E = 1$ GeV). The baseline lengths corresponding to experiments such as T2K, NO ν A and DUNE have been shown by vertical lines in the figure. For concreteness, Table 3.6 provides the range of variation of $A_{\mu e}$ for a fixed energy of $E = 1$ GeV in T2K, NO ν A and DUNE.

In Fig.3.4, the CP asymmetry parameter $A_{\mu e}$ is plotted against the beam energy E for four possible cases (Table 3.5) separately for T2K, NO ν A and DUNE for both types of mass ordering. In generating these plots, the atmospheric mixing angle θ_{23} has been taken to be within its currently allowed 3σ range while the remaining neutrino oscillation parameters have been kept fixed at their best fit values.

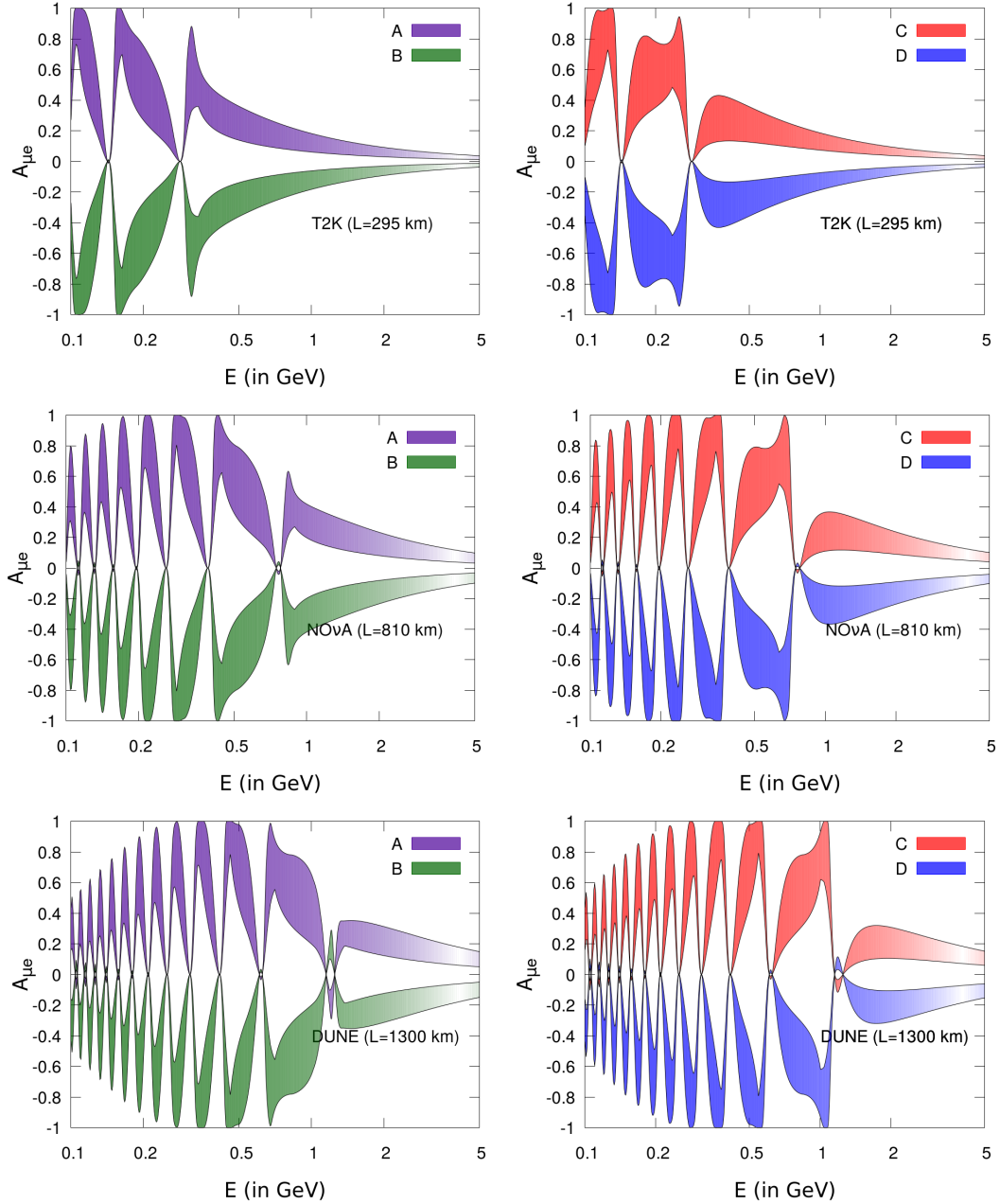


Figure 3.4: Variation of the CP asymmetry parameter with beam energy E for different baselines lengths of $L = 295$ km, 810 km and 1300 km corresponding to T2K, NO ν A and DUNE respectively for both NO and IO; the numerical distinction between the two types of ordering is insignificant for the 3σ range of θ_{23} .

Table 3.6: Prediction of the ranges of $|A_{\mu e}|$ with $E = 1\text{GeV}$

Experiment	T2K	NO ν A	DUNE
Case A, B	0.04 – 0.18	0.14 – 0.44	0.14 – 0.64
Case C, D	0.05 – 0.19	0.09 – 0.39	0.45 – 0.90

Table 3.7: Prediction of the ranges of $|A_{\mu e}|$ in T2K, NO ν A, DUNE

T2K			
Energy	$E = 0.5 \text{ GeV}$	$E = 1.0 \text{ GeV}$	$E = 2.0 \text{ GeV}$
Case A,B	0.14-0.37	0.07-0.21	0.05-0.10
Case C,D	0.14-0.37	0.06-0.19	0.05-0.10
NOνA			
Energy	$E = 0.5 \text{ GeV}$	$E = 1.0 \text{ GeV}$	$E = 2.0 \text{ GeV}$
Case A,B	0.31-0.80	0.21-0.43	0.08-0.24
Case C,D	0.29-0.79	0.10-0.38	0.13-0.29
DUNE			
Energy	$E = 0.5 \text{ GeV}$	$E = 1.0 \text{ GeV}$	$E = 2.0 \text{ GeV}$
Case A,B	0.39-0.98	0.21-0.64	0.15-0.30
Case C,D	0.41-0.97	0.61-0.87	0.13-0.32

3.4.3 Flavor flux ratios at neutrino telescopes

Given the necessary background in Sec.1.4, one can define certain flavor flux ratios R_l ($l = e, \mu, \tau$) at the neutrino telescope as

$$R_l \equiv \frac{\phi_l^T}{\sum_m \phi_m^T - \phi_l^T} = \frac{1 + \sum_i |U_{li}|^2 \Delta_i}{2 - \sum_i |U_{li}|^2 \Delta_i}, \quad (3.32)$$

where $m = e, \mu, \tau$ and U is as in (5.11). Since $s_{13}^2 \approx 0.01$, $\mathcal{O}(s_{13}^2)$ terms can be neglected. Then the approximate expressions for the flux ratios become

$$\begin{aligned} R_e &\equiv \frac{\phi_e^T}{\phi_\mu^T + \phi_\tau^T} \approx \frac{1 + \frac{1}{2} \sin^2 2\theta_{12} \cos 2\theta_{23} + \frac{1}{2} \sin 4\theta_{12} \sin 2\theta_{23} s_{13} \cos \delta}{2 - \frac{1}{2} \sin^2 2\theta_{12} \cos 2\theta_{23} - \frac{1}{2} \sin 4\theta_{12} \sin 2\theta_{23} s_{13} \cos \delta}, \\ R_\mu &\equiv \frac{\phi_\mu^T}{\phi_e^T + \phi_\tau^T} \approx \frac{1 + \{c_{23}^2(1 - \frac{1}{2} \sin^2 2\theta_{12}) - s_{23}^2\} \cos 2\theta_{23} - \frac{1}{4} \sin 4\theta_{12} \sin 2\theta_{23} s_{13} \cos \delta (4c_{23}^2 - 1)}{2 - \cos^2 2\theta_{23} + \frac{1}{2} \sin^2 2\theta_{12} \cos 2\theta_{23} c_{23}^2 + \frac{1}{4} (3 - 4s_{23}^2) \sin 4\theta_{12} \sin 2\theta_{23} s_{13} \cos \delta}, \\ R_\tau &\equiv \frac{\phi_\tau^T}{\phi_e^T + \phi_\mu^T} \approx \frac{1 + \{s_{23}^2(1 - \frac{1}{2} \sin^2 2\theta_{12}) - c_{23}^2\} \cos 2\theta_{23} - \frac{1}{4} \sin 4\theta_{12} \sin 2\theta_{23} s_{13} \cos \delta (4s_{23}^2 - 1)}{2 + \cos^2 2\theta_{23} + \frac{1}{2} \sin^2 2\theta_{12} \cos 2\theta_{23} c_{23}^2 + \frac{1}{4} (3 - 4c_{23}^2) \sin 4\theta_{12} \sin 2\theta_{23} s_{13} \cos \delta}. \end{aligned} \quad (3.33)$$

Note that each R_l depends on $\cos \delta$ which from (3.23) is given by

$$\cos \delta = \pm (\sqrt{\cos^2 \theta \sin^2 2\theta_{23} - \sin^2 \theta \cos^2 2\theta_{23}}) / \sin 2\theta_{23}. \quad (3.34)$$

With $\theta = \pi/2 + \epsilon$ for any arbitrary ϵ , positive or negative, we can write

$$\cos \delta = \pm (\sqrt{\sin^2 \epsilon \sin^2 2\theta_{23} - \cos^2 \epsilon \cos^2 2\theta_{23}}) / \sin 2\theta_{23} \quad (3.35)$$

which is the same whether ϵ is positive or negative. For either sign, this explains why each R_l in Fig.3.5 and 3.6 is symmetric about $\theta = \pi/2$ though the allowed range of θ is not (Table 5.2). The ‘ \pm ’ sign in (3.35) tells us that for a fixed θ (equivalently, for a fixed ϵ), and fixed θ_{23} , each R_l is double-valued except for $\theta = \pi/2$ (i.e., $\epsilon = 0$)

where $\cos \delta = 0$ from (3.35) and (3.23). However, instead of two discrete values of R_l , a continuous band is obtained for a fixed θ since θ_{23} has been allowed to vary in its current 3σ range while the other mixing angles are held fixed at their best fit values.

In the figure below, we plot the variation of the flavor flux ratios R_l with the $\mu\tau$ mixing parameter θ in its allowed range for both normal and inverted types of mass ordering. Unlike the CP asymmetry parameter in neutrino oscillation experiments, these flavor flux ratios are different for NO and IO—specifically in the allowed ranges of θ . An exact CP transformed $\mu\tau$ interchange ($\text{CP}^{\mu\tau}$) antisymmetry leads to $R_e = R_\mu = R_\tau = 1/2$ irrespective of the mass ordering. This can be clearly seen from the approximate expressions of flux ratios in (3.33), in the limit $\theta = \pi/2$ or equivalently, $\theta_{23} = \pi/4$ and $\cos \delta = 0$. But a small deviation from $\text{CP}^{\mu\tau}$ (anti)symmetry may lead to a drastic change of the flux ratios as is clear from the sharp edges of the allowed parameter spaces on either side of $\theta = \pi/2$.

In order to obtain precise predictions for flavor flux ratios, a precise value of θ must be specified. In particular, precise measurements of δ and θ_{23} can be used to pinpoint a value of θ from Eq.(3.23). As an illustration, the best fit value of $\delta = 234^\circ$ (278°) and $\theta_{23} = 47.2^\circ$ (48.1°) for NO (IO), the value of θ turns out to be 34.75° (75.9°). The contours corresponding to the best fit values of the mixing angles has now been indicated in Fig.3.5 and Fig.3.6. Now, it can be clearly seen that, as θ deviates from $\pi/2$, the flavor flux ratios deviate drastically from 0.5 and the corresponding values have been tabulated in Table 8. The quantitative predictions of flux ratio θ deviating from $\pi/2$ has now been summarized in Table 3.8 the current best fit values 215° (284°) of δ and 49.6° (49.8°) of θ_{23} to obtain θ to be 34.75° (75.9°) for NO(IO) case. The corresponding values of R_e , R_μ and R_τ have been found to be 0.456 (0.465), 0.529 (0.525) and 0.516 (0.512) respectively. It is interesting to note that while the predicted value of R_e is less than 0.5 those of R_μ and R_τ are greater

than 0.5. If this best fit values change in future, the corresponding predictions for R_l can be easily obtained using the formulae (3.32) and (3.34) to test or falsify our proposal.

Table 3.8: Prediction for the values of flux ratios (R_l) for $\theta \neq \pi/2$ [12]

Ordering \downarrow	bf value of δ	bf value of θ_{23}	θ	R_e	R_μ	R_τ
NO	234°	47.2°	53.70°	0.456	0.529	0.516
IO	278°	48.1°	79.74°	0.465	0.525	0.512

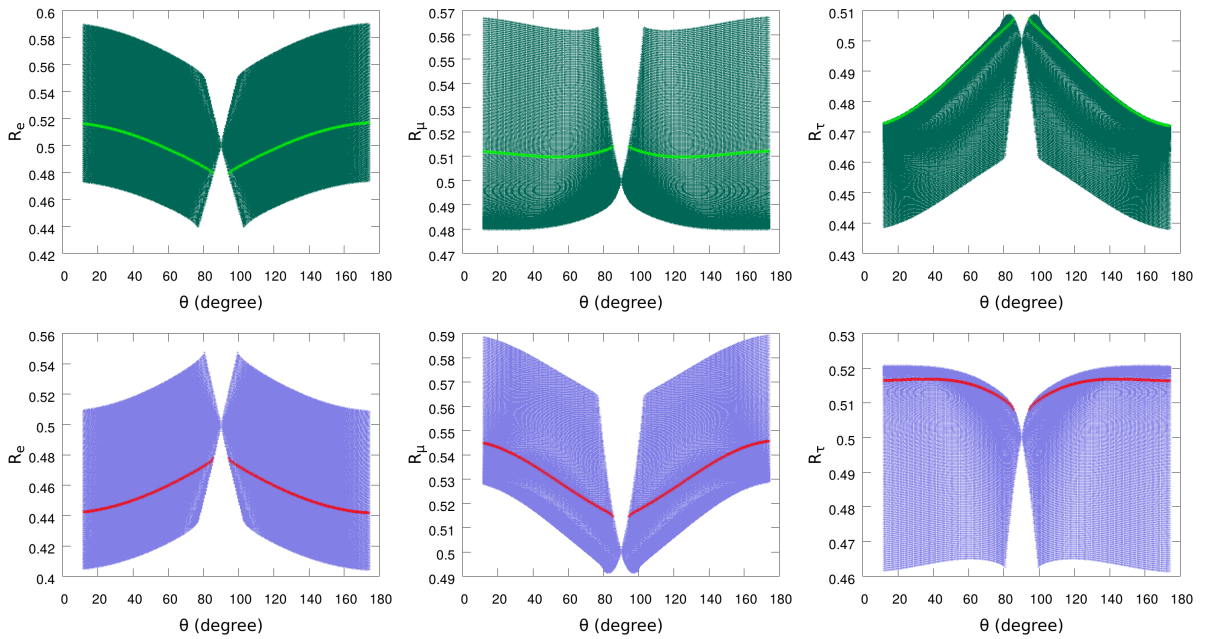


Figure 3.5: Flux ratios R_e, R_μ, R_τ vs. the $\mu\tau$ -mixing parameter θ for normal ordering, where the three mixing angles have been allowed to vary over their 3σ ranges. The green(red) line in each plot of the upper(lower) panel corresponds to the best fit value of the mixing angles. The plots in the upper (lower) panel correspond to $\cos \delta \geq 0(\leq 0)$.

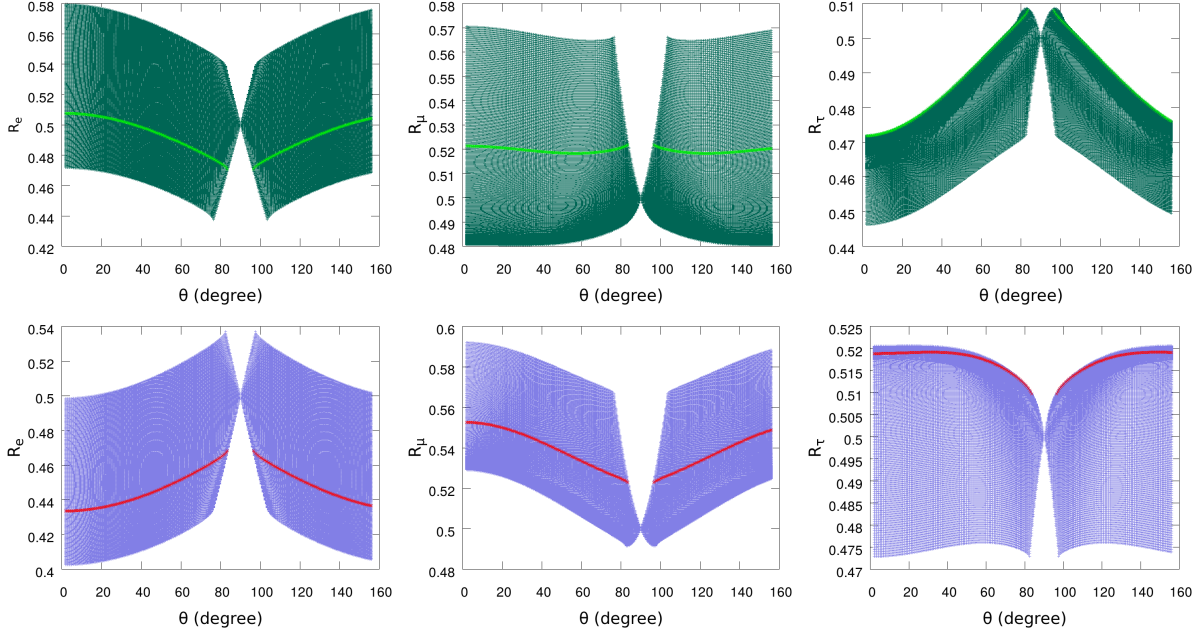


Figure 3.6: Flux ratios R_e, R_μ, R_τ vs. the $\mu\tau$ -mixing parameter θ for inverted ordering where the three mixing angles have been allowed to vary over their 3σ ranges. The green(red) line in each plot of the upper(lower) panel corresponds to the best fit value of the mixing angles. The plots in the upper (lower) panel correspond to $\cos \delta \geq 0(\leq 0)$.

3.5 Summary and conclusions

We have proposed a CP transformed mixed $\mu\tau$ antisymmetry in the light neutrino Majorana mass matrix M_ν implemented in the Lagrangian by a generalized CP transformation on left-chiral flavor neutrino fields. We explore its consequences in leptonic CP violation. The Dirac CP phase δ , which is in general nonmaximal, is found to be correlated with both the $\mu\tau$ mixing parameter θ and the atmospheric mixing angle θ_{23} . For a nonmaximal δ , one of the Majorana phases is neither zero nor π , thereby leading to a nonvanishing Majorana CP violation. Moreover, we discuss

the consequences of our proposal on the $\beta\beta 0\nu$ decay process in relation to ongoing and upcoming experiments. We have also investigated the quantitative variation of the CP asymmetry parameter $A_{\mu e}$ as a function of beam energy for different baseline lengths as appropriate for different experiments. We have further obtained the implications of $\mu\tau$ mixing on flavor flux ratios $R_{e,\mu,\tau}$ at neutrino telescopes such as IceCube. While an exact $\mu\tau$ interchange antisymmetry leads to $R_e = R_\mu = R_\tau = 0.5$, any tiny departure will cause a significant deviation in the flux ratios, as has been explained quantitatively. Further, a careful measurement of these flux ratios in future can put additional constraints on the parameter θ .

Chapter 4

Complex extension of the residual

$\mathbb{Z}_2 \times \mathbb{Z}_2$ symmetry in scaling neutrino

Majorana mass matrix

4.1 Introduction

In this chapter, we present a study of the consequences of the complex extension of the residual $\mathbb{Z}_2 \times \mathbb{Z}_2$ [124] symmetry that corresponds to the scaling ansatz [6, 7, 118–121, 190] in conjunction with a nonstandard CP transformation on light neutrino Majorana mass matrix. We first consider a general light neutrino Majorana mass matrix M_ν^0 that enjoys an invariance under a scaling ansatz as an effective low energy symmetry. Next, we interpret the latter as a residual $\mathbb{Z}_2 \times \mathbb{Z}_2$ symmetry. Due to the prediction of a vanishing reactor mixing angle θ_{13} (now excluded at more than 5.2σ [115]) such a symmetry have to suitably modified. We use these \mathbb{Z}_2 generators to implement generalized CP transformations, and instead of an

ordinary $\mathbb{Z}_2 \times \mathbb{Z}_2$ symmetry, we now demand a generalized or CP extended $\mathbb{Z}_2 \times \mathbb{Z}_2$ as an effective residual symmetry that extends the scaling ansatz to its complex counterpart. In this case, the resulting mass matrices have a more complicated scaling relationship between its elements, and are further reconstructed through the type-I seesaw mechanism (cf. Sec.1.3).

As explained in Sec.1.6, though is nontrivial to combine a flavor and a CP symmetry, a consistent definition for both of them is possible when they satisfy certain consistency conditions are met. At low energy this combined symmetry must be broken to different residual symmetries in the neutrino and the charged lepton sector, since it is known that at least a common residual CP symmetry in both the sector would imply a vanishing CP violation [99, 102, 103]. Although here we do not focus on the explicit construction of the high energy flavor group, throughout the analysis we assume a diagonal charged lepton mass matrix which is protected by a residual symmetry G_ℓ after the spontaneous breaking of the combination of CP and flavor symmetry at high energy. Depending upon the breaking pattern, there may also be a trivial or a nontrivial CP symmetry in the charged lepton sector [167]. However, as pointed out, the final residual CP symmetries in both the sectors should be different.

Finally, using the oscillation constraints, tantalizing predictions on the low energy parameters such as neutrino masses, neutrinoless double beta decay, CP violating phases are obtained. Due to the presence of three massive right handed (RH) neutrinos, baryogenesis via leptogenesis scenario is also explored. Interesting conclusions such as octant sensitivity of the atmospheric mixing angle θ_{23} , preconditioned by the observed range of the final baryon asymmetry Y_B and nonoccurrence of unflavored leptogenesis are also drawn.

This chapter is organized as follows. Section 4.2 contains a brief discussion on residual symmetry and scaling ansatz with a possible modification to the ansatz

by extending the former with a nonstandard CP transformation. In section 4.3 we discuss a type-I seesaw extension of the analysis made in the previous section. Section 4.4 contains a discussion about baryogenesis via leptogenesis scenario related to the present model. In section 4.5 we present detail results of the numerical analysis. A discussion on the sensitivity of the heavier neutrinos to the obtained results for the final Y_B is presented in section 4.6. Section 4.7 concludes the entire discussion with some promising remarks.

4.2 Modification to scaling neutrino mass matrix with generalized $\mathbb{Z}_2 \times \mathbb{Z}_2$

Before going to an explicit details of our work, let us first discuss the residual $\mathbb{Z}_2 \times \mathbb{Z}_2$ symmetry proposed in Ref. [1]. A Majorana neutrino mass matrix M_ν enjoys a $\mathbb{Z}_2 \times \mathbb{Z}_2$ flavor symmetry which can be envisaged as a remnant symmetry of some horizontal flavor group. These horizontal symmetry groups are preferably finite groups since in that case the theory has a more predictive power due to the discrete number of choices for the residual symmetries G_i [1]. A bottom up as well as a top down approach for a viable horizontal group has been studied in the first one of Ref. [1].

We interpret the Strong Scaling Ansatz (SSA) proposed in Ref. [6, 7], as a residual $\mathbb{Z}_2 \times \mathbb{Z}_2$ symmetry. Since SSA leads to a vanishing θ_{13} , a possible modification to this has been made by generalizing the two independent ordinary \mathbb{Z}_2 invariance to their complex counterpart, i.e., two independent \mathbb{Z}_2^{CP} invariance. Thus the SSA has been extended to its complex version by means of a generalized $\mathbb{Z}_2 \times \mathbb{Z}_2$ symmetry (see Ref. [124] for another such extension in case of TBM mixing). Let us discuss the

methodology of the present analysis:

We consider a column wise scaling relations in the elements of M_ν^0 in flavor space as

$$\frac{(M_\nu^0)_{e\mu}}{(-M_\nu^0)_{e\tau}} = \frac{(M_\nu^0)_{\mu\mu}}{(-M_\nu^0)_{\mu\tau}} = \frac{(M_\nu^0)_{\tau\mu}}{(-M_\nu^0)_{\tau\tau}} = k, \quad (4.1)$$

where k is a real and positive dimensionless scaling factor. The superscript ‘0’ on M_ν symbolizes SSA as a leading order matrix in this analysis. Now the structure for M_ν^0 dictated by the ansatz of (4.1) comes out as

$$M_\nu^0 = \begin{pmatrix} P & -Qk & Q \\ -Qk & Rk^2 & -Rk \\ Q & -Rk & R \end{pmatrix}. \quad (4.2)$$

Here P, Q, R are a priori unknown, complex mass dimensional quantities. The minus sign in (4.1) has been considered to be in conformity with the PDG convention [112].

The matrix in (4.2) is diagonalized by a unitary matrix U^0 having a form

$$U^0 = \begin{pmatrix} c_{12}^0 & s_{12}^0 e^{i\alpha} & 0 \\ -\frac{ks_{12}^0}{\sqrt{1+k^2}} & \frac{kc_{12}^0}{\sqrt{1+k^2}} e^{i\alpha/2} & \frac{1}{\sqrt{1+k^2}} e^{i\beta/2} \\ \frac{s_{12}^0}{\sqrt{1+k^2}} & -\frac{c_{12}^0}{\sqrt{1+k^2}} e^{i\alpha/2} & \frac{k}{\sqrt{1+k^2}} e^{i\beta/2} \end{pmatrix}, \quad (4.3)$$

where α, β represents the Majorana phases, $c_{12}^0 = \cos \theta_{12}^0$ and $s_{12}^0 = \sin \theta_{12}^0$ which are computed in terms of the parameters of M_ν^0 . SSA predicts a vanishing θ_{13} (hence no measurable leptonic Dirac CP-violation) as one can see from (4.3) and an Inverted Ordering (IO) (i.e., $m_{2,1} > m_3$), with $m_3 = 0$. Therefore, we modify the ansatz to generate a non-zero θ_{13} using the paradigm of residual symmetry. In the first step, we obtain the G_a matrices using the relation

$$G_a^{(k)} = U^0 d_a U^{0\dagger} \quad (4.4)$$

with $G_a^{(k)}$ as the \mathbb{Z}_2 generators for a scaling ansatz invariant M_ν . Therefore, M_ν^0 will then satisfy the invariance equation

$$\left(G_a^{(k)}\right)^T M_\nu^0 G_a^{(k)} = M_\nu^0. \quad (4.5)$$

Now using (4.4) we calculate the corresponding $G_a^{(k)}$ ($a = 1, 2, 3$) matrices and present them as

$$G_1^{(k)} = \begin{pmatrix} \cos 2\theta_{12}^0 & -k(1+k^2)^{-1/2} \sin 2\theta_{12}^0 & -(1+k^2)^{-1/2} \sin 2\theta_{12}^0 \\ -k(1+k^2)^{-1/2} \sin 2\theta_{12}^0 & -(1+k^2)^{-1}(k^2 \cos 2\theta_{12}^0 + 1) & -k(1+k^2)^{-1}(1 - \cos 2\theta_{12}^0) \\ -(1+k^2)^{-1/2} \sin 2\theta_{12}^0 & -k(1+k^2)^{-1}(1 - \cos 2\theta_{12}^0) & -(1+k^2)^{-1}(k^2 + \cos 2\theta_{12}^0) \end{pmatrix}, \quad (4.6)$$

$$G_2^{(k)} = \begin{pmatrix} -\cos 2\theta_{12}^0 & k(1+k^2)^{-1/2} \sin 2\theta_{12}^0 & -(1+k^2)^{-1/2} \sin 2\theta_{12}^0 \\ k(1+k^2)^{-1/2} \sin 2\theta_{12}^0 & (1+k^2)^{-1}(k^2 \cos 2\theta_{12}^0 - 1) & -k(1+k^2)^{-1}(1 + \cos 2\theta_{12}^0) \\ -(1+k^2)^{-1/2} \sin 2\theta_{12}^0 & -k(1+k^2)^{-1}(1 + \cos 2\theta_{12}^0) & -(1+k^2)^{-1}(k^2 - \cos 2\theta_{12}^0) \end{pmatrix}, \quad (4.7)$$

$$G_3^{(k)} = \begin{pmatrix} -1 & 0 & 0 \\ 0 & (1-k^2)(1+k^2)^{-1} & 2k(1+k^2)^{-1} \\ 0 & 2k(1+k^2)^{-1} & -(1-k^2)(1+k^2)^{-1} \end{pmatrix}. \quad (4.8)$$

Note that all the $G_a^{(k)}$ matrices are symmetric by construction. Now to modify SSA, we generalize this $\mathbb{Z}_2 \times \mathbb{Z}_2$ by implementing CP transformations on the neutrino fields [100, 126, 171, 191] with the \mathbb{Z}_2 generators ($G_a^{(k)} = G_a^{(k)T}$) as¹

$$\nu_{L\alpha} \rightarrow i(G_a^{(k)})_{\alpha\beta\gamma} \nu_{L\beta}^C. \quad (4.9)$$

¹The matrices that represent the CP symmetry should be symmetric [102].

This extends the real horizontal invariance of M_ν^0 in (4.5) to its complex counterpart, i.e.

$$\left(G_a^{(k)}\right)^T M_\nu G_a^{(k)} = M_\nu^*. \quad (4.10)$$

Therefore the SSA, which could be thought of as a $\mathbb{Z}_2 \times \mathbb{Z}_2$ residual symmetry, has now been modified to a complex $\mathbb{Z}_2 \times \mathbb{Z}_2$ symmetry. This is often also referred to as a generalized $\mathbb{Z}_2 \times \mathbb{Z}_2$ symmetry of M_ν [124]. We show in the following subsections that there exists only two independent ways in which such a complex extension can be implemented.

4.2.1 Case I: Complex extension of $G_{2,3}^{(k)}$ Invariance

The complex invariance relations of M_ν related to $G_{2,3}^{(k)}$ is now written as

$$\left(G_{2,3}^{(k)}\right)^T M_\nu G_{2,3}^{(k)} = M_\nu^*, \quad (4.11)$$

which in turn implies

$$\left(G_1^{(k)}\right)^T M_\nu G_1^{(k)} = M_\nu \quad (4.12)$$

owing to the closure property of the $G_a^{(k)}$ ($a = 1, 2, 3$) matrices.

Eq.(4.11) leads to a most general Majorana neutrino mass matrix of the form

$$M_\nu^{MS1} = \begin{pmatrix} p & -q_1 k + i \frac{q_2}{k} & q_1 + i q_2 \\ -q_1 k + i \frac{q_2}{k} & r - \frac{s(k^2-1)}{k} + i \frac{2q_2 \kappa_+}{\sqrt{1+k^2}} & s + i \frac{q_2 \kappa_+ (k^2-1)}{k\sqrt{1+k^2}} \\ q_1 + i q_2 & s + i \frac{q_2 \kappa_+ (k^2-1)}{k\sqrt{1+k^2}} & r - i \frac{2q_2 \kappa_+}{\sqrt{1+k^2}} \end{pmatrix} \quad (4.13)$$

with

$$r = (sk + p) - q_1 \sqrt{1 + k^2} \left(\kappa_+ - \frac{1}{\kappa_+} \right), \quad (4.14)$$

$$\kappa_+ = (\cot 2\theta_{12}^0 + \operatorname{cosec} 2\theta_{12}^0). \quad (4.15)$$

Here p , $q_{1,2}$, r and s are real, mass dimensional quantities and the superscript ‘ MS ’ stands for ‘Modified Scaling’. It has already been shown in Ref. [119] that $(G_3^{(k)})^T M_\nu G_3^{(k)} = M_\nu^*$ leads to the results

$$\tan \theta_{23} = k^{-1}, \quad (4.16)$$

$$\sin \alpha = \sin \beta = \cos \delta = 0. \quad (4.17)$$

Now in the present case, the overall real $G_1^{(k)}$ (cf. Eq.(4.12)) invariance of M_ν fixes the first column of U_{PMNS} to the first column of U^0 . Therefore, one gets the relation between the solar and the reactor mixing angle as

$$|\cos \theta_{12} \cos \theta_{13}| = \cos \theta_{12}^0 \Rightarrow \sin^2 \theta_{12} = 1 - \cos^2 \theta_{12}^0 (1 + \tan^2 \theta_{13}). \quad (4.18)$$

4.2.2 Case II: Complex extension of $G_{1,3}^{(k)}$ Invariance

In this case, the complex invariance relations of M_ν due to $G_{1,3}^{(k)}$ can be written as

$$\left(G_{1,3}^{(k)} \right)^T M_\nu G_{1,3}^{(k)} = M_\nu^*, \quad (4.19)$$

which leads to

$$\left(G_2^{(k)} \right)^T M_\nu G_2^{(k)} = M_\nu. \quad (4.20)$$

Eq.(4.19) leads to the mass matrix M_ν^{MS2} having a form same as M_ν^{MS1} as given in (4.13) where κ_+ is replaced with $\kappa_- = -1/\kappa_+$. Similar to the previous case, a complex invariance due to $G_3^{(k)}$ leads to the predictions

$$\tan \theta_{23} = k^{-1}, \quad (4.21)$$

$$\sin \alpha = \sin \beta = \cos \delta = 0. \quad (4.22)$$

Now the overall real $G_2^{(k)}$ (cf. Eq.(4.20)) invariance of M_ν fixes the second column of U_{PMNS} to the second column of U^0 which gives rise to a relation between the solar and the reactor mixing angle as

$$|\sin \theta_{12} \cos \theta_{13}| = \sin \theta_{12}^0 \Rightarrow \sin^2 \theta_{12} = \sin^2 \theta_{12}^0 (1 + \tan^2 \theta_{13}). \quad (4.23)$$

Similar to the previous two cases, complex invariance due to $G_{1,2}^{(k)}$ lead to an overall real invariance due to $G_3^{(k)}$ which in turn leads to a vanishing θ_{13} . This case must therefore be discarded.

For both the viable cases, three CP phases have been obtained, namely, $\cos \delta = 0, \alpha, \beta = 0$ or π . Thus, there remains 6 real free parameters $p, q_{1,2}, s, k$ and κ_+ (or θ_{12}^0) (cf. Eq.(4.13)) in both M_ν^{MS1} and M_ν^{MS2} . However, one can trivially track the parameters k and θ_{12}^0 on account of the relations in (4.16) or (4.21) and (4.18) or (4.23). Thus, the remaining four parameters account for one mixing angle and three neutrino masses. However, to fix the absolute neutrino mass scale, we use additional constraints from baryogenesis and has been discussed in the numerical section.

We note that the prediction of the CP phases in the extended SSA scheme are identical to the case of $\text{CP}^{\mu\tau}$ [109, 192, 193]. Therefore the question arises how one

might distinguish the $\text{CP}^{\mu\tau}$ and the extended SSA experimentally? First of all, both the Strong Scaling Ansatz (SSA) and the $\mu\tau$ symmetry lead to $\theta_{13} = 0$ at the leading order and therefore, has to be abandoned. However, one can in principle differentiate SSA from the $\mu\tau$ reflection symmetry via their predictions of atmospheric mixing angle θ_{23} . The former in general predicts a nonmaximal θ_{23} (for $k \neq 1$) given by $\theta_{23} = \tan^{-1}(k^{-1})$ while a maximal value ($\theta_{23} = \pi/4$) is predicted by the latter.

Furthermore, in the extended scheme, besides the similar predictions for the CP phases an arbitrary nonvanishing value of the reactor mixing angle θ_{13} is predicted in both the cases (extended SSA and $\text{CP}^{\mu\tau}$). However, the prediction on the θ_{23} is different for each case. Interestingly, even after the extension, the value of θ_{23} survives for both the cases i.e., $\theta_{23} = \tan^{-1}(k^{-1})$ for the SSA as well as extended SSA and $\theta_{23} = \pi/4$ for $\mu\tau$ symmetry and its extended version ($\text{CP}^{\mu\tau}$). If experiments find a nonmaximal θ_{23} at a significant confidence level (recently there is a hint from $\text{NO}\nu\text{A}$ regarding the nonmaximality of θ_{23} at 2.6σ CL [194]) then the $\text{CP}^{\mu\tau}$ symmetry will be excluded while our proposal of an extended SSA (that predicts a nonmaximal θ_{23} in general) will continue to survive.

Before proceeding further we should comment on the fulfillment of the consistency conditions [99, 103, 104] as mentioned in the introduction. Here we have discussed two cases. In the first one $G_{2,3}^{(k)}$ are the CP symmetries which further result in a $G_1^{(k)}$ invariance of the mass term while in the second case, the CP generators $G_{1,3}^{(k)}$ lead to an invariance of the mass term due to the $G_2^{(k)}$. Now the consistency condition in case of a \mathbb{Z}_2 group implies [99]

$$X_r \rho_r^*(g) X_r^{-1} = \rho_r(g), \quad (4.24)$$

where X_r is a unitary matrix representing CP symmetry which acts on a generic

multiplet φ as

$$X_r \varphi(x) \xrightarrow{\text{CP}} X_r \varphi(x') \quad (4.25)$$

with $x' = (t, -\mathbf{x})$ and $\rho_r(g)$ is a representation for the element g of the flavor group in an irreducible representation \mathbf{r} . In our analysis, $G_i^{(k)}$'s are real, and hence, the condition in (4.24) turns out to be

$$\begin{aligned} G_{2,3}^{(k)} G_1^{(k)} (G_{2,3}^{(k)})^{-1} &= G_1^{(k)} \quad \text{for Case I;} \\ G_{1,3}^{(k)} G_2^{(k)} (G_{1,3}^{(k)})^{-1} &= G_2^{(k)} \quad \text{for Case II.} \end{aligned} \quad (4.26)$$

Since $(G_i^{(k)})^2 = 1$, $(G_i^{(k)})^{-1} = G_i^{(k)}$ and each $G_i^{(k)}$ commutes with each other, the consistency condition is trivially satisfied for both the cases. However the main challenge is to ensure that such conditions are fulfilled for the larger (embedding) symmetries [102–104] which we do not explore here in this work.

Resolving the shortcomings of SSA, both the viable modified SSA matrices, referred as M_ν^{MS1} and M_ν^{MS2} , possess intriguing phenomenology. This has been discussed in section 4.5 on numerical analysis. For the time being let's focus on the implementation of the symmetry in a more specific way. So far we have discussed a possible complex extension for a general M_ν , not so about the origin of the neutrino masses. This would be interesting to see the effects of generalized $\mathbb{Z}_2 \times \mathbb{Z}_2$ on a particular mechanism that generates the light neutrino masses. Obviously, the choice depends upon the phenomenological interest. Here we choose the type-I seesaw mechanism and investigate possible consequences of the generalized $\mathbb{Z}_2 \times \mathbb{Z}_2$ to explore the phenomena of baryogenesis via leptogenesis. A detailed discussion about these has been presented in the next two sections. First, we show the reconstruction of the effective modified SSA matrices through type-I seesaw mechanism with proper

implementation of the symmetry on the constituent matrices (m_D and M_R). Then we discuss some aspects of baryogenesis via leptogenesis related to this scheme.

4.3 Reconstruction of modified scaling matrices with type-I seesaw

For the realization of generalized $\mathbb{Z}_2 \times \mathbb{Z}_2$ in the context of type-I seesaw mechanism, we define two separate ‘ G ’ matrices G_L and G_R for ν_L and N_R fields respectively. Now the CP transformations are defined on these fields as [145]

$$\nu_{L\alpha} \rightarrow i(G_L)_{\alpha\beta}\gamma^0\nu_{L\beta}^C, \quad N_{R\alpha} \rightarrow i(G_R)_{\alpha\beta}\gamma^0N_{R\beta}^C. \quad (4.27)$$

With m_D as a Dirac type and M_R as a diagonal nondegenerate Majorana type mass matrix, the Lagrangian for type-I seesaw

$$-\mathcal{L} = \bar{N}_{iR}(m_D)_{i\alpha}l_{L\alpha} + \frac{1}{2}\bar{N}_{iR}(M_R)_i\delta_{ij}N_{jR}^C + \text{h.c.} \quad (4.28)$$

leads to the effective 3×3 light neutrino Majorana mass matrix M_ν as

$$M_\nu = -m_D^T M_R^{-1} m_D. \quad (4.29)$$

Now the invariance of the mass terms of (4.28) under the CP transformations defined in (4.27) leads to the relations

$$G_R^\dagger m_D G_L = m_D^*, \quad G_R^\dagger M_R G_R^* = M_R^*. \quad (4.30)$$

Eqs.(4.29) and (4.30) together imply $G_L^T M_\nu G_L = M_\nu^*$. Now, specifying G_L by $G_i^{(k)}$, we obtain the key equation

$$\left(G_i^{(k)}\right)^T M_\nu G_i^{(k)} = M_\nu^*. \quad (4.31)$$

Since M_R is taken to be diagonal i.e., $M_R = \text{diag}(M_1, M_2, M_3)$, the corresponding symmetry generator matrix G_R is diagonal [145] with entries ± 1 , i.e.,

$$(G_R)_{lm} = \pm \delta_{lm}. \quad (4.32)$$

which implies for each G_L , there are eight different structures for G_R that correspond to eight different choices of m_D . However, a straightforward computation shows that for the case-I, the G_R matrix compatible with $G_2^{(k)}$ and $G_3^{(k)}$ should be taken as $(G_R)_2 = \text{diag}(1, 1, 1)$ and $(G_R)_3 = \text{diag}(-1, -1, -1)$ respectively. Similarly for Case-II also, those are taken as $(G_R)_1 = \text{diag}(1, 1, 1)$ and $(G_R)_3 = \text{diag}(-1, -1, -1)$ for $G_1^{(k)}$ and $G_3^{(k)}$. It can be shown that all the other choices of G_R are incompatible with scaling symmetry. Therefore, the first of (4.30) leads to

$$\begin{aligned} m_D G_3 &= -m_D^*, m_D G_2 = m_D^* && \text{for Case-I} \\ m_D G_3 &= -m_D^*, m_D G_1 = m_D^* && \text{for Case-II.} \end{aligned} \quad (4.33)$$

For both the cases as discussed above, the most general form of m_D that satisfies the constraints of (4.33) can be parameterized as

$$m_D^{MS} = \begin{pmatrix} a & b_1 + ib_2 & -b_1/k + ib_2k \\ e & c_1 + ic_2 & -c_1/k + ic_2k \\ f & d_1 + id_2 & -d_1/k + id_2k \end{pmatrix} \quad (4.34)$$

with

$$b_1 = \pm ak(1 + k^2)^{-1/2}\kappa_{\pm}, c_1 = \pm ek(1 + k^2)^{-1/2}\kappa_{\pm}, d_1 = \pm fk(1 + k^2)^{-1/2}\kappa_{\pm}. \quad (4.35)$$

Here the ‘ \pm ’ sign in the expressions of b_1, c_1 and d_1 are for Case-I and Case-II respectively. In (4.34) a, e, f, b_2, c_2 and d_2 are six a priori unknown real mass dimensional quantities and k is a real, positive, dimensionless parameter. Now using the seesaw relation in (4.29), it is easy to reconstruct the effective mass matrices M_{ν}^{MS1} and M_{ν}^{MS2} for Case-I and Case-II respectively. In Table 4.1, we present the parameters of the effective light neutrino mass matrix in terms of the Dirac and Majorana components.

Table 4.1: Parameters of M_{ν} .

$p = -\left(\frac{a^2}{M_1} + \frac{e^2}{M_2} + \frac{f^2}{M_3}\right)$ $q_1 = -\frac{\kappa_{\pm} p}{\sqrt{1+k^2}}$ $q_2 = -k\left(\frac{ab_2}{M_1} + \frac{ec_2}{M_2} + \frac{fd_2}{M_3}\right)$ $s = -\frac{\kappa_{\pm}^2 pk}{1+k^2} + k\left(\frac{b_2^2}{M_1} + \frac{c_2^2}{M_2} + \frac{d_2^2}{M_3}\right)$ $r = (sk + p) - q_1 \sqrt{1+k^2} \left(\kappa_{\pm} - \frac{1}{\kappa_{\pm}}\right)$
--

Once again ‘ \pm ’ sign in κ are for Case-I and Case-II respectively.

Before we conclude this section, we would like to address the following: it is clear from (4.8) and (4.32) that the matrices \overline{G}_L and G_R are of different form. This is since we choose to work in a basis where M_R is diagonal but m_D is not (“leptogenesis basis” [145]). However that does not mean that the left handed and right handed field must transform differently. The form of G_R , i.e., $G_R = \text{diag}(\pm 1, \pm 1, \pm 1)$ is obtained purely for the diagonal M_R matrix. In principle one may assume same residual symmetry (say G) in the matrices m_D and M_R when both of them are nondiagonal.

However, in a basis where M_R is diagonal the symmetry in the nondiagonal M_R ultimately changes to $G_R = \text{diag}(\pm 1, \pm 1, \pm 1)$ while the symmetry in the left handed field remains the same.

To see this explicitly, we consider the Lagrangian of (4.28) with a nondiagonal M_R . Now M_R could be diagonalized by a unitary matrix U_N as

$$U_N^\dagger M_R U_N = M_R^d = \text{diag}(M_1, M_2, M_3), \quad (4.36)$$

where M_R^d is a real diagonal matrix with nondegenerate eigenvalues. Eq.(4.30) can now be rewritten as

$$G^\dagger m_D G = m_D^*, \quad G^\dagger M_R G^* = M_R^*, \quad (4.37)$$

where we have assumed same symmetry for both the fields. Now the second equation of (4.37) and (4.36) together imply

$$U_N^T G^\dagger U_N = d^\dagger, \quad (4.38)$$

where d is a diagonal matrix with $d_{jj} = \pm 1$. In the basis where the RH neutrino mass matrix is diagonal one can have a modified Dirac matrix as

$$m_D \rightarrow m'_D = U_N^\dagger m_D. \quad (4.39)$$

Thus the first equation of (4.37) and (4.38) give

$$U_N^* d^\dagger U_N^\dagger m_D G = m_D^* \quad \text{or} \quad d^\dagger m'_D G = m_D'^*, \quad (4.40)$$

where m'_D is defined in (4.39). Thus starting from a basis where M_R is nondiagonal,

we obtain the identical complex symmetry condition on the Dirac mass matrix as given in (4.30) in the basis where M_R is diagonal. This is worth mentioning that the matrix d is basically the matrix G_R of (4.32) since they both are diagonal with entries ± 1 .

4.4 Baryogenesis via leptogenesis

An introduction to the framework of baryogenesis via leptogenesis were already given in Sec. 1.5.1. Here, we first note that the flavor sum of the second term in (1.87) is

$$\sum_{\alpha} \text{Im}[h_{ji}(m_D)_{i\alpha}(m_D^*)_{j\alpha}] = \text{Im}[h_{ji}h_{ij}] = \text{Im}|h_{ji}|^2 = 0, \quad (4.41)$$

while the first term is proportional to $\text{Im}(h_{ij}^2)$. Now for both the cases in our model, h has a generic form

$$h = \begin{pmatrix} a^2(1 + \kappa_{\pm}^2) + b_2^2(1 + k^2) & ae(1 + \kappa_{\pm}^2) + (1 + k^2)b_2c_2 & af(1 + \kappa_{\pm}^2) + (1 + k^2)b_2d_2 \\ ae(1 + \kappa_{\pm}^2) + (1 + k^2)b_2c_2 & e^2(1 + \kappa_{\pm}^2) + c_2^2(1 + k^2) & ef(1 + \kappa_{\pm}^2) + (1 + k^2)c_2d_2 \\ af(1 + \kappa_{\pm}^2) + (1 + k^2)b_2d_2 & ef(1 + \kappa_{\pm}^2) + (1 + k^2)c_2d_2 & f^2(1 + \kappa_{\pm}^2) + d_2^2(1 + k^2) \end{pmatrix} \quad (4.42)$$

with the subscripts ‘ \pm ’ refer to Case-I and Case-II respectively. We note that h in (4.42) is a real matrix so that the flavor-summed CP asymmetry ε_i vanishes. Therefore, unflavored leptogenesis (relevant for the high temperature regime) does not take place for any N_i in this model. In general, any pre-existing asymmetry produced by the heavier RH neutrinos ($N_{2,3}$) get washed out by L -violating N_1 interactions [72] unless certain fine-tuned conditions (discussed in the Sec.4.6) are satisfied. In the present context, we assume that only the decay of N_1 matters in generating the CP asymmetry, and hence, ε_1 is the only relevant quantity for unflavored leptogenesis,

which vanishes in our model.

Next, we concentrate on computing the α -flavored CP asymmetry in terms of x_{12} , x_{13} and the elements of m_D . These are necessary ingredients for the fully flavored and the τ -flavored regimes. We find a vanishing value² of ε_1^e while $\varepsilon_1^{\mu,\tau}$ are calculated as

$$\varepsilon_1^\mu = \zeta [b_2 k^2 (\chi_1 + \chi_2) + b_1 (\chi_3 + \chi_4) - b_2 \chi_5] = -\varepsilon_1^\tau. \quad (4.43)$$

In (4.43) the real parameters ζ and χ_i ($i = 1 - 5$) are defined as

$$\zeta = [4\pi v^2 (b_1^2 + (a^2 + b_1^2 + b_2^2)k^2 + b_2 k^4)]^{-1}, \quad (4.44)$$

$$\chi_1 = b_2 (1 + k^2) [c_1 c_2 A_{12} + d_1 d_2 A_{13}], \quad (4.45)$$

$$\chi_2 = c [c_1 e A_{12} + d_1 f A_{13}], \quad (4.46)$$

$$\chi_3 = b_2 (1 + k^2) [c_1^2 A_{12} - k^2 (c_2^2 A_{12} - d_2^2 A_{13}) + d_1^2 A_{13}], \quad (4.47)$$

$$\chi_4 = -a k^2 [c_2 e A_{12} + d_2 f A_{13}], \quad (4.48)$$

$$\chi_5 = (1 + k^2) [c_1 c_2 A_{12} + d_1 d_2 A_{13}] \quad (4.49)$$

where $A_{ij} = g(x_{ij}) + (1 - x_{ij})^{-1}$.

Now for $T \sim M_1 < 10^9$ GeV regime, Y_B is well approximated with [68]

$$Y_B \simeq -\frac{12}{37g^*} \left[\varepsilon_i^e \eta \left(\frac{151}{179} \tilde{m}_e \right) + \varepsilon_i^\mu \eta \left(\frac{344}{537} \tilde{m}_\mu \right) + \varepsilon_i^\tau \eta \left(\frac{344}{537} \tilde{m}_\tau \right) \right] \quad (4.50)$$

where \tilde{m}_α are the wash-out masses, defined as

$$\tilde{m}_\alpha = \frac{|(m_D)_{1\alpha}|^2}{M_1} \quad (\alpha = e, \mu, \tau), \quad (4.51)$$

²This is also true for $\text{CP}^{\mu\tau}$ [195, 196] since $(m_D)_{1e}$, $(m_D)_{2e}$ and h are all real as in our case.

$\eta(\tilde{m}_\alpha)$ is the efficiency factor that accounts for the inverse decay and the L -violating scattering processes and g^* is the number of relativistic degrees of freedom in the thermal bath having a value $g^* \approx 106.75$ in the SM. And for $10^9 \text{ GeV} < T \sim M_1 < 10^{12} \text{ GeV}$, Y_B is approximated with [68]

$$Y_B \simeq -\frac{12}{37g^*} \left[\varepsilon_i^{(2)} \eta \left(\frac{417}{589} \tilde{m}_2 \right) + \varepsilon_i^\tau \eta \left(\frac{390}{589} \tilde{m}_\tau \right) \right], \quad (4.52)$$

where $\tilde{m}_2 = \sum_{\alpha=e,\mu} \tilde{m}_\alpha = \tilde{m}_e + \tilde{m}_\mu$ and $\varepsilon_i^{(2)} = \sum_{\alpha=e,\mu} \varepsilon_i^\alpha = \varepsilon_i^e + \varepsilon_i^\mu$.

At the end we would like to mention the following: Existing literature such as [145, 195, 196] also discussed the phenomena of leptogenesis under the framework of residual CP symmetry. They also pointed out the nonoccurrence of unflavored leptogenesis and only the viability of τ -flavored scenario in case of a preserved residual CP symmetry (in particular $\text{CP}^{\mu\tau}$) in the neutrino sector. Interestingly, Ref. [145, 195] pointed out M_1 to be $\mathcal{O}(10^{11} \text{ GeV})$ to produce Y_B in the observed range which is also true for our analysis (see numerical section). However the final analysis in Ref. [145, 195] is to some extent different from our analysis. In [145, 195], the authors present the variation of Y_B with a single model parameter for a fixed value of $M_1(5 \times 10^{11} \text{ GeV})$ and for the best fit values of the oscillation parameters. In our analysis, we stick to the near best fit values of the Yukawa parameters for which Y_B is positive. However, as we shall see in the numerical section, we can only constrain the Yukawa parameters scaled by the RH neutrino masses. Thus for a particular set of scaled parameters we can vary the value of M_1 freely and obtain an upper and a lower bound on M_1 corresponding to the observed upper and lower bound of Y_B . Another point is that in our analysis the sign of the final Y_B depends upon the primed Yukawa parameters and not on the CP phases. However, Ref. [196] discusses how in a residual CP scheme the sign of Y_B depends upon the low energy CP phases through a correction to the m_D matrix.

4.5 Numerical analysis: methodology and discussion

In order to assess the viability of our theoretical conjecture and consequent outcomes, we present a numerical analysis in substantial detail for both the viable cases. Our method of analysis and organization are as follows. First, we utilize the (3σ) values of globally fitted neutrino oscillation data (Table 4.2), together with an upper bound of 0.23 eV [53] on the sum of the light neutrino masses arising from PLANCK. To fix the absolute neutrino mass scale we assume $m_{max} \approx \sqrt{|\Delta m_{23}|^2}$ which is in general used in the type-I seesaw like models to be consistent with Davidson-Ibarra bound [153]. We can also dispense with the possibility of weak washout $K_\alpha = \tilde{m}_\alpha/10^{-3} < 1$ which strongly depends upon the initial conditions and likely to be disfavored by the current oscillation data [146]. We first constrain the parameter space in terms of the rescaled (primed) parameters defined below.

$$\begin{aligned} a &\longrightarrow a' = \frac{a}{\sqrt{M_1}}, e \longrightarrow e' = \frac{e}{\sqrt{M_2}}, \\ f &\longrightarrow f' = \frac{f}{\sqrt{M_2}}, b_{1,2} \longrightarrow b'_{1,2} = \frac{b_{1,2}}{\sqrt{M_1}}, \\ c_{1,2} &\longrightarrow c'_{1,2} = \frac{c_{1,2}}{\sqrt{M_2}}, d_{1,2} \longrightarrow d'_{1,2} = \frac{d_{1,2}}{\sqrt{M_3}}. \end{aligned} \quad (4.53)$$

Then we explore the predictions of the present model in the context of the $\beta\beta_{0\nu}$ experiments for each of the cases. Finally, in order to estimate the value of Y_B we make use of these constrained parameters with a subtlety. Since we have only constrained the primed parameters, there remains a freedom of various set of independent choices for the parameters of m_D (unprimed) along with M_i , for a given set of primed parameters. Note that for the computation of Y_B we need to feed the unprimed parameters and M_i separately. However, for the entire parameter space of primed parameters, it is impractical to generate the unprimed ones for different values of M_i as one ends up with infinite number of choices. For this, from the

entire parameter space of the primed parameters, we have considered only that set of primed parameters which corresponds to a positive value of Y_B (sign of Y_B depends upon the primed parameters) and observables that lie near their best-fit values as dictated by the oscillation data. Then varying M_1 , we generate the corresponding unprimed set (parameters of m_D). Note that here we take only M_1 as the free parameter assuming $M_{i+1}/M_i = 10^3$ for $i = 1, 2$. Thus for each value of M_1 and corresponding unprimed parameters we obtain the final baryon asymmetry Y_B . Since Y_B has an observed upper and lower bound, we get an upper and a lower bound for M_1 also. Let's now present the numerical results of our analysis in systematic way.

Constraints from oscillation data

For each of the viable cases, both the normal ordering (NO) and inverted ordering (IO) of light neutrino masses are found to be permitted over a respectable size of parameter space consistent with the aforementioned experimental constraints. This is interesting since the ordinary SSA predicts $m_3 = 0$, and thus, inverted light neutrino mass ordering (see Sec.4.2). However in the extended case both the mass orderings are allowed due to the fact that the matrices M_ν^{MS1} and M_ν^{MS2} have nonzero determinant. The ranges of the primed parameters for both the cases I and II are graphically shown in Fig.4.1-4.4. These plots are basically two dimensional projection of a coupled six dimensional parameter space. In order to constrain the parameter space, the explicit analytic relations that have been implemented in the computer program can be found in Ref. [186] which discusses explicit expressions for the masses and mixing angles for a general 3×3 Majorana mass matrix.

In both the cases, reduction in the number of parameters upon rescaling led

to a constrained range for each of the light neutrino masses as depicted in Table 4.3. It has been found that all the light neutrino mass spectrum are hierarchical. Interestingly, though the upper bound on $\Sigma_i m_i$ is fed in as an input constraint, the bound has not been reached up in our model irrespective of the mass ordering. The predictions on $\Sigma_i m_i$ are tabulated in Table 4.3 for each of the cases.

Table 4.2: Input values fed into the analysis [13].

Parameters	θ_{12} (degrees)	θ_{23} (degrees)	θ_{13} (degrees)	Δm_{21}^2 $10^{-5}(\text{eV}^2)$	$ \Delta m_{31}^2 $ $10^{-3}(\text{eV}^2)$
3σ ranges/ others	31.29 – 35.91	38.3 – 53.3	7.87 – 9.11	7.02 – 8.09	2.32 – 2.59
Best fit values (NO)	33.48	42.3	8.50	7.50	2.46
Best fit values (IO)	33.48	49.5	8.51	7.50	2.45

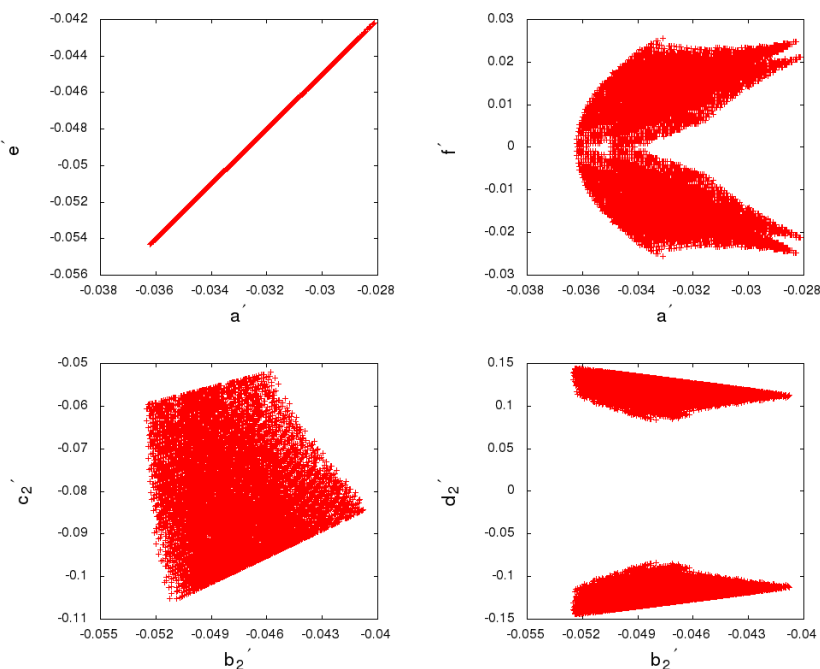


Figure 4.1: Case-I: Plots of the primed parameters for a normal mass ordering.

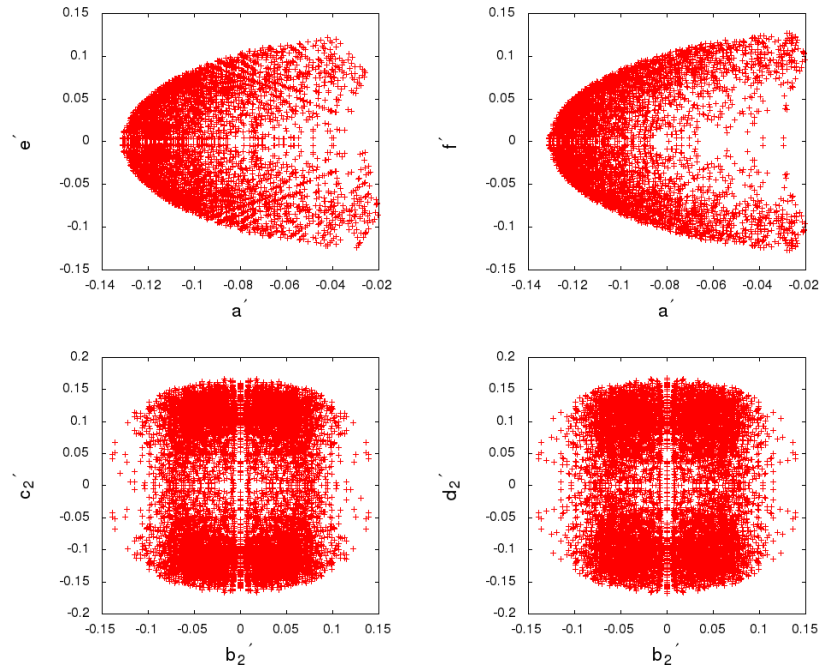


Figure 4.2: Case-I: Plots of the primed parameters for a inverted mass hierarchy.

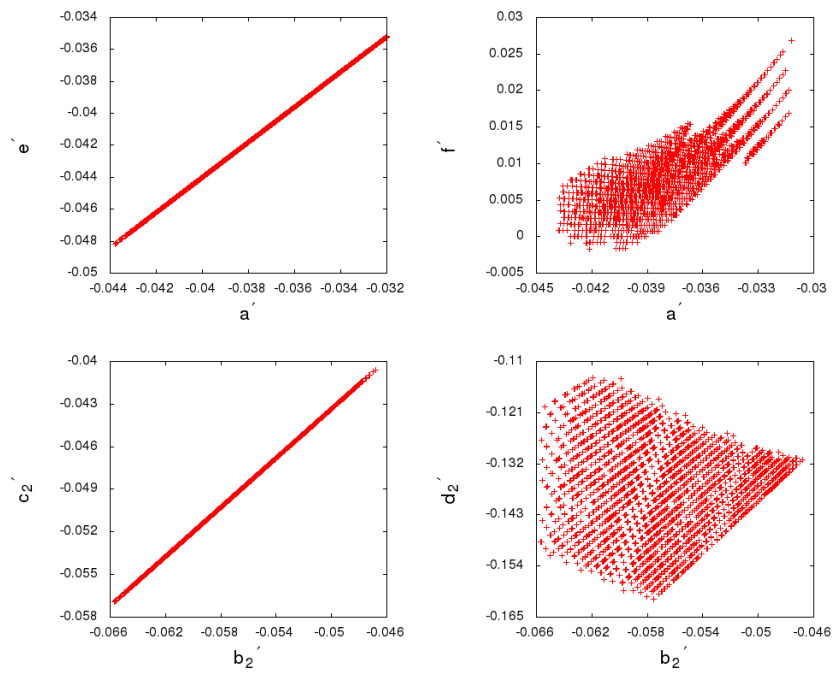


Figure 4.3: Case-II: Plots of the primed parameters for a normal mass ordering.

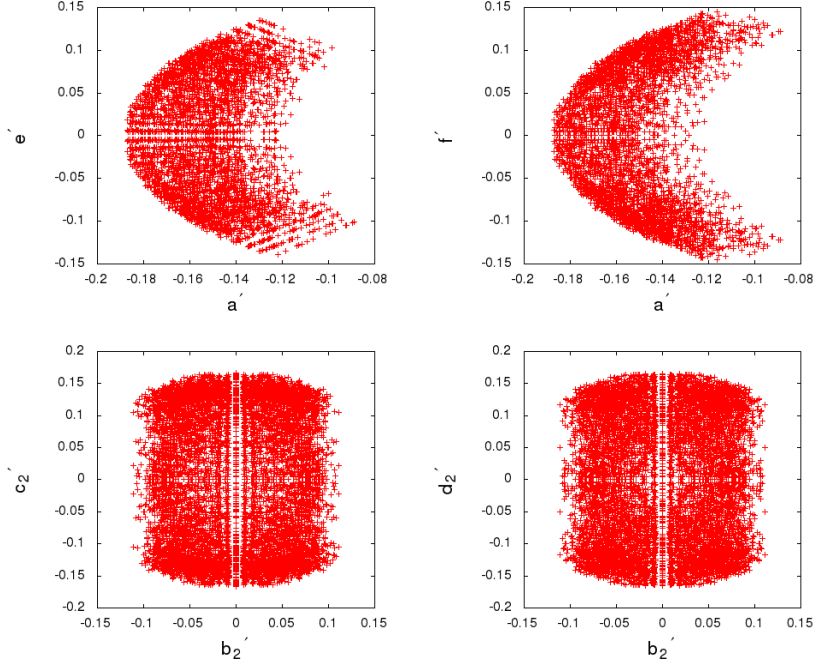


Figure 4.4: Case-II: Plots of the primed parameters for a normal mass ordering.

Table 4.3: Predictions on the light neutrino masses and $\sum_i m_i$.

Case-II					
Normal Ordering			Inverted Ordering		
$m_1/10^{-3}$	$m_2/10^{-3}$	$m_3/10^{-3}$	$m_1/10^{-3}$	$m_2/10^{-3}$	$m_3/10^{-3}$
(eV)	(eV)	(eV)	(eV)	(eV)	(eV)
4.0 – 8.5	9.28 – 12.0	49 – 52	47 – 61	49 – 62	9 – 36
$\sum_i m_i < 0.08$ eV			$\sum_i m_i < 0.16$ eV		
Normal Ordering			Inverted Ordering		
$m_1/10^{-3}$	$m_2/10^{-3}$	$m_3/10^{-3}$	$m_1/10^{-3}$	$m_2/10^{-3}$	$m_3/10^{-3}$
(eV)	(eV)	(eV)	(eV)	(eV)	(eV)
4.1 – 8.8	9.23 – 13.1	48 – 52	47 – 60	49 – 61	10 – 38
$\sum_i m_i < 0.08$ eV			$\sum_i m_i < 0.16$ eV		

Neutrinoless double beta decay ($\beta\beta_{0\nu}$)

In subsection 3.4.1, we introduced the $0\nu\beta\beta$ decay process. Using the PDG parametrization convention for U_{PMNS} [112], the M_{ee} can be written as

$$M_{ee} = c_{12}^2 c_{13}^2 m_1 + s_{12}^2 c_{13}^2 m_2 e^{i\alpha} + s_{13}^2 m_3 e^{i(\beta-2\delta)}. \quad (4.54)$$

Significant upper limits on $|M_{ee}|$ are available from various ongoing experiments. For instance, KamLAND-Zen [197] have constrained $|M_{ee}| < 0.35$ eV. However, till date the most impressive upper bound of 0.22 eV on $|M_{ee}|$ is provided by GERDA phase-I data [198] which is likely to be lowered even further by GERDA phase -II data [189] to around 0.098 eV. As shown in Ref. [119], existence of $G_3^{(k)}$ in M_ν leads to four pairs of values of the CP-violating Majorana phases α and β for each neutrino mass ordering. Since $|M_{ee}|$ is sensitive to these phases, we get four different plots for each mass ordering. In Fig.5.2 we present the plots of $|M_{ee}|$ vs. the lightest neutrino mass ($m_{1,3}$) for both the mass orderings in Case-I only. Apart from slight changes in the upper and lower limits on $m_{1,3}$, Case-II also leads to similar plots since it also predicts same results on CP violating phases (i.e. $\cos \delta = 0, \alpha, \beta = 0$ or π).

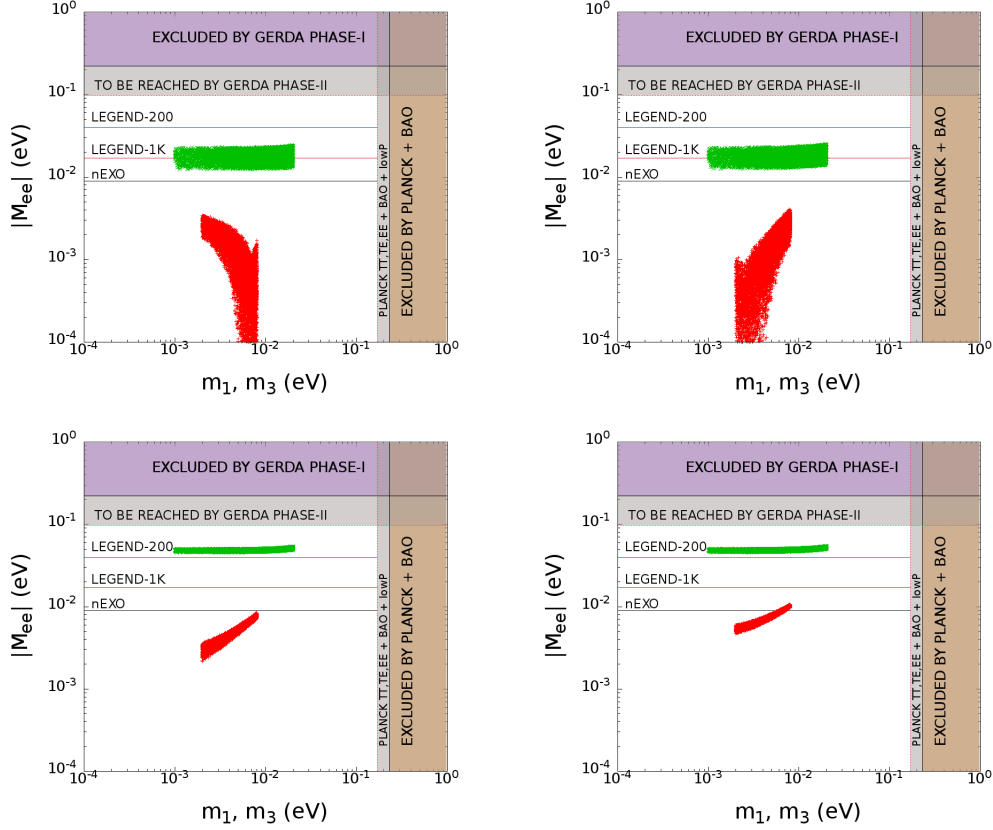


Figure 4.5: Plot of $|M_{ee}|$ vs. the lightest neutrino mass: the top two figures represent Case A: $\alpha = \pi$, $\beta = 0$ (left) and Case B: $\alpha = \pi$, $\beta = \pi$ (right) while the figures in the lower panel represent Case C: $\alpha = 0$, $\beta = 0$ (left) and Case D: $\alpha = 0$, $\beta = \pi$ (right).

This is evident from Fig.5.2 that $|M_{ee}|$ in each plot leads to an upper limit which is below the reach of the GERDA phase-II data. However, predictions of our model could be probed by GERDA + MAJORANA experiments [199]. Sensitivity reach of other promising experiments such as LEGEND-200 (40 meV), LEGEND-1K (17 meV) and nEXO (9 meV) [11] are also shown in Fig.5.2. Note that for each case, the entire parameter space corresponding to the inverted mass ordering could be excluded by the nEXO reach. One can also explain the nature of the plots analytically. Let us first consider the inverted mass ordering. In this case, with the approximations

$m_3 \simeq 0$ and $m_1 \simeq m_2$, $|M_{ee}|$ simplifies to

$$|M_{ee}| = \sqrt{|\Delta m_{32}|^2 c_{13}^2 [\{1 - s_{12}^2 (1 - \cos \alpha)\}^2 + s_{12}^4 \sin^2 \alpha]^{1/2}}. \quad (4.55)$$

Clearly, $|M_{ee}|$ is not sensitive to the phases β and δ . On the other hand, for $\alpha = \pi$ and 0 (4.55) further simplifies to

$$|M_{ee}| = \sqrt{|\Delta m_{32}|^2 c_{13}^2 [1 - 2s_{12}^2]^2}, \text{ and } |M_{ee}| = \sqrt{|\Delta m_{32}|^2 c_{13}^2} \quad (4.56)$$

respectively. Therefore, for $\alpha = \pi$ (cases A, B), $|M_{ee}|$ is suppressed as compared to the case $\alpha = 0$ (cases C, D). Now for a NO, in addition to the s_{13} suppression, there is a significant interference between the first two terms. If $\alpha = 0$, the first two terms interfere constructively and we obtain a lower bound ($\sim 10^{-3}$ eV for Case C and $\sim 5 \times 10^{-3}$ eV for Case D) despite it being a case of NO of the light neutrinos. This is one of the crucial results of the present analysis. On the other hand, for $\alpha = \pi$, the first two terms interfere destructively and thus a sizable cancellation between them brings down the value of $|M_{ee}|$ and results in the kinks that is depicted in the lower curves in the top two figures.

Baryogenesis via flavored leptogenesis

As mentioned in the beginning of the numerical section, to get a positive Y_B , we were obliged to use those value of the primed parameters for which the low energy neutrino parameters predicted from our model lie close to their best fit values dictated by the oscillation experiment. To facilitate this purpose, we define a variable χ^2 in (4.57) that measures the deviation of the parameters from their best fit values.

$$\chi^2 = \sum_{i=1}^5 \left[\frac{\mathcal{O}_i(th) - \mathcal{O}_i(bf)}{\Delta \mathcal{O}_i} \right]^2. \quad (4.57)$$

In (4.57)) \mathcal{O}_i denotes the i^{th} neutrino oscillation observable among $\Delta m_{21}^2, \Delta m_{32}^2, \theta_{12}, \theta_{23}$ and θ_{13} and the summation runs over all of them. The parenthetical th stands for the numerical value of the observable given by our model, whereas bf denotes the best fit value (cf. Table 4.2). $\Delta\mathcal{O}_i$ in the denominator stands for the measured 1σ range of \mathcal{O}_i . For numerical computation, we choose $M_{i+1}/M_i = 10^3$ ($i = 1, 2$)³. First we calculate χ^2 as a function of the primed parameters in their constrained range. For a fixed value of M_1 , we then start with the minimum value of χ^2 and we keep on increasing it until Y_B attains a positive value. For that particular χ^2 i.e., for a particular set of primed parameters, we are then able to generate a large set of unprimed parameters by varying M_1 over a wide range and can calculate Y_B for each value of M_1 . Let's discuss our results case by case for each mass ordering.

Case-I: Y_B for normal mass ordering of light neutrinos:

$M_1 < 10^9$ GeV: In this regime, all three lepton flavors (e, μ, τ) are distinguishable. Since $\varepsilon_1^e = 0$, we need to individually evaluate $\varepsilon_1^{\mu, \tau}$ only. Numerically, the maximum value of $|\varepsilon_1^{\mu, \tau}|$ is found to be $\sim 10^{-8}$. Y_B in the observed range cannot be generated with such a small CP asymmetry parameter. Theoretically, this can be understood as an interplay between various quantities. A unique feature in the present model is that the nonzero value of θ_{13} and ε_i originated from the imaginary part of the m_D matrix.

10^9 GeV $< M_1 < 10^{12}$ GeV: Before calculating final Y_B , we have to look first at the wash-out parameters $K_\alpha = \tilde{m}_\alpha/10^{-3}$ relevant to this mass regime. Since in this regime only τ flavor is distinguishable, there are two wash-out parameters, K_τ and $K_2 = K_e + K_\mu$. As shown in the first plot of Fig.4.6, the entire range of these

³In the next section a detailed discussion is given regarding the sensitivity of Y_B to the chosen hierarchy of M_i .

parameters is not much greater than 1 for the observed range of Y_B . Thus the efficiency factor in (4.52) can be written for this mild wash-out scenario [68] as

$$\eta(\tilde{m}_\alpha) = \left[\left(\frac{\tilde{m}_\alpha}{8.25 \times 10^{-3}} \right)^{-1} + \left(\frac{0.2 \times 10^{-3}}{\tilde{m}_\alpha} \right)^{-1.16} \right]^{-1}. \quad (4.58)$$

We then perform a χ^2 scanning of the primed parameters. It has been found that for $\chi_{min}^2 = 0.083$ one can have Y_B positive. Basically, In our scheme, (4.52) of the present manuscript can be written as

$$Y_B \simeq \frac{12}{37g^*} \varepsilon_1^\mu \left[\eta\left(\frac{390}{589} \tilde{m}_\tau\right) - \eta\left(\frac{417}{589} \tilde{m}_2\right) \right]. \quad (4.59)$$

Thus the sign of Y_B depends upon the sign of ε_1^μ and the quantity in brackets. Next, we take a particular set from the primed parameter space, calculate the corresponding χ^2 and then Y_B . This has been seen that data sets corresponding to $\chi^2 < 0.083$ cannot produce positive Y_B , since for those, we get positive values of ε_1^μ but negative values for the bracketed quantity. A complete data set of the primed parameters and corresponding values of the observables are tabulated in Table 4.4 for $\chi_{min}^2 = 0.083$. The other parameters i.e., b_1, c_1, d_1 can be calculated using (4.35).

Table 4.4: Parameters and observables corresponding $\chi^2 = 0.083$ for normal mass ordering.

a'	e'	f'	b'_2	c'_2	d'_2	χ^2
-0.036	-0.050	0.003	-0.052	-0.059	-0.122	0.083
observables		θ_{13}	θ_{12}	θ_{23}	$\Delta m_{21}^2 \times 10^5$	$ \Delta m_{31} ^2 \times 10^3$
$\chi^2 = 0.083$		8.42^0	33.04^0	42.54^0	7.57 (eV)^2	2.55 (eV)^2

Finally, given the primed data set for that χ_{\min}^2 , M_1 is varied widely to have Y_B in the observed range. For each value of M_1 , a set of values of the unprimed parameters $\{a, e, f, b_1, c_1, d_1, b_2, c_2, d_2\}$ is generated. Final Y_B is then calculated for each values of M_1 and the corresponding unprimed set.

A careful surveillance of Fig.4.7 reveals that we can obtain an upper and a lower bound on M_1 from the observed range of Y_B . To show this clearly, two straight lines have been drawn parallel to the abscissa in the mentioned plot: one at $Y_B = 8.55 \times 10^{-11}$ and the other at $Y_B = 8.77 \times 10^{-11}$. The values of M_1 , where the straight lines meet the Y_B vs M_1 curve, yield the allowed lower and upper bounds on M_1 , namely $(M_1)_{lower} = 2.17 \times 10^{11}$ GeV and $(M_1)_{upper} = 2.23 \times 10^{11}$ GeV. To explain this linear correlation between M_1 and Y_B one could see the expression for ε_1^μ in (4.62). As one can see from (4.62), ε_1^α is composed of two terms. The first term is proportional to M_1/M_j while the second term is proportional $(M_1/M_j)^2$. Now for the assumed hierarchical scenario ($M_3 \gg M_2 \gg M_1$), the first term dominates (cf. Eq.4.63) and effectively ε_1^α becomes proportional to M_1 (theoretically which is not the case due to the presence of the second term). Now in (4.52), in the expression of Y_B , the wash-out parameters only depend upon the primed parameters. Thus effectively the final baryon asymmetry Y_B is also proportional to M_1 . One might also ask about the narrow range for M_1 as we see in the Fig.4.7. Basically we have presented our result for a particular set of primed parameters (for $\chi_{min}^2 = 0.083$).

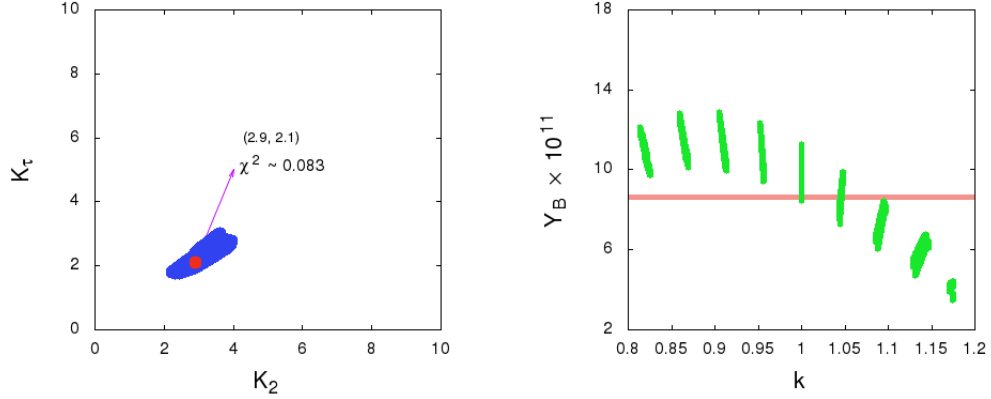


Figure 4.6: The plot on the left panel shows the range of the wash-out parameters. The red dot corresponds to the minimum value of χ^2 for which a set of primed parameters has been taken to compute Y_B . The plot on the right panel shows a variation of Y_B vs k . The red band in the same plot indicates the observed range of Y_B .

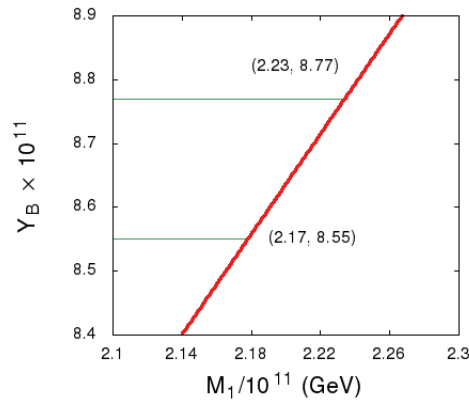


Figure 4.7: A plot of the final Y_B for different values of M_1 for a normal light neutrino mass ordering.

From Table 4.4, we infer that $\theta_{23} = 42.54^\circ$ corresponding to $\chi_{min}^2 = 0.083$. Since theoretically θ_{23} is related only with a single model parameter k (cf. Eq.(4.16)) and

unlike the other parameters of m_D (discussed earlier in this section) value of k does not depend upon the variation of M_1 , θ_{23} remain fixed for the entire range of M_1 that corresponds to the observed range of Y_B . Thus an experimentally appealing conclusion of this scheme is that, given the observed range of Y_B , the octant of θ_{23} is determined ($< \pi/4$). One can also check the sensitivity of the produced Y_B to the entire range of θ_{23} in a slightly different way. It is trivial to find out the analytic form of Y_B that explicitly depend upon θ_{23} , by replacing $k = (\tan \theta_{23})^{-1}$ in the expression of ε_1'' and m_α in (4.59). Thus for a fixed value of M_1 one can use the entire parameter space of the primed parameters and k to compute the final Y_B . From the plot on the right panel of Fig.4.6, we see that the value of k is always greater than 1 for Y_B to be in the observed range (represented by the red narrow strip in Fig.4.6). This is certainly for a particular value of $M_1(6.79 \times 10^{11}\text{GeV})$. As previously mentioned, Y_B is almost proportional to M_1 , thus lowering the value of the latter below $6.79 \times 10^{11}\text{GeV}$ would cause a downward movement of the overall pattern of the Y_B vs. k plot in Fig.4.6. Thus for the observed range of Y_B , along with the values $k > 1$, there would be other values of k which are less than one. It is seen that for the normal mass ordering in Case-II a similar lower limit on M_1 exist that dictates the octant of θ_{23} for the the observed range of Y_B .

It should be emphasized that the lower bound obtained in the second method is different from that obtained in the first. This is simply because the ways of obtaining these bounds are different. In the first method, keeping k and the primed parameters fixed at their best-fit values M_1 is freely varied so as to obtain the observed range of Y_B which in turn enables us to determine an upper and lower bound on M_1 . In the second method, for a fixed value of M_1 , we compute Y_B using the entire parameter space for k and the primed parameters. The plot of Y_B vs. k in Fig.4.6 for $M_1 = 6.79 \times 10^{11}\text{GeV}$ represents the lower bound on M_1 above which we always get $k > 1$ for the observed range of Y_B . If we further lower the value of M_1 from $6.79 \times 10^{11}\text{GeV}$, in the second

approach, it would lead to a downward movement of Y_B vs k curve in Fig.4.6 or in Fig.4.9. In that case both $k > 1$ and $k < 1$ values are possible for the observed range of Y_B . Obviously this has an impact on the results obtained in the first method. From the first method we know that if we choose the best fit value of k , the allowed range of M_1 should be read from Fig.4.7. This does not necessarily mean that for this range of M_1 , other values of k are not possible (obviously those values of k should not be the best fit values then) since the range shown in Fig.4.7 is below $M_1 = 6.79 \times 10^{11}$ GeV.

$M_1 > 10^{12}$ GeV: It has been shown that $Y_B = 0$ here for our model.

Case-I: Y_B for inverted mass ordering of light neutrinos:

Following the same procedure as for the normal mass ordering, a final discussion for each regime is summarized as follows.

$M_1 < 10^9$ GeV: Similar to the normal ordering, the $|\varepsilon_1^{\mu,\tau}|$ can have values at most the order of 10^{-8} which is not sufficient to let Y_B come within its observed range.

10^9 GeV $< M_1 < 10^{12}$ GeV: Unlike the previous case the ranges of the the wash-out parameters (cf. Fig.4.8) favors a strong wash-out scenario.

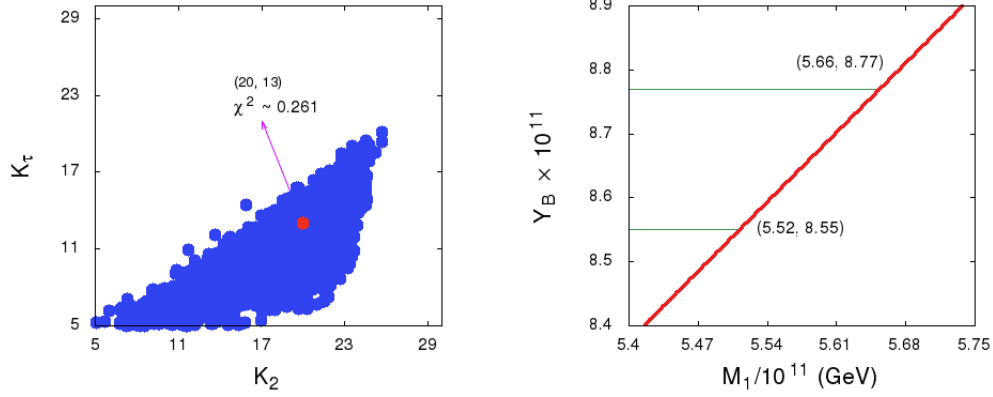


Figure 4.8: The plot on the left panel shows the range of the wash-out parameters. The red dot corresponds to the minimum value of χ^2 for which a set of primed parameter has been taken to compute Y_B . The plot on the right panel shows final Y_B for different values of M_1 for the inverted light neutrino mass ordering.

Thus the efficiency factor in (4.52) can be written for this strong wash-out scenario [68] as

$$\eta(\tilde{m}_\alpha) = \left[\left(\frac{0.55 \times 10^{-3}}{\tilde{m}_\alpha} \right)^{1.16} \right]. \quad (4.60)$$

For $\chi_{min}^2 = 0.261$, a set of primed parameters is obtained (cf. Table 4.5). Then similar to the previous case, varying M_1 in a wide range, a lower and upper bound on M_1 , namely $(M_1)_{lower} = 5.52 \times 10^{11}$ GeV and $(M_1)_{upper} = 5.66 \times 10^{11}$ GeV is obtained for the observed range of Y_B . A plot of Y_B vs M_1 is shown in the right panel of Fig.4.8.

$M_1 > 10^{12}$ GeV: Once again, $Y_B = 0$ in this regime, for the present model.

Table 4.5: Parameters and observables corresponding $\chi^2 = 0.261$ for inverted hierarchy.

a'	e'	f'	b'_2	c'_2	d'_2	χ^2
-0.043	-0.065	0.116	0.130	-0.019	0.039	0.261
observables		θ_{13}	θ_{12}	θ_{23}	$\Delta m_{21}^2 \times 10^5$	$ \Delta m_{31} ^2 \times 10^3$
$\chi^2 = 0.261$		8.54^0	34.07^0	49.37^0	7.53 (eV)^2	2.40 (eV)^2

Case-II: Y_B for normal mass ordering of light neutrinos: The analysis has been done exactly in the same way as was in the previous case. A systematic presentation of the obtained results is the following.

$M_1 < 10^9$ GeV: Again, Y_B in the observed range cannot be generated due to the small value of $|\varepsilon_1^{\mu,\tau}|$.

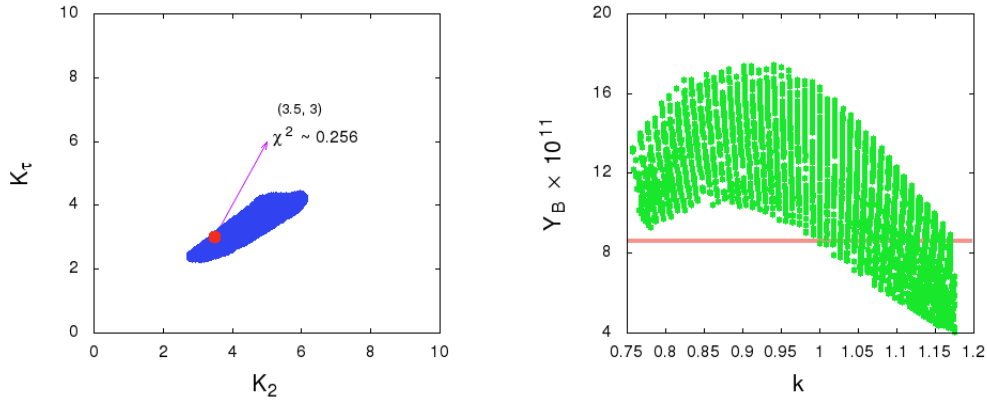


Figure 4.9: The plot on the left panel shows the range of the wash-out parameters. The red dot corresponds to the minimum value of χ^2 for which a set of primed parameter has been taken to compute Y_B . The plot on the right panel shows a variation of Y_B vs k . The red band in the same plot indicates the observed range of Y_B .

10^9 GeV $< M_1 < 10^{12}$ GeV: Similar to the previous normal hierarchical case, the

wash-out parameters here also suggest a mild wash-out scenario (cf. Fig.4.9). For $\chi^2_{min} = 0.256$, a set of rescale parameter has been found and then varying M_1 in a wide range, a lower and a upper bound on M_1 are obtained as shown in the Fig.4.10. Note that in this case also $\theta_{23} < \pi/4$ (Table 4.6) for the minimum χ^2 that produce Y_B positive and in the observed range. Similar to the case of normal mass ordering in Case-I, here we also show a Y_B vs k plot (cf. Fig.4.9) and infer that there exists a lower limit $8.2 \times 10^{11}\text{GeV}$ on M_1 for which $k > 1$, i.e., $\theta_{23} < \pi/4$ for Y_B to be in the observed range.

Table 4.6: Parameters and observables corresponding $\chi^2 = 0.256$ for normal mass ordering.

a'	e'	f'	b'_2	c'_2	d'_2	χ^2
-0.042	-0.046	-0.005	-0.065	-0.056	-0.128	0.256
observables		θ_{13}	θ_{12}	θ_{23}	$\Delta m_{21}^2 \times 10^5$	$ \Delta m_{31} ^2 \times 10^3$
$\chi^2 = 0.256$		8.37^0	33.08^0	43.49^0	7.55 (eV)^2	2.55 (eV)^2

$M_1 > 10^{12}$ GeV: It has been shown that $Y_B = 0$ here for our model.

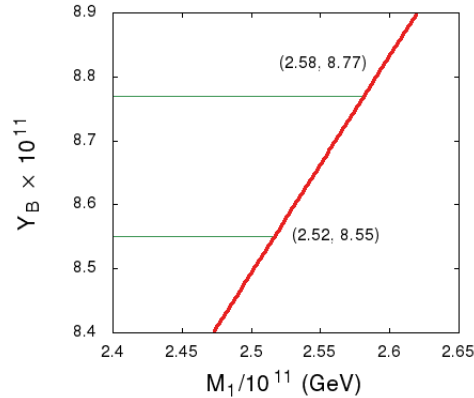


Figure 4.10: A plot of the final Y_B for different values of M_1 for the normal light neutrino mass ordering.

Case-II: Y_B for inverted mass ordering of light neutrinos:

Proceeding exactly in the same manner as for the normal mass ordering, a brief discussion for each regime goes as follows.

$M_1 < 10^9$ GeV: Similar to the normal ordering, the $|\varepsilon_1^{\mu,\tau}|$ can have values at most the order of 10^{-8} which is not sufficient to let Y_B come within its observed range.

10^9 GeV $< M_1 < 10^{12}$ GeV: Unlike the previous case the ranges of the wash-out parameters (cf. Fig.4.11) favors a strong wash-out scenario. For $\chi^2_{min} = 0.041$ a set of primed parameters is obtained (cf Table 4.7). Then similar to the previous case varying M_1 in a wide range a lower and upper bound on M_1 , namely $(M_1)_{lower} = 5.27 \times 10^{11}$ GeV and $(M_1)_{upper} = 5.40 \times 10^{11}$ GeV is obtained for the observed range of Y_B . A plot of Y_B vs M_1 is shown in the right panel of Fig.4.11.

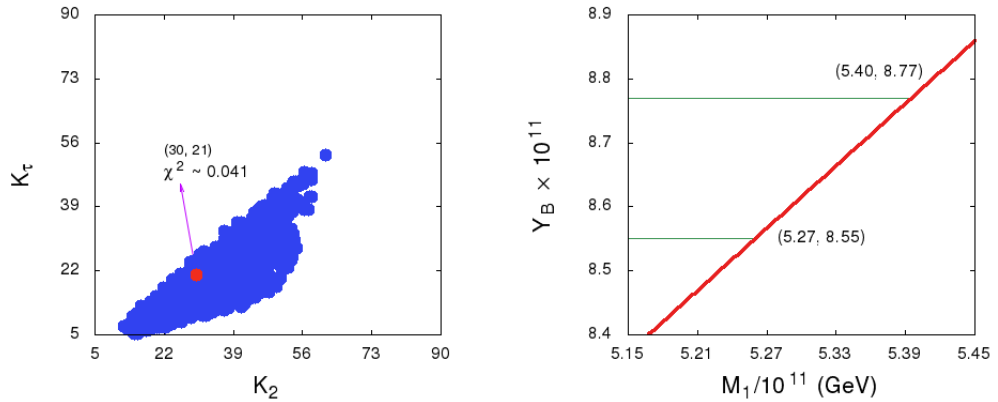


Figure 4.11: The plot on the left panel shows the range of the wash-out parameters. The red dot corresponds to the minimum value of χ^2 for which a set of primed parameter has been taken to compute Y_B . The plot on the right panel shows final Y_B for different values of M_1 for the inverted light neutrino mass ordering.

Table 4.7: Parameters and observables corresponding $\chi^2 = 0.041$ for inverted hierarchy.

a'	e'	f'	b'_2	c'_2	d'_2	χ^2
-0.123	-0.084	0.123	0.104	-0.052	-0.096	0.041
observables		θ_{13}	θ_{12}	θ_{23}	$\Delta m_{21}^2 \times 10^5$	$ \Delta m_{31} ^2 \times 10^3$
$\chi^2 = 0.041$		8.71^0	33.43^0	49.23^0	7.58 (eV)^2	2.44 (eV)^2

$M_1 > 10^{12}$ GeV: Once again, $Y_B = 0$ here for the present model.

A compact presentation of the final conclusions regarding Y_B from the numerical analysis is given in Table 4.8.

Table 4.8: Final statements on Y_B for different mass regimes.

Type	$M_1 < 10^9$ GeV	10^9 GeV $< M_1 < 10^{12}$ GeV	$M_1 > 10^{12}$ GeV
Normal Ordering	Excluded since Y_B is below the observed range for any χ^2 .	Y_B within the observed range for $\chi_{min}^2 = 0.083$.	Excluded since $Y_B = 0$.
Inverted Ordering	Excluded since Y_B is below the observed range for any χ^2 .	Y_B within the observed range for $\chi_{min}^2 = 0.261$.	Excluded since $Y_B = 0$.
Type	$M_1 < 10^9$ GeV	10^9 GeV $< M_1 < 10^{12}$ GeV	$M_1 > 10^{12}$ GeV
Normal Ordering	Excluded since Y_B is below the observed range for any χ^2 .	Y_B within the observed range for $\chi_{min}^2 = 0.256$.	Excluded since $Y_B = 0$.
Inverted Ordering	Excluded since Y_B is below the observed range for any χ^2 .	Y_B within the observed range for $\chi_{min}^2 = 0.041$.	Excluded since $Y_B = 0$.

Before concluding this section, we emphasize that in this model, the imaginary part of m_D^{MS} (cf. Eq.(4.34)) plays a very crucial role. Absence of the latter leads to a

vanishing θ_{13} , and thus undetermined value of δ and most importantly a vanishing ε_i^α . Therefore, the model addresses a common origin of θ_{13} , CP violation and leptogenesis. However, although the parameters in the imaginary part of m_D^{MS} are correlated with Y_B , from (4.43) we see the parameter b_1 is also very much sensitive to ε_1^α . For example, when $b_2 = 0$ and $c_2, d_2 \neq 0$, (4.43) simplifies to

$$\varepsilon_1^\mu = 4\pi v^2 [b_1^2 + (a^2 + b_1^2)k^2]^{-1} b_1 \chi_4 = -\varepsilon_1^\tau, \quad (4.61)$$

where $\chi_4 = f(c_2, d_2)$ as defined in (4.48). Now if b_1 vanishes ε_1^μ , hence, Y_B vanishes but due to nonvanishing value of c_2, d_2 one obtains $\theta_{13} \neq 0$. However, to obtain a nonzero Y_B , along with a nonvanishing b_1 , one always needs $\chi_4 \neq 0$ which in turn implies a nonzero θ_{13} . Thus in this model a nonzero θ_{13} does not always imply a nonzero Y_B but the reverse is not true.

4.6 Effect of $N_{2,3}$ on final Y_B

In the present analysis, the effect of the two heavier neutrinos (N_2, N_3) on the final baryon asymmetry has been neglected with the assumption that the asymmetries produced by the decays of both N_2 and N_3 get washed out [72]. In this section, we present a brief discussion on the sensitivity of the heavier neutrinos to final Y_B . There are two ways that such a sensitivity might arise as elaborated below.

Indirect effect of $N_{2,3}$:

Although the neutrino oscillation data have been fitted with the primed parameters, (cf. (4.53)), one needs to evaluate the unprimed parameters (i.e. the matrix elements of m_D) for computing quantities relevant to leptogenesis e.g., ε_1^α . It

is interesting to inquire whether the final Y_B is affected by the chosen hierarchies of the RH neutrinos. It turns out that the final Y_B is not much sensitive to $M_{2,3}$. To better appreciate this, we note that the CP asymmetry parameters of (1.87) simplifies to

$$\varepsilon_1^\alpha = -\frac{1}{4\pi v^2 h_{11}} \left(\frac{3}{2} \sum_{j=2,3} \frac{M_1}{M_j} \text{Im}[h_{1j}(m_D)_{1\alpha}(m_D^*)_{j\alpha}] + \sum_{j=2,3} \frac{M_1^2}{M_j^2} \text{Im}[h_{j1}(m_D)_{1\alpha}(m_D^*)_{j\alpha}] \right) \quad (4.62)$$

after approximating $g(x_{1j})$ to $g(x_{1j}) = -\frac{3}{2\sqrt{x_{1j}}}$ for $x_{1j} \gg 1$. The last term of (4.62) is of $\mathcal{O}(x_{1j}^{-2})$, and hence, heavily suppressed. The first term has two parts for $j = 2, 3$. The $j = 3$ term has negligible effect on ε_1^α since $M_3 \gg M_1$ and the values of f, d_1 and d_2 are of $\mathcal{O}(m_D)$. With this, for $j = 2$ term, ε_1^α simplifies to

$$\varepsilon_1^\mu = -\frac{3M_1}{8\pi v^2 h_{11}} [(ae' + b_1c'_1 + b_2c'_2)(b_2c'_1 + b_1c'_2)] = -\varepsilon_1^\tau \quad (4.63)$$

with $\varepsilon_1^e = 0$ as already shown in Sec.4.4. Since the primed parameters are already fixed by the oscillation data, $\varepsilon_1^{\mu,\tau}$ are practically insensitive to the value of M_2 . However, for the numerical computation of the final baryon asymmetry, we take into account each term in (4.62) with two different mass hierarchical schemes for the heavy neutrinos, e.g, $M_{i+1}/M_i = 10^2$ and $M_{i+1}/M_i = 10^4$ where i can take the values 1, 2. Note that in the previous section we have already computed Y_B for $M_{i+1}/M_i = 10^3$. The outcome of the numerical analysis is that though the chosen mass ratios of the RH neutrinos are altered, changes in the lower and upper bounds on M_1 are not significant for the observed range of Y_B . For convenience, for each case and light neutrino mass ordering, the variation of Y_B with M_1 for different mass ratios has been presented in Table 4.9.

It can be seen from Table 4.9 that the upper and lower bounds on M_1 are slightly different for each hierarchical cases. As explained earlier, while the first term of (4.62) is not sensitive to the chosen hierarchies the second term does contribute to the ε_1^μ and

therefore, to the final Y_B value. Thus, for the same value of M_1 , the contribution from the second term in (4.62) is larger for $M_{i+1}/M_i = 10^2$ and smaller for $M_{i+1}/M_i = 10^4$ w.r.t the case $M_{i+1}/M_i = 10^3$. Hence, for the case where $M_{i+1}/M_i = 10^2$, the slope of the Y_B vs. M_1 curve is greater than the case where $M_{i+1}/M_i = 10^3$. As a consequence, both the upper and the lower bounds are slightly lowered for the given range of Y_B . Similarly, we find the the bounds are slightly increased for the case $M_{i+1}/M_i = 10^4$.

Table 4.9: Bounds on M_1 for different mass ratios of the RH neutrinos ($i = 1, 2$).

Case-I: Normal ordering (NO) of light neutrinos			
Hierarchies \rightarrow	$M_{i+1}/M_i = 10^2$	$M_{i+1}/M_i = 10^3$	$M_{i+1}/M_i = 10^4$
Upper bound (GeV)	2.21×10^{11}	2.23×10^{11}	2.25×10^{11}
Lower bound (GeV)	2.16×10^{11}	2.17×10^{11}	2.18×10^{11}
Case-I: Inverted ordering (IO) of light neutrinos			
Hierarchies \rightarrow	$M_{i+1}/M_i = 10^2$	$M_{i+1}/M_i = 10^3$	$M_{i+1}/M_i = 10^4$
Upper bound (GeV)	5.64×10^{11}	5.66×10^{11}	5.67×10^{11}
Lower bound (GeV)	5.51×10^{11}	5.52×10^{11}	5.54×10^{11}
Case-II: Normal ordering (NO) of light neutrinos			
Hierarchies \rightarrow	$M_{i+1}/M_i = 10^2$	$M_{i+1}/M_i = 10^3$	$M_{i+1}/M_i = 10^4$
Upper bound (GeV)	2.57×10^{11}	2.58×10^{11}	2.59×10^{11}
Lower bound (GeV)	2.50×10^{11}	2.52×10^{11}	2.54×10^{11}
Case-II: Inverted ordering (IO) of light neutrinos			
Hierarchies \rightarrow	$M_{i+1}/M_i = 10^2$	$M_{i+1}/M_i = 10^3$	$M_{i+1}/M_i = 10^4$
Upper bound (GeV)	5.38×10^{11}	5.40×10^{11}	5.42×10^{11}
Lower bound (GeV)	5.25×10^{11}	5.27×10^{11}	5.28×10^{11}

Direct effect of N_2 :

For the sake of simplicity, we consider here the effect of N_2 only. It has been shown

in Ref. [73] that, due to a decoherence effect, a finite lepton asymmetry generated from the decays of N_2 become protected against N_1 -washout and survives down to the electroweak scale and contributes to the final baryon asymmetry. However, for this to take place, two wash-out factors $\Delta_1 = \frac{h_{11}}{M_1 m^*}$ and $\Delta_2 = \frac{h_{22}}{M_2 m^*}$ must respectively meet the conditions $\Delta_1 \gg 1$ and $\Delta_2 \not\gg 1$ with $m^* = 1.66\sqrt{g^*}\pi v^2/M_{Pl} \approx 10^{-3}$ eV.

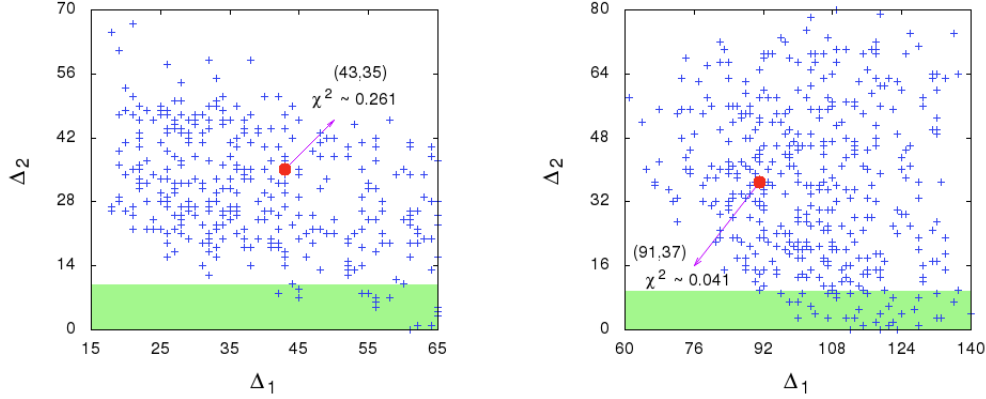


Figure 4.12: Plots of the wash-out parameters Δ_1 and Δ_2 for inverted light neutrino mass ordering for both the cases. The red dot corresponds to the corresponding χ^2_{min} for which we calculate the final baryon asymmetry.

Here, the criterion $\Delta_1 \gg 1$ indicates that faster N_1 interactions destroy the coherence among the states produced by N_2 . Thus a component of the lepton asymmetry produced by N_2 survives orthogonal to N_1 -states and gets protected against N_1 -washout. A mild wash-out of the lepton asymmetry produced by N_2 due to N_2 -interactions is expressed by the condition $\Delta_2 \not\gg 1$. For this scenario, a considerable amount of N_2 -generated lepton asymmetry survives during the phase of N_1 -leptogenesis. It has been found that for each of the cases discussed in this chapter, for a NO, both the wash-out parameters $\Delta_{1,2} < 10$. Thus faster N_1 interaction do not take place and criterion for successful N_2 leptogenesis is not satisfied. On the other hand, for IO, the allowed parameter space favors large values of Δ_2 in excess

of 10 except at the bottom (the green band). Thus the $\Delta_2 \not\gg 1$ condition is violated in most of the region. Moreover the χ^2_{min} values, for which we compute final Y_B strongly violates the condition $\Delta_2 \not\gg 1$. Few allowed points with $\Delta_2 < 10$ correspond to values of χ^2 above 0.8 which is much higher than χ^2_{min} for which we obtain Y_B in the observed range. Therefore, for our calculation, any direct effect of N_2 is not significant.

4.7 Summary and conclusion

We interpret the Strong Scaling Ansatz (SSA) in a Majorana neutrino mass matrix as the consequence of a residual $\mathbb{Z}_2 \times \mathbb{Z}_2$ symmetry. Since SSA predicts a vanishing value of θ_{13} , and hence, no measurable Dirac CP violation, it is modified by invoking a nonstandard CP transformation. We address the resulting symmetry as a generalized $\mathbb{Z}_2 \times \mathbb{Z}_2$ symmetry. Depending upon the manner in which the symmetry is implemented, there are several cases all of which have been explored in substantial detail. For each case, besides the predictions of maximal Dirac CP violation ($\delta = \pm\pi/2$) and Majorana CP conservation ($\alpha, \beta = 0, \pi$), numerically permissible ranges for the light neutrino masses as well as the $\beta\beta 0\nu$ decay parameter $|M_{ee}|$ has been obtained. Next, we show how such a generalized $\mathbb{Z}_2 \times \mathbb{Z}_2$ invariance can arise in the type-I seesaw framework and explore the possibility of baryogenesis via leptogenesis. Typical structure of the Dirac mass matrix m_D leads to a common origin of θ_{13} , leptonic CP violation and nonzero CP asymmetry parameter ε_i^α . Though we primarily focus the N_1 -leptogenesis, we discuss the effect of the heavier neutrinos $N_{2,3}$ on the final baryon asymmetry Y_B . We show that the heavier neutrinos might affect the final Y_B in two different ways: either via the chosen hierarchy of the RH neutrinos or through the asymmetry generated by the heavy neutrino itself (for simplicity we

have assumed only the effect of N_2 , i.e., N_2 leptogenesis). We found that the final Y_B is not sensitive to the chosen hierarchy of the RH neutrinos since the leading order term in ε_1^α is independent of the chosen hierarchy. In the numerical analysis we restrict ourselves to the near best-fit values of the oscillation parameters for which a positive value of Y_B is obtained. We found that the conditions for N_2 leptogenesis are not satisfied for those best-fit points. Thus N_2 -leptogenesis is also not so sensitive to the final Y_B . For each of the cases and irrespective of the light neutrino mass ordering, only τ -flavored leptogenesis scenario ($10^9 \text{ GeV} < T \sim M_1 < 10^{12} \text{ GeV}$) is found to be feasible one to generate Y_B in the observed range with the other regimes $T \sim M_1 > 10^{12}$ and $T \sim M_1 < 10^9 \text{ GeV}$ being ruled out analytically as well as numerically. The best-fit parameters for which we calculate the final Y_B , lead to the value of $\theta_{23} < \pi/4$ for NO and $\theta_{23} > \pi/4$ for IO for both Case-I and Case-II. We also found an upper and a lower bound on the lightest (M_1) of the heavy neutrino masses for each case. Finally, for a fixed value of M_1 , we also investigate the sensitivity of θ_{23} on the final Y_B . Though both neutrino mass ordering are allowed, the NO comes with an interesting prediction. It has been shown and explained in Sec.4.5 that in both the NO scenarios, there exist lower limits on M_1 , above which any value of M_1 corresponds to $\theta_{23} < \pi/4$ for Y_B to lie in the observed range.

Chapter 5

Implications of the Friedberg-Lee invariance in a neutrino mass model with $\mu\tau$ -flavored CP symmetry

5.1 Introduction

Various neutrino mass models with definitive statements about the mass ordering and the absolute scale of three light neutrino masses are yet to be tested. Also, since the octant of the atmospheric mixing angle θ_{23} remains uncertain, a precise prediction of θ_{23} can be used to exclude and discriminate models in the light of future precision measurements. For the Dirac CP phase δ , the current best-fit values are close to 234° for NO and 278° for IO. While the possibility of CP conservation ($\sin \delta = 0$) is allowed at slightly above 1σ , one of the CP violating value $\delta = \pi/2$ is disfavored at 99% CL. Thus, the remaining CP violating value $\delta = 3\pi/2$ and deviations around it still remain potentially viable possibilities. Also the rapid development of the long

baseline experiments such as T2K [200], NO ν A [194] and also $0\nu\beta\beta$ experiments such as KamLandZen [197], GERDA [189, 198] is expected to shortly resolve the above issues. Thus, from the perspective of neutrino mass model building, this is a moment of paramount importance, since many existing models that predict θ_{23} , δ and the mass ordering will be challenged through precise future measurements of these quantities.

As mentioned earlier, discrete flavor symmetries [92, 94, 99, 201] have always been quite popular paradigm in building highly predictive models of neutrino mass and mixing. These include the celebrated $\mu\tau$ interchange symmetry [113, 159–161] which, in its pristine form, was excluded after the discovery of a nonvanishing reactor mixing angle θ_{13} (now confirmed at more than 5.2σ [115]). However, it has now been revived with a simple change of usage-by using the $\mu\tau$ -interchange symmetry as the generator of a nonstandard CP symmetry ($\text{CP}^{\mu\tau}$) [100, 109]:

$$\nu_{Ll} \rightarrow iG_{lm}\gamma^0\nu_{Lm}^C, \quad (5.1)$$

instead of an exact $\mu\tau$ -interchange flavor symmetry: $\nu_{Ll} \rightarrow G_{lm}\nu_{Lm}$, in the effective neutrino Majorana mass term in the low-energy Lagrangian (density)

$$-\mathcal{L}_{\text{mass}}^\nu = \frac{1}{2}\overline{\nu_{Ll}^C}(M_\nu)_{lm}\nu_{Lm} + \text{h.c.} \quad (5.2)$$

Here, $\nu_{Ll}^C = C\overline{\nu_{Ll}}^T$. While the indices l, m span the lepton flavor indices e, μ, τ , the subscript L denotes left-handed flavor neutrino fields. M_ν is a complex symmetric matrix ($M_\nu^* \neq M_\nu = M_\nu^T$) in lepton flavor space. Though $\text{CP}^{\mu\tau}$ was proposed few years back [109, 144], recently it has gathered a lot of attention [102–105, 110, 123–125, 129, 130, 202–204] due to its exact prediction: $\theta_{23} = \pi/4$ and $\delta = \pi/2$ or $3\pi/2$ (Co-bimaximal mixing [205]), which is also a recent hint from from T2K. To make $\text{CP}^{\mu\tau}$ more predictive, a sizable body of research has been done combining CP symmetry

with other flavor symmetries [99], despite the fact that at very high energy, it is nontrivial to have a consistent theory of CP combined with flavor symmetry [102,103].

One particular generalization [3, 8] of (5.1) is $\text{CP}^{\mu\tau\theta}$ which is implemented in the neutrino Majorana mass by means of the field transformation

$$\nu_{Ll} \rightarrow iG_{lm}^\theta \gamma^0 \nu_{Lm}^C \quad (5.3)$$

where $G^{\mu\tau\theta}$ has the generic form

$$G^{\mu\tau\theta} = \begin{pmatrix} -1 & 0 & 0 \\ 0 & -\cos \theta & \sin \theta \\ 0 & \sin \theta & \cos \theta \end{pmatrix}, \quad (5.4)$$

in the flavor space. Here, ‘ θ ’ being an arbitrary mixing parameter that mixes the $\nu_{L\mu}$ and $\nu_{L\tau}$ flavors. It is worth noticing that $\theta = \pi/2$ reduces the mixing symmetry $G_{lm}^{\mu\tau\theta}$ to the interchange symmetry $G_{lm}^{\mu\tau}$ and any nonzero value of $\theta - \pi/2$ has the potential to account for the deviation from $\text{CP}^{\mu\tau}$. Though, in general, CP symmetries are highly predictive in terms of mixing angles and CP-violating phases, for most of the cases, it lacks information regarding light neutrino masses and mass ordering unless one invokes additional flavor symmetries to reduce the number of parameters [99], e.g, by the means of ‘texture zeros’ in the light neutrino mass matrix [110, 204].

In order to obtain testable predictions about neutrino masses and mixing, we consider a Friedberg-Lee (FL) transformation [206–211]

$$\nu_{Ll} \rightarrow iG_{lm}^{\mu\tau\theta} \gamma^0 \nu_{Lm}^C + \eta l \xi. \quad (5.5)$$

in combination with (5.3). This leads to

$$M^\nu \boldsymbol{\eta} = 0, \quad \text{and} \quad (G^{\mu\tau\theta})^T M_\nu G^{\mu\tau\theta} = M_\nu^*, \quad (5.6)$$

where η_l ($l = e, \mu, \tau$) are three arbitrary complex numbers, $\boldsymbol{\eta} = (\eta_e \ \eta_\mu \ \eta_\tau)^T$ and ξ is a fermionic Grassmann field [206]. Note that, (5.5) is a simple CP generalization of the ordinary (general) FL transformation (also known as twisted FL symmetry [212,213])

$$\nu_{Ll} \rightarrow G_{lm}^{\mu\tau\theta} \nu_{Lm} + \eta_l \xi \quad (5.7)$$

leading to

$$M^\nu \boldsymbol{\eta} = 0, \quad \text{and} \quad (G^{\mu\tau\theta})^T M_\nu G^{\mu\tau\theta} = M_\nu. \quad (5.8)$$

Amongst many of the interesting results (which we shall discuss in the next section) that emerge as a consequence of the transformation in (5.5), it is worthwhile to stress two important departures from $\text{CP}^{\mu\tau}$.

- First of all, as mentioned earlier, $G_{lm}^{\mu\tau\theta}$ in (5.4) is a $\mu\tau$ mixing symmetry. It reduces to ‘ $\mu\tau$ -interchange’ in the limit $\theta \rightarrow \pi/2$ which we address in rest of this chapter as ‘ $\mu\tau$ -interchange limit (MTIL)’. It is now trivial to anticipate that the mixing parameter $\theta (\neq \pi/2)$ conspires for the departure from maximal δ and θ_{23} . However, we show in this chapter that despite the generalization from $\text{CP}^{\mu\tau}$ to $\text{CP}^{\mu\tau\theta}$, the additionally imposed FL symmetry only allows a tiny deviation from the maximality of δ .

- The first condition in (5.6) is satisfied for a nontrivial eigenvector $\boldsymbol{\eta}$ if $\det M_\nu = 0$ which means at least one of the light neutrino masses is zero. Thus, by construction, this model predicts the absolute light neutrino mass scale.

For a consistent phenomenological analysis, apart from fitting the neutrino

oscillation global-fit data, we study here the impact of $\text{CP}^{\mu\tau\theta}$ symmetry on $\nu_\mu \rightarrow \nu_e$ oscillation in the long baseline experiments such as NO ν A, T2K and DUNE. In addition, in the context of recent discovery of high energy neutrino events at IceCube [41–45], assuming high energy neutrinos originate purely from distant astrophysical sources¹, we also calculate the flux-ratios which will be measured with enhanced statistics at advanced neutrino telescopes (e.g. IceCube and ANTARES) in near future. These calculations show that any potential deviation from the democratic 1:1:1 distribution of flux ratios [51, 214–216] can lead to predictions on the octant of θ_{23} in our model.

The rest of the chapter is organized as follows. Sec.5.2 contains the most general parametrization of M_ν that is invariant under (5.5), thereby satisfying the conditions of (5.6). Sec.5.3 deals with the evaluation of Majorana phases α, β and the leptonic Dirac CP phase δ for both types of mass ordering analysed in two different subsections. The numerical analysis in Sec.5.4 comprises of four subsections. Subsec.5.4.1 entails the extraction of the allowed parameter space and the prediction of light neutrino masses, whereas Subsec.5.4.2 deals with the prediction on neutrinoless double beta decay process. Subsec.5.4.3 discusses of the range of variation of the oscillation probability $P_{\mu e}$ and the CP asymmetry parameter $A_{\mu e}$ in experiments such as T2K, NO ν A and DUNE for both NO and IO. Subsec.5.4.4 comments on the possibility of determining the octant of θ_{23} from futuristic measurements of flavor flux ratios in neutrino telescopes such as IceCube.

¹We consider high energy neutrinos originating from pp and $p\gamma$ collisions.

5.2 FL transformed $CP^{\mu\tau\theta}$ invariance of M_ν

Using (5.6), a 3×3 symmetric mass matrix can most generally be parametrized as²:

$$M_\nu = \begin{pmatrix} -\frac{2a_1}{(1+c_\theta)} \frac{\eta_2}{\eta_1} & a_1 + ia_2 & -a_1 t_{\frac{\theta}{2}} + ia_2 t_{\frac{\theta}{2}}^{-1} \\ a_1 + ia_2 & c_1 t_{\frac{\theta}{2}} - a_1 \frac{\eta_1}{\eta_2} - ia_2 (1+c_\theta) \frac{\eta_1}{\eta_2} & c_1 - ia_2 t_{\frac{\theta}{2}}^{-1} c_\theta \frac{\eta_1}{\eta_2} \\ -a_1 t_{\frac{\theta}{2}} + ia_2 t_{\frac{\theta}{2}}^{-1} & c_1 - ia_2 t_{\frac{\theta}{2}}^{-1} c_\theta \frac{\eta_1}{\eta_2} & c_1 t_{\frac{\theta}{2}}^{-1} - a_1 \frac{\eta_1}{\eta_2} + ia_2 (1+c_\theta) \frac{\eta_1}{\eta_2} \end{pmatrix}, \quad (5.9)$$

where $c_\theta \equiv \cos \theta$, $s_\theta \equiv \sin \theta$ and $t_{\theta/2} = \tan \frac{\theta}{2}$. For simplicity, we restrict to a reasonable choice that η_i are a priori arbitrary complex numbers with same phases, so that the ratios $\frac{\eta_1}{\eta_1}$, $\frac{\eta_2}{\eta_3}$ and $\frac{\eta_3}{\eta_1}$ are all real and positive. In (5.9), there are five real free parameters: a_1 , a_2 , c_1 , $\frac{\eta_1}{\eta_2}$ and θ which can be well constrained by existing neutrino oscillation global-fit data. It is to be noted that (5.9) does not contain the parameter η_3 owing to a consistency relation of the form $\frac{\eta_2}{\eta_3} = -\frac{(1+c_\theta)}{s_\theta}$. The mass matrix M_ν in (5.9) can be diagonalized by a similarity transformation with a unitary matrix U :

$$U^T M_\nu U = M_\nu^d \equiv \text{diag} (m_1, m_2, m_3), \quad (5.10)$$

where m_i ($i = 1, 2, 3$) are real and we assume that $m_i \geq 0$. Without any loss of generality, we work in the diagonal basis of the charged lepton so that U can be related to the $PMNS$ mixing matrix U_{PMNS} as

$$U = P_\phi U_{PMNS} \equiv P_\phi \begin{pmatrix} c_{12}c_{13} & e^{i\frac{\alpha}{2}} s_{12}c_{13} & s_{13}e^{-i(\delta-\frac{\beta}{2})} \\ -s_{12}c_{23} - c_{12}s_{23}s_{13}e^{i\delta} & e^{i\frac{\alpha}{2}} (c_{12}c_{23} - s_{12}s_{13}s_{23}e^{i\delta}) & c_{13}s_{23}e^{i\frac{\beta}{2}} \\ s_{12}s_{23} - c_{12}s_{13}c_{23}e^{i\delta} & e^{i\frac{\alpha}{2}} (-c_{12}s_{23} - s_{12}s_{13}c_{23}e^{i\delta}) & c_{13}c_{23}e^{i\frac{\beta}{2}} \end{pmatrix}, \quad (5.11)$$

²In rest of the chapter, η_e , η_μ and η_τ are referred to as η_1 , η_2 and η_3 respectively.

where $P_\phi = \text{diag}(e^{i\phi_1}, e^{i\phi_2}, e^{i\phi_3})$ is an unphysical diagonal phase matrix and $c_{ij} \equiv \cos \theta_{ij}$, $s_{ij} \equiv \sin \theta_{ij}$ with the mixing angles $\theta_{ij} \in [0, \pi/2]$. We work within the PDG convention [112] but denote our Majorana phases by α and β . CP-violation enters through nontrivial values of the Dirac phase δ and of the Majorana phases α, β where $\delta, \alpha, \beta \in [0, 2\pi]$.

5.3 Impact of mass ordering on mixing angles and CP properties

Eqs.(5.6) and (5.10) jointly imply [109]

$$G^\theta U^* = U \tilde{d}. \quad (5.12)$$

where $\tilde{d} = \text{diag}(\tilde{d}_1, \tilde{d}_2, \tilde{d}_3)$, where each \tilde{d}_i ($i = 1, 2, 3$) is either +1 or -1, and therefore (5.12) can be written in the following explicit form:

$$\begin{pmatrix} -1 & 0 & 0 \\ 0 & -c_\theta & s_\theta \\ 0 & s_\theta & c_\theta \end{pmatrix} \begin{pmatrix} U_{e1}^* & U_{e2}^* & U_{e3}^* \\ U_{\mu 1}^* & U_{\mu 2}^* & U_{\mu 3}^* \\ U_{\tau 1}^* & U_{\tau 2}^* & U_{\tau 3}^* \end{pmatrix} = \begin{pmatrix} \tilde{d}_1 U_{e1} & \tilde{d}_2 U_{e2} & \tilde{d}_3 U_{e3} \\ \tilde{d}_1 U_{\mu 1} & \tilde{d}_2 U_{\mu 2} & \tilde{d}_3 U_{\mu 3} \\ \tilde{d}_1 U_{\tau 1} & \tilde{d}_2 U_{\tau 2} & \tilde{d}_3 U_{\tau 3} \end{pmatrix}. \quad (5.13)$$

Eq.(5.13) is equivalent to nine equations for the three rows:

$$\begin{aligned} -U_{e1}^* &= \tilde{d}_1 U_{e1}, & -U_{e2}^* &= \tilde{d}_2 U_{e2}, & -U_{e3}^* &= \tilde{d}_3 U_{e3}, \\ -U_{\mu 1}^* c_\theta + U_{\tau 1}^* s_\theta &= \tilde{d}_1 U_{\mu 1}, & -U_{\mu 2}^* c_\theta + U_{\tau 2}^* s_\theta &= \tilde{d}_2 U_{\mu 2}, & -U_{\mu 3}^* c_\theta + U_{\tau 3}^* s_\theta &= \tilde{d}_3 U_{\mu 3} \\ U_{\mu 1}^* s_\theta + U_{\tau 1}^* c_\theta &= \tilde{d}_1 U_{\tau 1}, & U_{\mu 2}^* s_\theta + U_{\tau 2}^* c_\theta &= \tilde{d}_2 U_{\tau 2}, & U_{\mu 3}^* s_\theta + U_{\tau 3}^* c_\theta &= \tilde{d}_3 U_{\tau 3} \end{aligned} \quad (5.14)$$

It is useful to construct the following two rephasing invariant quantities, that are independent of the unphysical phases, for calculating the Majorana phases:

$$I_1 = U_{e1}U_{e2}^*, \quad I_2 = U_{e1}U_{e3}^*. \quad (5.15)$$

From the first row of (5.14), we get,

$$I_1 = \tilde{d}_1\tilde{d}_2U_{e1}^*U_{e2}, \quad I_2 = \tilde{d}_1\tilde{d}_2U_{e1}^*U_{e3} \quad (5.16)$$

Using the above expressions for $I_{1,2}$, in (5.15) and (5.16), we obtain the relations,

$$c_{12}s_{12}c_{13}^2e^{-i\alpha/2} = \tilde{d}_1\tilde{d}_2c_{12}s_{12}c_{13}^2e^{i\alpha/2} \quad (5.17)$$

and

$$c_{12}s_{13}c_{13}e^{i(\delta-\beta/2)} = \tilde{d}_1\tilde{d}_3c_{12}s_{13}c_{13}e^{-i(\delta-\beta/2)}. \quad (5.18)$$

From (5.17) and (5.18), we find,

$$e^{-i\alpha} = \tilde{d}_1\tilde{d}_2, \quad e^{2i(\delta-\beta/2)} = \tilde{d}_1\tilde{d}_3, \quad (5.19)$$

i.e., either $\alpha = 0$ or $\alpha = \pi$, and either $\beta = 2\delta$ or $\beta = 2\delta - \pi$. Therefore, four distinct pairs of values are possible for the Majorana phases. From the third row of (5.14), taking the absolute square, we obtain,

$$|U_{\tau 3}|^2 = (U_{\mu 3}^*s_\theta + U_{\tau 3}^*c_\theta)(U_{\mu 3}s_\theta + U_{\tau 3}c_\theta) \quad (5.20)$$

$$\Rightarrow \cot 2\theta_{23} = \cot \theta \cos(\phi_2 - \phi_3). \quad (5.21)$$

Similarly, the absolute square of the second relation in the third row in (5.14) is devoid of the unphysical phase difference $(\phi_2 - \phi_3)$, and we get,

$$\cos^2 \delta = \cos^2 \theta \sin^2(\phi_2 - \phi_3) = \frac{\cos^2 \theta \sin^2 2\theta_{23} - \sin^2 \theta \cos^2 \theta_{23}}{\sin^2 2\theta_{23}}. \quad (5.22)$$

Note that, both the relations, i.e., (5.21) and (5.22) reduce to the co-bimaximal prediction of $\text{CP}^{\mu\tau}$ in the MTIL, as expected. We also stress that the relations (5.19), (5.21) and (5.22) hold irrespective of the neutrino mass ordering.

Now, due to FL invariance, M_ν has a vanishing eigenvalue with corresponding normalized eigenvector given by

$$\mathbf{v} = N^{-1} \begin{pmatrix} -\frac{\eta_1}{\eta_2} \cot \frac{\theta}{2} \\ -\cot \frac{\theta}{2} \\ 1 \end{pmatrix} e^{i\gamma}, \quad \text{with } N = \left[\left(1 + \frac{\eta_1^2}{\eta_2^2}\right) \cot^2 \frac{\theta}{2} + 1 \right]^{1/2}, \quad (5.23)$$

where γ is an arbitrary phase signifying that the normalized eigenvector is unique up to an overall phase. If the zero eigenvalue is associated with $m_1 = 0$ ($m_3 = 0$), we discover additional consequences for the normal (inverted) ordering.

5.3.1 Normal ordering

Here, \mathbf{v} is associated with the first column of PMNS. Equating \mathbf{v} with the first column of U in (5.11), we get,

$$c_{12}c_{13} = N^{-1} \frac{\eta_1}{\eta_2} \cot \frac{\theta}{2}, \quad \phi_1 = \gamma + \pi, \quad (5.24)$$

$$s_{12}c_{23} + c_{12}s_{23}s_{13}e^{i\delta} = N^{-1} \cot \frac{\theta}{2} e^{i(\gamma - \phi_2)}, \quad (5.25)$$

$$s_{12}s_{23} - c_{12}c_{23}s_{13}e^{i\delta} = N^{-1}e^{i(\gamma-\phi_3)}. \quad (5.26)$$

Note that, (5.25) and (5.26) together imply

$$s_{12}^2 = N^{-2}[\cot^2 \frac{\theta}{2} + s_{23}^2 + 2s_{23}c_{23} \cot \frac{\theta}{2} \cos(\phi_2 - \phi_3)]. \quad (5.27)$$

Taking the product of (5.25) with the complex conjugate of (5.26), and taking its imaginary part, we obtain,

$$\sin^2 \delta = \frac{\cot^2 \frac{\theta}{2} \sin^2(\phi_2 - \phi_3)}{\left[1 + \left(1 + \frac{\eta_1^2}{\eta_2^2}\right) \cot^2 \frac{\theta}{2}\right]^2 c_{12}^2 s_{12}^2 s_{13}^2}. \quad (5.28)$$

Eliminating $\sin^2(\phi_2 - \phi_3)$ and using (5.22), we finally get

$$\cos^2 \delta = \frac{\sin^2 2\theta_{12}s_{13}^2 \cos^2 \theta}{\sin^2 2\theta_{12}s_{13}^2 \cos^2 \theta + 4\left[1 + \left(1 + \frac{\eta_1^2}{\eta_2^2}\right) \cot^2 \frac{\theta}{2}\right]^2 \cot^2 \frac{\theta}{2}}. \quad (5.29)$$

Using (5.27) and eliminating $\cos(\phi_2 - \phi_3)$ from (5.21), we obtain,

$$\cos^2 \theta_{23} = \frac{\left[\left\{1 + \left(1 + \frac{\eta_1^2}{\eta_2^2}\right) \cot^2 \frac{\theta}{2}\right\} s_{12}^2 - 1\right] \cot \theta + \cot \frac{\theta}{2}}{(\cot^2 \frac{\theta}{2} - 1) \cot \theta + 2 \cot \frac{\theta}{2}}. \quad (5.30)$$

As we shall see in the numerical analysis in the next section, though in general $\cos \delta \neq 0$ for NO, the numerically allowed range of δ is very close to $3\pi/2$, lying in the narrow interval $269.6^\circ - 270.4^\circ$. Since the possibility of $\delta = \pi/2$ is excluded at more than 99% CL, by maximal CP violation, we refer only to $\delta = 3\pi/2$.

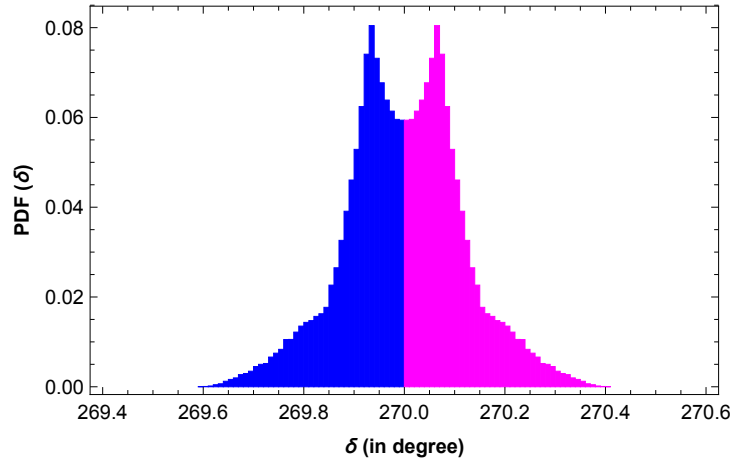


Figure 5.1: Probability distribution of the Dirac CP phase δ for normal mass ordering. It is evident that the values which are very close to 270° are most probable. To be numerically precise, $\int_{270}^{270 \pm 0.2} PDF(\delta) d\delta = 0.795$. Thus upon a large number of random trial (we choose that number to be 10^6), there is 80 % probability that δ will be in the range 270 ± 0.2 .

5.3.2 Inverted ordering

In this case, \mathbf{v} is associated with the third column of PMNS. Equating \mathbf{v} with the third column of U in (5.11), we get,

$$s_{13} = N^{-1} \frac{\eta_1}{\eta_2} \cot \frac{\theta}{2}, \quad \phi_1 - \delta + \beta/2 = \gamma + \pi, \quad (5.31)$$

$$c_{13}s_{23} = N^{-1} \cot \frac{\theta}{2}, \quad \phi_2 + \frac{\beta}{2} = \gamma + \pi, \quad (5.32)$$

$$c_{13}c_{23} = N^{-1}, \quad \phi_3 + \frac{\beta}{2} = \gamma. \quad (5.33)$$

Note that, (5.32) and (5.33) together imply

$$\tan \theta_{23} = \cot \frac{\theta}{2}, \quad (\phi_2 - \phi_3) = \pi, \quad (5.34)$$

which is consistent with the relation (5.21). Note that, since the unphysical phase difference $(\phi_2 - \phi_3) = \pi$, it follows from (5.22) that the Dirac CP violation is maximal irrespective of the value of θ_{23} i.e.,

$$\cos \delta = 0. \quad (5.35)$$

Clearly, since the Dirac CP phase deviates slightly from its maximal value only for the NO, and both types of mass ordering in this model predict arbitrary nonmaximality in θ_{23} , it is difficult to make comments on the mass ordering, only from the measurement of these two parameters. Though any large nonmaximality in δ will rule out $\text{CP}^{\mu\tau}$ as well as this model ($\text{CP}^{\mu\tau\theta} + \text{FL}$), however, if the experiments favour nonmaximal θ_{23} along with a maximal value of δ the latter model will survive while the former will be in tension.

5.4 Numerical analysis

5.4.1 Parameter Estimation

In this section, we present a comprehensive numerical analysis to demonstrate the phenomenological viability of our scheme, and explore its implications on neutrino phenomenology in general. It is organized as follows. We utilize the (3σ) ranges of the globally fitted neutrino oscillation data [12] together with the upper bound of 0.17 eV [187] on the sum of the light neutrino masses from PLANCK and other

cosmological observations in Table 5.1. The allowed ranges of the parameters of M_ν are tabulated in Table 5.2. Subsequently, we discuss neutrinoless double beta decay, CP asymmetry in neutrino oscillations and flavor flux ratios at neutrino telescopes and provide corresponding predictions in our model in three separate subsections.

Table 5.1: Input values used in the analysis [12]

Parameter	θ_{12} degrees	θ_{23} degrees	θ_{13} degrees	Δm_{21}^2 $10^{-5}(\text{eV})^2$	$ \Delta m_{31}^2 $ $10^{-3}(\text{eV}^2)$
3σ ranges (NO)	31.42 – 36.05	40.3 – 51.5	8.09 – 8.98	6.80 – 8.02	2.399 – 2.593
3σ ranges (IO)	31.43 – 36.06	41.3 – 51.7	8.14 – 9.01	6.80 – 8.02	2.369 – 2.562
Best fit values (NO)	33.62	47.2	8.54	7.40	2.494
Best fit values (IO)	33.62	48.1	8.58	7.40	2.465

Table 5.2: Output values of the parameters of M_ν

Parameters	$a_1/10^{-3}$	$a_2/10^{-3}$	$c/10^{-3}$	$ \frac{\eta_1}{\eta_2} $	θ°
NO	−4.0 – 4.0	−6.5 – 6.5	−28 – +28	+1.79 – +2.11	79.6 – 101.6
IO	−2.7 – +2.7	−36.0 – +36.0	−11.6 – +11.6	+0.18 – +0.23	77.0 – 94.4

5.4.2 Neutrinoless double beta ($0\nu\beta\beta$) decay process

An introduction to the $0\nu\beta\beta$ decay process was already given in Sec.3.4.1 of Chapter 3. We recall that the half-life was given by

$$\frac{1}{T_{1/2}^{0\nu}} = G_{0\nu} |\mathcal{M}|^2 |M_{ee}|^2 m_e^{-2}, \quad (5.36)$$

where $G_{0\nu}$ denote the two-body phase space factor, \mathcal{M} is the nuclear matrix element (NME), m_e is the mass of the electron and M_{ee} is the (1,1) element of the effective light neutrino mass matrix M_ν . Using the PDG parametrization convention for U_{PMNS} , the M_{ee} can be written as

$$M_{ee} = c_{12}^2 c_{13}^2 m_1 + s_{12}^2 c_{13}^2 m_2 e^{i\alpha} + s_{13}^2 m_3 e^{i(\beta-2\delta)}. \quad (5.37)$$

For the normal ordering, since δ deviates from $\pi/2$ or $3\pi/2$, and $m_1 = 0$ as a direct consequence of the FL symmetry, (5.37) simplifies to the following four different possibilities for the four sets of α, β values as obtained in (5.19) of Sec 5.3:

(i) $\alpha = 0, \beta = 2\delta \Rightarrow M_{ee} = s_{12}^2 c_{13}^2 m_2 + s_{13}^2 m_3,$

(ii) $\alpha = 0, \beta = 2\delta - \pi \Rightarrow M_{ee} = s_{12}^2 c_{13}^2 m_2 - s_{13}^2 m_3,$

(iii) $\alpha = \pi, \beta = 2\delta \Rightarrow M_{ee} = -s_{12}^2 c_{13}^2 m_2 + s_{13}^2 m_3$ and,

(iv) $\alpha = \pi, \beta = 2\delta - \pi \Rightarrow M_{ee} = -s_{12}^2 c_{13}^2 m_2 - s_{13}^2 m_3.$ Since the observations give upper bounds on $|M_{ee}|$, cases (i) and (iv) give identical predictions, as can be clearly seen from the upper left and lower right panels of Fig.5.2. Similar situations occur for cases (ii) (upper right panel) and (iii) (lower left panel) in Fig.5.2.

For the inverted ordering, $\delta = \pi/2$ or $3\pi/2$, and $m_3 = 0$. Here, due to the latter condition, the expression (5.37) becomes independent of β and reduces to two different possibilities:

(a) $\alpha = 0, \beta = 0, \pi \Rightarrow M_{ee} = c_{12}^2 c_{13}^2 m_1 + s_{12}^2 c_{13}^2 m_2,$

(b) $\alpha = \pi, \beta = 0, \pi \Rightarrow M_{ee} = c_{12}^2 c_{13}^2 m_1 - s_{12}^2 c_{13}^2 m_2.$

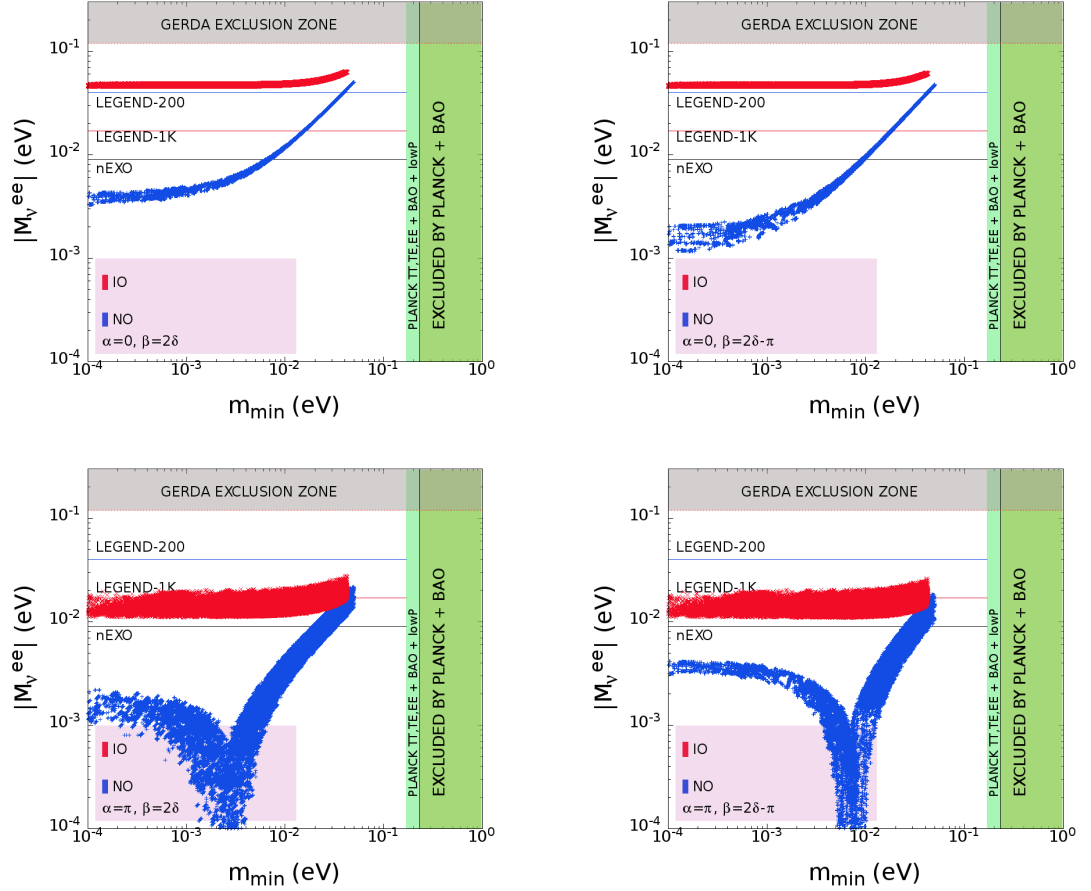


Figure 5.2: Plots of $|M^{ee}|$ vs. m_{min} for both types of mass ordering with four possible choices of the Majorana phases α and β .

The plots of $|M_{ee}|$ versus the sum of the light neutrino masses $\sum_i m_i$ for both NO and IO are displayed in Fig.5.2. Several upper limits on $|M_{ee}|$ from various ongoing and upcoming experiments have been shown. It is evident from Fig.5.2 that $|M_{ee}|$ in each plot leads to an upper limit which is below the sensitivity reach of the GERDA phase-II experimental data. The upper bounds on $|M_{ee}|$ from experiments such as LEGEND-200 (40 meV), LEGEND-1K (17 meV) and nEXO (9 meV) [11], shown in Fig.5.2, can probe our model better. Note that, for each case, the entire parameter space corresponding to the inverted mass ordering is likely to be ruled out in case nEXO does not observe any $0\nu\beta\beta$ signal covering its entire reach.

5.4.3 Effect of CP asymmetry in neutrino oscillations

Following the discussion in Sec.3.4.2, we recall that the CP asymmetry parameter is given by

$$A_{\mu e} = \frac{P(\nu_\mu \rightarrow \nu_e) - P(\bar{\nu}_\mu \rightarrow \bar{\nu}_e)}{P(\nu_\mu \rightarrow \nu_e) + P(\bar{\nu}_\mu \rightarrow \bar{\nu}_e)} = \frac{2\sqrt{P_{atm}}\sqrt{P_{sol}} \sin \Delta_{32} \sin \delta}{P_{atm} + 2\sqrt{P_{atm}}\sqrt{P_{sol}} \cos \Delta_{32} \cos \delta + P_{sol}}. \quad (5.38)$$

In the present case, δ is given by (5.29) and (5.35) for NO and IO respectively. Fig.5.3 represents the variation of $P_{\mu e}$ and $A_{\mu e}$ against the baseline length L for an IO, i.e., for $\delta = 3\pi/2$, while Fig.5.5 gives same plots for δ given by (5.29) i.e., for NO. The baseline lengths T2K, NO ν A and DUNE are indicated in these figures by vertical lines. In Fig.5.4 and 5.6 the CP asymmetry $A_{\mu e}$ is plotted against the beam energy E for the same three experiments for IO and NO respectively.

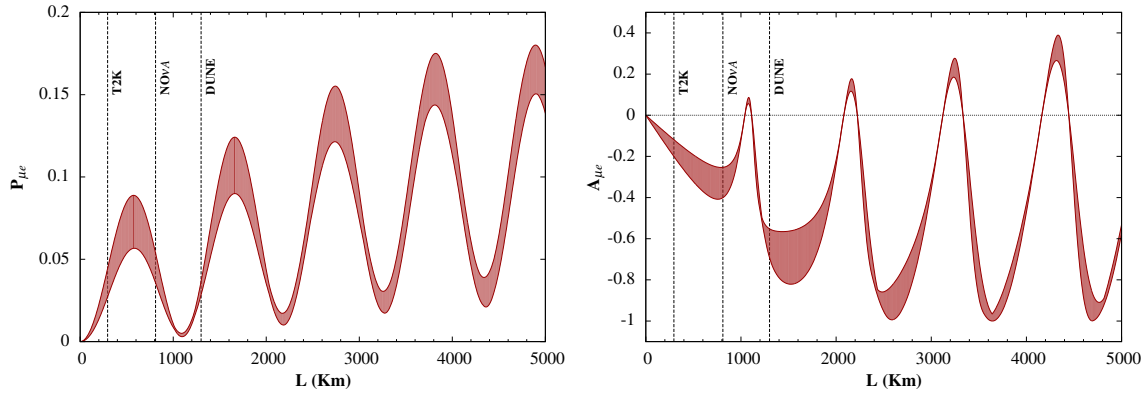


Figure 5.3: Variation of $P_{\mu e}$ and $A_{\mu e}$ against the baseline length L for IO ($E = 1$ GeV). The plots are for $\delta = 3\pi/2$ and the bands correspond to 3σ ranges in θ_{12} and θ_{13} . The three vertical dashed lines indicate observations at three different baseline lengths: $L = 295$ Km (T2K), $L = 810$ Km (NO ν A) and $L = 1300$ Km (DUNE).

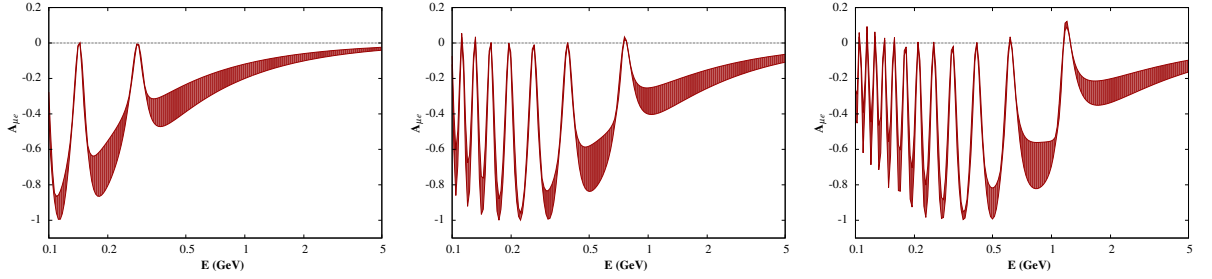


Figure 5.4: Plots of $A_{\mu e}$ with energy E for fixed baseline lengths corresponding to different experiments in case of IO. Fig.(a) is for T2K with $L = 295\text{Km}$; fig.(b) is for $\text{NO}\nu\text{A}$ with $L = 810\text{Km}$ and fig.(c) is for DUNE with $L = 1300\text{Km}$. The plot is for $\delta = 3\pi/2$, while the bands and the horizontal dashed lines have the same specifications as in fig. 5.3.

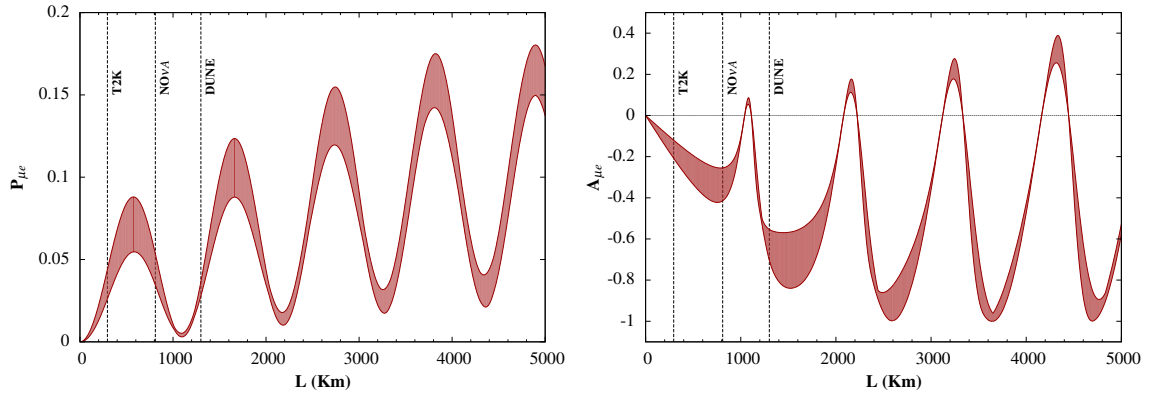


Figure 5.5: Plots of $P_{\mu e}$ and $A_{\mu e}$ with different baseline lengths L for NO ($E = 1\text{GeV}$). The bands of the plots correspond to 3σ ranges of the mixing angles and also the ranges for the parameters $79.6^\circ < \theta < 101.6^\circ$ and $1.79 < |\eta_1/\eta_2| < 2.11$. In this case, δ is not fixed, but varies over a range predicted from (5.29) with the same ranges of the mixing angles, and model parameters θ and η_1/η_2 . The three vertical dashed lines and the horizontal dotted line specify the same as in Fig.5.3.

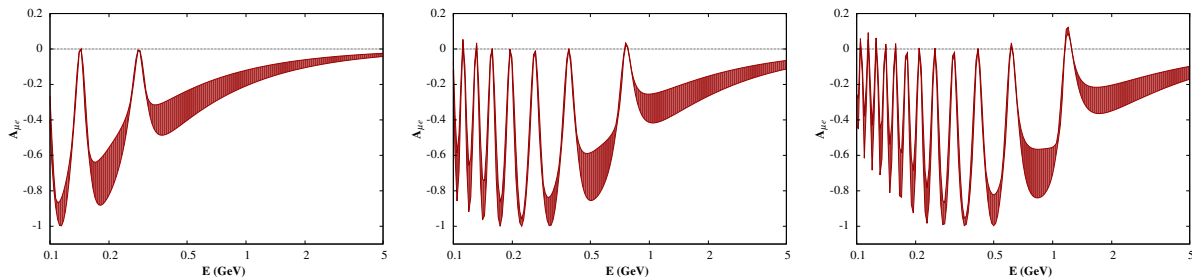


Figure 5.6: Plots of $A_{\mu e}$ with energy E for fixed baseline lengths corresponding to different experiments in case of NO. Fig.(a) is for T2K with $L = 295\text{Km}$; fig.(b) is for $\text{NO}\bar{\nu}A$ with $L = 810\text{Km}$ and fig.(c) is for DUNE with $L = 1300\text{Km}$. The plots and their widths have same specifications as in fig. 5.5. The horizontal dotted lines $A_{\mu e} = 0$ specify CP conservation.

5.4.4 Octant of θ_{23} from flavor flux measurement at neutrino telescope

With the background laid out in Sec.1.4, one can define certain flavor flux ratios R_l ($l = e, \mu, \tau$) at the neutrino telescope as

$$R_l \equiv \frac{\phi_l^T}{\sum_m \phi_m^T - \phi_l^T} = \frac{1 + \sum_i |U_{li}|^2 \Delta_i}{2 - \sum_i |U_{li}|^2 \Delta_i}, \quad (5.39)$$

where $l, m = e, \mu, \tau$ and U is given in (5.11). Each R_l depends on all the three mixing angles and $\cos \delta$. For NO, θ_{23} and $\cos \delta$ are given by (5.30) and (5.29) while for IO the corresponding quantities are given by (5.34) and (5.35) respectively. For both types of ordering, we show in Fig.5.7 the variation of $R_{e,\mu,\tau}$ w.r.t θ in its phenomenologically allowed range (Table 5.2) using the exact expressions in (5.39).

For NO, θ_{23} can be eliminated in favor of θ and η_1/η_2 . Keeping the latter fixed at a value 1.5, we show in Fig.5.7 (left panel) the contour corresponding to the best-fit

values of θ_{12} and θ_{13} , while the bands arise when θ_{12} and θ_{13} are allowed to vary in their current 3σ ranges. It should be emphasized that the contours corresponding to $\cos \delta > 0$ and $\cos \delta < 0$ are practically indistinguishable, and therefore, we show the contours and bands only for the case $\cos \delta > 0$.

Next, for the IO, θ_{23} can be eliminated in favor of θ only. The resulting variation of $R_{e,\mu,\tau}$ w.r.t θ are displayed in the right panel of Fig.5.7. In generating these plots, the mixing angles θ_{12} and θ_{13} are again allowed to vary in their current experimental 3σ ranges. The contours within the bands represent the case when θ_{12} and θ_{13} are kept fixed at their best-fit values. Unlike NO, the expressions for R_i in case of IO are relatively simple and has been used in the following to explain the nature of the plots. The expressions for $R_{e,\mu,\tau}$ for IO are:

$$\begin{aligned}
 R_e &\approx \frac{2 - \sin^2 2\theta_{12}c_\theta}{4 + \sin^2 2\theta_{12}c_\theta}, \\
 R_\mu &\approx \frac{1 + \frac{1}{4}\sin^2 2\theta_{12}c_\theta + (1 - \frac{1}{4}\sin^2 2\theta_{12})c_\theta^2}{2 - \frac{1}{4}\sin^2 2\theta_{12}c_\theta - (1 - \frac{1}{4}\sin^2 2\theta_{12})c_\theta^2}, \\
 R_\tau &\approx \frac{1 + \frac{1}{4}\sin^2 2\theta_{12}c_\theta - (1 - \frac{1}{4}\sin^2 2\theta_{12})c_\theta^2}{2 - \frac{1}{4}\sin^2 2\theta_{12}c_\theta + (1 - \frac{1}{4}\sin^2 2\theta_{12})c_\theta^2},
 \end{aligned} \tag{5.40}$$

where we have used (5.35), (5.34) and neglected terms of $\mathcal{O}(s_{13}^2)$. It is evident from the approximate expressions (5.40) that in the exact $\mu\tau$ interchange limit $\theta = \frac{\pi}{2}$, all the flavor flux ratios converge to the value $\frac{1}{2}$. It is clear from the figure (as well as from the approximate expression of R_e) that for $R_e < \frac{1}{2}$ ($R_e > \frac{1}{2}$), we have $\theta < \frac{\pi}{2}$ ($\theta > \frac{\pi}{2}$). Since (5.34) implies $2\theta_{23} = \pi - \theta$, observed value of R_e will give a definite value of θ_{23} . In particular, $\theta > \frac{\pi}{2}$ implies $\theta_{23} < \frac{\pi}{4}$ and vice versa. Similar conclusion can be made from the observed value of R_μ . Though the expression for R_μ in (5.40) is quadratic in $\cos \theta$, only one of the roots of this equation belongs to the numerically allowed range of θ (Table 5.2). However, a definite observational value of R_τ cannot unambiguously predict the value of θ . This is because of the quadratic

dependence of R_τ on c_θ (clearly visible from Fig.5.7) specifically for $\theta < \pi/2$. For consistency, the unique value of θ determined from the future precision measurement of R_e (or R_μ) leads to a theoretical prediction of the ranges of R_μ (or R_e) and R_τ which should in turn match the observed values of R_μ (or R_e) and R_τ . Alternatively, if θ_{23} is measured with significant precision in a complementary experiment (e.g. long baseline experiments), the range of each R_l can be uniquely predicted for all l , which can in turn be compared against the future IceCube observations.

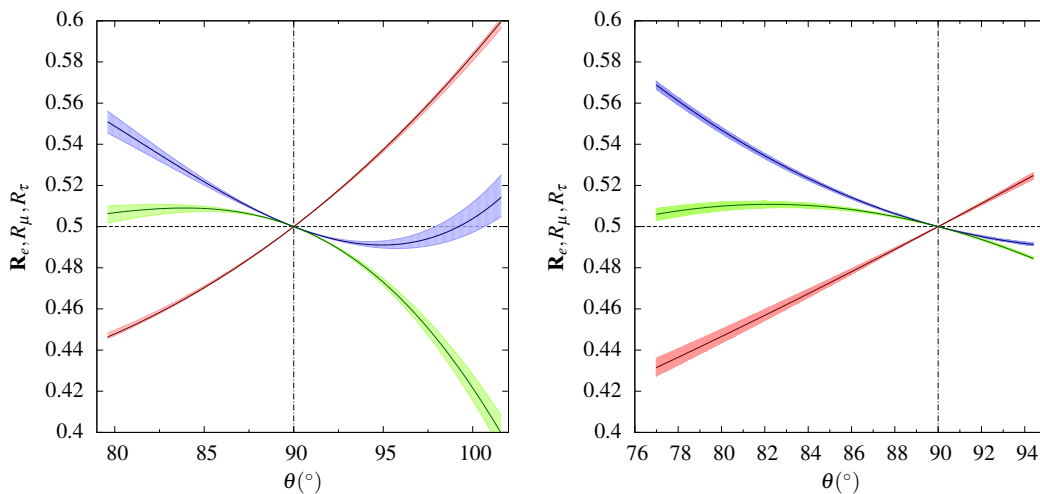


Figure 5.7: Variation of the flavor the flux ratios R_e (red), R_μ (blue) and R_τ (green) with θ for NO (left panel) and for IO (right panel). The solid lines represent plots for the best-fit values of the mixing angles and the bands are caused by the current 3σ ranges of the mixing angles θ_{12} and θ_{13} . The horizontal axes in both plots correspond to the numerically obtained ranges of θ in Table 5.2, which is different in NO and IO. For the NO case, η_1/η_2 is fixed at 1.0.

5.5 Summary and conclusion

In this chapter, we describe the work where we propose an invariance of the light neutrino Majorana mass term under a mixed $\mu\tau$ -flavored CP symmetry ($CP^{\mu\tau\theta}$),

compounded with a generalised Friedberg-Lee (FL) transformation on the left-chiral flavor neutrino fields. In this model, while both types of mass ordering are viable with a nondegenerate neutrino mass spectrum, a vanishing value for the smallest light neutrino mass results as a direct consequence of FL invariance. While the atmospheric mixing angle θ_{23} is in general nonmaximal ($\theta_{23} \neq \pi/4$), the Dirac CP phase δ is exactly maximal ($\delta = \pi/2, 3\pi/2$) for IO and nearly maximal for NO due to $\cos \delta \propto \sin \theta_{13}$. However, the departure from maximality does not exceed 0.4° on either side of $\delta = 3\pi/2$. One of the Majorana phases, α , is restricted to lie at its CP conserving values while the other, β , is linearly related with δ leading to a tiny Majorana CP violation. For the IO, θ_{23} is, in general, nonmaximal but δ is maximal irrespective of the value of θ_{23} . For the NO, the Majorana CP violation sneaking through the Majorana phase β is numerically insignificant so that the model essentially predicts vanishing Majorana CP violation. Evidently, any substantial deviation of δ from $3\pi/2$, will exclude our model. After fitting the neutrino oscillation global fit data, we also consider a numerical analysis of $\nu_\mu \rightarrow \nu_e$ oscillation which is expected to show up Dirac CP violation in different long baseline experiments. Finally, assuming purely astrophysical sources, we compute the Ultra High Energy (UHE) neutrino flavor flux ratios at the neutrino telescopes. From this, we comment on the predictability of the octant of θ_{23} .

Chapter 6

Maximal zero textures in the framework of Linear and Inverse Seesaw

6.1 Introduction

In type-I seesaw, the lightness of the neutrinos is attributed to scale identified with the mass of the lightest of the heavy neutrinos N_{Ri} . Since the latter is constrained to be $(M_R)_{\text{lightest}} \geq 10^8$ GeV [153, 217] the scale of new physics is beyond the reach of ongoing collider experiments. On the other hand, a seesaw scale in the TeV range can be realized in some other variants such as Linear and Inverse seesaw mechanisms by incorporating singlet neutral fermions S_{Li} in addition to N_{Ri} . Both mechanisms can potentially explain the smallness of neutrino mass through a small lepton-number breaking mass matrix.

As explained in Sec.1.3, in Linear seesaw [30, 218–221], the low energy light

neutrino mass matrix M_ν reads

$$M_\nu \approx -M(m^{-1}m_D^T) - [M(m^{-1}m_D^T)]^T \quad (6.1)$$

and that for the Inverse seesaw is given by

$$M_\nu \approx m_D m^{-1} \mu_S (m_D m^{-1})^T. \quad (6.2)$$

Till date, since there exists only five experimentally measured quantities, namely, the two mass-square differences and three mixing angles (cf. Sec.1.6), the standard approach is to reduce the number of parameters by postulating some symmetry in the Lagrangian or by assuming vanishing of certain elements of M_ν or at a more fundamental level, for the mass matrices comprising M_ν (also dictated by some underlying symmetry), called texture zeros. In this chapter, we discuss the work which investigates both the Linear and Inverse seesaw mechanisms incorporating the idea of maximal zero textures [108, 122, 137, 222–238] subjected to the assumption of nonvanishing eigenvalues of M_ν . For the phenomenologically viable maximal zero textures of M_ν , we explore maximal zero textures of the matrices comprising M_ν using the following strategies:

i) First, we obtain the maximal zero textures of charged lepton mass matrix (M_ℓ) with three nonzero, nondegenerate eigenvalues. This gives rise to five minimal textures of M_ℓ .

ii) Next, we assume that M_ν has nonvanishing eigenvalues i.e., $\det(M_\nu) \neq 0$. As a consequence, the formula 6.1 (6.2) immediately implies that each of the three matrices m_D , m and M (μ_S) must also be nonsingular and unambiguously dictates all possible maximal zero textures for linear (inverse) seesaw.

iii) Fixing a particular minimal structure of m_D and M (m) in Linear (Inverse) seesaw, we work out the maximal zero textures of m (μ_S) by analysing zeros in different entries of m (μ_S) for Linear (Inverse) seesaw.

iv) To facilitate the analysis, we utilize the Frampton, Glashow and Marfatia condition [222] to discard the phenomenologically disallowed maximal zero textures of M_ν and those matrices m and μ_S for the Linear and Inverse seesaw respectively which lead to such M_ν .

v) Finally, we explore numerically the parameter space of the survived matrices utilizing the neutrino oscillation global fit data and predict $\Sigma_i m_i$, $|M_{11}|$, J_{CP} , δ along with the hierarchical structure of neutrino masses.

This chapter is organized as follows. Sec.6.2 contains the minimal textures of the charged lepton mass matrix M_ℓ . Viable mass matrices with maximal texture zeros in Linear and Inverse seesaw are discussed in Sec. 6.3 and 6.4 respectively. Finally, a summary is presented in Sec. 6.5.

6.2 Maximal zero textures of charged lepton mass matrix

A generic charged lepton mass matrix M_ℓ can be parametrized as

$$M_\ell = \begin{pmatrix} A' e^{ia'} & B' e^{ib'} & C' e^{ic'} \\ D' e^{id'} & E' e^{ie'} & F' e^{if'} \\ G' e^{ig'} & H' e^{ih'} & K' e^{ik'} \end{pmatrix}. \quad (6.3)$$

We look for maximum zero textures (minimum number of parameters) of M_ℓ such that $\det(M_\ell M_\ell^\dagger) \neq 0$ (or nonvanishing eigenvalues for M_ℓ). A careful inspection of the quantity $\det(M_\ell M_\ell^\dagger)$ reveals six possible maximal zero textures and are presented in Table 6.1. Interestingly, for all these matrices, $M_\ell M_\ell^\dagger$ is diagonal and therefore, the

Table 6.1: Maximal zero textures of the charged lepton mass matrix M_ℓ

$\begin{pmatrix} A'e^{ia'} & 0 & 0 \\ 0 & B'e^{ib'} & 0 \\ 0 & 0 & C'e^{ic'} \end{pmatrix}$	$\begin{pmatrix} 0 & 0 & A'e^{ia'} \\ 0 & B'e^{ib'} & 0 \\ C'e^{ic'} & 0 & 0 \end{pmatrix}$	$\begin{pmatrix} A'e^{ia'} & 0 & 0 \\ 0 & 0 & B'e^{ib'} \\ 0 & C'e^{ic'} & 0 \end{pmatrix}$
$\begin{pmatrix} 0 & 0 & A'e^{ia'} \\ B'e^{ib'} & 0 & 0 \\ 0 & C'e^{ic'} & 0 \end{pmatrix}$	$\begin{pmatrix} 0 & A'e^{ia'} & 0 \\ 0 & 0 & B'e^{ib'} \\ C'e^{ic'} & 0 & 0 \end{pmatrix}$	$\begin{pmatrix} 0 & A'e^{ia'} & 0 \\ B'e^{ib'} & 0 & 0 \\ 0 & 0 & C'e^{ic'} \end{pmatrix}$

mixing arises only from the neutrino sector of the Lagrangian i.e., $U_{PMNS} = U_\nu$.

6.3 Texture zeros in Linear seesaw

For an invertible $n \times n$ square matrix A , and two $n \times m$ rectangular matrices B and C , one has

$$\det(A + BC^T) = \det(I_m + C^T A^{-1}B) \det A \quad (6.4)$$

Since we assume $\det(M_\nu) \neq 0$, 6.1 implies that $\det(Mm^{-1}m_D^T) \neq 0$ which in turn implies that M , m^{-1} and m_D^T must be nonsingular. Since, for a matrix A , $\det(A) = \det(A^T)$, $\det(A^{-1}) = 1/\det(A)$, we obtain that M , m and m_D must also be nonsingular. The resulting textures are presented in Table 6.2, Table 6.3 and Table 6.4 respectively.

Table 6.2: Six zero textures of m_D with $\det(m_D) \neq 0$

Minimal (6-zero) textures of m_D with $\det(m_D) \neq 0$					
$m_D^1 = \begin{pmatrix} Ae^{ia} & 0 & 0 \\ 0 & Be^{ib} & 0 \\ 0 & 0 & Ce^{ic} \end{pmatrix}$	$m_D^2 = \begin{pmatrix} 0 & 0 & Ae^{ia} \\ 0 & Be^{ib} & 0 \\ Ce^{ic} & 0 & 0 \end{pmatrix}$	$m_D^3 = \begin{pmatrix} Ae^{ia} & 0 & 0 \\ 0 & 0 & Be^{ib} \\ 0 & Ce^{ic} & 0 \end{pmatrix}$			
$m_D^4 = \begin{pmatrix} 0 & 0 & Ae^{ia} \\ Be^{ib} & 0 & 0 \\ 0 & Ce^{ic} & 0 \end{pmatrix}$	$m_D^5 = \begin{pmatrix} 0 & Ae^{ia} & 0 \\ 0 & 0 & Be^{ib} \\ Ce^{ic} & 0 & 0 \end{pmatrix}$	$m_D^6 = \begin{pmatrix} 0 & Ae^{ia} & 0 \\ Be^{ib} & 0 & 0 \\ 0 & 0 & Ce^{ic} \end{pmatrix}$			

Table 6.3: Six zero textures of M with $\det(M) \neq 0$

Six zero textures of M with $\det(M) \neq 0$					
$M^1 = \begin{pmatrix} Xe^{ix} & 0 & 0 \\ 0 & Ye^{iy} & 0 \\ 0 & 0 & Ze^{iz} \end{pmatrix}$	$M^2 = \begin{pmatrix} 0 & 0 & Xe^{ix} \\ 0 & Ye^{iy} & 0 \\ Ze^{iz} & 0 & 0 \end{pmatrix}$	$M^3 = \begin{pmatrix} Xe^{ix} & 0 & 0 \\ 0 & 0 & Ye^{iy} \\ 0 & Ze^{iz} & 0 \end{pmatrix}$			
$M^4 = \begin{pmatrix} 0 & 0 & Xe^{ix} \\ Ye^{iy} & 0 & 0 \\ 0 & Ze^{iz} & 0 \end{pmatrix}$	$M^5 = \begin{pmatrix} 0 & Xe^{ix} & 0 \\ 0 & 0 & Ye^{iy} \\ Ze^{iz} & 0 & 0 \end{pmatrix}$	$M^6 = \begin{pmatrix} 0 & Xe^{ix} & 0 \\ Ye^{iy} & 0 & 0 \\ 0 & 0 & Ze^{iz} \end{pmatrix}$			

Table 6.4: Minimal (6-zero) textures of m with $\det(m) \neq 0$

Minimal (6-zero) textures of m with $\det(m) \neq 0$					
$m^1 = \begin{pmatrix} Pe^{ip} & 0 & 0 \\ 0 & Qe^{iq} & 0 \\ 0 & 0 & Re^{ir} \end{pmatrix}$	$m^2 = \begin{pmatrix} 0 & 0 & Pe^{ip} \\ 0 & Qe^{iq} & 0 \\ Re^{ir} & 0 & 0 \end{pmatrix}$	$m^3 = \begin{pmatrix} Pe^{ip} & 0 & 0 \\ 0 & 0 & Qe^{iq} \\ 0 & Re^{ir} & 0 \end{pmatrix}$			
$m^4 = \begin{pmatrix} 0 & 0 & Pe^{ip} \\ Qe^{iq} & 0 & 0 \\ 0 & Re^{ir} & 0 \end{pmatrix}$	$m^5 = \begin{pmatrix} 0 & Pe^{ip} & 0 \\ 0 & 0 & Qe^{iq} \\ Re^{ir} & 0 & 0 \end{pmatrix}$	$m^6 = \begin{pmatrix} 0 & Pe^{ip} & 0 \\ Qe^{iq} & 0 & 0 \\ 0 & 0 & Re^{ir} \end{pmatrix}$			

6.3.1 Effective M_ν in Linear seesaw

We confine to the minimal structures of M_ν as given in the Ref. [222] in which it was shown that for a phenomenologically viable M_ν , the number of independent zeros should be atmost two. With such a criterion in view, we begin with maximum zeros

in the matrix m for a given m_D and M . It turns out that for six zeros in m (Table 6.4), all the emerged M_ν has either three or more independent zeros. Therefore, discarding such textures we start with five zero textures of m . Though in general, there exists 126 such textures of m , the criterion of nonvanishing eigenvalues of M_ν (which requires m to be nonsingular) drastically reduces the number of nonsingular five zero textures of m from 126 to 36 and are presented in Table 6.6.

Interestingly, only the combinations given in Table 6.5 gives rise to phenomenologically viable M_ν and all of them leads to a single generic structure as

$$\begin{pmatrix} \times & \times & \times \\ \times & 0 & \times \\ \times & \times & 0 \end{pmatrix}. \quad (6.5)$$

All the remaining combinations are discarded because they either lead to three independent zeros or two independent zeros that are not consistent with the current data. For a compact view, the allowed combinations of m_D , M and m are presented in Table 6.5.

Table 6.5: Compositions for Allowed Realizations of M_ν

	$M \rightarrow$					
$m_D \downarrow$	M^1	M^2	M^3	M^4	M^5	M^6
m_D^1	m^{16}, m^{23}	m^{12}, m^{17}	m^9, m^{36}	m^5, m^{22}	m^3, m^{18}	m^{29}, m^{34}
m_D^2	m^{10}, m^{25}	m^{14}, m^{21}	m^2, m^{15}	m^{28}, m^{31}	m^8, m^{33}	m^4, m^{19}
m_D^3	m^9, m^{36}	m^5, m^{22}	m^{16}, m^{23}	m^{12}, m^{27}	m^{29}, m^{34}	m^3, m^{18}
m_D^4	m^2, m^{15}	m^{28}, m^{31}	m^{10}, m^{25}	m^{14}, m^{21}	m^4, m^{19}	m^8, m^{33}
m_D^5	m^1, m^{24}	m^{11}, m^{32}	m^{26}, m^{35}	m^6, m^{13}	m^{17}, m^{20}	m^7, m^{30}
m_D^6	m^{26}, m^{35}	m^6, m^{13}	m^1, m^{24}	m^{11}, m^{31}	m^7, m^{30}	m^{17}, m^{20}

Table 6.6: Viable 5-zero textures of m

5 zero textures of m		
$m^1 = \begin{pmatrix} Pe^{ip} & Se^{is} & 0 \\ 0 & Qe^{iq} & 0 \\ 0 & 0 & Re^{ir} \end{pmatrix}$	$m^2 = \begin{pmatrix} Pe^{ip} & 0 & Se^{is} \\ 0 & Qe^{iq} & 0 \\ 0 & 0 & Re^{ir} \end{pmatrix}$	$m^3 = \begin{pmatrix} Pe^{ip} & 0 & 0 \\ Se^{is} & Qe^{iq} & 0 \\ 0 & 0 & Re^{ir} \end{pmatrix}$
$m^4 = \begin{pmatrix} Pe^{ip} & 0 & 0 \\ 0 & Qe^{iq} & Se^{is} \\ 0 & 0 & Re^{ir} \end{pmatrix}$	$m^5 = \begin{pmatrix} Pe^{ip} & 0 & 0 \\ 0 & Qe^{iq} & 0 \\ Se^{is} & 0 & Re^{ir} \end{pmatrix}$	$m^6 = \begin{pmatrix} Pe^{ip} & 0 & 0 \\ 0 & Qe^{iq} & 0 \\ 0 & Se^{is} & Re^{ir} \end{pmatrix}$
$m^7 = \begin{pmatrix} Se^{is} & Pe^{ip} & 0 \\ Qe^{iq} & 0 & 0 \\ 0 & 0 & Re^{ir} \end{pmatrix}$	$m^8 = \begin{pmatrix} 0 & Pe^{ip} & Se^{is} \\ Qe^{iq} & 0 & 0 \\ 0 & 0 & Re^{ir} \end{pmatrix}$	$m^9 = \begin{pmatrix} 0 & Pe^{ip} & 0 \\ Qe^{iq} & Se^{is} & 0 \\ 0 & 0 & Re^{ir} \end{pmatrix}$
$m^{10} = \begin{pmatrix} 0 & Pe^{ip} & 0 \\ Qe^{iq} & 0 & Se^{is} \\ 0 & 0 & Re^{ir} \end{pmatrix}$	$m^{11} = \begin{pmatrix} 0 & Pe^{ip} & 0 \\ Qe^{iq} & 0 & 0 \\ Se^{is} & 0 & Re^{ir} \end{pmatrix}$	$m^{12} = \begin{pmatrix} 0 & Pe^{ip} & 0 \\ Qe^{iq} & 0 & 0 \\ 0 & Se^{is} & Re^{ir} \end{pmatrix}$
$m^{13} = \begin{pmatrix} Se^{is} & 0 & Pe^{ip} \\ Qe^{iq} & 0 & 0 \\ 0 & Re^{ir} & 0 \end{pmatrix}$	$m^{14} = \begin{pmatrix} 0 & Se^{is} & Pe^{ip} \\ Qe^{iq} & 0 & 0 \\ 0 & Re^{ir} & 0 \end{pmatrix}$	$m^{15} = \begin{pmatrix} 0 & 0 & Pe^{ip} \\ Qe^{iq} & Se^{is} & 0 \\ 0 & Re^{ir} & 0 \end{pmatrix}$
$m^{16} = \begin{pmatrix} 0 & 0 & Pe^{ip} \\ Qe^{iq} & 0 & Se^{is} \\ 0 & Re^{ir} & 0 \end{pmatrix}$	$m^{17} = \begin{pmatrix} 0 & 0 & Pe^{ip} \\ Qe^{iq} & 0 & 0 \\ Se^{is} & Re^{ir} & 0 \end{pmatrix}$	$m^{18} = \begin{pmatrix} 0 & 0 & Pe^{ip} \\ Qe^{iq} & 0 & 0 \\ 0 & Re^{ir} & Se^{is} \end{pmatrix}$
$m^{19} = \begin{pmatrix} Se^{is} & Pe^{ip} & 0 \\ 0 & 0 & Qe^{iq} \\ Re^{ir} & 0 & 0 \end{pmatrix}$	$m^{20} = \begin{pmatrix} 0 & Pe^{ip} & Se^{is} \\ 0 & 0 & Qe^{iq} \\ Re^{ir} & 0 & 0 \end{pmatrix}$	$m^{21} = \begin{pmatrix} 0 & Pe^{ip} & 0 \\ Se^{is} & 0 & Qe^{iq} \\ Re^{ir} & 0 & 0 \end{pmatrix}$
$m^{22} = \begin{pmatrix} 0 & Pe^{ip} & 0 \\ 0 & Se^{is} & Qe^{iq} \\ Re^{ir} & 0 & 0 \end{pmatrix}$	$m^{23} = \begin{pmatrix} 0 & Pe^{ip} & 0 \\ 0 & 0 & Qe^{iq} \\ Re^{ir} & Se^{is} & 0 \end{pmatrix}$	$m^{24} = \begin{pmatrix} 0 & Pe^{ip} & 0 \\ 0 & 0 & Qe^{iq} \\ Re^{ir} & 0 & Se^{is} \end{pmatrix}$
$m^{25} = \begin{pmatrix} Pe^{ip} & Se^{is} & 0 \\ 0 & 0 & Qe^{iq} \\ 0 & Re^{ir} & 0 \end{pmatrix}$	$m^{26} = \begin{pmatrix} Pe^{ip} & 0 & Se^{is} \\ 0 & 0 & Qe^{iq} \\ 0 & Re^{ir} & 0 \end{pmatrix}$	$m^{27} = \begin{pmatrix} Pe^{ip} & 0 & 0 \\ Se^{is} & 0 & Qe^{iq} \\ 0 & Re^{ir} & 0 \end{pmatrix}$
$m^{28} = \begin{pmatrix} Pe^{ip} & 0 & 0 \\ 0 & Se^{is} & Qe^{iq} \\ 0 & Re^{ir} & 0 \end{pmatrix}$	$m^{29} = \begin{pmatrix} Pe^{ip} & 0 & 0 \\ 0 & 0 & Qe^{iq} \\ Se^{is} & Re^{ir} & 0 \end{pmatrix}$	$m^{30} = \begin{pmatrix} Pe^{ip} & 0 & 0 \\ 0 & 0 & Qe^{iq} \\ 0 & Re^{ir} & Se^{is} \end{pmatrix}$
$m^{31} = \begin{pmatrix} Se^{is} & 0 & Pe^{ip} \\ 0 & Qe^{iq} & 0 \\ Re^{ir} & 0 & 0 \end{pmatrix}$	$m^{32} = \begin{pmatrix} 0 & Se^{is} & Pe^{ip} \\ 0 & Qe^{iq} & 0 \\ Re^{ir} & 0 & 0 \end{pmatrix}$	$m^{33} = \begin{pmatrix} 0 & 0 & Pe^{ip} \\ Se^{is} & Qe^{iq} & 0 \\ Re^{ir} & 0 & 0 \end{pmatrix}$
$m^{34} = \begin{pmatrix} 0 & 0 & Pe^{ip} \\ 0 & Qe^{iq} & Se^{is} \\ Re^{ir} & 0 & 0 \end{pmatrix}$	$m^{35} = \begin{pmatrix} 0 & 0 & Pe^{ip} \\ 0 & Qe^{iq} & 0 \\ Re^{ir} & Se^{is} & 0 \end{pmatrix}$	$m^{36} = \begin{pmatrix} 0 & 0 & Pe^{ip} \\ 0 & Qe^{iq} & 0 \\ Re^{ir} & 0 & Se^{is} \end{pmatrix}$

Parametrization and phase rotation

To be explicit, we parametrize one set of combination (m_D^3 and m^9) and (m_D^3 and m^{36}) which gives rise to M_ν given in Eq.(6.5). To extract the relevant phases out of these allowed M_ν , let us parametrize them in a generic way as

$$M_\nu = \begin{pmatrix} K_1 e^{ik_1} & K_2 e^{ik_2} & K_3 e^{ik_3} \\ K_2 e^{ik_2} & 0 & K_4 e^{ik_4} \\ K_3 e^{ik_3} & K_4 e^{ik_4} & 0 \end{pmatrix} \quad (6.6)$$

where for m_D^3 with m^9 combination:

$$\begin{aligned} K_1 e^{ik_1} &= \frac{2Ae^{ia-ip-iq+is+ix} SX}{PQ}, & K_2 e^{ik_2} &= -\frac{Ae^{ia-ip+iy} Y}{P}, \\ K_3 e^{ik_3} &= -\frac{Ce^{ic-iq+ix} X}{Q}, & K_4 e^{ik_4} &= -\frac{Be^{ib-ir+iz} Z}{R}. \end{aligned} \quad (6.7)$$

and for m_D^3 with m^{36} combination:

$$\begin{aligned} K_1 e^{ik_1} &= \frac{2Ae^{ia-ip-ir+is+ix} SX}{PR}, & K_2 e^{ik_2} &= -\frac{Be^{ib-ir+ix} X}{R}, \\ K_3 e^{ik_3} &= -\frac{Ae^{ia-ip+iz} Z}{P}, & K_4 e^{ik_4} &= -\frac{Ce^{ic-iq+iy} Y}{Q}. \end{aligned} \quad (6.8)$$

6.4 Maximal zero textures in Inverse seesaw

As before we consider the minimal nonsingular textures of m_D (presented in Table 6.2) and m (Table 6.7) whereas the minimal texture of μ_S contains only two-independent complex parameters due to its anti-symmetry and given by the 3 possible textures presented in Table 6.8.

However, it turns out that if the number of zeros in μ_S is greater than three (as

Table 6.7: Minimal (6-zero) textures of m

Minimal (6-zero) textures of m					
$m^1 = \begin{pmatrix} X e^{ix} & 0 & 0 \\ 0 & Y e^{iy} & 0 \\ 0 & 0 & Z e^{iz} \end{pmatrix}$	$m^2 = \begin{pmatrix} 0 & 0 & X e^{ix} \\ 0 & Y e^{iy} & 0 \\ Z e^{iz} & 0 & 0 \end{pmatrix}$	$m^3 = \begin{pmatrix} X e^{ix} & 0 & 0 \\ 0 & 0 & Y e^{iy} \\ 0 & Z e^{iz} & 0 \end{pmatrix}$			
$m^4 = \begin{pmatrix} 0 & 0 & X e^{ix} \\ Y e^{iy} & 0 & 0 \\ 0 & Z e^{iz} & 0 \end{pmatrix}$	$m^5 = \begin{pmatrix} 0 & X e^{ix} & 0 \\ 0 & 0 & Y e^{iy} \\ Z e^{iz} & 0 & 0 \end{pmatrix}$	$m^6 = \begin{pmatrix} 0 & X e^{ix} & 0 \\ Y e^{iy} & 0 & 0 \\ 0 & 0 & Z e^{iz} \end{pmatrix}$			

Table 6.8: Minimal (4-independent zero) textures of μ_S

Minimal (4-independent zero) textures of μ_S					
$\mu_S^1 = \begin{pmatrix} 0 & 0 & R e^{ir} \\ 0 & S e^{is} & 0 \\ R e^{ir} & 0 & 0 \end{pmatrix}$	$\mu_S^2 = \begin{pmatrix} P e^{ip} & 0 & 0 \\ 0 & 0 & T e^{it} \\ 0 & T e^{it} & 0 \end{pmatrix}$	$\mu_S^3 = \begin{pmatrix} 0 & Q e^{iq} & 0 \\ Q e^{iq} & 0 & 0 \\ 0 & 0 & V e^{iv} \end{pmatrix}$			

in Table 6.8), all the emerged M_ν contain three or more independent zeros and hence rejected. Therefore, to obtain viable structures of M_ν we stick with the nonsingular two zero textures of μ_S and are presented in Table 6.9. Interestingly, unlike Linear seesaw, we note that Inverse seesaw leads to all the seven viable two zero textures ($M_\nu^1 - M_\nu^7$) of M_ν given in Ref. [222]. In a compact way, in Table 6.10 we present all the combinations that generate these textures of M_ν .

Table 6.9: 2-independent zero textures for μ_S

2-independent-zero textures for μ_S								
$\mu_S^1 = \begin{pmatrix} 0 & 0 & Re^{ir} \\ 0 & Se^{is} & Te^{it} \\ Re^{ir} & Te^{it} & Ve^{iv} \end{pmatrix}$	$\mu_S^2 = \begin{pmatrix} 0 & Qe^{iq} & Re^{ir} \\ Qe^{iq} & Se^{is} & 0 \\ Re^{ir} & 0 & Ve^{iv} \end{pmatrix}$	$\mu_S^3 = \begin{pmatrix} 0 & Qe^{iq} & 0 \\ Qe^{iq} & Se^{is} & Te^{it} \\ 0 & Te^{it} & Ve^{iv} \end{pmatrix}$						
$\mu_S^4 = \begin{pmatrix} Pe^{ip} & 0 & Re^{ir} \\ 0 & 0 & Te^{it} \\ Re^{ir} & Te^{it} & Ve^{iv} \end{pmatrix}$	$\mu_S^5 = \begin{pmatrix} Pe^{ip} & Qe^{iq} & Re^{ir} \\ Qe^{iq} & 0 & 0 \\ Re^{ir} & 0 & Ve^{iv} \end{pmatrix}$	$\mu_S^6 = \begin{pmatrix} Pe^{ip} & Qe^{iq} & 0 \\ Qe^{iq} & 0 & Te^{it} \\ 0 & Te^{it} & Ve^{iv} \end{pmatrix}$						
$\mu_S^7 = \begin{pmatrix} Pe^{ip} & 0 & Re^{ir} \\ 0 & Se^{is} & Te^{it} \\ Re^{ir} & Te^{it} & 0 \end{pmatrix}$	$\mu_S^8 = \begin{pmatrix} Pe^{ip} & Qe^{iq} & Re^{ir} \\ Qe^{iq} & Se^{is} & 0 \\ Re^{ir} & 0 & 0 \end{pmatrix}$	$\mu_S^9 = \begin{pmatrix} Pe^{ip} & Qe^{iq} & 0 \\ Qe^{iq} & Se^{is} & Te^{it} \\ 0 & Te^{it} & 0 \end{pmatrix}$						
$\mu_S^{10} = \begin{pmatrix} Pe^{ip} & Qe^{iq} & Re^{ir} \\ Qe^{iq} & 0 & Te^{it} \\ Re^{ir} & Te^{it} & 0 \end{pmatrix}$	$\mu_S^{11} = \begin{pmatrix} 0 & Qe^{iq} & Re^{ir} \\ Qe^{iq} & Se^{is} & Te^{it} \\ Re^{ir} & Te^{it} & 0 \end{pmatrix}$	$\mu_S^{12} = \begin{pmatrix} 0 & Qe^{iq} & Re^{ir} \\ Qe^{iq} & 0 & Te^{it} \\ Re^{ir} & Te^{it} & Ve^{iv} \end{pmatrix}$						

 Table 6.10: Compositions for Realization of two-zero M_ν textures with $m_D = m_D^1$

μ_S	$m \rightarrow$					
	m^1	m^2	m^3	m^4	m^5	m^6
μ_S^1	M_ν^1	\times	M_ν^2	M_ν^6	\times	M_ν^5
μ_S^2	\times	M_ν^4	\times	M_ν^4	M_ν^3	M_ν^3
μ_S^3	M_ν^2	M_ν^6	M_ν^1	\times	\times	\times
μ_S^4	M_ν^5	\times	M_ν^6	M_ν^2	M_ν^5	M_ν^1
μ_S^5	\times	M_ν^5	\times	M_ν^1	\times	M_ν^2
μ_S^6	M_ν^3	M_ν^3	M_ν^4	\times	M_ν^6	\times
μ_S^7	M_ν^4	\times	M_ν^3	M_ν^3	M_ν^4	M_ν^4
μ_S^8	\times	M_ν^1	\times	M_ν^5	M_ν^2	M_ν^6
μ_S^9	M_ν^6	M_ν^2	M_ν^5	\times	M_ν^1	\times
μ_S^{10}	M_ν^7	\times	M_ν^7	\times	\times	\times
μ_S^{11}	\times	\times	\times	M_ν^7	\times	M_ν^7
μ_S^{12}	\times	M_ν^7	\times	\times	M_ν^7	\times

Similar to Table 6.10, five more tables can be obtained for $m_D^2 - m_D^6$. However, all those combinations also lead to all seven possible two-zero textures but with different combinations of m_D , m and μ_S . We are not listing all these tables.

6.4.1 Effective M_ν and its parametrization

 Table 6.11: Effective allowed M_ν from Inverse seesaw

Effective allowed M_ν from Inverse seesaw		
M_ν	Phase rotated M_ν	Parametrization
$\begin{pmatrix} 0 & 0 & K_1 e^{ik_1} \\ 0 & K_2 e^{ik_2} & K_3 e^{ik_3} \\ K_1 e^{ik_1} & K_3 e^{ik_3} & K_4 e^{ik_4} \end{pmatrix}$	$m_0 \begin{pmatrix} 0 & 0 & 1 \\ 0 & y_1 & y_2 \\ 0 & y_2 & y_3 e^{i\alpha} \end{pmatrix}$	$m_0 = K_1, K_2/K_1 = y_1,$ $K_3/K_1 = y_2, K_4/K_1 = y_3,$ $\alpha = (k_2 - 2k_3 + k_4)$
$\begin{pmatrix} 0 & K_1 e^{ik_1} & 0 \\ K_1 e^{ik_1} & K_2 e^{ik_2} & K_3 e^{ik_3} \\ 0 & K_3 e^{ik_3} & K_4 e^{ik_4} \end{pmatrix}$	$m_0 \begin{pmatrix} 0 & 1 & 0 \\ 1 & y_1 & y_2 \\ 0 & y_2 & y_3 e^{i\alpha} \end{pmatrix}$	$m_0 = K_1, K_2/K_1 = y_1,$ $K_3/K_1 = y_2, K_4/K_1 = y_3,$ $\alpha = (k_2 - 2k_3 + k_4)$
$\begin{pmatrix} K_1 e^{ik_1} & K_2 e^{ik_2} & 0 \\ K_2 e^{ik_2} & 0 & K_3 e^{ik_3} \\ 0 & K_3 e^{ik_3} & K_4 e^{ik_4} \end{pmatrix}$	$m_0 \begin{pmatrix} 1 & y_1 & 0 \\ y_1 & 0 & y_2 \\ 0 & y_2 & y_3 e^{i\alpha} \end{pmatrix}$	$m_0 = K_1, K_2/K_1 = y_1,$ $K_3/K_1 = y_2, K_4/K_1 = y_3,$ $\alpha = (2k_2 - 2k_3 + k_4 - k_1)$
$\begin{pmatrix} K_1 e^{ik_1} & 0 & K_2 e^{ik_2} \\ 0 & K_4 e^{ik_4} & K_3 e^{ik_3} \\ K_2 e^{ik_2} & K_3 e^{ik_3} & 0 \end{pmatrix}$	$m_0 \begin{pmatrix} 1 & 0 & y_1 \\ 0 & y_3 & y_2 e^{i\alpha} \\ y_1 & y_2 e^{i\alpha} & 0 \end{pmatrix}$	$m_0 = K_1, K_2/K_1 = y_1,$ $K_3/K_1 = y_2, K_4/K_1 = y_3,$ $\alpha = \frac{1}{2}(k_1 - 2k_2 + 2k_3 - k_4)$
$\begin{pmatrix} K_1 e^{ik_1} & 0 & K_2 e^{ik_2} \\ 0 & 0 & K_3 e^{ik_3} \\ K_2 e^{ik_2} & K_3 e^{ik_3} & K_4 e^{ik_4} \end{pmatrix}$	$m_0 \begin{pmatrix} 0 & 0 & y_1 \\ 0 & 0 & y_2 \\ y_1 & y_2 & y_3 e^{i\alpha} \end{pmatrix}$	$m_0 = K_1, K_2/K_1 = y_1,$ $K_3/K_1 = y_2, K_4/K_1 = y_3,$ $\alpha = (k_1 - 2k_2 + k_4)$
$\begin{pmatrix} K_1 e^{ik_1} & K_2 e^{ik_2} & 0 \\ K_2 e^{ik_2} & K_4 e^{ik_4} & K_3 e^{ik_3} \\ 0 & K_3 e^{ik_3} & 0 \end{pmatrix}$	$m_0 \begin{pmatrix} 1 & y_1 & 0 \\ y_1 & y_3 e^{i\alpha} & y_2 \\ 0 & y_2 & 0 \end{pmatrix}$	$m_0 = K_1, K_2/K_1 = y_1,$ $K_3/K_1 = y_2, K_4/K_1 = y_3,$ $\alpha = (k_1 - 2k_2 + k_4)$
$\begin{pmatrix} K_1 e^{ik_1} & K_2 e^{ik_2} & K_3 e^{ik_3} \\ K_2 e^{ik_2} & 0 & K_4 e^{ik_4} \\ K_3 e^{ik_3} & K_4 e^{ik_4} & 0 \end{pmatrix}$	$m_0 \begin{pmatrix} y_1 & 1 & y_2 \\ 1 & 0 & y_3 e^{i\alpha} \\ y_2 & y_3 e^{i\alpha} & 0 \end{pmatrix}$	$m_0 = K_2, K_1/K_2 = y_1,$ $K_3/K_2 = y_2, K_4/K_2 = y_3,$ $\alpha = (k_1 - k_2 - k_3 + k_4).$

We parametrize all emerged viable M_ν matrices in Table 6.11 in a generic way where K_i and k_i are functions of the elements of m_D , m and μ_S . We are not listing explicit expressions of each K_i and k_i parameters as there are many different functions for K_i and k_i .

6.4.2 Numerical analysis

The matrix M_ν obtained in Linear seesaw case Eqn.(6.8) is similar to the matrix M_ν^7 obtained in Inverse seesaw case. In order to perform the numerical analysis we use the experimental constraints (Table 6.12) arising from the global fit oscillation data. We note that the first two matrices (M_ν^1 and M_ν^2) of Table 6.11 do not trigger

Table 6.12: Input experimental values [14]

Quantity	3σ ranges
$ \Delta m_{31}^2 $ (N)	$2.30 < \Delta m_{31}^2 (10^3 eV^{-2}) < 2.64$
$ \Delta m_{31}^2 $ (I)	$2.20 < \Delta m_{31}^2 (10^3 eV^{-2}) < 2.54$
Δm_{21}^2	$7.11 < \Delta m_{21}^2 (10^5 eV^{-2}) < 8.18$
θ_{12}	$31.8^\circ < \theta_{12} < 37.8^\circ$
θ_{23}	$39.4^\circ < \theta_{23} < 53.1^\circ$
θ_{13}	$8^\circ < \theta_{13} < 9.4^\circ$

$\beta\beta_{0\nu}$ decay, due to $|M_{11}| = 0$ for these two matrices. Therefore, we categorize all the matrices presented in Table 6.11 into two different classes.

Class I: Parameter ranges for allowed M_ν with $|M_{11}| \neq 0$

For the numerical analysis of the matrices $M_\nu^3, M_\nu^4, M_\nu^5, M_\nu^6$ we use the experimental constraints (Table 6.12) arising from the global fit oscillation data. It is seen that all the parameters are constrained in a very narrow range and we present them in Table 6.13. The matrices predict a constrained range of δ phase along with an upper bound on the sum of three light neutrino masses ($\Sigma_i m_i$) well below the upper limit dictated by the PLANCK and other astrophysical experiments [53]. For all the four matrices we get normal hierarchical spectrum of neutrino masses. The value of M_{11} are also far below the present experimental probing region [239].

Table 6.13: Parameter ranges of the matrices with $|M_{11}| \neq 0$

M_ν	y_1, y_2, y_3	$ \delta (\text{deg})$	$J_{CP} \times 10^3$	$\sum m_i(\text{eV})$	$ M_{11} \times 10^2(\text{eV})$
m_ν^3	$y_1 : 0.06 - 0.125,$ $y_2 : 1.11 - 1.23,$ $y_3 : 0.24 - 0.50$	3.96 – 5.25	2.3 – 3.6	0.146 – 0.215	4.2 – 6.8
m_ν^4	$y_1 : 0.06 - 0.23,$ $y_2 : 1.118 - 1.386,$ $y_3 : 0.259 - 0.866$	6.51 – 7.65	3.8 – 4.8	0.116 – 0.210	3 – 6.4
m_ν^5	$y_1 : (7.98 - 8) \times 10^{-2},$ $y_2 : 1.15 - 1.18,$ $y_3 : 0.39 - 0.41$	9.0 – 9.4	5.25 – 5.27	0.14 – 0.172	4.8 – 5.1
m_ν^6	$y_1 : 0.11 - 0.14,$ $y_2 : 1.17 - 1.27,$ $y_3 : 0.40 - 0.66$	5.72 – 7.53	1.29 – 2.59	0.128 – 0.173	3.5 – 5.1
m_ν^7	$y_1 : 1.30 - 1.34,$ $y_2 : 0.85 - 0.89,$ $y_3 : 0.79 - 0.82$	0	0	0.127 – 0.131	0.022 – 0.023

Class II: Parameter ranges of the matrices with $|M_{11}| = 0$

Unlike the previous case, this class of matrices (M_ν^1 and M_ν^2) allow a sizable parameter space compatible with the experimental data. However, the matrices also predict constraint ranges of δ phase and $\Sigma_i m_i$. We present plots of these parameters in figure 6.1 and figure 6.2 respectively. From the first two plots of figure 6.1 the ranges of the parameters read as $1.69 < y_1 < 2.93$, $1.47 < y_2 < 2.97$ and $1.37 < y_3 < 3.16$.

The Dirac CP phase is constrained as $-25^\circ < \delta < 25^\circ$ and the sum of the light neutrino masses ($\Sigma_i m_i$) is obtained within the range $0.094 \text{ eV} < \Sigma_i m_i < 0.18 \text{ eV}$ which is well below the present experimental upper bound. In figure 6.2 we present the parameter ranges for M_ν^2 . The matrix M_ν^2 also allow a sizable parameter space and are depicted in first two plots of figure 6.2. The ranges of y_1 , y_2 and y_3 can be read as $1.58 < y_1 < 3.4$, $1.5 < y_2 < 3$ and $1.5 < y_3 < 2.96$. Similar to the previous

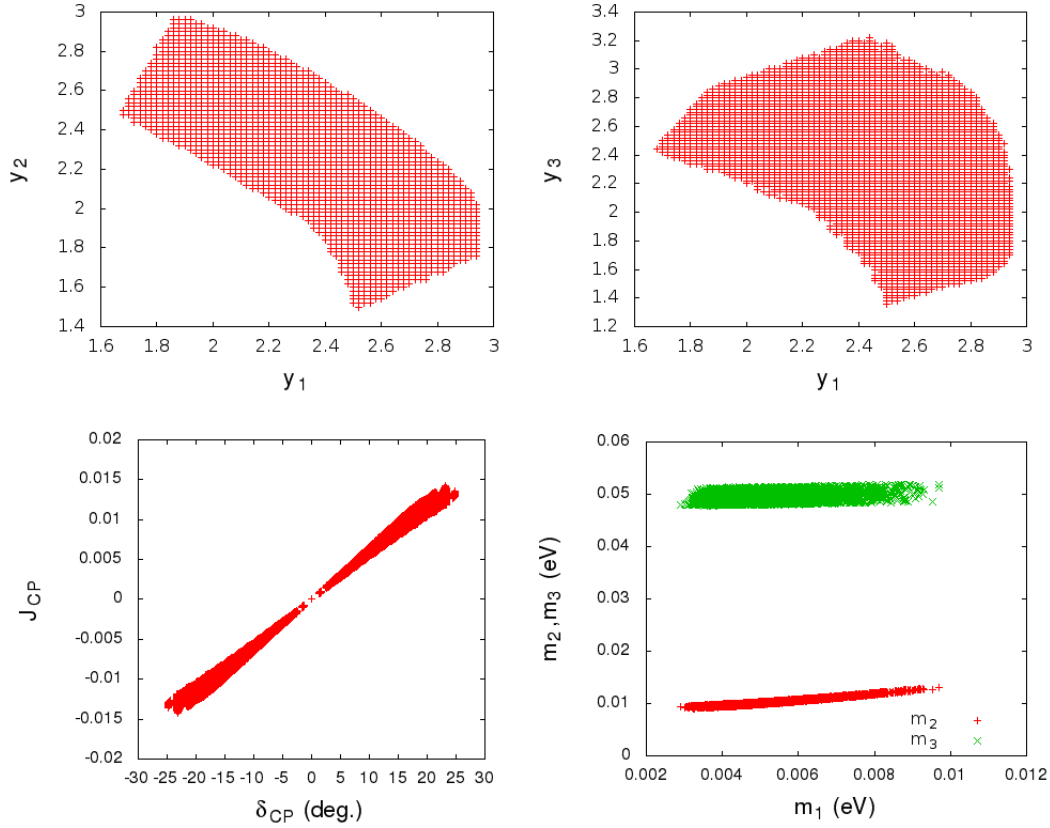


Figure 6.1: The first two figures of the top row represent the parameter space for M_ν^1 matrix. Left plot of the bottom row is the variation of J_{CP} with δ and the right figure shows the hierarchy (normal) of the model.

case, for this matrix also the ranges for δ and $\sum_i m_i$ are constrained in a very narrow range as $-8^\circ < \delta < 8^\circ$, $0.09 \text{ eV} < \sum_i m_i < 0.16 \text{ eV}$. The hierarchy is normal and is depicted in the extreme right plot of the bottom row of figure 6.2.

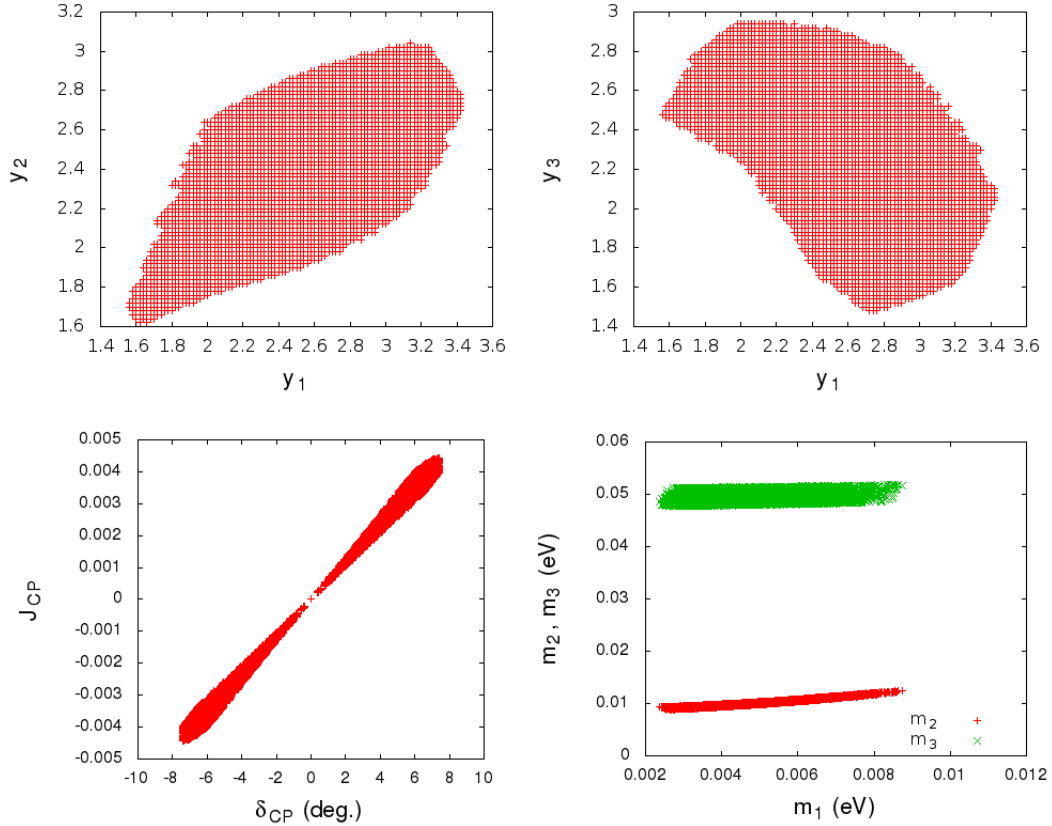


Figure 6.2: The first two figures of the top row represent the parameter space for M_ν^2 matrix. Left plot of the bottom row is the variation of J_{CP} with δ and the right figure shows the hierarchy (normal) of the model.

6.5 Summary

In this chapter, we present an elaborate analysis the Linear and Inverse seesaw mechanisms with the assumption of a minimal nonsingular structure the light neutrino Majorana mass matrix M_ν . The nonsingular nature of M_ℓ together with the assumption of $\det(M_\nu) \neq 0$ dictates the possible minimal structures for the constituent matrices. It has been found in this minimalistic approach that the maximum number of zeros that can be accommodated in matrix ‘ m ’ is five and that for ‘ μ_S ’ is three for Linear and Inverse seesaw respectively in order to obtain a phenomenologically allowed M_ν . Next, we use neutrino oscillation global fit data to obtain the allowed

parameter spaces and obtain predictions on $\sum_i m_i$, $|M_{11}|$, J_{CP} , δ and the neutrino mass spectrum. In particular, all the matrices predict nonvanishing and highly constrained range of δ together with the normal hierarchical spectrum. Numerical analysis shows that two zero textures cannot give rise to large CP violation, and therefore if a maximal Dirac CP violation established in future, this simplistic textures shall be ruled out. However, we can possibly continue to have the same scheme in the neutrino sector but with other nontrivial charged lepton mass matrices such that $h_\ell = M_\ell M_\ell^\dagger$ is not diagonal to obtain large CP-violating phase.

Chapter 7

Summary and conclusions

Various experiments have conclusively established that neutrinos undergo flavor oscillation and therefore must have tiny masses. Neutrino masses require us to construct various extension of the SM which acts as a window to probe new physics. Though several low energy neutrino observables have now been measured with significant precision, there exists a few such as the Dirac CP phase, the Majorana phases etc which are yet to be measured. The octant of the atmospheric mixing angle, the sign of the atmospheric mass-square difference (and hence, the neutrino mass ordering) and the absolute scale of the neutrino mass still remains undetermined. Due to null results of $0\nu\beta\beta$ decay experiments, the perplexing nature of neutrinos, Dirac or Majorana, also has not been settled yet. In this thesis, we have discussed some predictive low energy neutrino mass models with various residual symmetries and implication of some of them in type-I seesaw leptogenesis.

In chapter 1, we have delineated the general theory of neutrino masses and mixing, some of ways of incorporating neutrino masses by enlarging the particle content of the SM, a brief summary of UHE neutrinos and the general theory and

methodology of baryogenesis via leptogenesis in type-I seesaw relevant for the thesis.

In chapter 2, we discuss how the well-known correlations between δ and θ_{23} , arising as a result of two \mathbb{Z}_2 symmetries associated with $\mu\tau$ interchange is altered if the latter is generalized to a symmetry that mixes the ν_μ and ν_τ flavors. In particular, we show that the condition of simultaneous maximality of δ and θ_{23} can be lifted even with a very tiny departure from the exact $\mu\tau$ interchange. Moreover, the current neutrino data on δ and θ_{23} can be explained better in this framework. We also discuss how the proposed mixing scenario could be realized with two simultaneous CP transformations leading to more predictive correlations between δ and the mixing angles θ_{ij} . Next, we analyze the ‘three flavor regime’ of leptogenesis within the CP extended framework and demonstrate that unlike the CP extended $\mu\tau$ interchange symmetry, a resonant leptogenesis is possible in the $\mu\tau$ mixing case and the resulting baryon asymmetry requires $\theta_{23} \neq \pi/4$ due to the fact that the baryon to photon ratio η_B vanishes in the limit of $\theta_{23} \rightarrow \pi/4$. The CP extended $\mu\tau$ mixing also serves as an example of a low energy effective model which provides an important insight into the off-diagonal terms of the flavor coupling matrix which have usually been neglected in literature to compute the final baryon asymmetry, in particular in the models with flavor symmetries.

In chapter 3, we propose a complex extension of $\mu\tau$ mixing antisymmetry in M_ν by a nonstandard CP transformation $\nu_{\alpha L} \rightarrow i\mathcal{G}_{\alpha\beta}\gamma^0\nu_{\beta L}^C$ where \mathcal{G} is a \mathbb{Z}_4 generator related to the \mathbb{Z}_2 generator G through the relation $\mathcal{G} = iG$. As a result $\mu\tau$ mixing parameter θ gets related with δ and θ_{23} as $\sin\delta = \pm\sin\theta/\sin 2\theta_{23}$. For arbitrary θ , both θ_{23} and δ are nonmaximal. For a nonmaximal δ , one of the two Majorana phases is different from 0 or π , leading to substantial Majorana CP violation with observable consequences for $\beta\beta 0\nu$ decay process. For all possible combination of α, β and δ the entire parameter space corresponding to the inverted mass ordering shall

be ruled out if nEXO, covering its entire reach, does not observe any $\beta\beta 0\nu$ signal. We have made a quantitative study of the effect of the CP asymmetry parameter $A_{\mu e}$ in long baseline neutrino oscillation experiments. We also make quantitative predictions of our scheme on Ultra High Energy (UHE) neutrino flavor flux ratios at neutrino telescopes. While exact CP transformed $\mu\tau$ interchange antisymmetry ($\theta = \pi/2$) leads to an exact equality among those ratios, taking a value 0.5, a tiny deviation can cause a drastic change in them. Measurement of UHE flavor flux with improved statistics will further constrain the parameter θ .

Chapter 4 is based on a CP extension of the residual symmetries associated with scaling ansatz invariant neutrino Majorana mass matrix M_ν . It changes the real invariances of M_ν to their complex counterparts which are referred to as ‘Modified Scaling’. We determine correlations between the mixing angles θ_{12} and θ_{13} and show that it leads to maximal Dirac CP violation and vanishing Majorana phases. Besides the testable predictions on $0\nu\beta\beta$ decay, we discuss interesting consequences for leptogenesis. Within the hierarchical scenario, we show that only τ -flavored leptogenesis is possible in this framework. For a NO (IO), θ_{23} is found to be less (greater) than $\pi/4$, for the final baryon asymmetry Y_B to lie in the observed range. An upper and a lower bound on the mass of N_1 and the effect of the heavier neutrinos $N_{2,3}$ on final Y_B has been subsequently estimated.

In chapter 5, we discuss a neutrino mass model with a CP extended $\mu\tau$ flavored symmetry of the effective light neutrino Lagrangian together with an additional invariance under a Friedberg-Lee (FL) transformation of the neutrino fields. The absolute scale of the light neutrino masses is fixed by the vanishing determinant of light Majorana neutrino mass matrix \mathcal{M}_ν . For both NO and IO, while θ_{23} is in general nonmaximal, δ is exactly maximal for IO and nearly maximal for NO due to $\cos\delta \propto \sin\theta_{13}$. For the NO, very tiny nonvanishing Majorana CP violation might

appear through one of the Majorana phases β , otherwise the model predicts vanishing Majorana CP violation. From the future precision measurement of θ_{23} , it is difficult to rule out the model. However, any large deviation of δ from its maximality, will exclude the model. Beside fitting the neutrino oscillation global fit data, we also explore $\nu_\mu \rightarrow \nu_e$ oscillation which is expected to reveal CP violation in different long baseline experiments. Finally, assuming pp and $p\gamma$ collisions as the source of the Ultra High Energy (UHE) neutrinos, statements have been made about the octant of θ_{23} . Conversely, a precision measurement of θ_{23} can be used to predict the allowed ranges of flavor flux ratios.

Chapter 6 is concerned with a detailed pedagogical analysis of the minimal textures of the matrices comprising the light neutrino Majorana mass matrix M_ν in low energy seesaw mechanisms. In particular, the Inverse and Linear seesaw mechanisms have been thoroughly investigated with maximal vanishing elements for the various matrices comprising M_ν with the assumption that its eigenvalues are nonvanishing. We show that the minimal structure of the charged lepton mass matrix allows only six possibilities. For the nonvanishing determinant of M_ν an extensive analysis is performed to derive the minimal textures of the matrices comprising M_ν in both linear and inverse seesaw. We find that the minimality allows the realization of all the phenomenologically allowed two-zero textures in Inverse seesaw but only one such texture is found to be allowed in linear seesaw.

Neutrinos play a crucial role to probe the physics beyond the Standard Model. In this thesis, we propose and explore some neutrino mass models with the hope that these can be tested in the ongoing and forthcoming experiments and throw some light on the physics beyond Standard Model.

Bibliography

- [1] C. S. Lam, “Symmetry of Lepton Mixing,” *Phys. Lett.*, vol. B656, pp. 193–198, 2007.
- [2] C. S. Lam, “The Unique Horizontal Symmetry of Leptons,” *Phys. Rev.*, vol. D78, p. 073015, 2008.
- [3] R. Samanta, R. Sinha, and A. Ghosal, “Model independent constraints on general $\mu\tau$ mixing from recent results on θ_{23} and δ ,” 2018.
- [4] S.-F. Ge, D. A. Dicus, and W. W. Repko, “ Z_2 Symmetry Prediction for the Leptonic Dirac CP Phase,” *Phys. Lett.*, vol. B702, pp. 220–223, 2011.
- [5] R. Sinha, R. Samanta, and A. Ghosal, “Generalized $\mathbb{Z}_2 \times \mathbb{Z}_2$ in scaling neutrino Majorana mass matrix and baryogenesis via flavored leptogenesis,” *JHEP*, vol. 12, p. 030, 2017.
- [6] L. Lavoura, “New model for the neutrino mass matrix,” *Phys. Rev.*, vol. D62, p. 093011, 2000.
- [7] R. N. Mohapatra and W. Rodejohann, “Scaling in the neutrino mass matrix,” *Phys. Lett.*, vol. B644, pp. 59–66, 2007.
- [8] R. Sinha, P. Roy, and A. Ghosal, “CP transformed mixed $\mu\tau$ antisymmetry for neutrinos and its consequences,” 2018.

- [9] R. Sinha, S. Bhattacharya, and R. Samanta, “Phenomenological implications of the Friedberg-Lee transformation in a neutrino mass model with $\mu\tau$ -flavored CP symmetry,” 2018.
- [10] R. Sinha, R. Samanta, and A. Ghosal, “Maximal Zero Textures in Linear and Inverse Seesaw,” *Phys. Lett.*, vol. B759, pp. 206–213, 2016.
- [11] M. Agostini, G. Benato, and J. Detwiler, “Discovery probability of next-generation neutrinoless double- β decay experiments,” *Phys. Rev.*, vol. D96, no. 5, p. 053001, 2017.
- [12] I. Esteban, M. C. Gonzalez-Garcia, M. Maltoni, I. Martinez-Soler, and T. Schwetz, “Updated fit to three neutrino mixing: exploring the accelerator-reactor complementarity,” *JHEP*, vol. 01, p. 087, 2017.
- [13] M. C. Gonzalez-Garcia, M. Maltoni, and T. Schwetz, “Global Analyses of Neutrino Oscillation Experiments,” *Nucl. Phys.*, vol. B908, pp. 199–217, 2016.
- [14] D. V. Forero, M. Tortola, and J. W. F. Valle, “Neutrino oscillations refitted,” *Phys. Rev.*, vol. D90, no. 9, p. 093006, 2014.
- [15] C. L. Cowan, F. Reines, F. B. Harrison, H. W. Kruse, and A. D. McGuire, “Detection of the free neutrino: A Confirmation,” *Science*, vol. 124, pp. 103–104, 1956.
- [16] G. Danby, J. M. Gaillard, K. A. Goulianos, L. M. Lederman, N. B. Mistry, M. Schwartz, and J. Steinberger, “Observation of High-Energy Neutrino Reactions and the Existence of Two Kinds of Neutrinos,” *Phys. Rev. Lett.*, vol. 9, pp. 36–44, 1962.
- [17] K. Kodama *et al.*, “Observation of tau neutrino interactions,” *Phys. Lett.*, vol. B504, pp. 218–224, 2001.

- [18] K. S. Hirata *et al.*, “Experimental Study of the Atmospheric Neutrino Flux,” *Phys. Lett.*, vol. B205, p. 416, 1988. [,447(1988)].
- [19] M. C. Goodman, “The Atmospheric neutrino anomaly in Soudan-2,” *Nucl. Phys. Proc. Suppl.*, vol. 38, pp. 337–342, 1995.
- [20] P. Anselmann *et al.*, “Solar neutrinos observed by GALLEX at Gran Sasso,” *Phys. Lett.*, vol. B285, pp. 376–389, 1992.
- [21] J. N. Abdurashitov *et al.*, “Results from SAGE,” *Phys. Lett.*, vol. B328, pp. 234–248, 1994.
- [22] P. Pal, *An Introductory Course of Particle Physics*. Taylor & Francis, 2014.
- [23] S. Choubey and P. Roy, “Testing maximality in muon neutrino flavor mixing,” *Phys. Rev. Lett.*, vol. 93, p. 021803, 2004.
- [24] E. K. Akhmedov, R. Johansson, M. Lindner, T. Ohlsson, and T. Schwetz, “Series expansions for three flavor neutrino oscillation probabilities in matter,” *JHEP*, vol. 04, p. 078, 2004.
- [25] P. B. Pal, “Dirac, Majorana and Weyl fermions,” *Am. J. Phys.*, vol. 79, pp. 485–498, 2011.
- [26] Y. Chikashige, R. N. Mohapatra, and R. D. Peccei, “Are There Real Goldstone Bosons Associated with Broken Lepton Number?,” *Phys. Lett.*, vol. 98B, pp. 265–268, 1981.
- [27] Y. Chikashige, R. N. Mohapatra, and R. D. Peccei, “Spontaneously Broken Lepton Number and Cosmological Constraints on the Neutrino Mass Spectrum,” *Phys. Rev. Lett.*, vol. 45, p. 1926, 1980. [,921(1980)].

- [28] G. B. Gelmini and M. Roncadelli, “Left-Handed Neutrino Mass Scale and Spontaneously Broken Lepton Number,” *Phys. Lett.*, vol. 99B, pp. 411–415, 1981.
- [29] E. K. Akhmedov, “Neutrino physics,” in *Proceedings, Summer School in Particle Physics: Trieste, Italy, June 21-July 9, 1999*, pp. 103–164, 1999.
- [30] H. Hettmansperger, M. Lindner, and W. Rodejohann, “Phenomenological Consequences of sub-leading Terms in See-Saw Formulas,” *JHEP*, vol. 04, p. 123, 2011.
- [31] A. Zee, “A Theory of Lepton Number Violation, Neutrino Majorana Mass, and Oscillation,” *Phys. Lett.*, vol. 93B, p. 389, 1980. [Erratum: *Phys. Lett.*95B,461(1980)].
- [32] L. Wolfenstein, “A Theoretical Pattern for Neutrino Oscillations,” *Nucl. Phys.*, vol. B175, pp. 93–96, 1980.
- [33] E. Ma, “Verifiable radiative seesaw mechanism of neutrino mass and dark matter,” *Phys. Rev.*, vol. D73, p. 077301, 2006.
- [34] R. Franceschini, T. Hambye, and A. Strumia, “Type-III see-saw at LHC,” *Phys. Rev.*, vol. D78, p. 033002, 2008.
- [35] R. N. Mohapatra and G. Senjanovic, “Neutrino Mass and Spontaneous Parity Nonconservation,” *Phys. Rev. Lett.*, vol. 44, p. 912, 1980. [,231(1979)].
- [36] R. N. Mohapatra and G. Senjanovic, “Neutrino Masses and Mixings in Gauge Models with Spontaneous Parity Violation,” *Phys. Rev.*, vol. D23, p. 165, 1981.
- [37] H. Georgi and S. L. Glashow, “Unity of All Elementary Particle Forces,” *Phys. Rev. Lett.*, vol. 32, pp. 438–441, 1974.

- [38] D. Chang, R. N. Mohapatra, and M. K. Parida, “A New Approach to Left-Right Symmetry Breaking in Unified Gauge Theories,” *Phys. Rev.*, vol. D30, p. 1052, 1984.
- [39] D. Chang, R. N. Mohapatra, and M. K. Parida, “Decoupling Parity and SU(2)-R Breaking Scales: A New Approach to Left-Right Symmetric Models,” *Phys. Rev. Lett.*, vol. 52, p. 1072, 1984.
- [40] R. N. Mohapatra, *UNIFICATION AND SUPERSYMMETRY. THE FRONTIERS OF QUARK - LEPTON PHYSICS*. Berlin: Springer, 1986.
- [41] M. G. Aartsen *et al.*, “First observation of PeV-energy neutrinos with IceCube,” *Phys. Rev. Lett.*, vol. 111, p. 021103, 2013.
- [42] M. G. Aartsen *et al.*, “Evidence for High-Energy Extraterrestrial Neutrinos at the IceCube Detector,” *Science*, vol. 342, p. 1242856, 2013.
- [43] M. G. Aartsen *et al.*, “Observation of High-Energy Astrophysical Neutrinos in Three Years of IceCube Data,” *Phys. Rev. Lett.*, vol. 113, p. 101101, 2014.
- [44] M. G. Aartsen *et al.*, “The IceCube Neutrino Observatory - Contributions to ICRC 2015 Part II: Atmospheric and Astrophysical Diffuse Neutrino Searches of All Flavors,” in *Proceedings, 34th International Cosmic Ray Conference (ICRC 2015): The Hague, The Netherlands, July 30-August 6, 2015*, 2015.
- [45] M. G. Aartsen *et al.*, “The IceCube Neutrino Observatory - Contributions to ICRC 2017 Part II: Properties of the Atmospheric and Astrophysical Neutrino Flux,” 2017.
- [46] S. Adrian-Martinez *et al.*, “The First Combined Search for Neutrino Point-sources in the Southern Hemisphere With the Antares and Icecube Neutrino Telescopes,” *Astrophys. J.*, vol. 823, no. 1, p. 65, 2016.

- [47] J. K. Becker, “High-energy neutrinos in the context of multimessenger physics,” *Phys. Rept.*, vol. 458, pp. 173–246, 2008.
- [48] Y. Sui and P. S. Bhupal Dev, “A Combined Astrophysical and Dark Matter Interpretation of the IceCube HESE and Throughgoing Muon Events,” *JCAP*, vol. 1807, no. 07, p. 020, 2018.
- [49] M. Ahlers and F. Halzen, “High-energy cosmic neutrino puzzle: a review,” *Rept. Prog. Phys.*, vol. 78, no. 12, p. 126901, 2015.
- [50] S. Hummer, M. Ruger, F. Spanier, and W. Winter, “Simplified models for photohadronic interactions in cosmic accelerators,” *Astrophys. J.*, vol. 721, pp. 630–652, 2010.
- [51] W. Rodejohann, “Neutrino Mixing and Neutrino Telescopes,” *JCAP*, vol. 0701, p. 029, 2007.
- [52] Z.-z. Xing, “A further study of $\mu\tau$ symmetry breaking at neutrino telescopes after the Daya Bay and RENO measurements of θ_{13} ,” *Phys. Lett.*, vol. B716, pp. 220–224, 2012.
- [53] P. A. R. Ade *et al.*, “Planck 2015 results. XIII. Cosmological parameters,” *Astron. Astrophys.*, vol. 594, p. A13, 2016.
- [54] A. Riotto, “Theories of baryogenesis,” in *Proceedings, Summer School in High-energy physics and cosmology: Trieste, Italy, June 29-July 17, 1998*, pp. 326–436, 1998.
- [55] J. M. Cline, “Baryogenesis,” in *Les Houches Summer School - Session 86: Particle Physics and Cosmology: The Fabric of Spacetime Les Houches, France, July 31-August 25, 2006*, 2006.

- [56] M. Dine and A. Kusenko, “The Origin of the matter - antimatter asymmetry,” *Rev. Mod. Phys.*, vol. 76, p. 1, 2003.
- [57] A. D. Sakharov, “Violation of CP Invariance, C asymmetry, and baryon asymmetry of the universe,” *Pisma Zh. Eksp. Teor. Fiz.*, vol. 5, pp. 32–35, 1967. [Usp. Fiz. Nauk161,no.5,61(1991)].
- [58] A. Yu. Ignatiev, N. V. Krasnikov, V. A. Kuzmin, and A. N. Tavkhelidze, “Universal CP Noninvariant Superweak Interaction and Baryon Asymmetry of the Universe,” *Phys. Lett.*, vol. 76B, pp. 436–438, 1978.
- [59] M. Yoshimura, “Unified Gauge Theories and the Baryon Number of the Universe,” *Phys. Rev. Lett.*, vol. 41, pp. 281–284, 1978. [Erratum: *Phys. Rev. Lett.*42,746(1979)].
- [60] S. Dimopoulos and L. Susskind, “On the Baryon Number of the Universe,” *Phys. Rev.*, vol. D18, pp. 4500–4509, 1978.
- [61] V. A. Rubakov and M. E. Shaposhnikov, “Electroweak baryon number nonconservation in the early universe and in high-energy collisions,” *Usp. Fiz. Nauk*, vol. 166, pp. 493–537, 1996. [Phys. Usp.39,461(1996)].
- [62] M. Trodden, “Electroweak baryogenesis,” *Rev. Mod. Phys.*, vol. 71, pp. 1463–1500, 1999.
- [63] I. Affleck and M. Dine, “A New Mechanism for Baryogenesis,” *Nucl. Phys.*, vol. B249, pp. 361–380, 1985.
- [64] M. Dine, L. Randall, and S. D. Thomas, “Baryogenesis from flat directions of the supersymmetric standard model,” *Nucl. Phys.*, vol. B458, pp. 291–326, 1996.

- [65] M. Fukugita and T. Yanagida, “Baryogenesis Without Grand Unification,” *Phys. Lett.*, vol. B174, pp. 45–47, 1986.
- [66] A. Riotto and M. Trodden, “Recent progress in baryogenesis,” *Ann. Rev. Nucl. Part. Sci.*, vol. 49, pp. 35–75, 1999.
- [67] S. Davidson, E. Nardi, and Y. Nir, “Leptogenesis,” *Phys. Rept.*, vol. 466, pp. 105–177, 2008.
- [68] A. Abada, S. Davidson, A. Ibarra, F. X. Josse-Michaux, M. Losada, and A. Riotto, “Flavour Matters in Leptogenesis,” *JHEP*, vol. 09, p. 010, 2006.
- [69] S. Antusch, S. F. King, and A. Riotto, “Flavour-Dependent Leptogenesis with Sequential Dominance,” *JCAP*, vol. 0611, p. 011, 2006.
- [70] N. S. Manton, “Topology in the Weinberg-Salam Theory,” *Phys. Rev.*, vol. D28, p. 2019, 1983.
- [71] B. Adhikary, M. Chakraborty, and A. Ghosal, “Flavored leptogenesis with quasidegenerate neutrinos in a broken cyclic symmetric model,” *Phys. Rev.*, vol. D93, no. 11, p. 113001, 2016.
- [72] W. Buchmuller, P. Di Bari, and M. Plumacher, “The Neutrino mass window for baryogenesis,” *Nucl. Phys.*, vol. B665, pp. 445–468, 2003.
- [73] G. Engelhard, Y. Grossman, E. Nardi, and Y. Nir, “The Importance of N_2 leptogenesis,” *Phys. Rev. Lett.*, vol. 99, p. 081802, 2007.
- [74] A. Pilaftsis and T. E. J. Underwood, “Resonant leptogenesis,” *Nucl. Phys.*, vol. B692, pp. 303–345, 2004.
- [75] S. L. Adler, “Axial vector vertex in spinor electrodynamics,” *Phys. Rev.*, vol. 177, pp. 2426–2438, 1969. [,241(1969)].

- [76] G. 't Hooft, “Symmetry Breaking Through Bell-Jackiw Anomalies,” *Phys. Rev. Lett.*, vol. 37, pp. 8–11, 1976. [,226(1976)].
- [77] P. B. Arnold, D. Son, and L. G. Yaffe, “The Hot baryon violation rate is $O(\alpha_w^5 T^4)$,” *Phys. Rev.*, vol. D55, pp. 6264–6273, 1997.
- [78] P. B. Arnold, D. T. Son, and L. G. Yaffe, “Effective dynamics of hot, soft nonAbelian gauge fields. Color conductivity and $\log(1/\alpha)$ effects,” *Phys. Rev.*, vol. D59, p. 105020, 1999.
- [79] V. A. Kuzmin, V. A. Rubakov, and M. E. Shaposhnikov, “On the Anomalous Electroweak Baryon Number Nonconservation in the Early Universe,” *Phys. Lett.*, vol. 155B, p. 36, 1985.
- [80] F. R. Klinkhamer and N. S. Manton, “A Saddle Point Solution in the Weinberg-Salam Theory,” *Phys. Rev.*, vol. D30, p. 2212, 1984.
- [81] P. B. Arnold and L. D. McLerran, “Sphalerons, Small Fluctuations and Baryon Number Violation in Electroweak Theory,” *Phys. Rev.*, vol. D36, p. 581, 1987.
- [82] W. Buchmuller, “Baryo- and leptogenesis (brief summary),” *ICTP Lect. Notes Ser.*, vol. 14, pp. 41–75, 2003.
- [83] M.-C. Chen, “TASI 2006 Lectures on Leptogenesis,” in *Proceedings of Theoretical Advanced Study Institute in Elementary Particle Physics : Exploring New Frontiers Using Colliders and Neutrinos (TASI 2006): Boulder, Colorado, June 4-30, 2006*, pp. 123–176, 2007.
- [84] E. W. Kolb and M. S. Turner, “The Early Universe,” *Front. Phys.*, vol. 69, pp. 1–547, 1990.
- [85] S. F. King, “Models of Neutrino Mass, Mixing and CP Violation,” *J. Phys.*, vol. G42, p. 123001, 2015.

- [86] S. F. King, “Neutrino mass models,” *Rept. Prog. Phys.*, vol. 67, pp. 107–158, 2004.
- [87] R. N. Mohapatra and A. Y. Smirnov, “Neutrino Mass and New Physics,” *Ann. Rev. Nucl. Part. Sci.*, vol. 56, pp. 569–628, 2006.
- [88] G. Altarelli and F. Feruglio, “Theoretical models of neutrino masses and mixings,” *Springer Tracts Mod. Phys.*, vol. 190, pp. 169–207, 2003. [,169(2002)].
- [89] J. W. F. Valle, “Neutrino physics overview,” *J. Phys. Conf. Ser.*, vol. 53, pp. 473–505, 2006.
- [90] E. Ma, “Plato’s fire and the neutrino mass matrix,” *Mod. Phys. Lett.*, vol. A17, pp. 2361–2370, 2002.
- [91] S. F. King and C. Luhn, “Neutrino Mass and Mixing with Discrete Symmetry,” *Rept. Prog. Phys.*, vol. 76, p. 056201, 2013.
- [92] G. Altarelli and F. Feruglio, “Discrete Flavor Symmetries and Models of Neutrino Mixing,” *Rev. Mod. Phys.*, vol. 82, pp. 2701–2729, 2010.
- [93] M. Tanimoto, “Generation of neutrino masses and mixings in gauge theories,” in *Weak interactions and neutrinos. Proceedings, 17th International Workshop, WIN’99, Cape Town, South Africa, January 24-30, 1999*, pp. 345–349, 1999.
- [94] H. Ishimori, T. Kobayashi, H. Ohki, Y. Shimizu, H. Okada, and M. Tanimoto, “Non-Abelian Discrete Symmetries in Particle Physics,” *Prog. Theor. Phys. Suppl.*, vol. 183, pp. 1–163, 2010.
- [95] C. S. Lam, “Determining Horizontal Symmetry from Neutrino Mixing,” *Phys. Rev. Lett.*, vol. 101, p. 121602, 2008.
- [96] D. A. Dicus, S.-F. Ge, and W. W. Repko, “Generalized Hidden Z_2 Symmetry of Neutrino Mixing,” *Phys. Rev.*, vol. D83, p. 093007, 2011.

- [97] H.-J. He and F.-R. Yin, “Common Origin of $\mu - \tau$ and CP Breaking in Neutrino Seesaw, Baryon Asymmetry, and Hidden Flavor Symmetry,” *Phys. Rev.*, vol. D84, p. 033009, 2011.
- [98] S.-F. Ge, H.-J. He, and F.-R. Yin, “Common Origin of Soft $\mu - \tau$ and CP Breaking in Neutrino Seesaw and the Origin of Matter,” *JCAP*, vol. 1005, p. 017, 2010.
- [99] S. F. King, “Unified Models of Neutrinos, Flavour and CP Violation,” *Prog. Part. Nucl. Phys.*, vol. 94, pp. 217–256, 2017.
- [100] W. Grimus and M. N. Rebelo, “Automorphisms in gauge theories and the definition of CP and P,” *Phys. Rept.*, vol. 281, pp. 239–308, 1997.
- [101] P. Chen, C.-C. Li, and G.-J. Ding, “Lepton Flavor Mixing and CP Symmetry,” *Phys. Rev.*, vol. D91, p. 033003, 2015.
- [102] R. Z. R. F. Feruglio, C. Hagedorn, “Lepton Mixing Parameters from Discrete and CP Symmetries,” *JHEP*, vol. 07, p. 027, 2013.
- [103] M. Holthausen, M. Lindner, and M. A. Schmidt, “CP and Discrete Flavour Symmetries,” *JHEP*, vol. 04, p. 122, 2013.
- [104] M.-C. Chen, M. Fallbacher, K. T. Mahanthappa, M. Ratz, and A. Trautner, “CP Violation from Finite Groups,” *Nucl. Phys.*, vol. B883, pp. 267–305, 2014.
- [105] F. Feruglio, C. Hagedorn, and R. Ziegler, “A realistic pattern of lepton mixing and masses from S_4 and CP,” *Eur. Phys. J.*, vol. C74, p. 2753, 2014.
- [106] R. N. Mohapatra and C. C. Nishi, “Implications of \hat{I}_{ij} - $\hat{I}\check{D}$ flavored CP symmetry of leptons,” *JHEP*, vol. 08, p. 092, 2015.
- [107] A. Ghosal and R. Samanta, “Probing texture zeros with scaling ansatz in inverse seesaw,” *JHEP*, vol. 05, p. 077, 2015.

- [108] R. Samanta and A. Ghosal, “Probing maximal zero textures with broken cyclic symmetry in inverse seesaw,” *Nucl. Phys.*, vol. B911, pp. 846–862, 2016.
- [109] W. Grimus and L. Lavoura, “A Nonstandard CP transformation leading to maximal atmospheric neutrino mixing,” *Phys. Lett.*, vol. B579, pp. 113–122, 2004.
- [110] C. C. Nishi and B. L. Sánchez-Vega, “ μ – τ reflection symmetry with a texture-zero,” *JHEP*, vol. 01, p. 068, 2017.
- [111] I. Girardi, S. T. Petcov, and A. V. Titov, “Predictions for the Leptonic Dirac CP Violation Phase: a Systematic Phenomenological Analysis,” *Eur. Phys. J.*, vol. C75, p. 345, 2015.
- [112] M. Tanabashi *et al.*, “Review of Particle Physics,” *Phys. Rev.*, vol. D98, no. 3, p. 030001, 2018.
- [113] R. N. Mohapatra and S. Nussinov, “Bimaximal neutrino mixing and neutrino mass matrix,” *Phys. Rev.*, vol. D60, p. 013002, 1999.
- [114] T. Fukuyama and H. Nishiura, “Mass matrix of Majorana neutrinos,” 1997.
- [115] F. P. An *et al.*, “New Measurement of Antineutrino Oscillation with the Full Detector Configuration at Daya Bay,” *Phys. Rev. Lett.*, vol. 115, no. 11, p. 111802, 2015.
- [116] W. Grimus, A. S. Joshipura, S. Kaneko, L. Lavoura, and M. Tanimoto, “Lepton mixing angle $\theta_{13} = 0$ with a horizontal symmetry D_4 ,” *JHEP*, vol. 07, p. 078, 2004.
- [117] W. Grimus, A. S. Joshipura, S. Kaneko, L. Lavoura, H. Sawanaka, and M. Tanimoto, “Non-vanishing U_{e3} and $\cos 2\theta_{23}$ from a broken Z_2 symmetry,” *Nucl. Phys.*, vol. B713, pp. 151–172, 2005.

- [118] A. S. Joshipura and W. Rodejohann, “Scaling in the Neutrino Mass Matrix, $\mu - \tau$ Symmetry and the See-Saw Mechanism,” *Phys. Lett.*, vol. B678, pp. 276–282, 2009.
- [119] R. Samanta, P. Roy, and A. Ghosal, “Extended scaling and residual flavor symmetry in the neutrino Majorana mass matrix,” *Eur. Phys. J.*, vol. C76, no. 12, p. 662, 2016.
- [120] R. Samanta, P. Roy, and A. Ghosal, “Complex Scaling in Neutrino Mass Matrix,” *Acta Phys. Polon. Supp.*, vol. 9, p. 807, 2016.
- [121] R. Samanta, M. Chakraborty, P. Roy, and A. Ghosal, “Baryon asymmetry via leptogenesis in a neutrino mass model with complex scaling,” *JCAP*, vol. 1703, no. 03, p. 025, 2017.
- [122] G. C. Branco, D. Emmanuel-Costa, M. N. Rebelo, and P. Roy, “Four Zero Neutrino Yukawa Textures in the Minimal Seesaw Framework,” *Phys. Rev.*, vol. D77, p. 053011, 2008.
- [123] R. N. Mohapatra and C. C. Nishi, “ S_4 Flavored CP Symmetry for Neutrinos,” *Phys. Rev.*, vol. D86, p. 073007, 2012.
- [124] S. Gupta, A. S. Joshipura, and K. M. Patel, “Minimal extension of tri-bimaximal mixing and generalized $Z_2 \times Z_2$ symmetries,” *Phys. Rev.*, vol. D85, p. 031903, 2012.
- [125] G.-J. Ding, S. F. King, C. Luhn, and A. J. Stuart, “Spontaneous CP violation from vacuum alignment in S_4 models of leptons,” *JHEP*, vol. 05, p. 084, 2013.
- [126] G.-J. Ding, S. F. King, and A. J. Stuart, “Generalised CP and A_4 Family Symmetry,” *JHEP*, vol. 12, p. 006, 2013.

- [127] P. Chen, C.-Y. Yao, and G.-J. Ding, “Neutrino Mixing from CP Symmetry,” *Phys. Rev.*, vol. D92, no. 7, p. 073002, 2015.
- [128] C. C. Nishi, “New and trivial CP symmetry for extended A_4 flavor,” *Phys. Rev.*, vol. D93, no. 9, p. 093009, 2016.
- [129] W. Rodejohann and X.-J. Xu, “Trimaximal μ - τ reflection symmetry,” *Phys. Rev.*, vol. D96, no. 5, p. 055039, 2017.
- [130] J. T. Penedo, S. T. Petcov, and A. V. Titov, “Neutrino mixing and leptonic CP violation from S_4 flavour and generalised CP symmetries,” *JHEP*, vol. 12, p. 022, 2017.
- [131] S. Blanchet and P. Di Bari, “Flavor effects on leptogenesis predictions,” *JCAP*, vol. 0703, p. 018, 2007.
- [132] P. S. B. Dev, P. Di Bari, B. Garbrecht, S. Lavignac, P. Millington, and D. Teresi, “Flavor effects in leptogenesis,” *Int. J. Mod. Phys.*, vol. A33, p. 1842001, 2018.
- [133] E. Nardi, Y. Nir, E. Roulet, and J. Racker, “The Importance of flavor in leptogenesis,” *JHEP*, vol. 01, p. 164, 2006.
- [134] R. Barbieri, P. Creminelli, A. Strumia, and N. Tetradis, “Baryogenesis through leptogenesis,” *Nucl. Phys.*, vol. B575, pp. 61–77, 2000.
- [135] S. Antusch, P. Di Bari, D. A. Jones, and S. F. King, “A fuller flavour treatment of N_2 -dominated leptogenesis,” *Nucl. Phys.*, vol. B856, pp. 180–209, 2012.
- [136] P. Di Bari and S. F. King, “Successful N_2 leptogenesis with flavour coupling effects in realistic unified models,” *JCAP*, vol. 1510, no. 10, p. 008, 2015.
- [137] R. Samanta, M. Chakraborty, and A. Ghosal, “Evaluation of the Majorana Phases of a General Majorana Neutrino Mass Matrix: Testability of hierarchical Flavour Models,” *Nucl. Phys.*, vol. B904, pp. 86–105, 2016.

- [138] M. Hirsch, S. Morisi, E. Peinado, and J. W. F. Valle, “Discrete dark matter,” *Phys. Rev.*, vol. D82, p. 116003, 2010.
- [139] Y. Hamada, T. Kobayashi, A. Ogasahara, Y. Omura, F. Takayama, and D. Yasuhara, “Revisiting discrete dark matter model: $\theta_{13} \neq 0$ and ν_R dark matter,” *JHEP*, vol. 10, p. 183, 2014.
- [140] P. H. Frampton and R. N. Mohapatra, “Possible gauge theoretic origin for quark-lepton complementarity,” *JHEP*, vol. 01, p. 025, 2005.
- [141] K. S. Babu and R. N. Mohapatra, “Predictive schemes for bimaximal neutrino mixings,” *Phys. Lett.*, vol. B532, pp. 77–86, 2002.
- [142] M. S. Berger and M. Dawid, “A Froggatt-Nielsen flavor model for neutrino physics,” 2019.
- [143] P. Chen, G.-J. Ding, F. Gonzalez-Canales, and J. W. F. Valle, “Generalized $\mu - \tau$ reflection symmetry and leptonic CP violation,” *Phys. Lett.*, vol. B753, pp. 644–652, 2016.
- [144] P. F. Harrison and W. G. Scott, “mu - tau reflection symmetry in lepton mixing and neutrino oscillations,” *Phys. Lett.*, vol. B547, pp. 219–228, 2002.
- [145] P. Chen, G.-J. Ding, and S. F. King, “Leptogenesis and residual CP symmetry,” *JHEP*, vol. 03, p. 206, 2016.
- [146] W. Buchmuller, P. Di Bari, and M. Plumacher, “Leptogenesis for pedestrians,” *Annals Phys.*, vol. 315, pp. 305–351, 2005.
- [147] P. Di Bari and L. Marzola, “SO(10)-inspired solution to the problem of the initial conditions in leptogenesis,” *Nucl. Phys.*, vol. B877, pp. 719–751, 2013.
- [148] N. Aghanim *et al.*, “Planck 2018 results. VI. Cosmological parameters,” 2018.

- [149] K. Moffat, S. Pascoli, S. T. Petcov, H. Schulz, and J. Turner, “Three-flavored nonresonant leptogenesis at intermediate scales,” *Phys. Rev.*, vol. D98, no. 1, p. 015036, 2018.
- [150] S. Blanchet, P. Di Bari, D. A. Jones, and L. Marzola, “Leptogenesis with heavy neutrino flavours: from density matrix to Boltzmann equations,” *JCAP*, vol. 1301, p. 041, 2013.
- [151] R. Samanta, P. Roy, and A. Ghosal, “Consequences of minimal seesaw with complex $\mu\tau$ antisymmetry of neutrinos,” *JHEP*, vol. 06, p. 085, 2018.
- [152] D. M. Barreiros, R. G. Felipe, and F. R. Joaquim, “Combining texture zeros with a remnant CP symmetry in the minimal type-I seesaw,” *JHEP*, vol. 01, p. 223, 2019.
- [153] S. Davidson and A. Ibarra, “A Lower bound on the right-handed neutrino mass from leptogenesis,” *Phys. Lett.*, vol. B535, pp. 25–32, 2002.
- [154] R. Samanta and M. Chakraborty, “A study on a minimally broken residual TBM-Klein symmetry with its implications on flavoured leptogenesis and ultra high energy neutrino flux ratios,” 2018.
- [155] P. S. Bhupal Dev, R. Franceschini, and R. N. Mohapatra, “Bounds on TeV Seesaw Models from LHC Higgs Data,” *Phys. Rev.*, vol. D86, p. 093010, 2012.
- [156] P. S. Bhupal Dev, P. Millington, A. Pilaftsis, and D. Teresi, “Flavour Covariant Transport Equations: an Application to Resonant Leptogenesis,” *Nucl. Phys.*, vol. B886, pp. 569–664, 2014.
- [157] M. Drewes, B. Garbrecht, D. Gueter, and J. Klaric, “Testing the low scale seesaw and leptogenesis,” *JHEP*, vol. 08, p. 018, 2017.

- [158] B. Garbrecht, “Why is there more matter than antimatter? Computational methods for leptogenesis and electroweak baryogenesis,” 2018.
- [159] C. S. Lam, “A 2-3 symmetry in neutrino oscillations,” *Phys. Lett.*, vol. B507, pp. 214–218, 2001.
- [160] E. Ma and M. Raidal, “Neutrino mass, muon anomalous magnetic moment, and lepton flavor nonconservation,” *Phys. Rev. Lett.*, vol. 87, p. 011802, 2001. [Erratum: *Phys. Rev. Lett.* 87, 159901 (2001)].
- [161] K. R. S. Balaji, W. Grimus, and T. Schwetz, “The Solar LMA neutrino oscillation solution in the Zee model,” *Phys. Lett.*, vol. B508, pp. 301–310, 2001.
- [162] A. Ghosal, “An $SU(2)(L) \times U(1)(Y)$ model with reflection symmetry in view of recent neutrino experimental result,” 2003.
- [163] A. Ghosal, “A neutrino mass model with reflection symmetry,” *Mod. Phys. Lett.*, vol. A19, pp. 2579–2586, 2004.
- [164] Z.-z. Xing and Z.-h. Zhao, “A review of $\hat{1}ij\text{-}\check{I}\check{D}$ flavor symmetry in neutrino physics,” *Rept. Prog. Phys.*, vol. 79, no. 7, p. 076201, 2016.
- [165] G.-J. Ding and Y.-L. Zhou, “Lepton mixing parameters from $\Delta(48)$ family symmetry and generalised CP,” *JHEP*, vol. 06, p. 023, 2014.
- [166] G.-J. Ding and S. F. King, “Generalized CP and $\Delta(96)$ family symmetry,” *Phys. Rev.*, vol. D89, no. 9, p. 093020, 2014.
- [167] C.-C. Li and G.-J. Ding, “Generalised CP and trimaximal TM_1 lepton mixing in S_4 family symmetry,” *Nucl. Phys.*, vol. B881, pp. 206–232, 2014.

- [168] S. F. King and T. Neder, “Lepton mixing predictions including Majorana phases from $\hat{\Gamma}(6n^2)$ flavour symmetry and generalised CP,” *Phys. Lett.*, vol. B736, pp. 308–316, 2014.
- [169] C.-C. Li and G.-J. Ding, “Lepton Mixing in A_5 Family Symmetry and Generalized CP,” *JHEP*, vol. 05, p. 100, 2015.
- [170] G.-J. Ding and Y.-L. Zhou, “Predicting lepton flavor mixing from $\Delta(48)$ and generalized CP symmetries,” *Chin. Phys.*, vol. C39, no. 2, p. 021001, 2015.
- [171] C. Hagedorn, A. Meroni, and E. Molinaro, “Lepton mixing from $\hat{\Gamma}(3n^2)$ and $\hat{\Gamma}(6n^2)$ and CP,” *Nucl. Phys.*, vol. B891, pp. 499–557, 2015.
- [172] A. Di Iura, C. Hagedorn, and D. Meloni, “Lepton mixing from the interplay of the alternating group A_5 and CP,” *JHEP*, vol. 08, p. 037, 2015.
- [173] I. Girardi, A. Meroni, S. T. Petcov, and M. Spinrath, “Generalised geometrical CP violation in a T’ lepton flavour model,” *JHEP*, vol. 02, p. 050, 2014.
- [174] L. L. Everett, T. Garon, and A. J. Stuart, “A Bottom-Up Approach to Lepton Flavor and CP Symmetries,” *JHEP*, vol. 04, p. 069, 2015.
- [175] L. L. Everett and A. J. Stuart, “Lepton Sector Phases and Their Roles in Flavor and Generalized CP Symmetries,” *Phys. Rev.*, vol. D96, no. 3, p. 035030, 2017.
- [176] S. F. King and C. C. Nishi, “ $\mu - \tau$ symmetry and the Littlest Seesaw,” *Phys. Lett.*, vol. B785, pp. 391–398, 2018.
- [177] S. F. King and Y.-L. Zhou, “Littlest $\mu - \tau$ seesaw,” 2019.
- [178] W. Grimus, S. Kaneko, L. Lavoura, H. Sawanaka, and M. Tanimoto, “ $\mu - \tau$ antisymmetry and neutrino mass matrices,” *JHEP*, vol. 01, p. 110, 2006.

- [179] A. S. Joshipura, “Neutrino masses and mixing from flavour antisymmetry,” *JHEP*, vol. 11, p. 186, 2015.
- [180] A. S. Joshipura and N. Nath, “Neutrino masses and mixing in A_5 with flavor antisymmetry,” *Phys. Rev.*, vol. D94, no. 3, p. 036008, 2016.
- [181] A. S. Joshipura and K. M. Patel, “Generalized μ - τ symmetry and discrete subgroups of $O(3)$,” *Phys. Lett.*, vol. B749, pp. 159–166, 2015.
- [182] J. Bernabeu, G. C. Branco, and M. Gronau, “CP Restrictions on Quark Mass Matrices,” *Phys. Lett.*, vol. 169B, pp. 243–247, 1986.
- [183] G. C. Branco, L. Lavoura, and M. N. Rebelo, “Majorana Neutrinos and CP Violation in the Leptonic Sector,” *Phys. Lett.*, vol. B180, pp. 264–268, 1986.
- [184] G. C. Branco, L. Lavoura, and J. P. Silva, “CP Violation,” *Int. Ser. Monogr. Phys.*, vol. 103, pp. 1–536, 1999.
- [185] M. H. Rahat, P. Ramond, and B. Xu, “Asymmetric tribimaximal texture,” *Phys. Rev.*, vol. D98, no. 5, p. 055030, 2018.
- [186] B. Adhikary, M. Chakraborty, and A. Ghosal, “Masses, mixing angles and phases of general Majorana neutrino mass matrix,” *JHEP*, vol. 10, p. 043, 2013. [Erratum: *JHEP*09,180(2014)].
- [187] N. Aghanim *et al.*, “Planck intermediate results. XLVI. Reduction of large-scale systematic effects in HFI polarization maps and estimation of the reionization optical depth,” *Astron. Astrophys.*, vol. 596, p. A107, 2016.
- [188] W. Rodejohann, “Neutrino-less Double Beta Decay and Particle Physics,” *Int. J. Mod. Phys.*, vol. E20, pp. 1833–1930, 2011.
- [189] B. Majorovits, “The search for $0\nu\beta\beta$ decay with the GERDA experiment: Status and prospects,” *AIP Conf. Proc.*, vol. 1672, p. 110003, 2015.

- [190] A. Blum, R. N. Mohapatra, and W. Rodejohann, “Inverted mass hierarchy from scaling in the neutrino mass matrix: Low and high energy phenomenology,” *Phys. Rev.*, vol. D76, p. 053003, 2007.
- [191] G. Ecker, W. Grimus, and H. Neufeld, “A Standard Form for Generalized CP Transformations,” *J. Phys.*, vol. A20, p. L807, 1987.
- [192] W. Grimus and L. Lavoura, “Models of maximal atmospheric neutrino mixing,” *Acta Phys. Polon.*, vol. B34, pp. 5393–5404, 2003.
- [193] W. Grimus and L. Lavoura, “ $\mu - \tau$ Interchange symmetry and lepton mixing,” *Fortsch. Phys.*, vol. 61, pp. 535–545, 2013.
- [194] P. Adamson *et al.*, “Measurement of the neutrino mixing angle θ_{23} in NOvA,” *Phys. Rev. Lett.*, vol. 118, no. 15, p. 151802, 2017.
- [195] P. Chen, G.-J. Ding, F. Gonzalez-Canales, and J. W. F. Valle, “Classifying CP transformations according to their texture zeros: theory and implications,” *Phys. Rev.*, vol. D94, no. 3, p. 033002, 2016.
- [196] C. Hagedorn and E. Molinaro, “Flavor and CP symmetries for leptogenesis and $0 \nu \beta\beta$ decay,” *Nucl. Phys.*, vol. B919, pp. 404–469, 2017.
- [197] K. Asakura *et al.*, “Search for double-beta decay of ^{136}Xe to excited states of ^{136}Ba with the KamLAND-Zen experiment,” *Nucl. Phys.*, vol. A946, pp. 171–181, 2016.
- [198] M. Agostini *et al.*, “Results on Neutrinoless Double- β Decay of ^{76}Ge from Phase I of the GERDA Experiment,” *Phys. Rev. Lett.*, vol. 111, no. 12, p. 122503, 2013.
- [199] N. Abgrall *et al.*, “The Majorana Demonstrator Neutrinoless Double-Beta Decay Experiment,” *Adv. High Energy Phys.*, vol. 2014, p. 365432, 2014.

- [200] K. Abe *et al.*, “Combined Analysis of Neutrino and Antineutrino Oscillations at T2K,” *Phys. Rev. Lett.*, vol. 118, no. 15, p. 151801, 2017.
- [201] S. T. Petcov, “Discrete Flavour Symmetries, Neutrino Mixing and Leptonic CP Violation,” *Eur. Phys. J.*, vol. C78, no. 9, p. 709, 2018.
- [202] N. Nath, Z.-z. Xing, and J. Zhang, “ $\mu - \tau$ Reflection Symmetry Embedded in Minimal Seesaw,” *Eur. Phys. J.*, vol. C78, no. 4, p. 289, 2018.
- [203] N. Nath, “ $\mu - \tau$ Reflection Symmetry and Its Explicit Breaking for Leptogenesis in a Minimal Seesaw Model,” 2018.
- [204] C. C. Nishi, B. L. Sánchez-Vega, and G. Souza Silva, “ $\mu\tau$ reflection symmetry with a high scale texture-zero,” *JHEP*, vol. 09, p. 042, 2018.
- [205] E. Ma, “Neutrino mixing: A_4 variations,” *Phys. Lett.*, vol. B752, pp. 198–200, 2016.
- [206] R. Friedberg and T. D. Lee, “A Possible Relation between the Neutrino Mass Matrix and the Neutrino Mapping Matrix,” *HEPNP*, vol. 30, pp. 591–598, 2006.
- [207] Z. Xing, H. Zhang, and S. Zhou, “Nearly Tri-bimaximal Neutrino Mixing and CP Violation from $\mu - \tau$ Symmetry Breaking,” *Phys. Lett. B*, vol. 641, pp. 189–197. 14 p, Jul 2006.
- [208] S. Luo and Z.-z. Xing, “Friedberg-Lee Symmetry Breaking and Its Prediction for θ_{13} ,” *Phys. Lett.*, vol. B646, pp. 242–247, 2007.
- [209] C.-S. Huang, T.-j. Li, W. Liao, and S.-H. Zhu, “Generalization of Friedberg-Lee Symmetry,” *Phys. Rev.*, vol. D78, p. 013005, 2008.
- [210] X.-G. He and W. Liao, “The Friedberg-Lee Symmetry and Minimal Seesaw Model,” *Phys. Lett.*, vol. B681, pp. 253–256, 2009.

- [211] Z.-h. Zhao, “Modified Friedberg-Lee symmetry for neutrino mixing,” *Phys. Rev.*, vol. D92, no. 11, p. 113001, 2015.
- [212] T. Araki and R. Takahashi, “Tri-Bimaximal Mixing from Twisted Friedberg-Lee Symmetry,” *Eur. Phys. J.*, vol. C63, pp. 521–526, 2009.
- [213] T. Araki and C. Q. Geng, “Leptogenesis in model with Friedberg-Lee symmetry,” *Phys. Lett.*, vol. B680, pp. 343–350, 2009.
- [214] J. G. Learned and S. Pakvasa, “Detecting tau-neutrino oscillations at PeV energies,” *Astropart. Phys.*, vol. 3, pp. 267–274, 1995.
- [215] S. Pakvasa, W. Rodejohann, and T. J. Weiler, “Flavor Ratios of Astrophysical Neutrinos: Implications for Precision Measurements,” *JHEP*, vol. 02, p. 005, 2008.
- [216] Z.-z. Xing and S. Zhou, “Implications of Leptonic Unitarity Violation at Neutrino Telescopes,” *Phys. Lett.*, vol. B666, pp. 166–172, 2008.
- [217] S. Blanchet, P. S. B. Dev, and R. N. Mohapatra, “Leptogenesis with TeV Scale Inverse Seesaw in $SO(10)$,” *Phys. Rev.*, vol. D82, p. 115025, 2010.
- [218] S. M. Barr, “A Different seesaw formula for neutrino masses,” *Phys. Rev. Lett.*, vol. 92, p. 101601, 2004.
- [219] M. Hirsch, S. Morisi, and J. W. F. Valle, “A4-based tri-bimaximal mixing within inverse and linear seesaw schemes,” *Phys. Lett.*, vol. B679, pp. 454–459, 2009.
- [220] M. Chakraborty, H. Z. Devi, and A. Ghosal, “Scaling ansatz with texture zeros in linear seesaw,” *Phys. Lett.*, vol. B741, pp. 210–216, 2015.
- [221] W. Wang and Z.-L. Han, “Radiative linear seesaw model, dark matter, and $U(1)_{B-L}$,” *Phys. Rev.*, vol. D92, p. 095001, 2015.

- [222] P. H. Frampton, S. L. Glashow, and D. Marfatia, “Zeroes of the neutrino mass matrix,” *Phys. Lett.*, vol. B536, pp. 79–82, 2002.
- [223] K. Whisnant, J. Liao, and D. Marfatia, “Constraints on texture zero and cofactor zero models for neutrino mass,” *AIP Conf. Proc.*, vol. 1604, pp. 273–278, 2014.
- [224] P. O. Ludl and W. Grimus, “A complete survey of texture zeros in the lepton mass matrices,” *JHEP*, vol. 07, p. 090, 2014. [Erratum: *JHEP*10,126(2014)].
- [225] W. Grimus and P. O. Ludl, “Correlations and textures in the neutrino mass matrix,” *PoS*, vol. EPS-HEP2013, p. 075, 2013.
- [226] J. Liao, D. Marfatia, and K. Whisnant, “Texture and Cofactor Zeros of the Neutrino Mass Matrix,” *JHEP*, vol. 09, p. 013, 2014.
- [227] H. Fritzsch, Z.-z. Xing, and S. Zhou, “Two-zero Textures of the Majorana Neutrino Mass Matrix and Current Experimental Tests,” *JHEP*, vol. 09, p. 083, 2011.
- [228] A. Merle and W. Rodejohann, “The Elements of the neutrino mass matrix: Allowed ranges and implications of texture zeros,” *Phys. Rev.*, vol. D73, p. 073012, 2006.
- [229] W. Wang, “Parallel Texture Structures with Cofactor Zeros in Lepton Sector,” *Phys. Lett.*, vol. B733, pp. 320–327, 2014. [Erratum: *Phys. Lett.*B738,524(2014)].
- [230] L. Lavoura, “Zeros of the inverted neutrino mass matrix,” *Phys. Lett.*, vol. B609, pp. 317–322, 2005.

- [231] A. Kageyama, S. Kaneko, N. Shimoyama, and M. Tanimoto, “Seesaw realization of the texture zeros in the neutrino mass matrix,” *Phys. Lett.*, vol. B538, pp. 96–106, 2002.
- [232] W. Wang, “Parallel Lepton Mass Matrices with Texture and Cofactor Zeros,” *Phys. Rev.*, vol. D90, no. 3, p. 033014, 2014.
- [233] S. Baek, H. Okada, and K. Yagyu, “Flavour Dependent Gauged Radiative Neutrino Mass Model,” *JHEP*, vol. 04, p. 049, 2015.
- [234] S. Choubey, W. Rodejohann, and P. Roy, “Phenomenological consequences of four zero neutrino Yukawa textures,” *Nucl. Phys.*, vol. B808, pp. 272–291, 2009. [Erratum: *Nucl. Phys.*B818,136(2009)].
- [235] B. Adhikary, A. Ghosal, and P. Roy, “ $\mu - \tau$ symmetry, tribimaximal mixing and four zero neutrino Yukawa textures,” *JHEP*, vol. 10, p. 040, 2009.
- [236] B. Adhikary, A. Ghosal, and P. Roy, “Baryon asymmetry from leptogenesis with four zero neutrino Yukawa textures,” *JCAP*, vol. 1101, p. 025, 2011.
- [237] B. Adhikary, A. Ghosal, and P. Roy, “Neutrino Masses, Cosmological Bound and Four Zero Yukawa Textures,” *Mod. Phys. Lett.*, vol. A26, pp. 2427–2435, 2011.
- [238] B. Adhikary, M. Chakraborty, and A. Ghosal, “Scaling ansatz, four zero Yukawa textures and large θ_{13} ,” *Phys. Rev.*, vol. D86, p. 013015, 2012.
- [239] M. Auger *et al.*, “Search for Neutrinoless Double-Beta Decay in ^{136}Xe with EXO-200,” *Phys. Rev. Lett.*, vol. 109, p. 032505, 2012.